Technische Universität München
TUM School of Life Sciences

Understanding Drug Synergy in Pancreatic Cancer: A Proteomic Study of Gemcitabine and ATR Inhibitors

Stefanie I. Höfer

Vollständiger Abdruck der von der TUM School of Life Sciences der Technischen Universität München zur Erlangung eines

Doktors der Naturwissenschaften (Dr. rer. nat.)

genehmigten Dissertation.

Vorsitz: Prof. Dr. Martin Klingenspor

Prüfende der Dissertation:

1. Prof. Dr. Bernhard Küster
2. Prof. Dr. Maximilian Reichert

Die Dissertation wurde am 06.08.2024 bei der Technischen Universität München eingereicht und durch die TUM School of Life Sciences am 28.11.2024 angenommen.

Abstract

Pancreatic ductal adenocarcinoma (PDAC) is a devastating disease in urgent need of new therapeutic strategies. The standard treatment of PDAC involves chemotherapeutics such as the DNA-damaging agent Gemcitabine (GEM), but chemoresistance is frequently observed. Combining GEM with targeted therapies, such as kinase inhibitors, is a promising strategy to overcome this resistance. Despite some clinical successes, the therapeutic impact of targeted therapy in PDAC remains marginal. Mechanistic insights into targeted therapies that synergize with GEM may aid the clinical development of such regimens. This study aimed to 1) assess the phenotypic efficacy of clinically relevant targeted therapies in combination with GEM in PDAC and 2) elucidate the mechanisms of synergy using mass spectrometry-based proteomics.

Therefore, a phenotypic drug screening of 146 targeted drugs alone and combined with GEM was conducted across 13 PDAC cell lines. Elimusertib, an inhibitor of the essential DNA damage response kinase Ataxia telangiectasia and Rad3 related (ATR), demonstrated the broadest efficacy, displaying synergy with GEM in 11 of 13 cell lines. Further testing of six additional ATR inhibitors confirmed the broad applicability of the observed synergy between Elimusertib and GEM. Chemoproteomic target deconvolution using Kinobeads identified ATR kinase as the sole common target of these inhibitors, although some compounds unexpectedly exhibited off-target effects.

Phosphoproteomic drug-perturbation experiments were performed on GEM and four clinical ATR inhibitors, including Elimusertib. Thereby, GEM induced a robust DNA damage response in AsPC1 cells, which was attenuated by ATR inhibition. A set of 36 SQ/TQ-phosphorylation sites, including known and potential new ATR substrates, emerged to explain drug synergy by ATR-mediated DNA damage response and transcriptional regulation. A novel substrate of ATR, CHEK1-p468, exhibited the strongest response to the combination treatment, underscoring its potential as a pharmacodynamic biomarker. The analysis of time-dependent changes in protein expression levels attributed non-canonical ATR-driven pathways to drug synergy. Notably, the ribonucleotide reductase subunit M2 (RRM2) was counter-regulated in abundance by GEM and Elimusertib, suggesting a pivotal role of nucleotide pool homeostasis in drug synergy.

Given the ongoing early clinical trials of several ATR inhibitors and the GEM-Elimusertib combination in PDAC, this study provides valuable phenotypic and mechanistic insights into the synergy between GEM and ATR inhibitors. It also demonstrates how mass spectrometry-based proteomics can be leveraged to understand the mechanisms underlying drug action and their combination. These findings may inform future clinical strategies and improve therapeutic outcomes for pancreatic cancer patients.

Zusammenfassung

Das duktale Pankreas-Adenokarzinom (englisch *pancreatic ductal adenocarcinoma*, PDAC) ist eine verheerende Krebserkrankung, die dringend neue therapeutische Ansätze benötigt. Die Standardbehandlung von PDAC umfasst Chemotherapeutika wie das DNA-schädigende Mittel Gemcitabin (GEM), wogegen Patienten jedoch häufig Chemoresistenz entwickeln. Die Kombination von GEM mit gezielten Therapien, wie Kinaseinhibitoren, ist eine vielversprechende Strategie, um diese Resistenz zu überwinden. Trotz einiger klinischer Erfolge bleibt der therapeutische Einfluss gezielter Therapien bei PDAC bislang jedoch marginal. Mechanistische Einblicke in gezielte Therapien, die mit GEM synergieren, könnten die klinische Entwicklung solcher Regime unterstützen. Diese Studie zielte darauf ab, 1) die phänotypische Wirksamkeit klinisch relevanter gezielter Therapien in Kombination mit GEM bei PDAC zu bewerten und 2) die Mechanismen der Synergie mittels Proteomik aufzudecken.

Daher wurde ein phänotypisches Medikamentenscreening von 146 zielbasierten Medikamenten, sowohl allein als auch in Kombination mit GEM, in 13 PDAC-Zelllinien durchgeführt. Elimusertib, ein Inhibitor der essentiellen DNA-Schadensantwort-Kinase *Ataxia telangiectasia and Rad3 related* (ATR), zeigte die breiteste Wirksamkeit und Synergie mit GEM in 11 von 13 Zelllinien. Weitere Tests von sechs zusätzlichen ATR inhibitoren bestätigten die breite Anwendbarkeit der beobachteten Synergie zwischen Elimusertib und GEM. Chemoproteomische Analysen mit Hilfe der Kinobeads-Technologie bestätigten die ATR-Kinase als das einzige gemeinsame Zielprotein dieser Inhibitoren, obwohl einige der Inhibitoren auch unerwartete Protein-Interaktionen zeigten.

Phosphoproteomische Zellbehandlungs-Experimente wurden mit GEM und vier klinischen ATR inhibitoren, einschließlich Elimusertib, durchgeführt. Dabei induzierte GEM eine robuste DNA-Schadensantwort in AsPC-1-Zellen, die nur teilweise durch die Behandlung mit ATR inhibitoren abgeschwächt wurde. Sechsunddreißig Phosphorylierungsstellen, einschließlich bekannter und potenziell neuer ATR-Substrate, traten als potenzielle Biomarker der Wirkstoffkombination hervor. CHEK1-p468 zeigte dabei die stärkste Reaktion auf die Kombinationstherapie. Weiterhin wurden zeitabhängige Veränderungen der Proteinexpression unter GEM und Elimusertib analysiert. Dies ergab, dass auch nicht-kanonische ATR-gesteuerte Wege an der Arzneimittelsynergie beteiligt sind. Bemerkenswert war, dass Ribonukleotidreduktase-Untereinheit 2 (englisch *ribonucleotide reductase subunit 2*, RRM2) in ihrer Expression durch GEM und Elimusertib gegensätzlich reguliert wurde, was auf eine zentrale Rolle im Mechanismus der Synergie hinweist.

Angesichts der laufenden frühen klinischen Studien mehrerer ATR inhibitoren und insbesondere der Kombination von GEM und Elimusertib in PDAC liefert diese Studie wertvolle phänotypische und mechanistische Einblicke in die Synergie zwischen GEM und ATR inhibitoren. Sie zeigt auch,

wie Massenspektrometrie-basierte Proteomik genutzt werden kann, um die Mechanismen zugrunde liegender Medikamente und deren Kombination zu verstehen. Diese Erkenntnisse könnten zukünftige klinische Strategien informieren und die therapeutischen Ergebnisse für Pankreaskrebs-Patienten verbessern.

TABLE OF CONTENTS

1 Introduction

1.1 Pancreatic cancer and the need for novel therapies

1.1.1 Clinical management of PDAC relies on chemotherapy

Therapeutic improvements in PDAC therapy are low compared to other cancers. Pancreatic adenocarcinoma (PDAC) is the most common form of pancreatic cancer, accounting for more than 85% of all pancreatic malignancies[1]. In 2023, the American Cancer Society estimated a total of 64,050 new pancreatic cancer cases and 50,550 deaths caused by the disease in the United States[2], underlining the need for novel therapeutic interventions. Within 1975 and 2018, the 5-year relative survival rates of all cancers combined have increased on average from 49% to 68% in the United States[2], with notable advancements in the prognosis of myeloma (from 25% to 58%) and leukemia (from 34% to 66%; **Figure 1**)[2]. Moreover, particularly hard-to-treat cancers such as that of the esophagus, liver, or bile duct have experienced some significant improvement, with patient survival rates having increased from < 6% to 21%[2]. In contrast, the prognosis of PDAC has only marginally advanced in the past decades, with an increase in the 5-year relative survival rate from 3% to 12%[2]. Despite this positive trend overall, this suggests a lack of substantial diagnostic and therapeutic breakthroughs in PDAC, highlighting the unmet clinical need for innovative therapies for this disease.

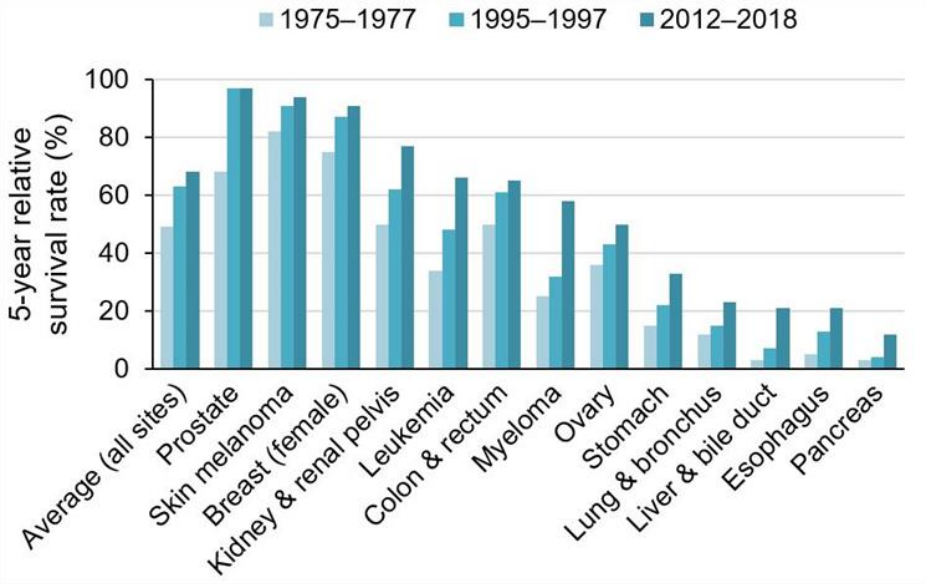

Figure 1. Trends in 5-year relative survival rates (%) per cancer site in the United States between 1975 and 2018. The numbers are based on patients diagnosed with the respective type of cancer between 1975-1977, 1995-1997, and 2012-2018. The average survival rates across all cancer sites include other cancers not shown here. The data was published by Siegel et al. (2023)[2] and is based on the National Cancer Institute's Surveillance, Epidemiology, and End Results program[3] (see also Siegel et al. (2023)[2]).

1 | Introduction

Chemotherapy is the mainstay of the clinical management of PDAC. As of today, the only potentially curative therapy for PDAC remains surgery[4]. However, about 80% of patients are found with locally advanced or metastatic disease, rendering them inoperable at the time of diagnosis[4]. Consequentially, the primary therapeutic goals for most PDAC patients remain tumor shrinkage and subsequent surgery or disease control and prolonged survival, primarily by systemic chemotherapy[4,5]. Although treatment plans are highly individual to the patient's initial performance status, the two most commonly used chemotherapeutic regimens are Gemcitabine (GEM) combined with nanoparticle albumin-bound (nab-)-Paclitaxel and FOLFIRINOX[4-6].

GEM is a nucleoside analog clinically used in PDAC since 1997, which acts as an antimetabolite that interferes with DNA replication in proliferating cells and ultimately induces programmed cell death[7,8]. In the phase III clinical trial that granted its approval, GEM demonstrated prolonged survival and enhanced quality of life in advanced PDAC patients compared to another antimetabolite, 5-fluorouracil[7]. In today's clinical practice, GEM is typically administered with nab-Paclitaxel, a tubulin-binding cytotoxic compound[9]. Compared to GEM alone, this combination increased the median overall survival of patients with metastatic PDAC from 6.7 months to 8.5 months and progression-free survival from 3.7 months to 5.5 months (phase III clinical trial MPACT)[10].

The other standard first-line therapy of PDAC is FOLFIRINOX, a four-drug regimen consisting of the cytotoxic agents 5-fluorouracil (antimetabolite), Irinotecan (topoisomerase inhibitor), Oxaliplatin (DNA-crosslinking agent), and the chemotherapy-modulator folinic acid[5,6]. In 2011, a clinical phase III trial revealed a superior median overall survival of patients with advanced PDAC that received FOLFORINOX compared to GEM monotherapy (11.1 months vs. 6.8 months; PRODIGE 4/ACCORD11 trial)[11]. However, despite its improved efficacy, the severe toxicological profile of FOLFIRINOX limits its use primarily to PDAC patients with good performance status[12]. Consequentially, individuals with poorer performance status are preferably given GEM plus nab-paclitaxel, GEM monotherapy, or a modified, less aggressive version of FOLFIRINOX (mFOLFIRINOX) by reducing or eliminating individual components from the original combination[5,13].

Although GEM plus nab-Paclitaxel and (m)FOLFIRINOX build the basis of PDAC clinical management, other systemic chemotherapy may be more recommended in some contexts. For instance, in PDAC patients harboring germline mutations in the DNA maintenance genes BRCA1, BRCA2, or PALB2 (5-9% of patients), the combination of GEM and the DNA-crosslinking agent Cisplatin has proven strong therapeutic efficacy[14]. Also, for patients with advanced PDAC who progressed on GEM-based first-line therapy, the combination of 5-fluorouracil and nanoliposomal Irinotecan is a recommended second-line intervention[15]. Finally, for post-operative chemotherapy

of tumor-resected patients, the combination of GEM and another antimetabolite, Capecitabine, is considered a standard therapy[16].

Targeted inhibitors have evolved as second-line therapy but with limited impact. In addition to systemic chemotherapy, targeted inhibitors have evolved in PDAC, yet with limited clinical impact. The first approved targeted therapy was the EGFR inhibitor Erlotinib combined with GEM[17]. In 2007, this combination demonstrated a statistically significant improvement in patient overall survival compared to GEM alone, but only by less than two weeks (6.2 months vs 5.9 months)[17]. More than ten years later, PARP1 inhibitor Olaparib was approved as maintenance therapy for a small subgroup of PDAC patients harboring germline mutations in BRCA1 or BRCA2, affecting 5-7% of patients[18]. In the approval-granting trial, Olaparib significantly increased median progression-free survival in this patient cohort to 7.4 months, compared to 3.8 months with a placebo (POLO trial)[18]. However, no improvement in overall survival was observed[18]. Finally, several tumor-agnostic targeted therapies have been approved for cancers with certain molecular features. For instance, the PD-L1-targeting antibody Pembrolizumab has been approved for the immunotherapy of advanced cancers harboring deficient DNA mismatch repair or high microsatellite instability[19]. Furthermore, the two TRK kinase inhibitors, Entrectinib and Larotrectinib, have been granted U.S. Food and Drug Administration (FDA) approval for solid cancers carrying a fusion in the NTRK gene[20,21]. However, these mutations are extremely rare in PDAC (~1%); hence, these therapies are limited to only very few patients[5,6]. Taken together, despite a few alternative advances, classical chemotherapy remains the current mainstay of PDAC management.

1.1.2 Mode of action of Gemcitabine and resistance mechanisms

GEM requires active cellular uptake and metabolism to become bioactive. GEM is a fundamental component of chemotherapy in PDAC and is also frequently used in other solid tumors, including non-small cell lung cancer (NSCLC), bladder, and breast cancer[22]. Given its broad application and significance in cancer therapy, the molecular mechanism of GEM has been extensively studied over the past decades. GEM is a synthetic analog of deoxycytidine, differing only by the addition of two fluorine atoms at the 2' position of the ribose ring (2′, 2′-difluoro deoxycytidine; dFdC; **Figure 2**). As a prodrug, GEM requires active transport into cells and subsequent metabolic conversion to its bioactive form[22]. Cellular uptake of GEM occurs through integral membrane proteins from the human nucleoside transporter family, primarily human equilibrative nucleoside transporter 1 (hENT1)[22,23]. Once inside the cell, GEM undergoes three phosphorylation steps: first, to its mono-phosphorylated form (dFdCMP) by deoxycytidine kinase (DCK); next, to its di-phosphorylated form (dFdCDP) by cytidine/uridine monophosphate kinase 1

(CMPK1); and finally, to its tri-phosphorylated, bioactive form (dFdCTP) by nucleoside diphosphate kinase A (NME1)[22].

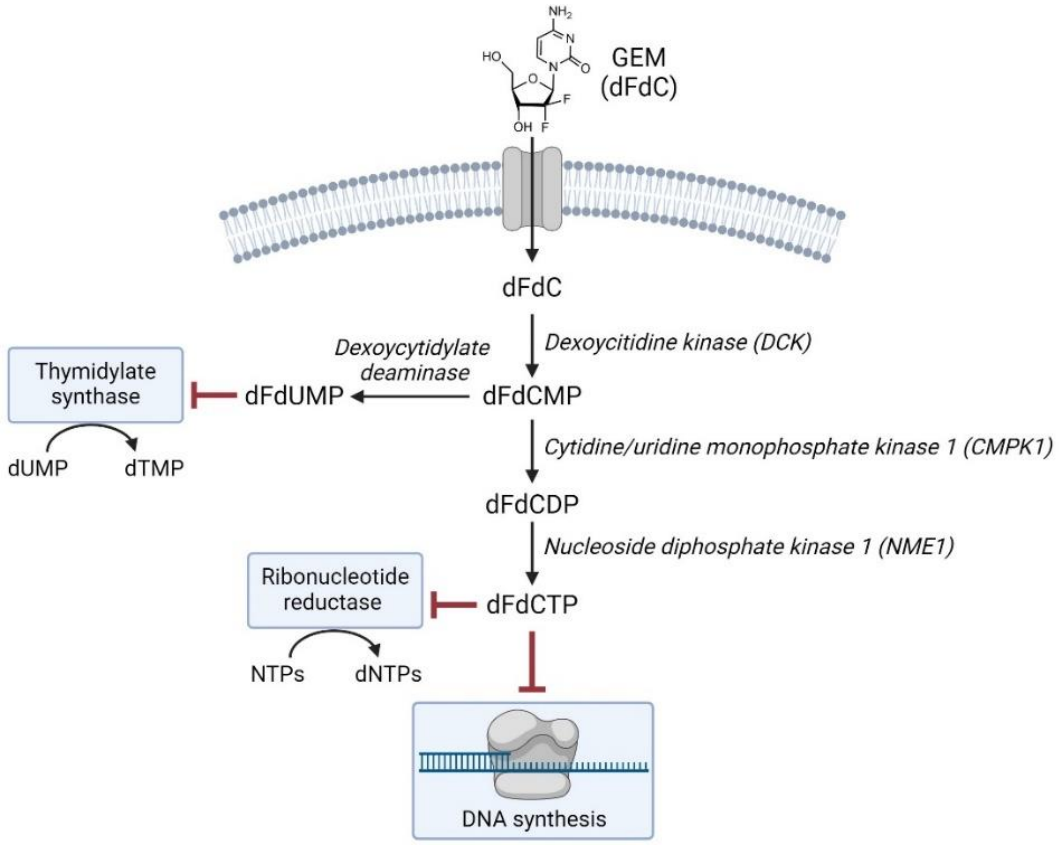

Figure 2. Cellular uptake, metabolism, and mode of action of GEM. GEM is phosphorylated by different kinases upon cellular uptake and inhibits DNA synthesis and dNTP metabolism enzymes. dFdC: 2′, 2′-difluorodeoxycytidine; dFdCMP, dFdCDP, and dFdCTP: mono-, di-, and tri-phosphorylated dFdC; dUMP: deoxyuridine monophosphate; dTMP: deoxythymidine monophosphate; dFdUMP: 2′-deoxy-2′,2′-difluorouridine monophosphate. Created with BioRender.com

Phosphorylated GEM is incorporated into newly synthesized DNA. The tri-phosphorylated form of GEM mimics deoxycytidine triphosphate (dCTP) and competes for incorporation into newly synthesized DNA in dividing cells[24]. This causes the termination of the replication process during the S-phase, triggering cell cycle arrest and the activation of DNA repair pathways[25]. However, GEM removal from DNA is hampered by different mechanisms. Upon incorporation of the pyrimidine analog, the DNA strand is elongated by one additional nucleotide before DNA polymerase terminates DNA synthesis[8,24]. This phenomenon, called ‘masked chain termination’, hides the faulty base from excision by DNA proofreading enzymes[24]. A second mechanism by which GEM escapes DNA repair has recently emerged: The direct inhibition of 3′-5′ exonuclease activity of DNA polymerase by all three phosphorylated forms of GEM[26]. The reduced proofreading function prevents the removal of incorporated GEM or the 3′-mismatched nucleotide from newly synthesized DNA strands[26]. The resulting accumulation of GEM at multiple replication sites in the DNA ultimately triggers programmed cell death, such as apoptosis[25].

GEM intermediates inhibit dNTP metabolism enzymes, leading to self-potentiation. Beyond the direct blockage of DNA synthesis, GEM and its intermediates also interfere with enzymes involved in the metabolism of deoxyribonucleotides (dNTP)[27]. This results in a misbalance in cellular dNTP pools, disrupting replication and DNA repair processes. Moreover, the dysregulation of cellular dNTP synthesis also displays a mechanism of self-potentiation, positively regulating the uptake, metabolism, and action of GEM[27]. For instance, the di-phosphorylated form of GEM inhibits ribonucleotide reductase, a key enzyme required for replenishing cellular dNTP pools by converting ribonucleotides to deoxyribonucleotides[27-29] (**Figure 2**). Inhibition of ribonucleotide reductase reduces intracellular dCTP levels, favoring the incorporation of GEM into DNA[27]. Low dCTP levels also elevate DCK activity, promoting the phosphorylation of GEM and its conversion to a bioactive compound[27].

Another more indirectly inhibited enzyme is thymidylate synthase (TYMS), which catalyzes the biosynthesis of deoxythymidine monophosphate (dTMP) during the *de novo* synthesis of deoxythymidine triphosphate (dTTP)[30] (**Figure 2**). It is enzymatically blocked by a side product of GEM metabolism, dFdUMP, produced from cellular deamination of GEM monophosphate (dFdCMP) by deoxycytidylate deaminase[30]. Noteworthy, deoxycytidylate deaminase is inhibited by GEM triphosphate. This promotes the cellular accumulation of bioactive GEM rather than the enzymatic conversion to dFdUMP, displaying another mechanism of self-potentiation of the chemodrug[30]. In summary, GEM's mode of action involves multiple mechanisms that disrupt DNA synthesis and replication, leading to its cytotoxicity. Importantly, its ability to interfere with dNTP metabolism and self-potentiate is key to its effectiveness as a chemotherapeutic agent.

Potential mechanisms of chemoresistance are implicated with GEM metabolism and kinase signaling. Despite the frequent use of GEM in treating PDAC, chemoresistance remains a significant clinical challenge[31,32]. On a molecular level, GEM resistance has been frequently linked to enzymes directly involved in the cellular uptake and metabolism of GEM. For instance, reduced expression of the hENT1 transporter protein has been linked to GEM resistance in pancreatic cancer patients[33,34]. Also, low expression levels of DCK, the enzyme responsible for the initial phosphorylation of GEM, have been found to correlate with reduced sensitivity in pancreatic cancer cells[35,36]. Furthermore, high expression levels of ribonucleotide reductase subunits RRM1 and RRM2 have been linked to GEM resistance in pancreatic cancer[36-38]. Finally, an increased activity of enzymes that catalyze the cellular export or the metabolic inactivation of GEM further contributes to chemoresistance; examples include ATP binding cassette proteins, which regulate GEM efflux out of the cell, and 5′-nucleotidases, which convert GEM nucleotides back to nucleosides[31,32].

In addition to these direct resistance mechanisms related to GEM uptake and metabolism, kinase-mediated signaling pathways have been linked to chemoresistance. For instance, a study utilizing

small interfering RNA to probe all human kinases in PDAC cells identified over 80 proteins associated with resistance to GEM-induced apoptosis, including those involved in cell cycle control and receptor-tyrosine kinase (RTK) signaling through the MAPK and the PI3K/AKT/mTOR axis[39,40]. Moreover, the tumor microenvironment in PDAC is characterized by a highly desmoplastic stroma, creating resistance by hindering drug delivery and penetration into tumor cells[41]. Kinase signaling pathways that promote stromal production, such as TGF-β receptor, Hedgehog, or Wnt signaling, are potential drivers of GEM chemoresistance[41,42]. These pathways involve kinases that could be inhibited by small molecules, highlighting the potential of targeted therapy to overcome chemoresistance.

1.1.3 Targeting PDAC vulnerabilities to overcome chemoresistance

Frequent mutations in KRAS activate targetable downstream signaling pathways. Several key signaling pathways are de-regulated in PDAC, displaying potential vulnerabilities for targeted therapy. Specifically, 12 core pathways and cellular processes have been identified as most frequently altered in PDAC patients based on genomic analyses[43] (**Figure 3a**). Intriguingly, some of these overlap with the pathways linked to GEM resistance before (see above), displaying a particular opportunity to combine GEM and targeted therapy in PDAC. Some of the most frequently altered pathways and cellular processes in PDAC are highlighted below, together with their potential targeted intervention.

Most PDAC patients (> 90%) harbor activating mutations in the KRAS oncogene, a GTPase that transduces cell growth signals via the MAPK and PI3K pathways[6,44] (**Figure 3b**). Given that KRAS mutations are considered a key driver of pancreatic carcinogenesis[6], it seems obvious to inhibit this protein through medical intervention. However, in the past, KRAS has been widely considered non-targetable, one reason being the challenge to establish a compound interaction affine enough to keep KRAS in its inactive state[6,45]. Only recently have covalent inhibitors of the KRAS G12C variant been approved for clinical use in lung cancer and were added to the National Comprehensive Cancer Network treatment guidelines for KRAS G12C-mutated pancreatic cancer[45-48]. However, the prevalence of the KRAS G12C variant in PDAC is extremely low (< 2%)[44], and inhibitors of more frequent variants such as KRAS G12D are only emerging recently[45,49,50].

In principle, targeting RTKs, such as EGFR, upstream of KRAS displays a viable targeting strategy, as demonstrated by the approved EGFR inhibitor Erlotinib (Chapter 1.1.1.). Alternatively, downstream kinase signaling, such as the KRAS-driven MAPK signaling pathway, including Raf, MEK, and ERK kinases, is well-described, and several inhibitors have been developed[51]. Also, the PI3K-signaling pathway downstream of RTKs, including AKT1 and mTOR, presents a cancer vulnerability[51]. However, the clinical success of such therapies has mostly been hampered by quickly acquired resistance[52]. Reported resistance mechanisms are the activation of parallel

signaling axis (e.g., PI3K, STAT3, or Hippo signaling in response to MEK inhibition) or alternative RTKs upstream of the MAPK or PI3K pathways[52].

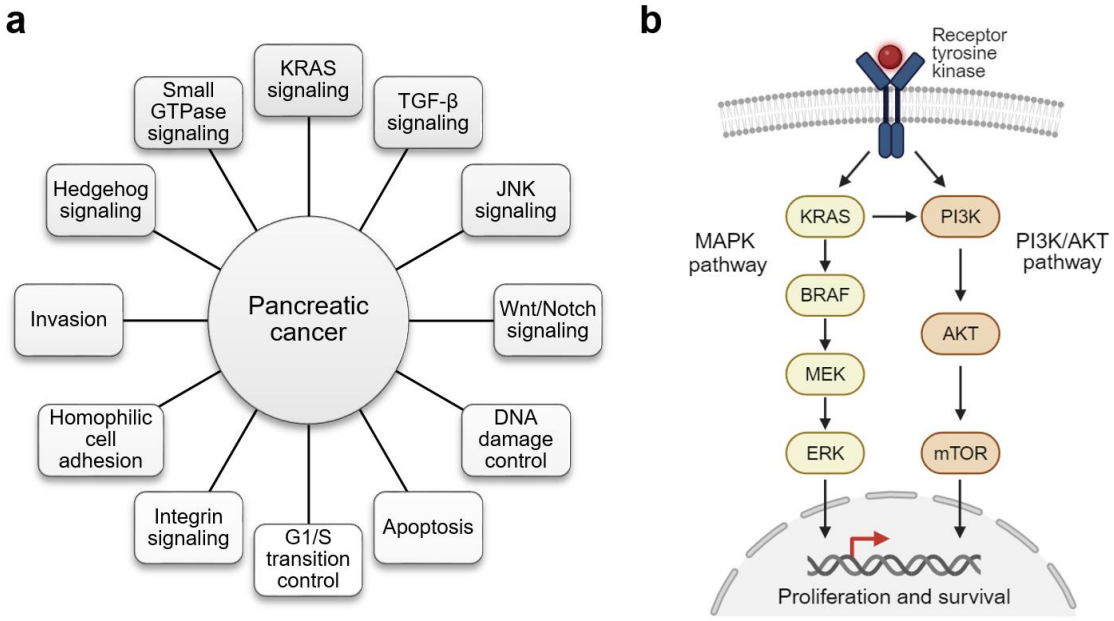

Figure 3. Potential vulnerabilities in PDAC for targeted therapy. a) Twelve core pathways and cellular processes frequently altered in PDAC[43]. Adapted from Jones et al. (2008)[43]. **b)** Schematic representation of the KRAS-driven MAPK and PI3K/AKT signaling pathways promoting cell proliferation and survival. Under normal conditions, these pathways are activated through receptor tyrosine kinase signaling in response to external stimuli. Inspired by Nikiforov and Nikiforova (2011)[53]. Created with BioRender.com.

Frequent loss of tumor suppressors in PDAC creates a vulnerability for targeted intervention. Another molecular characteristic of PDAC is mutations in tumor suppressor genes, most frequently TP53 (60-70%), CDKN2A (30-50%), or SMAD4 (20-50%)[54]. Under normal conditions, these tumor suppressors prevent uncontrolled proliferation and genome instability through cell cycle control, DNA repair, and pro-apoptotic signaling[55]. Deficiencies in these genes often render cancer cells heavily reliant on alternative pathways to sustain their growth and survival, known as synthetic essentiality[56]. Such compensatory pathways and dependencies create vulnerabilities that targeted therapies can address.

For instance, p53 is a central guardian of the G_1 checkpoint, and the loss of p53 function makes cancer cells highly dependent on the G_2 checkpoint to survive the accumulation of DNA damage (**Figure 4**). Therefore, targeting G_2/M checkpoint regulators, such as cyclin-dependent kinases, CHEK1, CHEK2, or WEE1, may cause pre-mature entry into mitosis and cell death[55,57]. A similar treatment strategy may be exploited for CDKN2A-deficient PDAC, as this tumor suppressor also controls the G_1/S transition in the cell cycle, yet by inhibition of CDK4/6[57]. In contrast, SMAD4 controls cell growth and mediates pro-apoptotic signaling of the TGF-β pathway[57]. Interestingly, in the absence of SMAD4, TGF-β signaling switches its function from a tumor suppressor to an oncogene, promoting cancer progression and metastasis[57]. This highlights that the TGF-β receptor is a potential target for therapeutic intervention in PDAC harboring SMAD4 deficiencies.

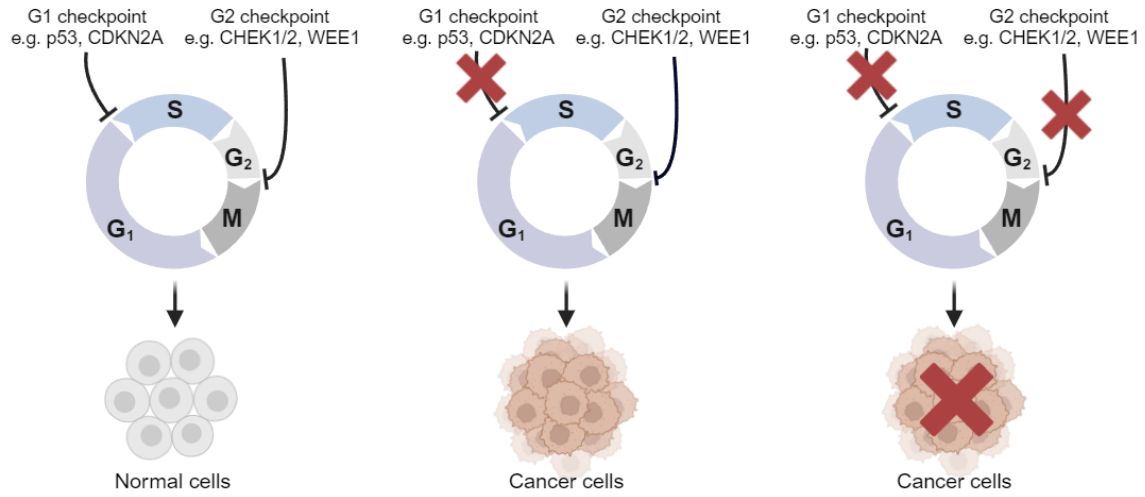

Figure 4. Concept of synthetic essentiality for cancers deficient in tumor suppressor genes, such as p53 or CDKN2A. Under normal conditions, both G_1 and G_2 checkpoints control cell division (left). In case of mutational loss of G_1 checkpoint control, uncontrolled cell proliferation can occur, leading to cancer (middle). If the G_2 checkpoint is additionally blocked, e.g., through medical intervention, cancer cells undergo programmed cell death (right). Created with BioRender.com.

The *status quo* of GEM-based combination therapy with targeted inhibitors in PDAC. The potential vulnerabilities of PDAC described above, together with the kinase-mediated signaling pathways connected to GEM resistance, imply their combination may be a valuable therapeutic strategy in PDAC. The general idea of combining GEM and targeted therapy for cancer therapy is not new. In PDAC alone, more than 300 clinical trials have been conducted on GEM-based combination therapies in the past 25 years, most frequently with other systemic chemotherapy (131 of 320 trials, or 41%; according to *clinicaltrials.gov* as of June 2024; **Figure 5a**). Noteworthy, the second and third most frequently tested GEM-based regimens in PDAC involved targeted therapy with either small molecule inhibitors (97 trials, or 30%) or biologics (62 trials, or 19%). In total, 58 unique targeted inhibitors have entered clinical stage in PDAC in GEM-based combination therapies, 14 drugs in the past five years alone (an increase of 25%; **Figure 5b**; **Appendix 1**). The inhibitors tested with GEM cover different targets (mostly kinases), but inhibitors of RTKs (RTKi) were most represented (11 different RTKi; **Figure 5c**). This increasing effort over the past 25 years implies a great interest in GEM-based combination therapies with molecularly targeted drugs. Nevertheless, the fact that only a single such combination emerged in PDAC (with EGFR inhibitor Erlotinib; Chapter 1.1.1) implies a low clinical success rate and the need for improved drug development strategies.

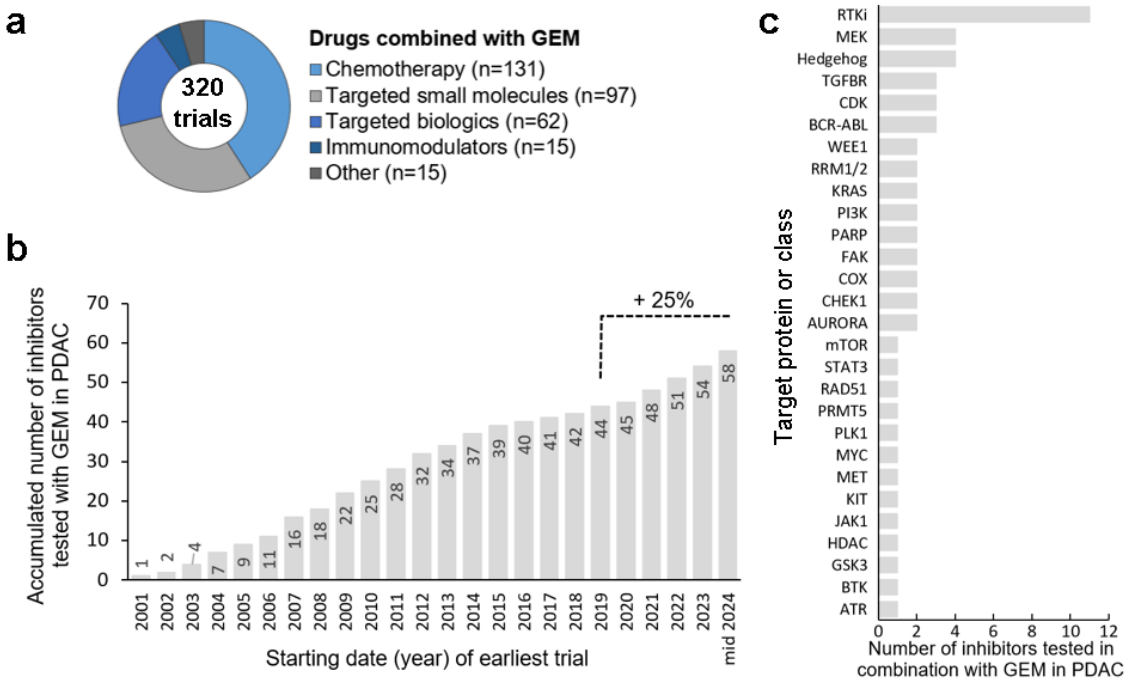

Figure 5. Overview of clinical trials of GEM-based combination therapies in PDAC. a) Fraction of clinical trials assessing GEM in combination with different therapies initiated since 2000, according to *clinicaltrials.gov* (as of June 2024). Only completed, active, or recruiting studies were considered. **b)** Accumulated number of inhibitors entering the clinical stage in combination with GEM in PDAC between 2001 and mid-2024. In the past five years, the number increased by 25%. **c)** The number of inhibitors tested in combination with GEM in PDAC between 2001 and mid-2024, grouped by target protein or class.

1.2 Targeting the ATR kinase-mediated DNA damage response

1.2.1 The roles of ATR, ATM, and DNA-PK in DNA damage response

Cells require a functional DNA damage response. Every cell in the human body constantly faces DNA damage, with an estimated tens of thousands of DNA lesions per day[58]. Such lesions include strand breaks, mismatches, chemical modifications, and cross-links of DNA, which can either arise from endogenous sources such as errors during DNA replication or reactive oxygen species or environmental factors such as radiation and chemical agents[59-61]. The accumulation of DNA lesions promotes genomic instability and can lead to senescence or programmed cell death if not sufficiently repaired[61,62]. Moreover, persistent DNA stress also promotes mutagenesis, which could initiate cancer through the stepwise acquisition of pro-tumorigenic mutations[63]. Therefore, an intact DNA damage response is crucial for all cells to protect them from fatal genomic instability and acquiring cancer-driving mutations.

DNA-PK, ATM, and ATR are the key regulators of cellular DNA damage response. Mammalian cells have evolved several DNA damage response pathways to cope with DNA defects, mainly orchestrated by three kinases: DNA-dependent protein kinase (DNA-PK), ataxia telangiectasia-mutated (ATM) and ataxia-telangiectasia, and Rad3-related (ATR)[60,61,64]. These proteins belong to the phosphatidylinositol 3-kinase-related kinase (PIKK) family and share substantial structural and functional similarities[65]. They trigger different cellular DNA damage tolerance and repair pathways, depending on the type of DNA lesion. In the presence of DNA double-strand breaks (DSBs), DNA-PK and ATM are primarily activated (**Figure 6**)[64]. DSBs pose a potential threat to cell survival, rendering their repair essential to cells[64]. Although several repair mechanisms exist, the main DSB repair pathways mediated by DNA-PK and ATM are non-homologous end-joining of the broken ends (NHEJ) and homologous recombination (HR), respectively[64]. NHEJ is a rapid yet error-prone mechanism for DSB repair that directly ligates DNA ends without the use of a sister chromatid or template[66]. This process can occur at any stage of the cell cycle but is predominantly active during the G_1- and G_2-phases[67]. In contrast, HR requires a template for DSB repair, ensuring a largely error-free process, and occurs during the S- and G_2-phases of the cell cycle[66,67]. To provide time for DNA repair, ATM further induces transient G_1-checkpoint activation by signal transduction through checkpoint kinase 2 (CHEK2) and p53[64]. If the DNA damage remains unrepaired and accumulates, ATM signaling can induce programmed cell death, such as apoptosis[64].

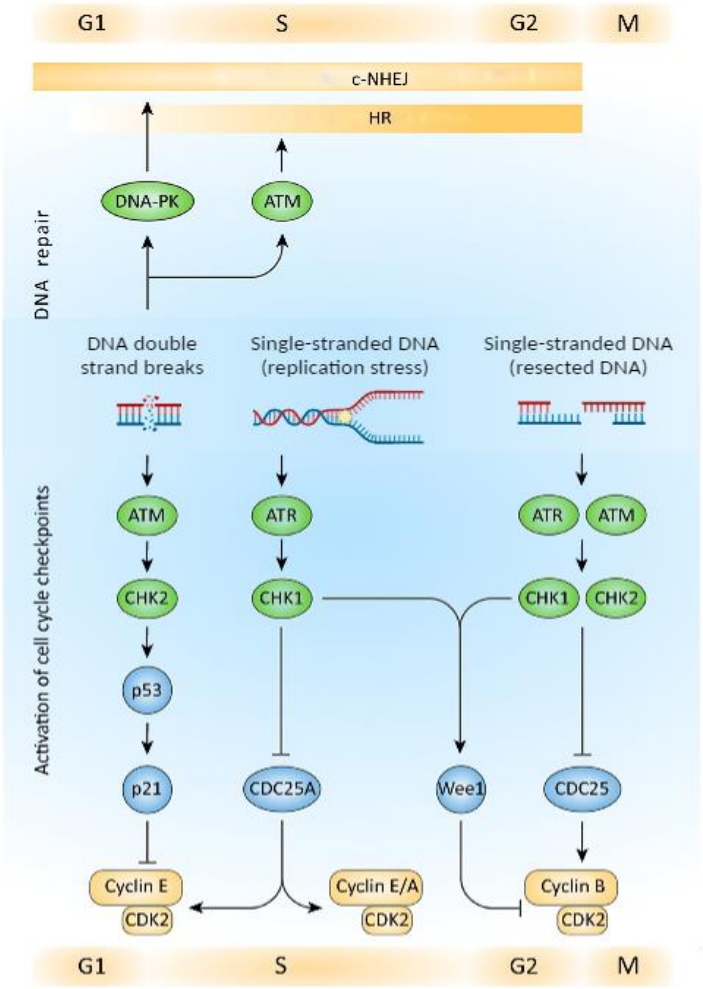

Figure 6. Overview of the DNA damage response orchestrated by DNA-PK, ATM, and ATR. These kinases respond to DNA double-strand breaks or the presence of single-stranded DNA by different DNA repair mechanisms and cell cycle control. Modified from Kantidze et al. (2018)[64]. Changes included the addition of schematic representations of DNA. Modified with BioRender.com.

In contrast to DNA-PK and ATM, ATR is primarily activated in the presence of single-stranded DNA (ssDNA), which primarily arises at stalled replication forks, or so-called replication stress[64]. Although the presence of ssDNA does not necessarily indicate DNA damage or breakage, its accumulation can eventually result in DSBs that pose a potential threat to cell survival. Therefore, ATR must adequately respond to maintain genomic integrity and prevent further DNA damage[64]. Its primary function is checkpoint activation by phosphorylation of downstream effectors, most importantly, checkpoint kinase 1 (CHEK1)[68-70]. Upon phosphorylation by ATR, CHEK1 promotes the proteasomal degradation of CDC25A, a phosphatase that removes inhibitory modifications on cyclin-dependent kinase 1 (CDK1) and CDK2. The activated CDKs lead to checkpoint activation in the S-phase and at the G_2/M transition[71]. Thereby, ATR ensures proper cell proliferation by preventing premature entry into mitosis and provides time for the cell to repair DNA lesions.

ATR and ATM were shown to partially overlap in their functional roles in cell cycle regulation and DNA repair[72,73]. For instance, as an alternative to replication stress, ssDNA can occur transiently at

the ends of resected DNA double-strand breaks during DNA repair, triggering G_2/M checkpoint activation by both ATR and ATM through phosphorylation of their effector proteins CHEK1 and CHEK2, respectively[64]. Moreover, although ATR is mostly known for its cell cycle-guarding role, it also mediates homologous recombination through direct phosphorylation of associated proteins, such as BRCA1[74]. In addition, both ATR and (to a lesser extent) ATM were reported to phosphorylate Fanconi anemia pathway proteins involved in the repair of DNA interstrand crosslinks, including FANCD2[75,76]. This overlap in substrates can be, in principle, explained by the kinases' shared preference to phosphorylate proteins at serine or threonine residues that are followed by glutamine (pSQ/pTQ)[72]. This pSQ/pTQ motif is characteristic of the PIKK protein family and is frequently used as a proxy for direct damage response signaling[72,73].

1.2.2 ATR-mediated replication stress response as cancer vulnerability

Replication stress is the primary source of ATR-activating ssDNA. The primary source of ssDNA, and therefore ATR activation, is replication stress. Replication stress occurs when DNA synthesis is hindered or slowed, leading to stalled replication forks[59,71,77]. Possible physical barriers that hinder the replisome from DNA synthesis include secondary DNA structures such as hairpins, G-quadruplexes, or R-loops[78] (**Figure 7**). Moreover, the replisome may occasionally collide with the transcription machinery, particularly in highly transcribed DNA regions[79]. Replication is further delayed by highly repetitive DNA sequences or misincorporated ribonucleotides and DNA lesions such as DNA-crosslinks, gaps, or misincorporated nucleotides[78]. In the presence of such hindrances, DNA polymerase is slowed while the replicative helicase, which proceeds the polymerase, continues unwinding the DNA[80]. This functional uncoupling of DNA synthesis and unwinding leads to excess ssDNA that activates an ATR-mediated response[80].

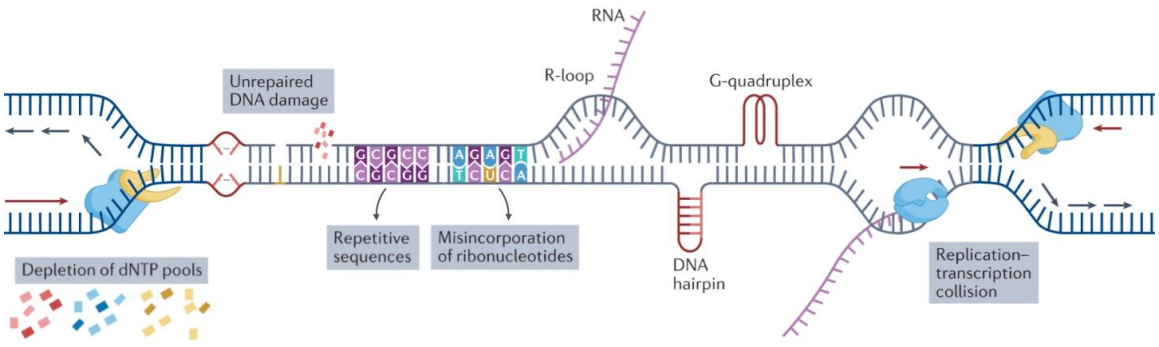

Figure 7. Different sources of cellular replication stress. Stalled replication forks occur in the presence of physical barriers such as DNA lesions or secondary DNA structures. Additional sources of replication stress include misincorporated ribonucleotides or reduced nucleotide (dNTP) pools. Modified from da Costa et al. (2023)[78]. Changes included re-arranging the depicted DNA lesions and the removal of origin firing as a source of replication stress. Modified with BioRender.com.

ATR regulates the cell cycle and DNA repair in response to replication stress. The activation of ATR in the presence of ssDNA is a multi-step process. Typically, it starts with the coating of ssDNA with replication protein A (RPA), which enables the recruitment of ATR to the site of DNA damage by another protein, ATRIP[60,71] (**Figure 8**). ATR activation further requires binding to TOPBP1 and the recruitment of a multi-protein complex consisting of the proteins RAD9, HUS1, and RAD1[60,81,82]. Once activated, ATR phosphorylates multiple downstream effectors that initiate several signaling cascades, most importantly checkpoint regulation and the initiation of repair mechanisms as described above.

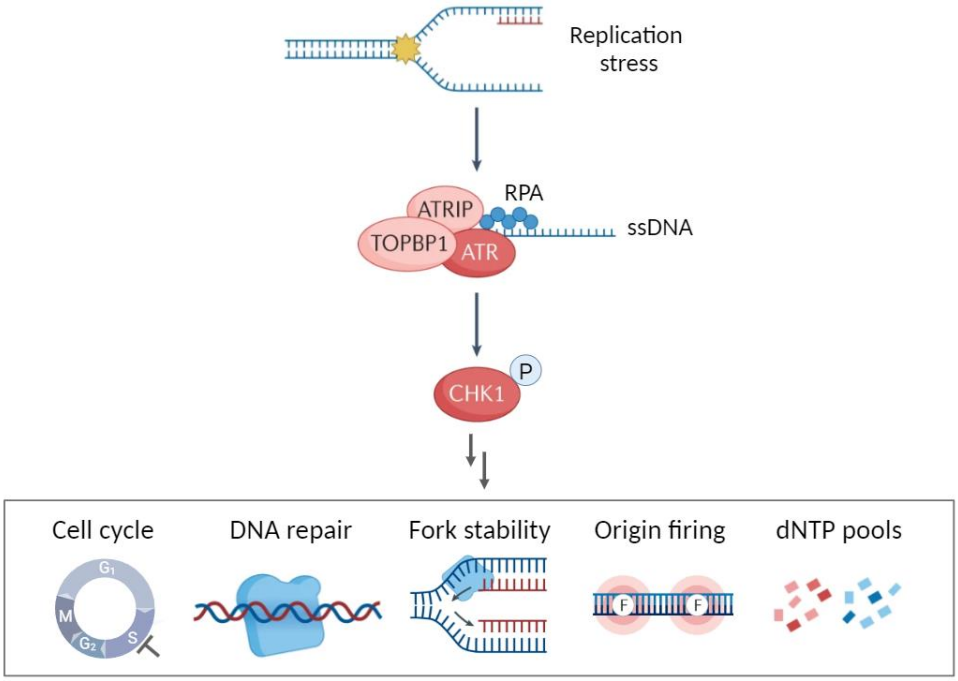

Figure 8. ATR activation upon replication stress and possible consequences. Single-stranded DNA (ssDNA) is formed upon replication stress, triggering ATR activation through several proteins and complexes. ATR phosphorylates CHEK1, initiating pathways involved in cell cycle regulation and DNA-repair. Also, ATR signaling stabilizes replication forks, regulates the firing of origins, and balances nucleotide (dNTP) pools. Modified from da Costa et al. (2023)[78]. Changes included the re-arrangement of individual elements and an overall reduction in complexity. Newly added were the schematic representation of cell cycle regulation and the encircled 'P' at CHEK1, indicating phosphorylation. Modified with BioRender.com.

Non-canonical roles of ATR signaling preserve genome integrity. ATR triggers additional mechanisms to tolerate replication stress and prevent further DNA lesions or breakage (**Figure 8**). For instance, inactive CDK1 and CDK2 stabilize replication forks and suppress origin firing, facilitating DNA repair processes[79]. Moreover, ATR signaling ensures sufficiently balanced dNTP levels throughout the cell cycle, which are required for DNA synthesis and repair. Specifically, ATR signaling inhibits ribonucleotide reductases (RRM1, RRM2) and deoxycytidine kinase (DCK), two enzymes crucial in nucleotide *de novo* synthesis and salvage, respectively[29,83,84]. Finally, ATR signaling enables DNA damage tolerance mechanisms that allow the cell to continue replication in the presence of unrepaired DNA. In so-called translesion synthesis, specialized

polymerases can bypass DNA lesions and continue DNA synthesis, leaving the lesion behind for later repair; this process is rather error-prone[79]. Alternatively, replication may continue by switching to the newly synthesized sister chromatid as a template, a more complex yet less error-prone bypass mechanism[79].

Targeting ATR signaling displays a potential anticancer strategy. The malfunction of replication stress response can lead to cell death, triggered by several mechanisms. First, stalled replication forks are prone to breakage, promoting the loss of genome integrity and the accumulation of potentially lethal DSBs. Moreover, detachment of the replisome machinery from the to-be-replicated DNA strand (so-called replication fork collapse) may lead to incomplete replication and fatal loss in genome integrity or pre-mature entry of damaged DNA into the G_2-phase, causing a mitotic catastrophe[78].

Cancer cells are particularly vulnerable to ATR-mediated replication stress due to their high proliferation rates, rendering ATR inhibition a viable anticancer strategy[85]. Many cancers, including PDAC, are driven by oncogenes like KRAS, leading to increased replication initiation and a higher risk of replication defects[85]. The chronic proliferation exhausts dNTP pools, further inhibiting DNA synthesis and slowing replication, thereby promoting replication-induced DNA damage[86]. In order to survive this extensive load of replication stress, cancer cells require functioning ATR signaling. Moreover, frequent mutations in tumor suppressor genes, such as p53 and CDKN2A, cause a loss in G_1-checkpoint control in PDAC cells, further increasing the dependency on functional cell cycle regulation such as by ATR (Chapter 1.1.3).

1.2.3 The rise of ATR kinase inhibitors in the clinics

Three ATR inhibitors are currently clinically investigated in PDAC. With ATR kinase being the essential regulator of cellular replication stress response, it displays a valuable target for anticancer therapy. Although no clinical approval of any ATR inhibitor (ATRi) exists, the rising number of trials initiated for various cancers over the past decade demonstrates their growing clinical significance (**Figure 9**). Eight ATRis are undergoing clinical investigation for multiple malignancies, either in monotherapy or combined with classical chemotherapy, targeted drugs, or radiotherapy (according to *clinicaltrials.gov* as of May 2024). Three of these ATRis are currently being evaluated for pancreatic cancer: Ceralasertib, Berzosertib, and Elimusertib (**Table 1**). With over 20 ongoing clinical trials across various malignancies, including one phase III study, Ceralasertib (AZD-6738)[87] is the most extensively investigated and clinically advanced ATRis. A phase III study currently assesses its efficacy combined with Durvalumab, an immunotherapeutic antibody, in advanced non-small cell lung cancer (NSCLC; *clinicaltrials.gov* identifier NCT05450692), based on the promising outcomes of the preceding phase II study[88]. In PDAC, a phase II trial evaluating Ceralasertib in combination with Durvalumab or PARP1 inhibitor Olaparib

has been initiated (NCT03682289). Also, a phase I trial investigating its combination with GEM will include PDAC patients in its dose-expansion phase (NCT03669601). Another frequently tested ATRi is Berzosertib (also known as VE-822, VX-970, or M6620), which exhibited favorable tolerability alone and in combination with Carboplatin or GEM in patients with advanced solid tumors[89,90]. Its combination with the topoisomerase inhibitor Irinotecan is undergoing safety evaluation in various solid tumors, including PDAC (phase I, NCT04616534). Finally, the third ATRi under clinical evaluation for PDAC is Elimusertib (BAY-1895344)[91]. Its safety profile, combined with GEM or topoisomerase inhibition, is currently being assessed in clinical phase I trials involving PDAC patients (NCT04616534, NCT04514497). Apart from this, several early-phase trials are presently testing Elimusertib in combination with other chemotherapy, targeted therapy, or radiation in multiple other cancer entities (based on *clinicaltrials.gov* as of May 2024; **Table 1**).

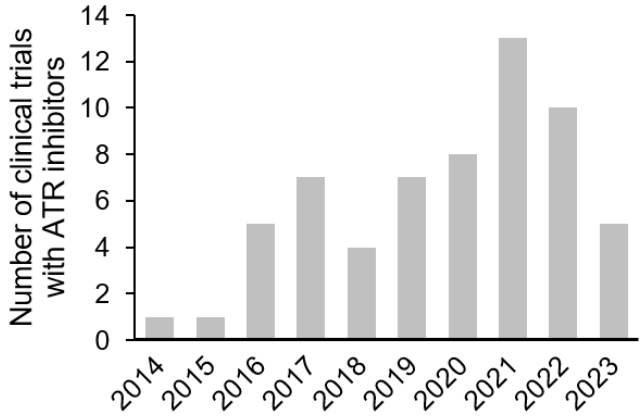

Figure 9. Number of clinical trials with ATR inhibitors initiated per year between 2014 and 2023 according to *clinicaltrials.gov* (as of May 2024). Only completed, active, or recruiting studies were considered.

Additional ATR inhibitors have entered the clinical stage only recently. Over the past five years, several novel ATRis have entered the clinical stage, although no trials have been initiated for pancreatic cancer yet. For instance, Tuvusertib (M1774), developed by Merck KGaA, has recently demonstrated a manageable safety profile across patients with advanced solid tumors in its ongoing first-in-human trial (NCT04170153)[92]. Only since 2023, seven additional trials (up to phase II) have been initiated to evaluate its efficacy as a single agent and in combination therapies across various cancers (based on *clinicaltrials.gov* as of May 2024; **Table 1**). Another promising candidate is Camonsertib (RP-3500), developed by Repare Therapeutics Inc., which is currently undergoing investigation in five early-phase studies based on its preclinical efficacy on tumor growth inhibition when combined with PARP1 inhibitors Olaparib or Niraparib (NCT04972110 and NCT04497116)[93]. Another novel ATRi is ART0380, developed by Artios Pharma Ltd. ART0380 is being evaluated in monotherapy and combination with Gemcitabine in advanced cancers (NCT04657068), and preliminary data suggests encouraging safety and clinical efficacy of this

regimen[94]. Most recently, ATG-018, developed by Antengene Corp., entered clinical trials after demonstrating preclinical efficacy in various cancer models[95]. A phase I trial is currently recruiting patients to evaluate the safety and efficacy of this novel ATRi in advanced solid tumors and hematological malignancies (NCT05338346).

In summary, ATR kinase signaling is critical in maintaining genomic stability and cell proliferation in response to replication stress, rendering its inhibition a promising anticancer strategy. The increasing frequency of novel ATRis entering clinical investigations mirrors the advancement of these agents toward clinically safe and effective therapeutics. The fact that only three of the eight clinical ATRis are currently being investigated in PDAC suggests considerable potential for the other inhibitors to be evaluated in this disease.

Table 1. Clinical ATR inhibitors and their number of clinical trials per phase. If applicable, additional information on trials conducted in pancreatic cancer patients is given. Data according to *clinicaltrials.gov* (as of May 2024). Only completed, active, or recruiting studies were considered.

ATR inhibitor	Number of clinical trials in phase				Clinical trial(s) in pancreatic cancer
	I	I/II	II	III	
Ceralasertib	5	2	13	1	Combination with Olaparib or Durvalumab (phase II, NCT03682289) Combination with Gemcitabine (phase I, NCT03669601; expansion phase will include PDAC patients)
Berzosertib	7	5	6	-	Combination with topoisomerase inhibitors (phase I, NCT04616534)
Elimusertib	5	2	-	-	Combination with topoisomerase inhibitors (phase I, NCT04514497) or Gemcitabine (phase I, NCT04616534)
Tuvusertib	5	1	2	-	-
Camonsertib	1	4	-	-	-
Gartisertib	1	-	-	-	-
ART0380	-	1	1	-	-
ATG-018	1	-	-	-	-

1.3 The use of proteomics to study a drug's mode of action

1.3.1 Knowledge of drug mechanisms aids therapeutic development

Mechanistic studies using proteomics aid the pre-clinical drug development process. Most drugs elicit their effects on biological systems through direct or indirect interaction with proteins, the key biochemically active units of cells[96]. Mass spectrometry (MS)-based proteomics is a technique for the large-scale study of proteins in biological samples, providing insights into protein identities, abundances, and modifications within a proteome[97]. MS-based proteomics can be employed in two ways to study the mode of action of a bioactive compound, as proposed by Meissner et al. (2023)[98]. First, the direct drug-target-interaction and the consequence on the target itself can be assessed by so-called chemical proteomics. This includes the affinity by which a drug binds its target, as well as the drug's effect on the target's biological activity, stability, and folding[98] (**Figure 10a**). Second, the global consequences of drug-target binding on other proteins in a cellular system can be assessed with global proteomics of drug-perturbed cells. Thereby, proteomics may reveal drug-induced changes in protein abundance, localization, post-translational modification, and interactions with other proteins or biomolecules within a cell[98] (**Figure 10b**).

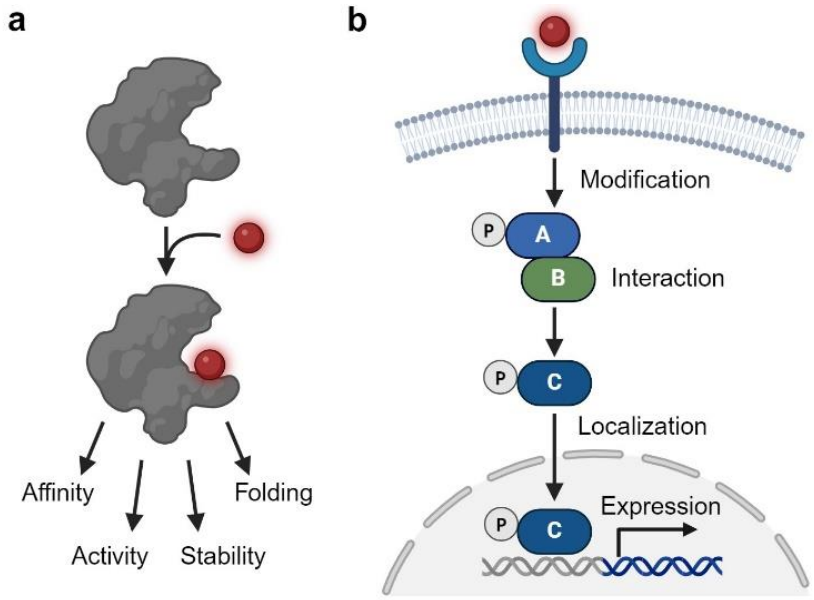

Figure 10. Two principles by which a drug's mechanism can be studied with MS-based proteomics. a) The direct interaction of a protein (grey) and a drug (red) can be characterized using chemical proteomics by measuring binding affinity and protein activity, stability, and folding changes. **b)** The global consequences of drug-target binding on protein modifications, interactions, localization, and abundance in a cell can be measured using global MS-based proteomics. Inspired by Meissner et al. (2022)[98].

An extensive knowledge of a drug's mode of action is crucial in developing new clinical therapies. The drug discovery and development process is typically initiated by either a target-based or a phenotype-based approach[99,100] (**Figure 11**). In the target-based approach, a compound library is

screened for interactions with a pre-defined target protein of interest. This target requires extensive validation prior to the screening campaign. In contrast, in the phenotypic approach, a drug library is screened for phenotypic efficacy in a pre-defined biological disease model. Such a target-agnostic screening campaign relies on the subsequent target identification and validation of the potential hit compounds[99]. Irrespective of the initial screening strategy, selected lead compounds are subjected to chemical optimization to increase their potency, selectivity, pharmacodynamics, and pharmacokinetics profiles. They are extensively tested in pre-clinical *in vivo* models before entering the clinical stage[99].

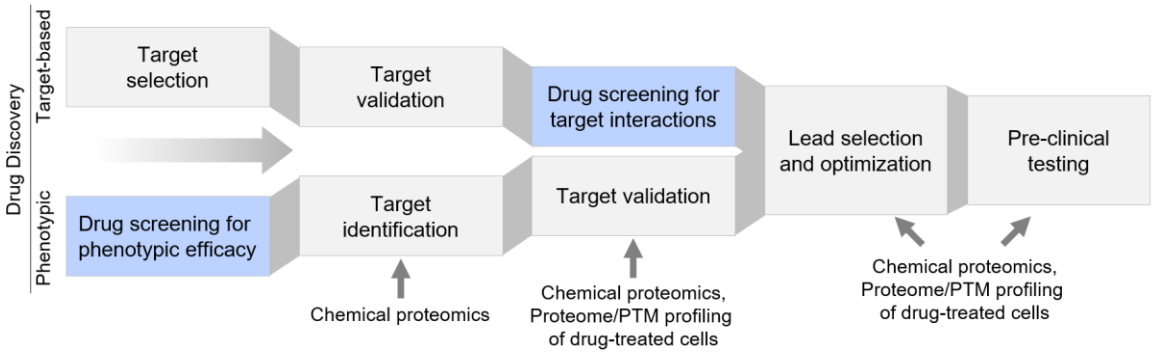

Figure 11. Flow-chart illustrating two different drug discovery strategies: Target-based and phenotype-based. The drug screening step is part of both strategies and is highlighted in blue. Additional text and arrows indicate which steps benefit from proteomics-aided mechanistic studies of a drug's mechanism by chemical proteomics or proteome profiling of drug-perturbed cells. PTM: Posttranslational modification. Inspired by Schirle et al. (2012)[99] and KhalKahl et al. (2019)[100].

Understanding the mode of action of potential hit, lead, or clinical candidates is highly desirable throughout the drug discovery and development process. For instance, chemical proteomics may be used at early stages for target identification and validation on a proteome-wide scale, explaining the drug's efficacy observed in phenotypic screening[99,100]. Thereby, previously unanticipated interactors of a compound, so-called 'off-targets', may be revealed. Although such polypharmacology may enhance drug efficacy, it may also contribute to adverse side-effects when used in organisms[101]. Eventually, such knowledge of a compound's target spectrum may rationalize the selection of potential hit candidates and guide chemical optimization of lead compounds towards improved safety profiles *in vivo*[99].

In addition, studying drug-induced changes on the proteome provides more evidence of drug-target-interactions and further helps to interpret the biological significance of target inhibition. For instance, the analysis of posttranslational modifications (PTMs), such as phosphorylation, may verify cellular target engagement of kinase inhibitors by changes in downstream signal transduction and other perturbed pathways[102]. Additionally, proteomic analysis of drug-treated cells may reveal pharmacodynamics biomarkers that correspond to the bioactivity of a drug and, thus its therapeutic efficacy[99]. Early knowledge of such biomarkers during pre-clinical investigation may allow their

incorporation in clinical trials, e.g., for patient stratification or to monitor cellular target engagement[103].

Beyond the benefits of proteomics-aided mechanistic studies on pre-clinical compounds, the retrospective analysis of clinically advanced or approved drugs offers several advantages. For instance, unbiased target deconvolution of these drugs can reveal novel drug-target interactions, which can rationalize their repurposing for different indications than initially intended[104]. Drug repurposing offers the advantage of accelerated clinical entry or re-approval due to the established toxicity profiles from previous clinical trials[105]. Hence, this approach is particularly beneficial for hard-to-treat cancers, such as PDAC, which urgently require new therapeutic options. Furthermore, analyzing a drug's mode of action alongside existing clinical data can elucidate potential mechanisms and biomarkers of resistance and retrospectively explain why certain treatments resulted in only partial responses or unexpected toxicity in patients[99]. This mechanistic understanding can rationalize the use of combination therapies or guide patient stratification in future clinical studies, thereby improving therapeutic outcomes and addressing clinical needs.

1.3.2 Chemoproteomic target deconvolution by affinity-based profiling

Competition assay for target validation in affinity-based target profiling. Chemical proteomics enables the detection and characterization of drug-target interactions on a proteome-wide scale. It covers an extensive toolbox of strategies, some of which utilize chemical tools or probes[98]. Chemical probes are typically created from a drug of interest and used as bait to capture target proteins from intact cells or cell extracts[106]. Therefore, the probes can be designed to enrich targets based on potent noncovalent interactions (affinity-based) or covalent interactions (activity-based probes)[106]. In contrast, probe-independent techniques exploit biophysical and biochemical principles to infer drug-target binding. For instance, such methods measure drug-induced changes in the thermal stability, rate of oxidation, or susceptibility to enzymatic proteolysis of proteins[98,106].

The classical affinity-based approach relies on a compound-functionalized matrix produced by chemically immobilizing a drug of interest (either the unmodified compound or a linkable analog) onto beads[107] (**Figure 12**). This compound-coupled matrix is then incubated with cell lysate to purify proteins based on their affinity to the immobilized drug. After several washing steps, only strong interactors are retained on the matrix, which are then digested and analyzed by liquid chromatography-tandem mass spectrometry (LC-MS/MS)[107,108].

During the enrichment step, proteins can bind non-specifically to the resin or the linker used for compound immobilization and may be falsely interpreted as true targets[109]. One strategy to increase confidence in identified targets is using an affinity matrix made of an inactive analog, which allows binders to be classified as unspecific. However, this approach typically involves extensive organic

synthesis and requires complete inactivity of the analog not to misclassify potential targets[109]. A conceptually simpler and more feasible alternative is a competition assay, in which the drug of interest is co-incubated with the affinity matrix in the lysate during the enrichment step[110] (**Figure 12**). This allows the unmodified drug in solution to compete for target binding with the immobilized drug on the beads. Proteins bound by the unmodified drug are occupied and thus not eligible for affinity purification by the matrix, while non-competed proteins can still be enriched[108]. As a result, true targets display decreased quantities in the LC-MS/MS readout compared to a vehicle, while the quantity of non-specific binders remains unchanged[108].

Competition with a series of drug concentrations rather than only a single dose generates dose-response relationships for each quantified drug-protein interaction. Subsequent curve fitting allows the calculation of half-maximum effect concentrations (EC_{50}) and the approximation of apparent dissociation constants (K_D^{app})[110,111]. These parameters describe the potency and binding affinity of drug-target interactions and are essential pharmacological indicators of drug effectiveness[112,113].

Kinobeads is a valuable technology for profiling kinase inhibitors. Immobilizing a small molecule for chemical proteomics requires a detailed understanding of its structure-affinity relationship to ensure that it retains its biological activity, and this process may not be feasible for all compounds. Kinobeads provide a highly valuable tool for chemoproteomic target deconvolution of kinase inhibitors specifically[110]. This technology uses beads coated with broad-spectrum kinase inhibitors to capture kinases from complex protein mixtures such as cell lysates[110]. Kinobeads have been employed as affinity matrices in competition assays for target deconvolution of various kinase inhibitors, which revealed previously unknown targets and mechanisms of these compounds. For instance, Kinobeads have identified novel targets of ABL kinase inhibitors and contributed to understanding their molecular mechanism in chronic myelogenous leukemia[110]. Also, retrospective target deconvolution of > 200 clinical kinase inhibitors[104] and > 1,000 pre-clinical tool compounds[114] with Kinobeads has revealed valuable insights on novel (off-)targets, molecular mechanisms, and potential indications of these bioactive compounds. Over the years, Kinobeads have undergone several optimizations to increase the coverage of kinases within the enriched proteome[115,116]. The latest generation of Kinobeads has been developed to enrich not only the ~300 kinases targeted by earlier versions but also members of the PI3K and PIKK families, thereby significantly extending its utility in target deconvolution of kinase inhibitors[116].

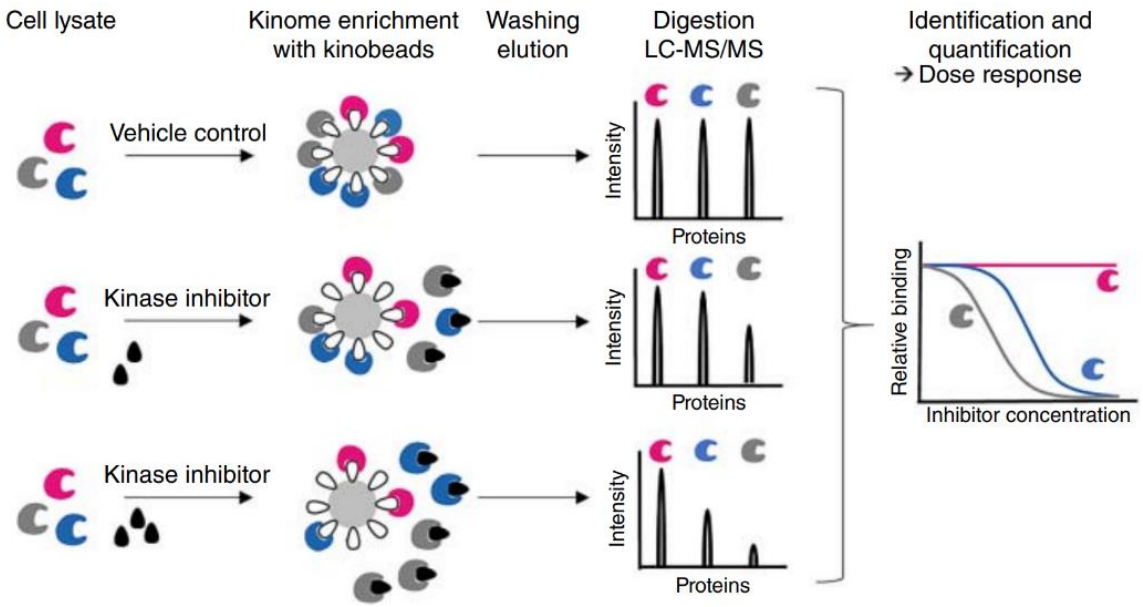

Figure 12. Competition-based pulldown workflow using Kinobeads as an affinity matrix. Cell lysate is incubated with Kinobeads and increasing concentrations of inhibitor. Proteins enriched by the Kinobeads are then digested and analyzed by LC-MS/MS. The resulting dose-response curves allow target identification and quantification of binding affinities. Figure from Reinecke et al. (2019)[117].

1.3.3 Phosphoproteomics to decipher a drug's effect on cellular signaling

Phosphorylation: Definition and significance in disease. Phosphorylation is a post-translational modification (PTM) catalyzed by kinases that regulates protein function, conformation, stability, subcellular localization, and interaction with other proteins[118]. This PTM controls various cellular processes such as cell proliferation, differentiation, metabolism, and apoptosis[119-121]. One example is the cellular DNA damage response reviewed above, in which ATR kinase mediates downstream signal transduction through the phosphorylation of proteins, mostly other kinases (Chapter 1.2.2). Protein phosphorylation occurs predominantly on serine (~85-90%), threonine (~10-15%), and tyrosine (< 1%) residues, and its reversal is catalyzed by phosphatases[120,122,123]. The balance between kinase and phosphatase activity is essential for maintaining normal cellular physiology, and its disruption can lead to disease[119]. In cancer, mutations often cause aberrant kinase activation and downstream signaling, promoting sustained cell division, angiogenesis, and resistance to apoptosis[124]. Targeted anti-cancer therapies are typically designed to inhibit the catalytic function of kinases, i.e., phosphorylation. Therefore, the global analysis of the drug-perturbed phosphoproteome can contribute to the understanding of molecular consequences of drug action in a biological context.

Experimental considerations for MS-based phosphoproteomics. Several techniques are available to measure protein phosphorylation, including immunohistochemistry, protein microarrays, and adaptations of western blotting. However, these methods depend on specific antibodies and offer only limited throughput[120,121]. In contrast, MS-based phosphoproteomics

enables the identification and quantification of over 10,000 phosphorylation sites in high throughput and without prior knowledge[120]. Moreover, MS-based phosphoproteomics provides high specificity through direct sequencing and localization of phosphorylation sites, enabling detailed studies of signaling pathways, disease mechanisms, and drug effects[120].

In bottom-up proteomics, samples are typically generated by the lysis of cells or tissue, followed by proteolytic digestion of proteins and sample clean-up through desalting. Additionally, phosphoproteomic samples require the enrichment of phosphorylated peptides prior to LC-MS/MS analysis due to the low stoichiometry of this PTM in cells[120]. This can be achieved by immobilized metal affinity chromatography, which utilizes the high affinity between negatively charged phosphate groups and positively charged metal ions, such as Fe^{3+}, on a resin)[120,125]. Enriched phosphorylated peptides can be eluted by a change in pH that disrupts the peptide-resin interaction or a phosphate-containing buffer that displaces bound peptides from the resin[126].

Different peptide quantification strategies are used in MS-based proteomics. While phosphoproteomic samples can be analyzed directly, labeling peptides for quantification with isobaric reagents, such as Tandem Mass Tags (TMT)[127], provides several benefits. With TMT reagents, peptides from different samples are tagged with isobaric labels that are indistinguishable in mass but release reporter ions of different masses upon fractionation in tandem MS (from MS2 or MS3 spectra)[128]. This enables the relative quantification of peptides from different samples (e.g., treatment conditions) in a single LC-MS/MS run. TMT-multiplexing enhances the throughput of proteomic studies and reduces variability in sample handling, as samples are typically labeled and pooled early during the sample preparation workflow[128]. Current TMT reagents allow multiplexing of up to 18 different conditions[129]. Moreover, TMT labeling reduces missing data across conditions within a single batch, which remains a common issue in label-free quantification[130]. While missing values are still a challenge in multi-batch TMT labeling experiments, elaborate bioinformatics tools such as SIMSI-Transfer that minimize this issue[131].

Experimental strategies to study drug-induced changes in cellular signaling. To study the impact of drugs on cellular signaling, cells can be treated with a drug of interest and the changes in protein phosphorylation can be measured by LC-MS/MS. Simple experimental setups involve single-dose treatments at specific incubation times and analyzing fold changes in PTM levels using t-test statistics (**Figure 13a**). A more elaborate alternative to this is a time-course experiment, in which cells are treated with a fixed drug concentration over multiple time points (**Figure 13b**). While time-series proteomic data can be challenging to analyze due to the dynamic nature of protein phosphorylation, it offers a more comprehensive view of a drug's mode of action by capturing temporal signaling changes[132,133]. Finally, and more recently, a dose-resolved drug treatment design with phosphoproteomic readout has been introduced, termed decryptM[102], in which cells are treated with increasing concentrations of a drug (**Figure 13c**). The resulting dose-dependent data is fitted

to a four-parameter regression model and classified into up- or down-regulated curves (e.g., using CurveCurator[134]). This analysis allows the determination of drug potencies for each phosphorylation site, in addition to their maximum regulation at high drug concentrations[102], providing valuable insights into a drug's mode of action. For instance, Zecha et al. (2023) employed decryptM on 31 anti-cancer drugs, including 10 kinase inhibitors, and successfully linked drug concentrations to direct target and pathway engagement, as well as potential off-target toxicity[102]. Moreover, Chang et al. (2024) utilized decryptM to provide novel mechanistic insights 21 lysine deacetylase inhibitors, revealing previously unknown substrate potencies on the phosphoproteome and acetylome levels[135]. These studies exemplify the use of decryptM on targeted inhibitors and illustrate the potential of dose-resolved PTM proteomics in providing detailed insights into drug mechanisms.

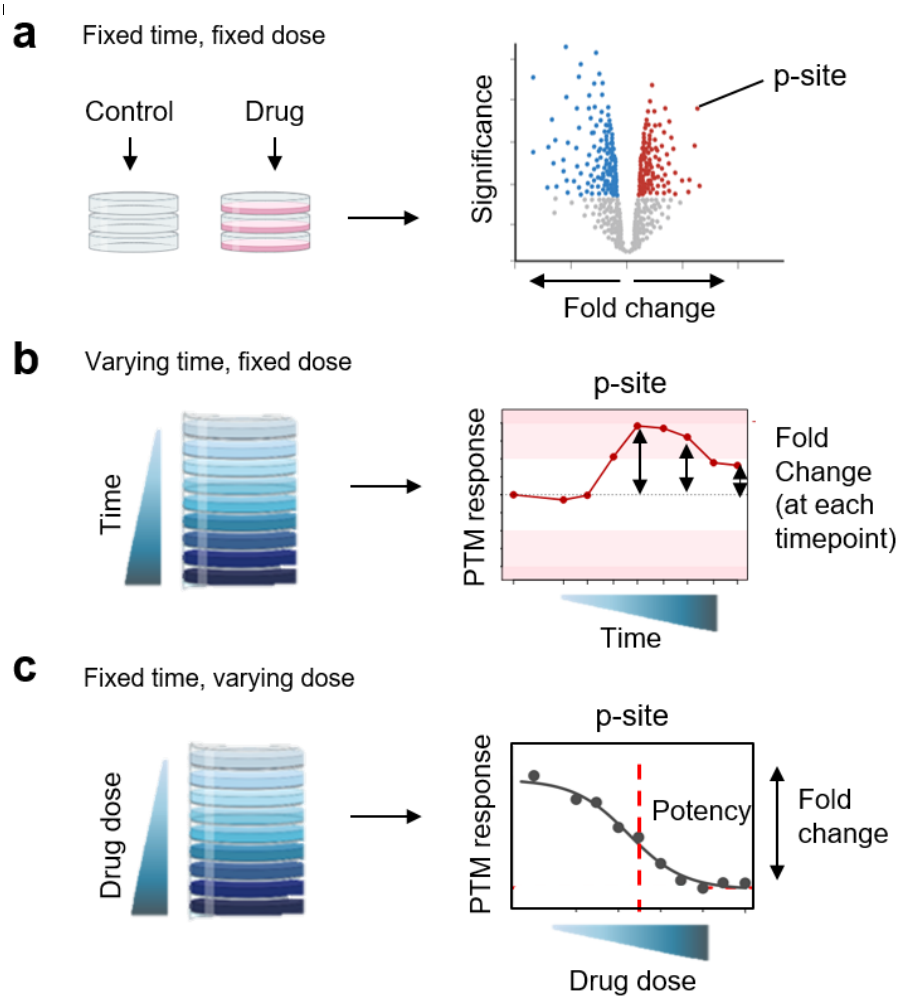

Figure 13. Different strategies for drug-treatment experiments with (phospho-)proteomic readout. a) Conventional drug-perturbation experiments apply a single drug dose and a fixed incubation time. Comparison to vehicle is performed by t-test statistical analysis of replicates. **b)** In time-series experiments, a fixed dose of a drug is incubated in cells for several consecutive time points. Typically, no regression can be made of the data given the complex PTM regulation over time. **c)** In decryptM, cells are treated with increasing doses of a drug for a fixed incubation time. Fitted dose-response curves provide information on drug potency. Created with BioRender.com.

1.4 Aim and Outline

PDAC is a lethal malignancy in desperate need for therapeutic advancements. Despite decades of chemotherapy being the standard of care, resistance to commonly used drugs such as GEM is frequently observed. One potential way to overcome this resistance is the combination of GEM with targeted therapies, such as kinase inhibitors. Currently, the clinical options for targeted therapy in PDAC are limited. However, frequently deregulated kinase signaling and pathway dependencies create vulnerabilities in PDAC that can be exploited by targeted therapies. One such vulnerability is the ATR-mediated replication stress response.

A thorough understanding of the molecular mode of action of drugs can significantly enhance the success of drug discovery and development. Also, the retrospective analysis of clinically advanced drugs may provide the potential for drug repurposing and offer a more rational basis for clinical re-use. Mass spectrometry-based proteomics is a powerful technique to characterize a drug's mechanism by systematically analyzing its interactions with targets and the indirect effects in a biological system.

This study aimed to mechanistically characterize synergistic combination of GEM and targeted therapies in PDAC using mass spectrometry-based proteomics. Thereby, the ultimate goal was to provide a resource of potential targeted therapies along with a mechanistic rationale, contributing to improved therapeutic strategies for PDAC. To identify effective synergistic interactions, a large-scale phenotypic profiling was initially conducted on PDAC cells (Chapter 3.1). Based on the results of this screen, mechanistic studies were performed on the combination of ATR kinase inhibitors and GEM using proteomics. First, the target landscape of seven ATR kinase inhibitors was characterized using chemical proteomics and the Kinobeads technology (Chapter 3.2). Then, the effects of GEM treatment and ATR inhibition on cellular signaling were analyzed through phosphoproteomics. Both time- and dose-dependent experimental designs were applied to gain deep mechanistic insights into the actions of both drugs individually and in combination (Chapter 3.3).

2 General Methods

2.1 Phenotypic drug screening and validation assays

2.1.1 Cell lines and drugs

Cell lines were purchased from ATCC (MiaPaCa-2, AsPC-1, PSN-1, BxPC-3, PANC-1), CLS (FAMPAC, Capan-1), DSMZ (PaTu-8988-T, Dan-G) or creative bioarray (HuP-T4). Cell lines Suit2-07, Colo-357, and HPDE were generously provided by Professor Kirsten Lauber (Ludwig-Maximilians-Universität, Germany). Cell lines were authenticated using STR fingerprinting (Suit2-07) or SNP profiling (all others) as provided by Multiplexion GmbH (Heidelberg, Germany). Cells were cultured at 37 °C and 5% CO_2 and regularly checked to be free of mycoplasma contamination (for detailed information on cell lines and culture media, see **Appendix 2**). All cell culture media and supplements were purchased from PAN biotech, except for bovine pituitary extract (Gibco #13028-014), keratinocyte-free medium (Gibco #17005042), and human epidermal growth factor (R&D Systems #236-EG). For large-scale drug screening, cell culture media were supplemented with penicillin and streptavidin (100 U/ml penicillin and 100 µg/ml streptomycin, Gibco #15140-122).

Library compounds were purchased from different vendors, including Selleckchem (Absource Diagnostics GmbH, Germany) and MedChemExpress (Hölzel Diagnostika Handels GmbH, Germany; **Appendix 3**). Additional ATR inhibitors were purchased from Selleckchen (Ceralasertib, #S7693; Berzosertib, #S7102; Gartisertib, #S9639; VE-821, #S8007; AZ-20, #S7050; ETP-46464, #S8050). Drug stock solutions were prepared at 10 mM in dimethyl sulfoxide (DMSO), except Perifosine and AZD-0156, dissolved in ethanol and Copanlisib, dissolved in 0.1 M hydrochloride. The identity of all compounds was confirmed by measuring their mass using LC-MS/MS at high resolution.

2.1.2 Drug combination screening

Before drug screening, all compounds were tested for media solubility with their final dilutions using a NEPHELOstar microplate reader (BMG LABTECH GmbH), and a counter screen was performed to detect false active compounds using the ATPlite 1step Luminescence Assay System. Drug dilution series ranging from 10 mM to 0.0002 mM in DMSO (1:3 dilution, 11 steps) were prepared using a Janus Gripper and a 384-channel Modular Dispense Technology dispensing head (revvity, previously Perkin Elmer, Waltham, MA, USA). Subsequently, small volumes were transferred to 384-well intermediate plates (Greiner Bio-One GmbH, Germany). GEM stock

solutions in DSMO (1 mM, 3 mM, 10 mM, 30 mM) were prepared manually. For drug screening, 1,000 to 5,000 cells were seeded into 384-well plates (CulturPlate™, Perkin Elmer, MA, USA) using a Multidrop™ Combi Reagent Dispenser (Thermo Fisher Scientific, Waltham, MA, USA) in 50 µl medium 24 h before drug treatment (seeding densities see **Appendix 2**). Compound intermediate plates were filled with water (1:45.5 dilution) using a Multidrop™ Combi Reagent Dispenser. Afterward, 2.5 µl of library drug serial dilutions were added to cells using a Janus Gripper, followed by the addition of either 2.5 µl vehicle (for single-agent treatment) or 2.5 µl of GEM (for drug combination treatments) using a Multidrop™ Combi Reagent Dispenser. The final concentration of DMSO in each well was 0.2%. The doses of GEM for combination screening were selected based on the cell lines' sensitivity towards GEM monotherapy (1 nM and 3 nM GEM for cell lines FAMPAC, Dan-G, Capan-1, Colo-357, PSN-1, HPDE, HuP-T4, BxPC-3, Suit2-07; 10 nM and 30 nM GEM for cell lines PaTu-8988-T, AsPC-1, PANC-1, MiaPaCa-2). Cells were incubated at 37 °C and 5% CO_2 for 72 h. Then, cell viability was measured using the ATPlite 1step Luminescence Assay System according to the manufacturer's protocol (Perkin Elmer, MA, USA) by detection of luminescence signals using an Envision Xcite 2104 plate reader with ultrasensitive luminescence detector (revvity, previously Perkin Elmer, MA, USA). Cells treated with vehicle were negative controls (eight wells per plate), and cells treated with 5 µM staurosporine were positive controls (sixteen wells per plate). Incubation effects were controlled manually based on control plates not containing any drug. The drug screen data quality was assessed by calculating plate-wise Z-prime[136] from positive and negative controls using the following formula (1), where SD is the standard deviation.

$$\text{Z-prime} = 1 - \frac{3SD_{pos} + 3SD_{neg}}{|mean_{pos} + mean_{neg}|} \quad (1)$$

All data was normalized to vehicle (plate-wise mean negative controls), and dose-response curves were fitted to a four-parameter log-logistic model. Additionally, area-under-curve (AUC, ranging between 0-100%) was calculated as described previously[133]. Drugs were considered efficacious as a single agent if AUC < 80%, $pEC_{50} > 6$, and $R^2 > 0.8$.

2.1.3 Drug synergy analysis

Synergistic effects were assessed by applying the concept of Bliss Independence[137]. In essence, using this model, a hypothetical dose-response curve describing the expected response when no combination effect occurs (i.e., additive response). Therefore, at each dose, the hypothetical (additive) combination response ($E_{A+B,Bliss}$) was calculated using formula (2), where $E_{A,experimental}$ and $E_{B,experimental}$ are the cell viability upon treatment with drugs A and B in monotherapy, respectively.

$$E_{A+B,Bliss} = E_{A,experimental} \cdot E_{A,experimental} \quad (2)$$

Combination effects were analyzed by comparing experimental and hypothetical data dose-response curves and calculating AUC shifts (AUC_{Δ} = $AUC_{hypothetical}$-$AUC_{experimental}$). Drug combinations were defined as synergistic if the summed AUC_{Δ} of the two GEM combinations (ΣAUC_{Δ}) >10% and if at least one of the two GEM combinations resulted in AUC < 80% and pEC_{50} > 6. Only combinations with R^2 > 0.8 were considered in the synergy analysis.

2.1.4 Cell proliferation and apoptosis assays

Cell proliferation and apoptosis assays, AsPC-1 cells were seeded at 5,000 cells per well into 96-well flat bottom plates (Eppendorf) and allowed to attach overnight. For proliferation assays, cells were treated either ATRi only (8 doses, 3 nM to 10,000 nM final), GEM only (8 doses, 1 nM to 3,000 nM final), titrated GEM combined with three sub-EC_{50} doses of ATRi, or vehicle (0.2% DMSO final concentration; **Table 2**). Cells were incubated at 37 °C and 5% CO_2 for 72 h, and cell confluence was read out using an Incucyte live-cell imaging platform (Sartorius; 10x magnification, four wells per well). Cell confluence was first normalized to the initial confluence and then to the vehicle not containing any drug (mean of n = 5). Dose-response curves were fitted with a four-parametric log model using the R package *drc*[138]. Shifts in curve EC_{50} between GEM monotherapy and combinations were determined to assess synergy. Experiments were performed in triplicates, and data was plotted as mean ± standard deviation. For apoptosis assays, seeded AsPC-1 cells were treated either with GEM only (1,000 nM), ATRi only (Elimusertib: 30 nM, Gartisertib: 30 nM, Berzosertib: 300 nM, Ceralasertib: 1,000 nM), a combination of GEM and ATRi (at the single drug doses), or vehicle (0.2% DMSO final concentration). Annexin V Red dye (Sartorius #4641) staining was performed on cells to monitor early apoptosis using half of the reagent recommended by the vendor. Using the Incucyte, images were taken every 8 h for 120 h. The red channel integrated intensity (RCU x μm^2) divided by cell confluence was used as an assay readout to account for treatment effects on cell growth.

Table 2. Three sub-EC_{50} concentrations (in nM) of ATRi used in combination experiments with GEM.

	Elimusertib	**Gartisertib**	**Berzosertib**	**Ceralasertib**	**AZ-20**	**VE-821**	**ETP-46464**
Dose 1 [nM]	3	3	30	100	10	300	30
Dose 2 [nM]	10	10	100	300	30	1000	100
Dose 3 [nM]	30	30	300	1000	300	3000	300

2.2 Chemoproteomic target profiling of ATR inhibitors using Kinobeads

2.2.1 Cell culture and lysis

AsPC-1 cells were cultured in DMEM (PAN Biotech) supplemented with 10% fetal bovine serum (PAN Biotech) and 1% non-essential amino acids (PAN Biotech) in 175 cm^2 cell culture flasks at 37 °C and 5% CO_2. After two passages, cells were seeded in 20 cm^2 dishes and grown until 80% confluence. Cells were washed twice with PBS and subsequently lysed in compound pulldown (CP) buffer (50 mM Tris-HCl pH 7.5, 5% glycerol, 150 mM NaCl, 1.5 mM $MgCl_2$, 25 mM NaF, 1 mM Na_3VO_4, 1 mM DTT) containing 0.8% IGEPAL-CA-630 (Sigma-Aldrich), protease inhibitor (SigmaFast; Sigma-Aldrich) and phosphatase inhibitors (prepared in-house according to phosphatase inhibitor cocktail 1, 2, and 3; Sigma-Aldrich), as previously described. The lysate was incubated on ice for 20 min and frozen at -80 °C overnight. Before use, the lysate was thawed carefully and cleared by ultracentrifugation at 4 °C (20 min at 52,000 x g). From the supernatant, protein concentration was determined using the Bradford assay (Thermo Fisher) according to the vendor's instructions and adjusted to 5 mg/ml in CP buffer containing 0.4% IGEPAL-CA-630.

2.2.2 Competition pulldown assay using Kinobeads

Dose-dependent competition pulldown assays with Kinobeads ε were performed as previously described, with minor differences[116]. In brief, AsPC-1 cell lysate (2.5 mg protein per pulldown) was incubated with different concentrations of compound solution (0.3 nM, 1 nM, 3 nM, 10 nM, 30 nM, 100 nM, 300 nM, 1,000 nM, 3,000 nM, 30,000 nM; 0.5% DMSO final) or vehicle for 45 min at 4 °C to allow drug-target binding. Subsequently, 17.5 µl of settled Kinobeads ε were added per well and incubated for 30 min at 4 °C for kinase pulldown. From the vehicle experiment, unbound proteins were collected and subjected to a second pulldown experiment with fresh Kinobeads ('pulldown of pulldown', PDPD). Bound proteins were denatured and reduced in 40 mM Tris-HCl pH 7.4, 8 M urea, and 50 mM DTT for 30 min, followed by alkylation with 55 mM chloroacetamide for another 30 min at room temperature. Subsequently, the urea concentration was reduced to 1-2 M by adding 40 mM Tris-HCl pH 7.4, followed by tryptic protein digest at 37 °C for 16 h. Protein digests were acidified with formic acid (FA) and desalted on SepPak tC18 µElution plates (Waters) using 0.1% FA in 40% acetonitrile as eluent. Desalted peptides were freeze-dried by vacuum centrifugation and stored at -20 °C until LC-MS/MS measurement.

2.2.3 LC-MS/MS measurement of Kinobeads-enriched samples

For LC-MS/MS, dried peptides were dissolved in 0.1% FA and analyzed on a Dionex Ultimate3000 nano HPLC (Thermo Fisher Scientific) coupled to an Orbitrap Fusion Tribrid mass spectrometer (Thermo Fisher Scientific) run in data-dependent mode. Peptides were first loaded onto a trap column (100 µm x 2 cm, packed in-house with 5 µm Reprosil-Gold C_{18} ODS-3 resin, Dr. Maisch, Ammerbuch) and washed with solvent A0 (0.1% FA in HPLC grade water) at a flow rate of 5 µl/min for 10 min. Subsequently, peptides were separated on an analytical column (75 µm x 40 cm, packed in-house with 5 µm Reprosil-Gold C_{18} ODS-3 resin, Dr. Maisch) at a flow rate of 300 nl/min with a 52 min gradient ranging from 4-32% solvent B (0.1% FA, 5% DMSO in acetonitrile) in solvent A1 (0.1% FA, 5% DMSO in HPLC grade water). MS1 spectra were acquired in the Orbitrap mass analyzed at a resolution of 60,000 (at m/z = 200) over a scan range of 360-1300 m/z with an automatic gain control (AGC) target value of $4e^5$ (normalized AGC target 100%) and a maximum injection time of 50 ms. For MS2 scans, up to 12 precursors were isolated with an isolation width of 1.2 Th and subjected to higher energy collision dissociation (HCD) fragmentation at 30% normalized collision energy. Fragmented precursor ions were analyzed in the Orbitrap at a resolution of 30,000 (at m/z = 200) with an AGC target value of $1e^5$ (normalized AGC target 200%) and a maximum injection time of 75 ms. The dynamic exclusion duration was set to 30 s.

2.2.4 Proteomic data analysis and target identification

For identification and quantification of peptides and proteins, raw files were searched against the human reference proteome (including isoforms; downloaded from UniProtKB[139] on March 16, 2021) using the search engine Andromeda embedded MaxQuant (v1.6.12.0)[140,141]. Cysteine carbamidomethylation was set as a fixed modification, and N-terminal acetylation and oxidized methionine were set as variable modifications. Additionally, label-free quantification (LFQ) and the match-between-runs feature were enabled. All searches were performed with 1% FDR on PSM and protein levels. In the resulting *proteingroups.txt* table, protein groups were filtered by potential contaminants, reversed hits, and proteins identified only by site. Residual protein binding on Kinobeads was defined as the LFQ intensity ratio between individual drug doses and vehicles. Dose-dependent curves were fitted using CurveCurator[134] (v0.4.1, default parameters) from these ratios. Kinases and other proteins were considered potential targets if curve goodness of fit (R^2) > 0.7, curve effect size > 0.5, curve slope > 0.2, and pEC_{50} > 6. Exceptions of these filter criteria were made upon manual inspection of dose-dependent reduction in MS/MS and unique peptide counts. Only proteins quantified with at least 4 unique peptides in the vehicle experiment were considered in the analysis. For the calculation of apparent dissociation constants (K_D^{app}), the EC_{50} value of each protein was multiplied with a correction factor. This correction factor estimated the protein depletion by Kinobeads and was the protein intensity ratio of the two subsequent vehicle pulldown

experiments (PDPD and vehicle, Chapter 2.2.2)[111]. The mean correction factor across all four experiments was used for each protein.

2.2.5 Calculation of CATDS scores for ATR

CATDS scores were calculated as described previously[108]. Here, CATDS scores were calculated for ATR kinase at the inhibitors' individual K_D^{app} for this kinase. In essence, the target engagement of ATR at this dose (0.5) was divided by the summed engagement of all targets, including ATR at this dose, using the following equation[108] (3).

$$CATDS_{ATR} = \frac{(target\ engagement)_{ATR}}{\sum(target\ engagement)_{all\ targets\ including\ ATR}} \quad (3)$$

The target engagement was calculated from the following equation[138,142] (4),

$$f(x) = c + \frac{d-c}{1+exp(b(log(x)-log(e)))} \quad (4)$$

where x is the concentration of interest (here, K_D^{app} of ATR), d the curve top, c the curve bottom, b the curve slope, and e the curve inflection point, or EC_{50}. Here, the curve slope and EC_{50} values were retrieved from CurveCurator, and the curve top and bottom parameters were set to 1 and 0, respectively, as suggested by Heinzlmeier[108]. Both kinase and non-kinase targets were included in the calculation of CATDS scores.

2.3 (Phospho-)proteomic drug perturbation experiments

2.3.1 Time- and dose-dependent drug treatments

For drug perturbation experiments, $10e^6$ AsPC-1 cells were seeded per 10 cm^2 cell culture dish and grown for 24 h. Then, the cell culture medium was replaced with fresh medium, and cells were allowed to grow for another 24 h prior to drug treatment. For time-resolved experiments, cells were treated with either 1 µM GEM or vehicle for eight different time points (15 min, 30 min, 1 h, 2 h, 4 h, 8 h, 12 h, 24 h). For time point 0, cells were treated with a vehicle and lysed immediately. The final DMSO concentration in time-dependent experiments was 0.1%. For decryptM experiments, cells were first pre-incubated with 1 µM GEM or vehicle for 3 h, followed by treatment with nine increasing concentrations of ATRi (1 nM, 3 nM, 10 nM, 30 nM, 100 nM, 300 nM, 1,000 nM, 3,000 nM and 10,000 nM in medium without FBS) or vehicle for one additional hour. The final DMSO concentration in decryptM experiments was 0.2%.

2.3.2 SDS cell lysis and protein quantification

Cells were lysed as described previously[143], with minor modifications. In short, the culture medium was removed, and cells were washed with PBS twice before adding 2% SDS in 40 mM Tris-HCl, pH 7.6, for cell lysis. After 5 min, cell lysate was collected and sonicated in a Bioruptor (Diagenode) for 10 min (30 s on, 30 s off). Then, DNA hydrolysis was performed by boiling samples at 95 °C for 10 min and subsequent incubation with 2% trifluoroacetic acid for 1 min. The reaction was quenched using 4% N-methylmorpholine. The cell lysate was cleared by centrifugation at 11,000 x g for 5 min, and the protein concentration in the supernatant was determined using the Pierce BCA Protein Assay Kit (Thermo Scientific) following the manufacturer's instruction.

2.3.3 SP3 sample cleanup- and tryptic digest

Lysate cleanup- and digest were performed using the SP3 method on an automated liquid handling system (Bravo AssayMAP, Agilent Technologies) as previously described[143,144], with minor differences. In essence, 200 µg of protein extract was mixed with 1,000 µg carboxylate beads (1:1 mixture of washed magnetic Sera-Mag SpeedBeads #45152105050250 and #65152105050250, Cytiva) in a 1 ml 96-well plate. Then, samples were precipitated on beads using 70% ethanol and washed thrice with 80% ethanol and once with 100% acetonitrile. Next, proteins were reduced and alkylated with 10 mM TCEP and 50 mM chloroacetamide in 100 mM EPPS/NaOH, pH 8.5, and 2 mM $CaCl_2$ for 1 h at 37 °C. Subsequently, samples were digested by adding trypsin in a 1:50 trypsin-to-protein ratio for 16 h at 37 °C. Peptides were recovered from the solution, acidified with 1% trifluoroacetic acid (TFA), and desalted on Chromabond HLB plates (30 um particle size, 10 mg capacity, Machery-Nagel). Thereby, 0.1% TFA was used for equilibration and peptide loading, and 0.1% TFA in 70% acetonitrile for peptide elution. Desalted peptides were freeze-dried by vacuum-centrifugation and stored at -20 °C until further use.

2.3.4 TMT labeling and multiplexing

Next, each treatment experiment was labeled with a different channel of TMT-multiplex reagent (Thermo Scientific). For decryptM, 11 conditions were labeled using TMT11-plex (**Table 3**), while 16 conditions were labeled for time-course experiments using TMTpro (**Table 4**). For labeling, stock solutions of each channel were prepared as 25 µg/µl in dry acetonitrile. Then, dried peptides were dissolved in 15 µl 100 mM EPPS, pH 8.5, and either 5 µl of a channel of TMT11-plex reagent (decryptM) or a channel of TMTpro-reagent (time-resolved experiment) were added to each sample. The reaction was incubated for 1 h at 23 °C and quenched by adding 0.4% hydroxylamine. Then, for each TMT multiplex experiment, the differently labeled peptides were pooled into a single vessel, acidified with 1% FA, and freeze-dried by vacuum-centrifugation. Then, labeled peptide

pools were desalted on C_{18} Sep-Pak cartridges (37-55 µm particle size, 50 mg capacity, Waters) using 0.1% FA for equilibration and peptide loading and 0.1% FA in 50% acetonitrile for peptide elution. Eluted peptides were freeze-dried by vacuum-centrifugation and stored at -20 °C until further use.

Table 3. TMT11 channel assignment in proteomic decryptM experiments (treatment length GEM: 4 h; ATRi: 1 h).

TMT11 channel	TMT11 reagent	Sample	Dose GEM [nM]	Dose ATRi [nM]
1	126	GEM+ATRi	1,000	10,000
2	127N	GEM+ATRi	1,000	3,000
3	127C	GEM+ATRi	1,000	1,000
4	128N	GEM+ATRi	1,000	300
5	128C	GEM+ATRi	1,000	100
6	129N	GEM+ATRi	1,000	30
7	129C	GEM+ATRi	1,000	10
8	130N	GEM+ATRi	1,000	3
9	130C	GEM+ATRi	1,000	1
10	131N	GEM	1,000	0
11	131C	Vehicle	0	0

Table 4. TMTpro channel assignment in proteomic time-series experiments (with 1 µM drug).

TMTpro channel	TMTpro reagent	Sample	Time point
1	126	Vehicle	0
2	127N	Drug	30 min
3	127C	Vehicle	30 min
4	128N	Drug	1 h
5	128C	Vehicle	1 h
6	129N	Drug	2 h
7	129C	Vehicle	2 h
8	130N	Drug	4 h
9	130C	Vehicle	4 h
10	131N	Drug	6 h
11	131C	Vehicle	6 h
12	132N	Drug	12 h
13	132C	Vehicle	12 h
14	133N	Drug	24 h
15	133C	Vehicle	24 h
16	134N	Drug	15 min

2.3.5 Offline basic reversed-phase fractionation

Offline basic reversed-phase (bRP) fractionation of labeled peptides was performed on a Vanquish HPLC (Thermo Scientific). Dried peptides were dissolved in 200 µl 25 mM ammonium bicarbonate, pH 8.0, and directly injected into a BEH130 XBridge C_{18} column (3.5 µm 4.6 x 250 mm, Waters). In the constant presence of 2.5 mM ammonium bicarbonate, pH 8.0, peptides were eluted using a 60 min gradient spanning 7% to 45% acetonitrile at a flow rate of 1000 µl/min. Ninety-six fractions were collected automatically starting 7 min after injection (30 s of collection

per fraction). The 96 fractions were acidified with 1% FA and pooled into 48 fractions. For global proteome analysis, 6 µg of peptides per fraction were collected in a separate plate, freeze-dried by vacuum-centrifugation, and stored at -20 °C. These samples were directly subjected to LC-MS/MS measurement (Chapter 2.3.7). In preparation for subsequent phospho-enrichment (only decryptM and time-series treatment with GEM), the remaining peptides in the 48 fractions were freeze-dried by vacuum-centrifugation and stored at -20 °C until further use.

2.3.6 Enrichment of phosphorylated peptides using IMAC

For decryptM and the time-series treatment with GEM, phosphorylated peptides were enriched by immobilized metal ion affinity chromatography (IMAC) using AssayMAP Fe(III)-NTA cartridges on the Bravo pipetting system (Agilent Technologies). In brief, the dried peptide fractions were dissolved in 0.1% TFA in 80% acetonitrile and further pooled from 48 to 12 fractions to reach a final volume of 200 µl per well. Then, the phosphopeptide enrichment protocol provided in the AssayMAP Bravo Protein Sample Prep Workbench v2.0 software (Agilent Technologies) was run. This protocol included the priming of cartridges with 150 µl 0.1% TFA in acetonitrile at 300 µl/min and subsequent equilibration with 150 µl 0.1% TFA in 80% acetonitrile at 10 µl/min. Afterward, pooled fractions were loaded onto the cartridges at 5 µl/min and washed three times using 150 µl 0.1% TFA in 80% acetonitrile at 50 µl/min. Enriched phosphorylated peptides were eluted with 60 µl 1% ammonium hydroxide at 5 µl/min. Finally, the collected eluates were acidified with 1% FA, freeze-dried by vacuum-centrifugation, and stored at -20 °C until LC-MS/MS measurement.

2.3.7 LC-MS/MS measurement of fractionated samples

Enriched phosphorylated peptides (TMT-labeled, 12 fractions) were measured in data-dependent mode on a Fusion Lumos Tribrid mass spectrometer (Thermo Scientific) coupled to a Dionex UltiMate 3000 RSLCnano System (Thermo Scientific) using MS3-quantification. In essence, dried peptides were dissolved in 50 mM sodium citrate buffer and injected into a trap column (100 µm x 2 cm, packed in-house with Reprosil-Gold C_{18} ODS-3 5 µm resin, Dr. Maisch, Ammerbuch). Subsequently, peptides were washed with solvent A0 (0.1 % formic acid in HPLC grade water) at a flow rate of 5 µl/min for 10 min. Then, peptides were separated on an analytical column (75 µm x 48 cm, packed in-house with Reprosil-Gold C_{18} 3 µm resin, Dr. Maisch, Ammerbuch) at a flow rate of 300 nl/min using an 80 min two-step gradient. Between minutes 0-64, the first gradient increased from 4% to 22.5 % solvent B (0.1% formic acid, 5 % DMSO in acetonitrile) in solvent A1 (0.1% formic acid, 5 % DMSO in HPLC grade water). The second gradient ranged from 22.5% to 32% solvent B in solvent A1 between minutes 65-80. Peptides were ionized using a nano source at 2.1 kV spray voltage. MS1 spectra were collected in the Orbitrap at a resolution of 60,000 (at 200 m/z) over a scan range of 360 to 1800 m/z. The AGC target value was set to $4e^5$, with a

maximum injection time of 50 ms. The cycle time between MS1 scans was 3 s. Precursor ions were isolated with a quadrupole isolation window of 0.7 Th, followed by collision-induced dissociation (CID) fragmentation in the linear ion trap using 35% normalized collision energy. Multistage activation was enabled. MS spectra were acquired in the Orbitrap at a resolution of 30,000 (auto scan range), with an AGC target value of $5e^4$, a maximum injection time of 60 ms, and the inject-beyond feature enabled. The dynamic exclusion duration was set to 90 s. A new batch of TMT reporter ions was isolated for a consecutive MS3 scan using charge state-dependent MS3 quadrupole isolation windows of 1.2 Th (z = 2), 0.9 Th (z = 3), and 0.7 Th (z = 4-6). Using synchronous precursor selection, the top 10 fragment ions of the MS2 scans were isolated and subjected to HCD fragmentation in the linear ion trap at 55% normalized collision energy. MS3 spectra were acquired in the Orbitrap at a resolution of 50,000 over a scan range of 100 to 1,000 m/z, with an AGC target of $1e^5$ and a maximum injection time of 120 ms.

LC-MS/MS measurement of non-enriched peptides (TMT-labeled, 48 fractions) was carried out on a micro-flow LC system built by combining a modified Vanquish pump with the autosampler of the Dionex UltiMate 3000 nano HPLC System (Thermo Scientific) coupled to an Orbitrap Fusion Lumos Tribrid instrument (Thermo Scientific). Dried peptides were reconstituted in 0.1% formic acid and loaded directly onto an Acclaim PepMap 100 C_{18} column (2 µm particle size, 1 mm inner diameter × 150 mm, Thermo Scientific) heated at 55 °C. Samples were separated using a 25 min linear gradient of 4-32% solvent B (solvent A: 0.1% formic acid, 3% DMSO in HPLC grade water; solvent B: 0.1% formic acid, 3% DMSO in acetonitrile) at a flow rate of 50 µl/min. Peptides were ionized using an electrospray voltage of 3.5 kV, a capillary temperature of 325 °C, and a vaporizer temperature of 125 °C. Sheath, aux, and sweep gas were used at a flow rate of 32, 5, and 0, respectively. MS1-spectra were acquired in the Orbitrap at a resolution of 60,000 (at 200 m/z) using a maximum injection time of 50 ms and an AGC target value of $4e^5$. The cycle time between MS1 scans was 1.2 s, and the dynamic exclusion was 50 s. Precursor ions were isolated with a quadrupole isolation window of 0.6 Th and fragmented by HCD using a normalized collision energy of 32%. MS2-spectra were acquired in the linear ion trap in rapid scan mode using a maximum injection time of 40 ms and an AGC target value of $1.2e^4$ (auto scan range). The top 8 fragment ions of the MS2 scans were isolated for MS3 using synchronous precursor selection with isolation windows of 1.2 Th and subjected to HCD fragmentation in the linear ion trap at 55% normalized collision energy. MS3 spectra were acquired in the Orbitrap at a resolution of 50,000 (at 200 m/z) over a scan range of 100 to 1,000 m/z, with an AGC target of $1e^5$ and a maximum injection time of 86 ms.

2.3.8 Data analysis of drug-perturbation experiments

Analysis of decryptM data. For peptide and protein identification and quantification, raw data was searched against the SwissProt human reference proteome UP000005640, including isoforms

(downloaded from UniProtKB[139] on March 16, 2021; 20,831 entries) using the search engine Andromeda embedded in MaxQuant[140,141] (v1.6.12.0). MS3-quantification via TMT11 was used with correction factors provided by the vendor. N-terminal acetylation, oxidized methionine, and phosphorylation (STY) were set as variable modifications, and cysteine carbamidomethylation as fixed modification. All other search parameters were set as default, except the protein false discovery rate, which was set to 100%. The resulting *evidence.txt* and *msms.txt* tables were subjected to SIMSI-Transfer[131] (v0.5.0) using a p10 threshold. Subsequently, potential contaminants and reversed hits were removed, and peptides were filtered for unambiguously assigned phosphorylation sites and a localization probability of > 0.75. Then, intensities of peptides containing the exact phosphorylation site(s) were summed up, followed by median-centering across all eleven channels. For decryptM, channels 1 to 10 (decryptM in GEM-treated cells) were submitted to CurveCurator[134] (v0.4.1) to retrieve information on significantly regulated dose-response relationships based on the SAM statistics, using A significance threshold limit of $\alpha = 0.05$ and $\log_2$ fold change threshold limit of 0.45 (default parameters)[134]. The resulting list of regulated peptides was further filtered for curve $pEC_{50} > 5$. Channel 11 served as a vehicle for the chemodrug treatment and was not used for curve fitting. Instead, all four TMT batches were normalized row-wise based on the median intensities of channels 10 and 11. Then, intensities were $\log_2$-transformed and submitted to two-sided statistical t-test analysis in Perseus[145], with at least three valid values in each group (GEM or vehicle) and correction for multiple hypothesis testing based on Benjamini-Hochberg[146]. Peptides were defined as significantly regulated if $\log_2$ fold changes > 1 and corrected *p*-values (*q*-values) < 0.01.

Analysis of time-series data. Peptide and protein identification and quantification of time-series data were also performed using the same MaxQuant version as above, with MS3 quantification via TMTpro. For phospho-proteome data, the same search parameters were applied as for decryptM (see above). For global proteome analysis, N-terminal acetylation and oxidized methionine were set as variable modifications, and cysteine carbamidomethylation as fixed modification. All other search parameters were set as default. The resulting *evidence.txt* (phospho-proteome data) and *proteingroups.txt* (global proteome data) were filtered to remove potential contaminants and reversed hits. Channels were median-centered, and ratios were calculated between treatments and controls (channel setup, see Chapter 2.3.4). Peptides and proteins were considered regulated if absolute $\log_2$ fold change > 1 in at least two consecutive time points. An additional threshold of absolute log2 fold change > 2 at 24 h was applied for protein regulation. The directionality of time-dependent regulation was assessed by the sum of $\log_2$ fold changes across all time points, indicating up-regulation if positive or down-regulation if negative.

Additional analysis and visualization tools. Sequence logos were generated using the PhosphoSitePlus online generator tool (https://phosphosite.org/sequenceLogoAction; v6.7.4)[147],

with the PSP Production algorithm and all phosphorylated serine sequences in PhosphoSitePlus as the background dataset. The y-axis of the sequence logo was termed 'normalized frequency change' based on the description of the PSP production algorithm provided by Hornbeck et al. (2012)[148]. Pathway enrichment and plotting of full proteome time-series data was performed using the web tool ShinyGo (http://bioinformatics.sdstate.edu/go/; v0.80)[149], using all quantified proteins as background dataset. STRING network analysis was done via the online tool embedded in the STRING website (https://string-db.org/; v12.0)[150]. Only proteins connected with each other were further analyzed and visualized in Cytoscape (v3.9.1)[151]. Pathway enrichment analysis on p-peptides regulated in the decryptM experiment was performed using PTMNavigator (https://proteomicsdb.org/analytics/ptmNavigator)[152]. In the input table, p-sites regulated by GEM alone were classified as up-regulated, and those regulated by the combination of GEM and ATRis as down-regulated. Of the top-enriched pathway, selected proteins were exported, and the color and style of regulated p-sites were modified manually. Created or modified figures and plots shown in this work were processed using BioRender (https://biorender.com/) and/or Adobe Illustrator (Adobe Inc.; v16.0.0). Chemical compound structures in this work were generated using ChemDraw (v23.0.1).

3 Results and Discussion

3.1 ATR inhibition synergizes with Gemcitabine in PDAC cells

Part of this work was included in the publication: Höfer, S.; Frasch, L.; Putzker, K.; Lewis, J.; Schürmann, H.; Leone, V.; Sakhteman, A.; The, M.; Bayer, F. P.; Müller, J.; Hamood, F.; Siveke, J. T.; Reichert, M.; Kuster, B. Gemcitabine and ATR inhibitors synergize to kill PDAC cells by blocking DNA damage response. Mol Syst Biol (2025)[153]. The article was published under a Creative Commons CC BY 4.0 license (https://creativecommons.org/licenses/by/4.0/). Some material published in the article, including several figure panels, have been adapted in this thesis.

In the context of the following work, one internship project (Teresa Rogler) and one Master's Thesis project (Larissa Frasch) were carried out under the supervision of Stefanie Höfer.

3.1.1 The potency landscape of clinical inhibitors in PDAC cells

To identify targeted drugs that synergize with Gemcitabine (GEM), phenotypic drug combination screening of 146 inhibitors and GEM was performed in 12 human PDAC cell lines and one hTERT-immortalized pancreatic duct cell line (HPDE, herein referred to as PDAC cell line for simplicity; **Figure 14**; **Appendix 2**; **Appendix 3**). The inhibitor library comprised primarily approved or clinically advanced compounds (87 approved, 46 phase III, 13 phase I or II according to *clinicaltrials.gov* as of June 2023). The majority of library drugs were kinase inhibitors (140 compounds), mainly targeting receptor tyrosine kinases (RTK) such as EGFR, VEGFR, and PDGFR (45), followed by inhibitors of JAK (12) and PI3K (9). The remaining six drugs were inhibitors of PARP1 (Olaparib, Talazoparib, Niraparib), STAT3 (Napapucasin), SMO (Glasdegib), and XPO1 (Selinexor). For drug screening, cells were treated with 11 doses of library drug (0.17 nM to 10,000 nM) alone or in combination with two fixed concentrations of GEM. Of the resulting ~1,900 drug combination pairs across all PDAC cells, shifts in dose-response relationships were analyzed to identify synergistic drug combinations. As a measure of data quality, a median z-prime of 0.87 was calculated from all positive and negative controls across 195 screening plates (Chapter 2.1.3 for details), indicating the high robustness of the drug screen readout[136]. All phenotypic data (single agent and combination profiling) can be downloaded and interactively explored in ProteomicsDB[154] (https://proteomicsdb.org/).

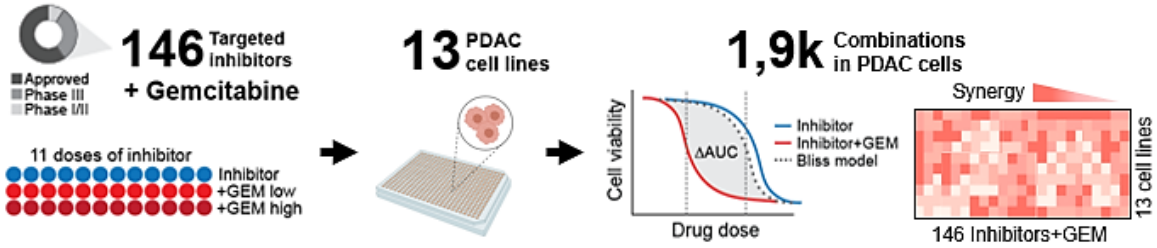

Figure 14. **Schematic overview of phenotypic drug combination screening of GEM and 146 clinically relevant inhibitors in 13 PDAC cell lines.** Cells were treated with 11 doses of inhibitor alone or in combination with two fixed doses of GEM. Drug synergy of the nearly 1,900 combination treatments was assessed through curve shift analysis. Created with Biorender.com.

The single-agent activity of the 146 drugs in PDAC cells was investigated first. From all inhibitors, about one-third (50 drugs) showed single-drug efficacy in at least one cell line (AUC < 80%, pEC_{50} > 6, and curve R^2 > 0.8; **Figure 15a**). Of these, 22 were efficacious in at least half of the cell line panel (median AUC < 80%, highlighted in blue in **Figure 15a**). Among the most potent drugs were the cell cycle inhibitors Dinaciclib (CDK inhibitor) and Volasertib (PLK1 inhibitor), displaying median AUCs of 40% and 54%, respectively, across all cell lines (**Figure 15b**, **Appendix 4**). Moreover, most cell lines responded particularly well to Sapanisertib (median AUC 54%), representing the most efficacious mTOR inhibitor in the screen (others were Rapamycin, Everolimus, Temsirolimus, and Ridaforolimus; median AUCs > 80%). Further, PDAC cells showed a reasonably strong response to SRC inhibitor Tirbanibulin (median AUC 60%) and MEK1/MEK2 dual inhibitors Cobimetinib, Copanlisib, and Trametinib (median AUC < 68%). To potentially reveal drug effects unrelated to pancreatic cancer, the immortalized pancreatic duct cell line HPDE was included in the screen. From all drugs, HPDE cells were most sensitive towards CDK inhibitor Dinaciclib (AUC = 38%) but also responded particularly strongly to mTOR inhibitor Sapanisertib, XPO1 inhibitor Selinexor, and RTK inhibitors Afatinib, Dacomitinib, and Neratinib (median AUC < 60%; **Figure 15a**). These findings imply a particular risk of potential cytotoxicity for these compounds when used in the clinics.

Finally, the sensitivity of each cell line towards GEM monotherapy was evaluated. Overall, GEM caused a strong response in most PDAC cells, with AUC values spanning 21% to 86% and half-maximum effect concentrations (EC_{50}) as low as 1 nM (**Figure 15c**). Based on this, the two doses of GEM for combination screening (GEM low, GEM high) were set as follows: 10 nM and 30 nM for the four least sensitive cell lines PANC-1, AsPC-1, MiaPaCa-2 and Patu-8988-T ($EC_{50,GEM} \gtrapprox$ 10 nM), and 1 nM and 3 nM GEM for all other cell lines ($EC_{50,GEM}$ < 10 nM; **Table 5**).

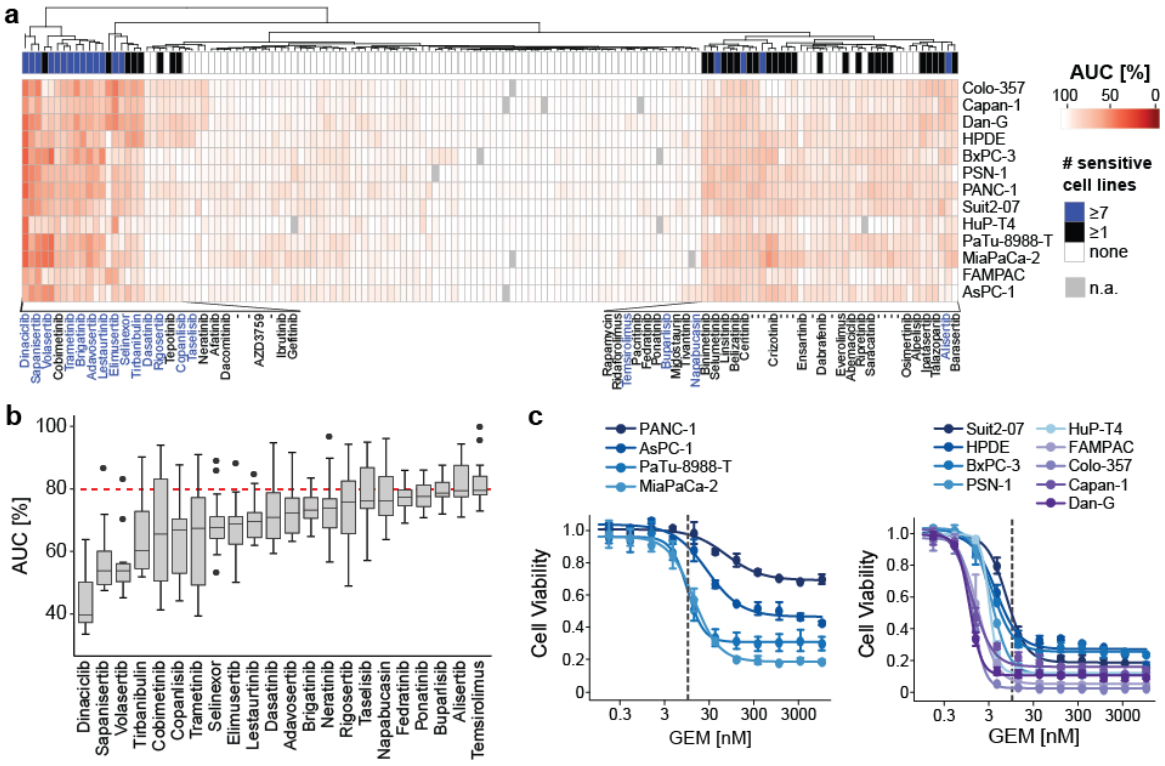

Figure 15. Single-drug efficacy of 146 inhibitors and GEM in PDAC cells. a) Area-under-curve (AUC, in %) of single drug treatments for all 146 inhibitors across 13 PDAC cell lines. A low AUC indicates high efficacy. Drugs showing efficacy in at least one cell line are annotated in black and labeled with text. Missing data (n.a.) is indicated in grey. **b)** Boxplot showing the AUC (in %) of the 22 most efficacious inhibitors (median AUC ≤ 80%, see red dashed line) across all cell lines (n = 13). **c)** Cell viability upon treatment with increasing doses of GEM as a single agent relative to the vehicle. Error bars indicate the ± standard deviation of duplicates. The dashed line marks an EC_{50} threshold of 10 nM, which was used to separate more resistant cell lines (left) from more sensitive cell lines (right).

Table 5. Potency (EC_{50}, in nM) and AUC (in %) of GEM monotherapy across 13 PDAC cell lines. Also, selected doses of GEM for drug screening (GEM low and GEM high, in nM) are shown.

Cell line	$EC_{50,GEM}$ [nM]	AUC_{GEM} [%]	GEM low [nM]	GEM high [nM]
PANC-1	72	86	10	30
AsPC-1	27	70	10	30
MiaPaCa-2	14	51	10	30
PaTu-8988-T	10	57	10	30
Suit2-07	8	47	1	3
HPDE	4	49	1	3
BxPC-3	4	46	1	3
PSN-1	3	35	1	3
HuP-T4	3	35	1	3
FAMPAC	2	25	1	3
Colo-357	1	21	1	3
Capan-1	1	32	1	3
Dan-G	1	26	1	3

3.1.2 Drug synergy between GEM and targeted therapy is rare and context-specific

The majority of clinical inhibitors lack synergy with GEM. The combination of two drugs can result in stronger or weaker phenotypic effects, depending on their molecular mechanism. Thereby, more potent phenotypic effects can either be additive (the effect of two individual drugs combined) or synergistic (any response exceeding the additive effect)[155]. In this work, the Bliss model of independence was applied to define the additive effect of two drugs and thus to estimate drug synergy[137] (see Chapter 2.1.3 for details). The model was used to calculate a hypothetical dose-response describing the additive effect of two drugs based on their single-drug efficacy. Subsequently, the simulated dose-response was compared to the experimental combination data by calculating shifts in the area-under-curve (AUC; **Figure 14**). To consider both GEM combinations, drug synergy was estimated by summing up the shift in AUC for both conditions ($\mathbf{\Sigma}AUC_{\Delta}$). From all tested compounds, only 18 targeted inhibitors displayed synergy with GEM in at least one cell line, defined by the following criteria: $\mathbf{\Sigma}AUC_{\Delta} > 10\%$, and AUC < 80%, $pEC_{50} > 6$, $R^2 > 0.8$ in at least one of the two GEM combinations (**Figure 16**). Even though RTK inhibitors comprised roughly one-third of the drug library, none exhibited synergy with GEM in any cell line. Interestingly, not even the combination of GEM and EGFR inhibitor Erlotinib demonstrated any synergy, albeit this drug regimen is clinically used in PDAC patients. Moreover, these 18 drugs did not include any drugs that displayed the highest single-drug efficacy before (Dinaciclib, Volasertib, Sapanisertib, Tirbanibulin; Chapter 3.1.1). Therefore, it can be assumed that the identified drug synergy is driven by drug mechanisms rather than the potency of the individual drugs.

Apart from synergy, another possible outcome of combination therapy is antagonism, which occurs if the response is lower than the additive effect (conceptually, $\mathbf{\Sigma}AUC_{\Delta} < 0$). A total of 30 compounds displayed antagonistic effects with GEM in at least one cell line (defined as $\mathbf{\Sigma}AUC_{\Delta} < -10\%$, and AUC < 80%, $pEC_{50} > 6$, $R^2 > 0.8$ in at least one of the two GEM combinations). Although this is nearly twice the number of synergizing drugs, the number of affected drug-cell line pairs was similar (56 antagonistic vs. 51 synergistic). This shows that antagonistic effects of individual drugs were contained to smaller subsets of PDAC cell lines, while synergistic combinations affected the cell line panel more broadly. Moreover, antagonistic effects appeared weaker across all affected cell lines than synergistic effects (median $\mathbf{\Sigma}AUC_{\Delta}$ of -14% vs. 22%). Although not further followed up in this work, these effects may be biologically relevant and warrant further investigation.

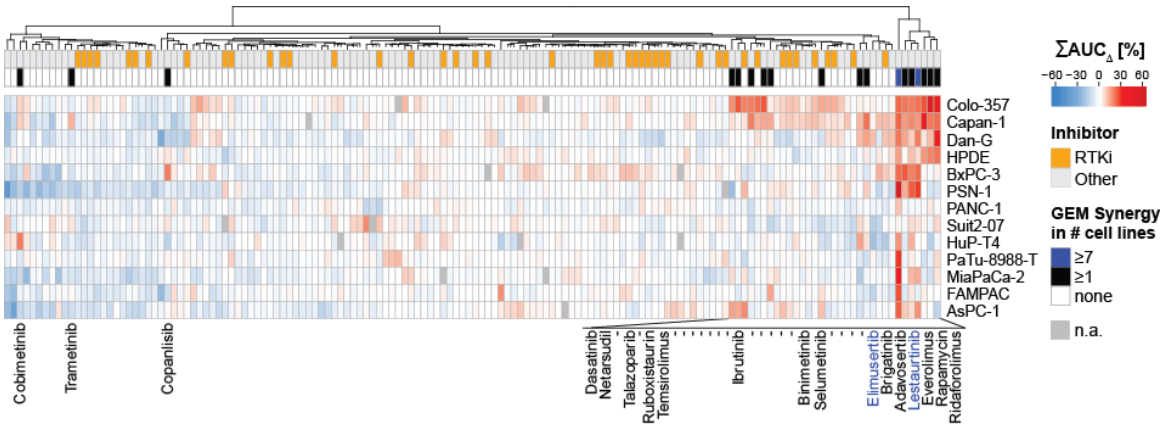

Figure 16. The summed shift in AUC (ΣAUC$_\Delta$, in %) upon combination with GEM for 146 library drugs across 13 PDAC cell lines. A high ΣAUC$_\Delta$ indicates high synergy. Inhibitors of receptor tyrosine kinases (RTKis) are annotated in orange, and all others are in light grey. Inhibitors that synergize with GEM in at least one cell line are annotated in black or blue if synergy occurs in seven or more cell lines. Only drugs showing synergy in at least one cell line are labeled with text. Missing data (n.a.) is indicated in dark grey.

Synergy between GEM and targeted therapy depends on the biological context. The 18 drugs that synergized with GEM comprised 17 kinase inhibitors and one non-kinase inhibitor (PARP1 inhibitor Talazoparib). Targeted kinases were involved in the PI3K/AKT/mTOR pathway, MAPK signaling, and cellular DNA damage response (ATR, WEE1; **Appendix 5**). Hierarchical clustering of combination effects grouped drugs by their target kinases and revealed the cellular context-specificity of combination effects (**Figure 17**). For instance, the three mTOR inhibitors (Everolimus, Rapamycin, and Ridaforolimus) synergized strongly with GEM in cell lines Colo-357, Capan-1, HPDE, and in part Dan-G (**Σ**AUC$_\Delta$ > 20% for most of these drug-cell line combinations), while other PDAC models remained largely unaffected. The mTOR inhibitor Temsirolimus displayed synergy with GEM in different cell lines (Capan-1, PANC-1) and did not cluster with the other mTOR inhibitors. Moreover, no single cell line was sensitized by combining GEM and mTOR inhibitor Sapanisertib. However, it was the most efficacious mTOR inhibitor in the single-drug screen (Chapter 3.1.1). Apart from this, another set of three inhibitors synergized with GEM in a different, broader subset of PDAC cell lines: Adavosertib (WEE-1 inhibitor), Brigatinib (ALK inhibitor), and Lestaurtinib (multi-kinase inhibitor). In combination with GEM, these drugs induced strong responses in five to seven cell lines, including FAMPAC, Patu-8988-T, and Colo-357, and in part also Dan-G, MiaPaCa-2, and AsPC-1 (median **Σ**AUC$_\Delta$ = 19% across all drug-cell line combinations). One explanation for their similar phenotypic behavior may be overlapping target engagement by these compounds, possibly also shared off-targets. To investigate this, data from two large-scale selectivity profiling studies based on the Kinobeads technology were mined[104,156]. In these datasets, Adavosertib displayed strong affinity to three kinases, including its designated target WEE1 (apparent dissociation constant (K_D^{app}) = 12 nM; ADK, K_D^{app} = 12 nM; MAP3K4, K_D^{app} = 52 nM; **Appendix 6**). In contrast to this, Brigatinib and Lestaurtinib were rather unselective and engaged > 20 different kinases at high affinity (K_D^{app} < 100 nM), including CHEK1

(K_D^{app} of 58 nM and 72 nM, respectively). There was no common target between the drugs, yet WEE1 and CHEK1 act as key cell cycle regulators in response to DNA damage[70,157]. Hence, considering that GEM is a DNA damage-inducing agent, the inhibition of DNA damage response by these drugs may explain their similar synergistic effects with the chemodrug.

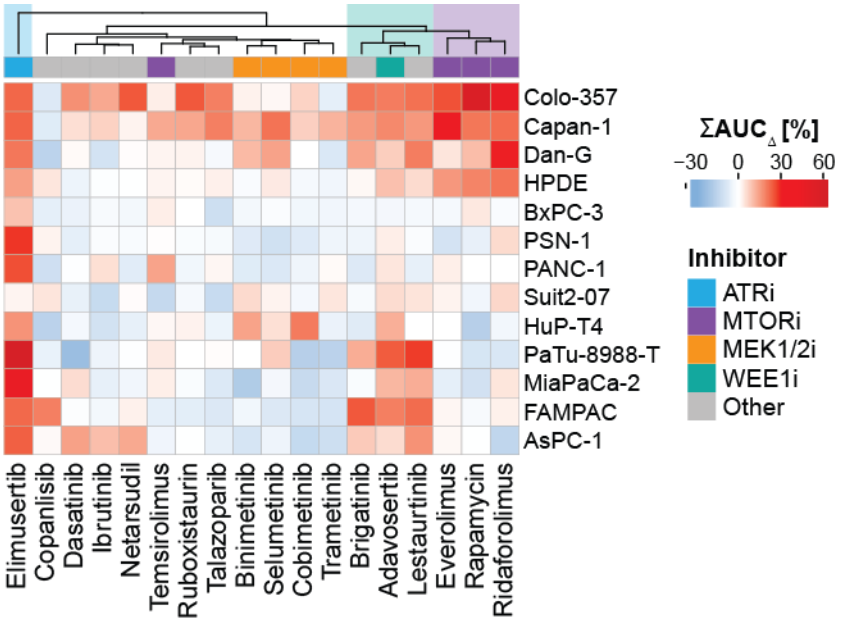

Figure 17. The summed shift in AUC (ΣAUC_Δ, in %) for the 18 drugs that synergized with GEM in at least one PDAC cell line. A high ΣAUC_Δ indicates high synergy. Inhibitor types are annotated by color. Three clusters of drugs described in the text are highlighted in blue, turquoise, and purple.

3.1.3 ATR inhibitor Elimusertib broadly synergizes with GEM in PDAC cell lines

Most synergistic drug combinations were efficacious in single or small subsets of PDAC cell lines only. In contrast, ATRi Elimusertib demonstrated synergy with GEM in 11 of the 13 screened PDAC models (**Figure 17**). In addition, the synergistic effects were remarkably strong, with ΣAUC_Δ > 20% in 9 cell lines and a maximum ΣAUC_Δ of 60% in PaTu-8988-T cells (**Table 6**). The chemosensitizing potential of Elimusertib was further manifested by large shifts in drug potency. As a single agent, the ATRi was potent across all cell lines, with EC_{50} values spanning 30 nM to 650 nM (median EC_{50} = 86 nM). Upon addition of GEM, the EC_{50} was reduced > 10-fold in most affected cell lines (**Figure 18a**, **Table 6**). The greatest potency shift was reached in cell line AsPC-1, where both GEM combinations reduced the EC_{50} from 58 nM to < 2 nM (**Figure 18b**). Interestingly, the cell lines most heavily sensitized by the combination treatment were also the least sensitive to GEM monotherapy (Chapter 3.1.1). Finally, GEM and Elimusertib also displayed synergy in the immortalized pancreatic duct cell line HPDE, but it exhibited the weakest response among all affected cell lines (ΣAUC_Δ = 15%).

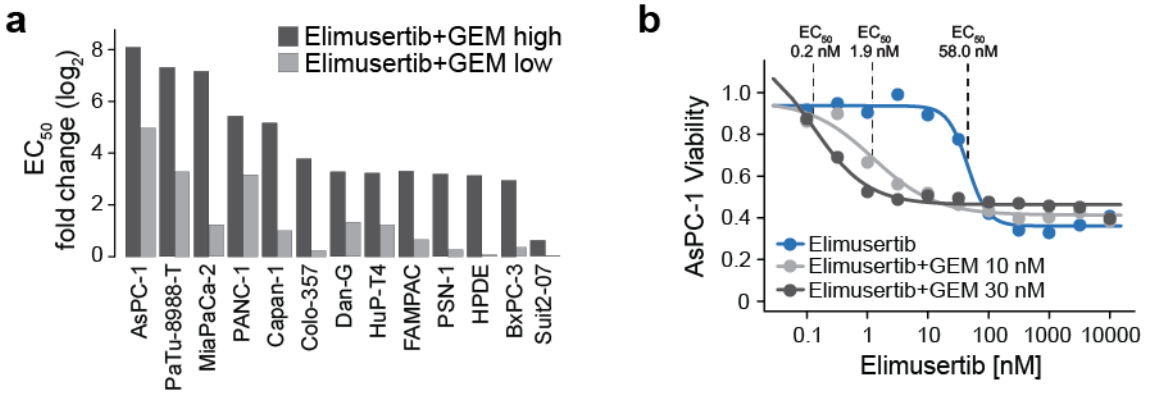

Figure 18. The combination of GEM and ATRi Elimusertib achieves strong shifts in potency in PDAC cells. a) Fold change in EC_{50} (log_2) upon combination of Elimusertib and GEM high (dark red) or GEM low (light red) across 13 PDAC cell lines. **b)** Viability curves upon Elimusertib alone (blue) or in combination with either 30 nM GEM (dark red) or 10 nM (light red) in AsPC-1 cells.

Table 6. The fold change in the potency of ATRi Elimusertib ($EC_{50,Elimusertib}$; in nM) upon the combination with GEM (GEM low or GEM high) and ΣAUC_{Δ} (in %) in 13 PDAC cell lines. Maximum potency shifts and ΣAUC_{Δ} are highlighted in blue text. Cell lines in which the synergy criteria were not reached are indicated in grey.

Cell line	$EC_{50,Elimusertib}$ [nM]	$EC_{50,Elimusertib}$ fold change upon GEM low	$EC_{50,Elimusertib}$ fold change upon GEM high	ΣAUC_{Δ} [%]	Synergy criteria met
AsPC-1	58	**31**	**272**	24	yes
PaTu-8988-T	110	10	159	**60**	yes
MiaPaCa-2	295	2	143	45	yes
PANC-1	648	9	43	26	yes
Capan-1	68	2	36	23	yes
Colo-357	29	1	14	23	yes
FAMPAC	44	2	10	22	yes
Dan-G	32	3	10	20	yes
HuP-T4	359	2	9	16	yes
PSN-1	124	1	9	28	yes
HPDE	104	1	9	15	yes
BxPC-3	55	1	8	9	no
Suit2-07	86	1	2	2	no

3.1.4 Synergy between GEM and ATRi is not restricted to Elimusertib

The extensive activity of ATRi Elimusertib and GEM in PDAC cells prompted further characterization of the chemo-sensitizing potential of this drug combination. Given that Elimusertib was the only ATRi in the initial drug screen, it was of particular interest whether the observed synergistic effects could be generalized to ATR inhibition. Additional phenotypic assays involving GEM and ATRis were conducted in AsPC-1 cells using a modified experimental setup- and different readouts to elucidate this. Thereby, GEM was titrated and combined with three fixed sub-EC_{50} doses of ATRi (reversed to the drug screen). Also, cell viability was measured via cell confluence, while the initial drug screen inferred cell viability from ATP levels (see Chapter 2.1.2 for details).

3 | Results and Discussion

First, the synergy between GEM and Elimusertib was validated. As expected, the addition of Elimusertib heavily sensitized AsPC-1 cells to the chemodrug, as seen by the substantial reduction in EC_{50} from 57 nM (GEM alone) to 5-17 nM (GEM combined with 3 nM, 10 nM, or 30 nM Elimusertib; **Figure 19a**). Notably, the EC_{50} of Elimusertib alone was 54 nM (**Appendix 5**), indicating that AsPC-1 cells were already chemo-sensitized by near non-effective doses of the ATRi. This corroborates the initial drug screen findings and provides further evidence of the phenotypic synergy between GEM and Elimusertib.

Subsequently, the same combination setup was employed to evaluate six additional ATRis, including three clinical (Berzosertib, Ceralasertib, Gartisertib) and three pre-clinical drugs (AZ-20, ETP-46464, VE-821). In monotherapy, only half of the ATRis demonstrated efficacy as single agents in AsPC-1 cells (Gartisertib, Berzosertib, AZ-20, EC_{50} < 1,000 nM vs. all others EC_{50} > 1,000 nM; **Appendix 7**). Nevertheless, except for ETP-46464, all compounds sensitized the cells to chemotherapy, mirroring the effect of Elimusertib observed before (**Figure 19b**). Notably, combining GEM with any of the four clinical ATRis resulted in stronger potency shifts compared to non-clinical compounds. In particular, Gartisertib exhibited similarly strong efficacy as Elimusertib, both in monotherapy and combined with GEM, emerging as one of the most active drug combinations.

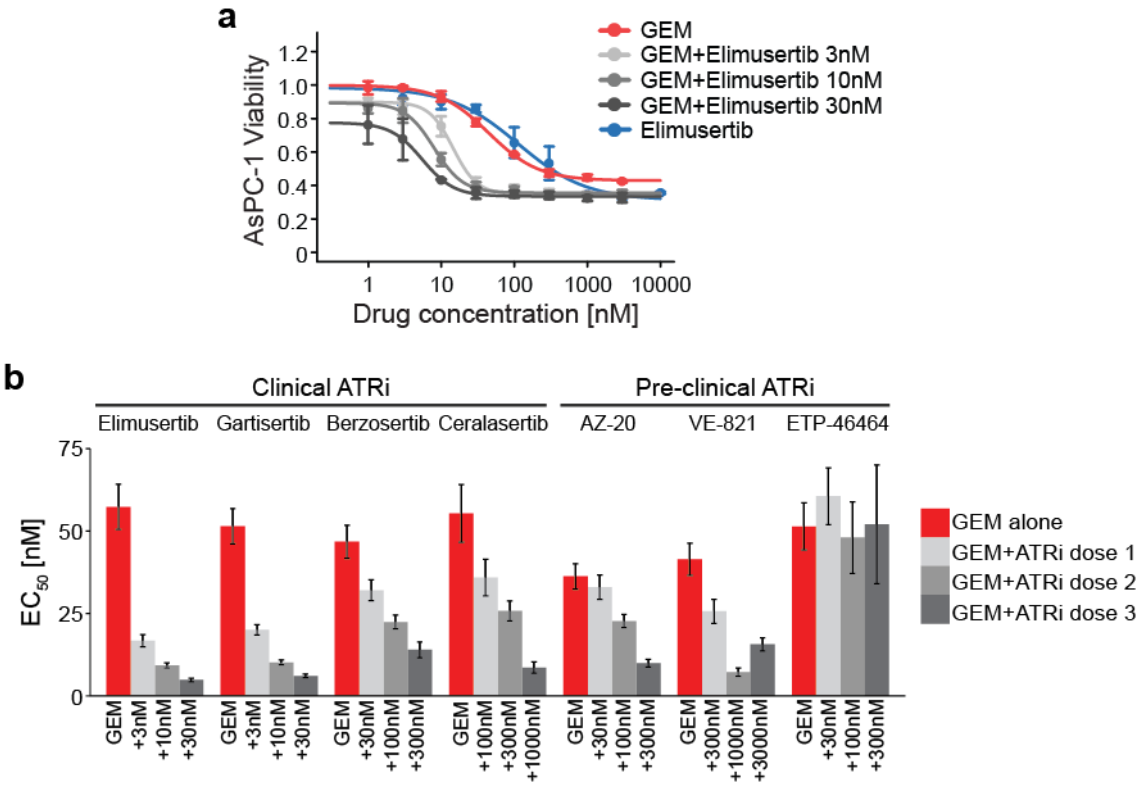

Figure 19. Cell proliferation experiments of Elimusertib and six additional ATRis with GEM in AsPC-1 cells. a) Viability of AsPC-1 cells after treatment with GEM only (red) or in combination with three sub-EC_{50} doses of Elimusertib (shades of grey) relative to the vehicle. Error bars indicate the ± standard deviation of triplicates. **b)** EC_{50} (in nM) of GEM only (red) or in combination with three sub-EC_{50} doses of ATRi (shades of grey). Error bars indicate the ± standard deviation of triplicates.

Many studies have shown that GEM induces apoptosis in PDAC cells[158-160]. To assess the impact of ATR inhibition on GEM-induced apoptosis, Annexin V was monitored in AsPC-1 cells treated with GEM and the four clinical ATRis over time. In combination with GEM, all four drugs led to an earlier onset of apoptosis in these cells compared to single drug treatments (all combinations: 24-32 h vs. GEM alone: 40-48 h, compared to a vehicle control; **Figure 20**). Moreover, the degree of apoptosis induced by the combination of GEM and either Elimusertib or Gartisertib (but not Berzosertib or Ceralasertib) surpassed that of GEM alone at the final time point, which aligned with their superior synergistic effects seen in the cell growth assays before. These results suggest that ATR inhibition accelerates GEM-induced apoptosis, adding further evidence of drug synergy. In summary, these data demonstrate the efficacy of Elimusertib and other ATRis with GEM on the level of both cell proliferation and GEM-induced apoptosis.

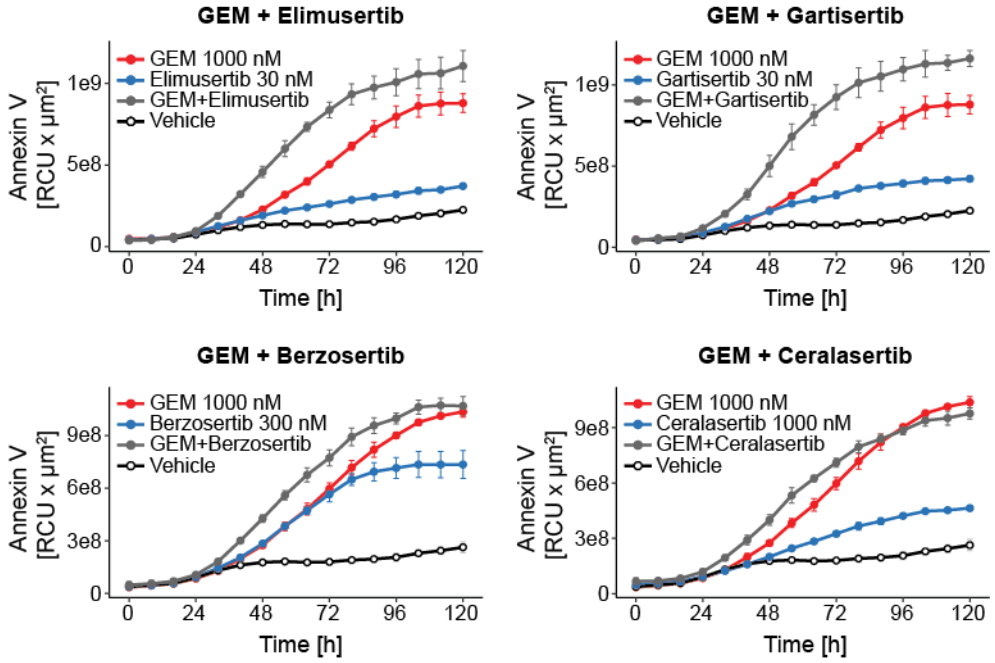

Figure 20. Early apoptosis in AsPC-1 cells treated with GEM only (red), ATRi only (blue), a combination of GEM and ATRi (grey), or vehicle (black circle) over time. Annexin V (in RCU x µm^2) was measured every 8 h until 120 h. The used drug doses are provided in the individual legends, and the doses used for combination are indicated.

3.1.5 Discussion

Comprehensive single-drug profiling suggests candidates for repurposing in PDAC. PDAC is a devastating disease with an unmet need for effective therapeutic strategies. This study explored the phenotypic efficacy of 146 clinically relevant inhibitors and their combination with GEM in 13 PDAC cell lines. Thereby, the single-drug data revealed several potential candidates for drug repurposing in pancreatic cancer. The repurposing of already approved or clinically advanced compounds poses the advantage of fastened clinical entry or re-approval due to their established safety profiles from prior trials[105].

One promising candidate was PLK1 inhibitor Volasertib, which induced a strong response in 12 out of 13 PDAC cell lines (median AUC = 54%). Volasertib has been clinically investigated for the treatment of AML (phase III)[161] and several solid tumors, including ovarian, lung, and ovarian cancer (phase II)[162-164]. Also, the FDA has granted orphan drug designation for rhabdomyosarcoma[165]. Intriguingly, while the efficacy of other PLK1 inhibitors has been studied in pancreatic cancer before[166-168], the antitumor activity of Volasertib has remained largely unexplored. Consequently, no clinical trial of Volasertib has been initiated for PDAC to date, although the drug screen suggests its strong therapeutic potential.

Another similarly effective drug in PDAC cells was SRC inhibitor Tirbanibulin (median AUC = 60%). This drug has been approved for actinic keratosis[169] and is currently being evaluated for skin cancer treatment (phase II, *clinicaltrials.gov* identifiers NCT06112522 and NCT05713760). Some ten years ago, clinical phase I trials evaluated Tirbanibulin for its use in patients with advanced malignancies, including pancreatic cancer (NCT00658970)[170]. However, despite a favorable pharmacokinetic profile, a tolerable safety profile, and preliminary evidence of antitumor activity[170], no subsequent trials have been initiated for PDAC. The high efficacy of Volasertib and Tirbanibulin in PDAC cells and the lack of relevant clinical trials strongly suggest further investigation into these drugs' therapeutic potential for PDAC patients.

A third highly active compound was mTOR inhibitor Sapanisertib, which induced strong phenotypic responses in nearly all PDAC models (AUC = 54%). This inhibitor demonstrated a manageable safety profile in previous clinical trials[171] and recently obtained fast-track designation by the FDA for squamous non-small cell lung cancer[172]. Currently, the clinical efficacy of Sapanisertib in various solid tumors, including pancreatic cancer, is being investigated (MATCH trial, phase II, NCT02465060)[173], and the pre-clinical data presented herein supports the clinical use of Sapanisertib in PDAC. Interestingly, a completed phase II trial reported the lack of efficacy of Sapanisertib in pancreatic neuroendocrine tumors, a different pancreatic cancer subtype[174]. The broad response of Sapanisertib observed across most PDAC models herein suggests its activity to be specific to the PDAC subtype.

Despite these encouraging findings, there is a possibility that these pre-clinical results may not translate into clinical efficacy in patients. For instance, the multi-CDK inhibitor Dinaciclib was the most active compound herein (median AUC = 40%), and its therapeutic potential has been demonstrated in both cellular and *in vivo* pre-clinical models of PDAC before[175-177]. However, Dinaciclib failed to show sufficient antitumor activity in advanced PDAC patients in a phase I trial testing its combination with the AKT inhibitor MK-7965 (NCT01783171)[178]. Although well-tolerated, the lack of preliminary response in this phase I study seemingly stopped any further clinical follow-up in PDAC, as no subsequent trials involving Dinaciclib have been initiated since

this study was completed in 2016[178]. Therefore, although the drug screen data suggests therapeutic efficacy, the actual clinical benefit of these compounds requires thorough investigation in patients.

The screened cell line panel involved the non-cancerous pancreatic duct cell line HPDE, which has been immortalized by the human telomerase reverse transcriptase gene and employed in previous studies to infer cytotoxicity[179,180]. Several suggested repurposing candidates induced a response in HPDE cells, suggesting potential safety risks when applied in patients. However, the fact that the majority of screened compounds are clinically advanced and thus surpassed safety criteria in prior clinical trials renders this interpretation questionable. For instance, HPDE cells were highly sensitive to Dinaciclib and Sapanisertib in the screen (AUCs of < 55%), yet both inhibitors demonstrated manageable safety profiles in clinical trials for PDAC before (see above). Therefore, the drug sensitivity in HPDE cells likely does not translate to clinically relevant toxicity. Presumably, using more advanced pre-clinical models, such as spheroid or organoid-like models derived from normal duct cells, could offer more reliable insights into potential safety risks from pre-clinical screening campaigns.

The combination of GEM with ATRi Elimusertib is currently in early clinical trials. Chemoresistance has been described as one of the key reasons for poor patient survival in PDAC. One potential way to improve therapeutic efficacy is the combination of standard chemotherapy, such as GEM, with inhibitors targeting specific signaling pathways. In addition to single-agent profiling (see above), this work provides a comprehensive resource of drug combination effects of the 146 targeted inhibitors combined with GEM. The most active drug regimen was the combination of GEM and ATR kinase inhibitor Elimusertib, exhibiting synergy in 11 out of 13 PDAC models. Moreover, follow-up experiments in AsPC-1 cells showed that the synergy could also be generalized to other ATRis.

In prior studies, several ATRis were reported to synergize with GEM in pre-clinical PDAC models before, including Ceralasertib[181], Berzosertib[182] (*in vitro* and *in vivo*), AZ-20[183], and VE-821[184] (*in vitro*). Only a single large-scale study by Zhang et al. (2023) systematically characterized the combination of three ATRis (but not Elimusertib) and GEM in a large panel of 62 cancer cell lines, including 4 PDAC[185]. Thereby, they detected a strong synergy between GEM and ATR inhibition in PDAC, supporting the findings of the current work. Moreover, they reported this regimen to synergize in other cancer types, indicating that drug synergy between GEM and ATR inhibition may also be a therapeutic option for other cancers as well.

Intriguingly, none of the pre-clinical studies mentioned above included Elimusertib specifically. In fact, the only prior evidence of its chemosensitizing ability comes from its combination with other DNA damage-inducing chemotherapies, including Oxaliplatin in PDAC[186]; Carboplatin, 5-FU, and Cisplatin in colorectal cancer[187,188]; and Carboplatin in ovarian cancer models[188]. Nevertheless, the

combination of Elimusertib and GEM is currently being clinically investigated for safety and preliminary efficacy in multiple cancer entities, including PDAC (phase I, NCT04616534). Hence, the data presented herein is the first systemic evidence of the pre-clinical efficacy of GEM and ATRi Elimusertib in PDAC and strongly supports its ongoing clinical trial in this malignancy.

Inhibition of ATR synergizes stronger with GEM than inhibition of downstream kinases. In the combinations screen, three additional drugs exhibited synergy with GEM, namely WEE1 inhibitor Adavosertib and the broad-spectrum inhibitors Brigatinib and Lestaurtinib, displaying off-target selectivity for CHEK1 (Chapter 3.1.2). CHEK1 and WEE1 are cell cycle regulators that act downstream of ATR kinase in response to damaged DNA[64,157], suggesting a similar drug synergy mechanism to ATRi Elimusertib. However, their combination with GEM was synergistic in only five to seven of the 13 PDAC cell lines, in contrast to Elimusertib, which affected nearly all cell lines. This implies that ATR inhibition synergizes with GEM across a broader range of PDAC tumors than the inhibition of downstream signaling kinases such as CHEK1 and WEE1.

Similar large-scale combination studies have also identified only partial synergy between GEM and inhibition of CHEK1 or WEE1 across PDAC cell panels. For instance, Jaaks et al. investigated the combination of GEM and 20 kinase inhibitors across 30 PDAC cell lines[189]. They found CHEK1 inhibitor AZD7762 to synergize most frequently among the tested drugs, yet in only half of the PDAC panel[189]. Similar observations were made in two other studies evaluating GEM-based combinations with CHEK inhibitors in NSCLC cells[190] and CHEK or WEE1 inhibitors across various other cancers (not including PDAC)[191]. However, these studies did not include any ATRis, rendering a direct comparison to the current work impossible. The superior efficacy and chemosensitizing ability of ATR inhibition observed herein may be explained by alternative downstream signaling independent of CHEK1 and WEE1. Some evidence for such an interpretation also comes from the single-drug screening data herein, in which Elimusertib was more broadly active than Adavosertib, Brigatinib, or Lestaurtinib (Chapter 3.1.2).

Context-dependent synergy warrants specific response markers. Finally, a notable observation from the drug combination screen was the tissue-specific nature of some synergistic interactions. For example, synergy between GEM and mTOR inhibitors was observed in only three to four PDAC cell lines, while other cell lines remained largely unaffected. Similarly, the aforementioned drugs Adavosertib, Brigatinib, and Lestaurtinib demonstrated synergy with GEM in five to seven PDAC cell lines exclusively. Moreover, although ATRi Elimusertib achieved strong responses in nearly all examined PDAC cell lines, the individual responses to the drug combination varied extensively. This raises the assumption that certain molecular features of these cells may divide responding into non-responding disease models, warranting further investigation of predictive biomarkers. A recent clinical trial on GEM and WEE1 inhibitor Adavosertib reported preliminary efficacy in PDAC (NCT02037230, phase I/II), rendering it a promising regimen. However,

although two studies of GEM and mTOR inhibitors have been initiated in PDAC, one has unknown results (Everolimus; phase I/II; NCT00560963), and the other was terminated for an unknown reason (Temsirolimus; phase I; NCT00593008; **Appendix 5**). The fact that these trials ended more than 10 years ago implies a lack of further interest of the community to follow-up on GEM and mTOR inhibition. Nevertheless, this study supports its use – provided that suitable biomarkers can be identified to identify responsive PDAC contexts.

All of the above clearly indicate the necessity to investigate the molecular mechanism underlying the observed synergistic effects. Specifically, mechanistic insights could provide a rationale for future or ongoing trials (e.g., GEM and ATRi Elimusertib), explain differences in efficacy (e.g., ATRi vs. CHEK1i vs. WEE1i), or reveal molecular markers of drug sensitivity (e.g., GEM and mTOR inhibitors in responding vs. non-responding cells). Such aspects can be addressed by mass spectrometry-based proteomics (Chapter 1.3), which was utilized in the following chapters. Based on the clinical relevance and robustly observed synergy, the following work was dedicated to unraveling the mechanism of drug synergy between GEM and ATR inhibitors.

3.2 ATR kinase inhibitors display different selectivity toward their putative target

Part of this work was included in the publication: Höfer, S.; Frasch, L.; Putzker, K.; Lewis, J.; Schürmann, H.; Leone, V.; Sakhteman, A.; The, M.; Bayer, F. P.; Müller, J.; Hamood, F.; Siveke, J. T.; Reichert, M.; Kuster, B. Gemcitabine and ATR inhibitors synergize to kill PDAC cells by blocking DNA damage response. Mol Syst Biol (2025)[153]. The article was published under a Creative Commons CC BY 4.0 license (https://creativecommons.org/licenses/by/4.0/). Some material published in the article, including several figure panels, have been adapted in this thesis.

In the context of the following work, one internship project (Larissa Frasch) was carried out under the supervision of Stefanie Höfer.

3.2.1 Designated target kinase ATR is the only common target protein

Based on the strong phenotypic synergy between GEM and ATR inhibition in PDAC cells (Chapters 3.1.3 and 3.1.4), the following work was dedicated to characterizing the drugs' mode of action using mass spectrometry-based proteomics. Chemoproteomic target deconvolution was initially employed to assess target engagement and potential off-target effects of seven ATRis (four clinical and three pre-clinical; **Figure 21**). Therefore, the latest version of the Kinobeads technology was utilized (Kinobeads ε). Kinobeads ε were chemically optimized to expand the previously captured kinome (more than 300 kinases) by additional enrichment of phosphatidylinositol 3-kinases (PI3Ks) and phosphatidylinositol 3-kinase-related kinases (PIKKs), including ATR[116].

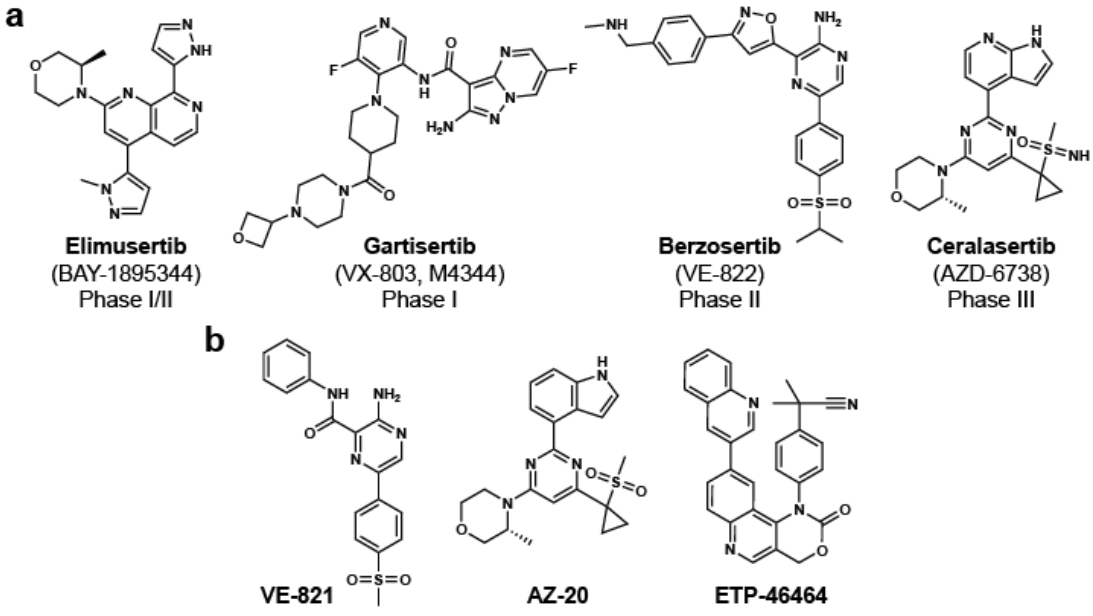

Figure 21. Chemical structures of the four clinical (**a**) and three pre-clinical (**b**) ATR inhibitors investigated in this study. For clinical inhibitors, synonyms and the highest reached clinical phase are indicated.

As expected, the designated target ATR was bound by all seven inhibitors in a dose-dependent fashion (**Figure 22a**). However, the drugs exhibited varying binding affinity to their target. While ATR was potently engaged by most drugs, including Elimusertib (apparent dissociation constant (K_D^{app}) < 10 nM), the interaction was comparably weak for the pre-clinical compound VE-821 and the clinical inhibitor Gartisertib (both $K_D^{app} \approx 300$ nM; **Figure 22b**; **Table 7**). Despite the differences in binding strength, ATR kinase was the only shared target among all tested inhibitors. Importantly, none of the other PIKK family members that are structurally related to ATR, such as ATM, DNA-PK, or mTOR[60], were bound by any of the drugs.

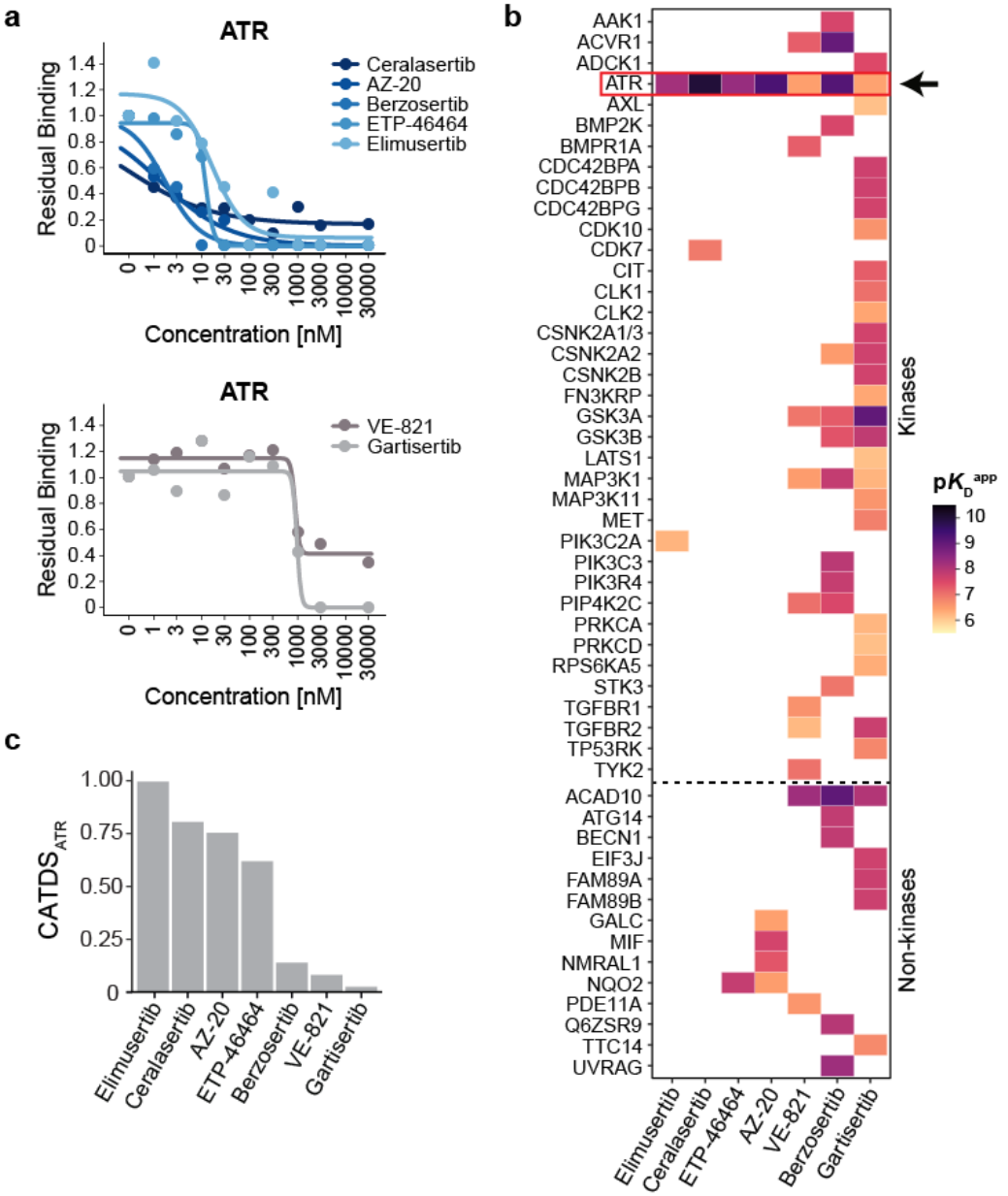

Figure 22. Target selectivity profiling of seven ATR inhibitors. a) Residual binding of ATR on Kinobeads upon increasing doses of ATR inhibitors Ceralasertib, AZ-20, Berzosertib, ETP-46464, and Elimusertib (upper panel), and VE-821 and Gartisertib (lower panel). **b)** Target proteins of all ATR inhibitors identified. Binding affinity is the -log$_{10}$ apparent

dissociation constant (pK_D^{app}). The dashed line separates target proteins into kinases and non-kinases. The designated target ATR is highlighted with a red rectangle and an arrow. **c)** Concentration and target-dependent selectivity scores (CATDS) for ATR kinase of seven ATR inhibitors. A high CATDS score indicates high target selectivity.

Table 7. Binding affinity, CATDS score for ATR, and number of (non-)kinase off-targets of the seven profiled ATR inhibitors.

ATR inhibitor	ATR K_D^{app} [nM]	$CATDS_{ATR}$	# Kinase off-targets	# Non-kinase off-targets
Elimusertib	6	1.0	1	0
Ceralasertib	< 1	0.8	1	0
AZ-20	< 1	0.8	0	4
ETP-46464	4	0.6	0	1
Berzosertib	< 1	0.1	11	5
VE-821	313	< 0.1	8	2
Gartisertib	340	< 0.1	24	5

3.2.2 Elimusertib and most other inhibitors are highly selective for ATR

Although all drugs were found to interact with ATR kinase, each of them also displayed off-target effects to a certain degree. As a measure of selectivity to their putative target kinase ATR, concentration and target-dependent selectivity (CATDS) scores[192] were calculated ($CATDS_{ATR}$). Essentially, the CATDS score is a metric that assesses the engagement of a target of interest (here, ATR) relative to the engagement of all targets, both on- and off-target, affected by a drug at a defined dose (here, the K_D^{app} of ATR; see Chapter 2.2.5 for details). Of all the tested compounds, the clinical ATR inhibitor Elimusertib was the most ATR-selective drug ($CATDS_{ATR}$ = 0.98; **Figure 22c**; **Table 7**). Elimusertib displayed ~80-fold stronger affinity to ATR over its single off-target PIK3C2A (ATR, K_D^{app} = 6 nM vs PIK3C2A, K_D^{app} = 518 nM). Similarly, Ceralasertib displayed sub-nanomolar affinity to ATR (K_D^{app} < 1 nM) and interacted with only one additional kinase, CDK7. However, since this off-target engagement was comparably strong (CDK7, K_D^{app} = 110 nM), Ceralasertib appeared less selective than Elimusertib ($CATDS_{ATR}$ = 0.8). Moreover, the two pre-clinical compounds AZ-20 and ETP-46464 displayed notable selectivity for ATR ($CATDS_{ATR}$ > 0.6). Both compounds exhibited off-target interactions with non-kinase proteins (ETP-46464 with NQO2, K_D^{app} = 15 nM; AZ-20 with FALC, MIF, NMRAL1, NQO2, all K_D^{app} = 23 nM to 326 nM), but binding affinities remained 4- and 80-fold weaker compared to ATR (both ATR, K_D^{app} < 4 nM).

3.2.3 Clinical ATR inhibitor Gartisertib is an unexpected multi-kinase inhibitor

Chemoproteomic target deconvolution revealed substantial off-target binding by three inhibitors, despite being marketed as highly selective inhibitors towards ATR: the investigational inhibitors Berzosertib and Gartisertib, and the pre-clinical compound VE-821 (all $CATDS_{ATR}$ < 0.2; **Figure 22c**)[182,193]. These drugs interacted with at least nine different kinases, including ATR. Berzosertib (formerly VE-822) and VE-821 are structural analogs arising from the same drug discovery

campaign[193], and proteome-wide target profiling identified five common target kinases (ATR, GSK3A, ACVR1, MAP3K1, and PIP4K2C), which were bound at different affinities by the analogs. Most importantly, Berzosertib displayed much-improved binding of ATR compared to VE-821 (K_D^{app} < 1 nM vs. K_D^{app} = 313 nM). However, Berzosertib also displayed similarly strong interaction with two off-targets, namely the kinase ACVR1 and the non-kinase ACAD10 (both K_D^{app} < 2 nM), which its structural predecessor did not engage. Therefore, despite its superior affinity for ATR, Berzosertib was found similarly unselective as VE-821 (both $CATDS_{ATR}$ < 0.2). Nevertheless, the clinical inhibitor Gartisertib demonstrated the highest degree of off-target engagement from all tested drugs, interacting with 25 different kinases, including ATR. Strikingly, nearly half of these were bound at > 10-fold higher affinity compared to their designated target (10 kinases, K_D^{app} < 30 nM vs. ATR, K_D^{app} = 340 nM). A substantial number of these were involved in cancer-related pathways. For instance, the most potent interaction was observed with GSK3, a multi-functional kinase taking part in pathways such as Wnt, Hedgehog, and PI3K signaling[194,195] (isoforms GSK3A, K_D^{app} < 1 nM and GSK3B, K_D^{app} < 15 nM). Further, several isoforms of CSNK2 (CSNK2A1/2/3 and CSNK2B) and CDC42BP (CDC42BPA/B/G), as well as TGFBR2, were bound at high affinity by Gartisertib (all K_D^{app} < 20 nM). Altogether, this renders Gartisertib a potent multi-kinase inhibitor with minimal selectivity for ATR ($CATDS_{ATR}$ < 0.1).

3.2.4 Discussion

Proteome-wide target profiling expands the current knowledge on ATR inhibitor selectivity. This work investigated the proteome-wide target selectivity of seven ATR inhibitors using Kinobeads. The majority of inhibitors displayed high affinity towards ATR (K_D^{app} < 10 nM), except for Gartisertib and VE-821, which were the least potent inhibitors ($K_D^{app} \approx$ 300 nM). Despite the presence of off-targets, the clinical ATRis Elimusertib and Ceralasertib remained highly selective for their designated target, similar to the pre-clinical compounds AZ-20 and ETP-46464 (all $CATDS_{ATR}$ > 0.6). These findings agree with previous studies reporting these compounds as highly potent and selective inhibitors of ATR[187,188,196]. In contrast to this, the clinical ATRi Berzosertib and Gartisertib and the non-investigational VE-821 exhibited low target selectivity for ATR ($CATDS_{ATR}$ < 0.15), although previously described as highly selective[182,193].

Of the two structural analogs, VE-821 and Berzosertib, only the latter entered clinical investigations due to its improved target selectivity and pharmacokinetic properties[193]. Here, the direct comparison revealed superior binding of ATR by Berzosertib by > 300-fold. This corroborates prior reports finding Berzosertib to display a 25-fold increased affinity for ATR compared to VE-821[182,193,197]. However, proteome-wide target deconvolution also discovered previously unanticipated off-targets[182,193] that may result in potential safety risks in the clinics, including ACVR1, BMPK2, and several isoforms of PI3K. However, considering that Berzosertib was well-tolerated in several

phase I clinical trials[89,90,198], these off-target effects may not translate into drug toxicity *in vivo*. Nevertheless, these unexpected off-target interactions may still be of essence in other cell- or tissue-specific contexts, warranting special care when testing this inhibitor in patients.

Among the newly discovered off-targets of the inhibitors were several non-kinases. One was the FAD-binding protein ACAD10, which was potently bound by three of the seven ATRis (K_D^{app} < 10 nM). ACAD10 plays a role in fatty-acid metabolism[199] and has been reported as off-target of other kinase inhibitors before[104]. Another example was the quinone oxidoreductase NQO2, an enzyme involved in cellular detoxification processes[200], bound by ETP-46464 and AZ-20 (K_D^{app} < 350 nM). It has been shown that NQO2 can interact with a multitude of compounds, including natural products and synthetic drugs, implying a very broad substrate specificity of this protein[110,200]. Nevertheless, the extent to which these ATRi interactions affect enzyme activity remains unclear, necessitating further investigation into the physiological consequences of these non-kinase off-target effects.

Newly discovered off-targets provide an explanation for high toxicity of Gartisertib *in vivo*. The most considerable discrepancy in the current literature was the potent off-target engagement by Gartisertib revealed in this work. Gartisertib is a relatively novel ATRi, and the only evidence of its selectivity is one published abstract stating 100-fold selectivity for ATR over 308 out of 312 kinases[201]. However, since the underlying data is undisclosed, the selectivity for the remaining four kinases remains unclear, let alone their identification. Here, several cancer-related kinases emerged as newly discovered off-targets of Gartisertib. Most strikingly, Gartisertib bound several cancer-related kinases with at least 10-fold higher affinity than ATR, likely translating into toxicities *in vivo*. For instance, among the most potently bound off-targets were GSK3, a multi-functional kinase taking part in Wnt, Hedgehog, and PI3K signaling[194,195], and TGFBR1, the signaling of which comprises both tumor-suppressing and oncogenic potential, promoting cell proliferation, differentiation, and migration[202]. Other newly discovered off-targets included CSNK2 (also known as CK1), which is frequently de-regulated in cancers and known to mediate cancer-related processes, including cell growth, angiogenesis, and apoptosis[203], and CDC42-binding kinases that promote cell motility and invasion, and likely play a role in tumor metastasis[204].

Although such polypharmacology of small molecule drugs may enhance efficacy, they may also drive drug toxicity *in vivo*[205]. In 2019, Gartisertib entered its first clinical trial, evaluating its safety for use in patients with solid tumors. Intriguingly, this trial was discontinued very recently due to liver toxicity[206]. The study authors attributed these adverse effects to the inhibition of UGT1A1, a liver enzyme involved in bilirubin glucuronidation, by Gartisertib and its metabolites[206]. The data presented herein provides an additional explanation: The potent inhibition of many cellular signaling pathways by Gartisertib could also affect the viability of non-cancerous cells. These findings on Gartisertib demonstrate the value of chemoproteomic in identifying potential toxicity

risks. When applied early during drug development, such knowledge can guide lead selection and optimization toward candidates with better safety profiles, ultimately preventing clinical failure.

Inhibition of DNA damage response via ATR, but not ATM or DNA-PK, likely explains drug synergy with GEM. Despite these newly revealed off-target effects, ATR kinase remained the only shared target of all inhibitors. This suggests a common mechanism through perturbation of the cellular DNA damage response. However, other PIKK family members, such as ATM and DNA-PK, also mediate cellular DNA damage signaling and share structural features[59,60], rendering them likely off-targets of ATR inhibitors (Chapter 1.2.1). In this work, no off-target effects were observed for any ATRis examined. Although there is prior evidence that these drugs also bind other PIKKs, previous studies consistently confirmed the inhibitors' high selectivity for ATR over these off-targets. For instance, Elimusertib was found to interact with multiple PIKKs, but selectivity for ATR was > 60-fold over mTOR (also a PIKK family member) and > 300-fold over ATM and DNA-PK[187]. Similarly, Ceralasertib and Berzosertib were found > 100-fold more selective towards ATR than its homologs ATM or DNA-PK[87,182]. Considering that only weak interactions with ATM or DNA-PK were evidenced for ATRi in the literature and none of these could be confirmed herein, these potential interactions with other PIKKs were considered negligible. From this, it was concluded that inhibition of DNA damage response via ATR (and not ATM or DNA-PK) remains the most likely explanation for the observed drug synergy with GEM.

Limitations of the Kinobeads assay for target deconvolution of ATR inhibitors. The Kinobeads assay comes with inherent limitations, which may explain the complete lack of affinity by the ATRis towards ATM or DNA-PK observed in the study (see above). First, the above studies measured these interactions *in vitro* using purified, pre-selected kinases at defined concentrations. In contrast, the current work employed largely unbiased target profiling in cell lysate, where the purity and quantity of individual proteins cannot be controlled. Consequently, drug-target binding may be disturbed by the numerous potential interaction partners and (bio-)molecules present in the complex protein mixture. Moreover, while critical assay parameters such as incubation time can easily be adapted *in vitro* to match the kinetics of a target-ligand-interaction, this is not feasible for *in lysate* assays. Instead, a single streamlined incubation time is applied, which may not allow every protein-ligand interaction to reach equilibrium during the competition assay. Finally, although working under mild conditions, slight changes in the protein structure may cause a drug to bind a target only weakly (or not at all) and potentially not lead to binding competition with the affinity matrix.

From this study, a few questions arise that yet remain to be explained. For instance, the translation into cellular target engagement remains unclear at this stage, as there were discrepancies between target selectivity and phenotypic combination effects in AsPC-1 cells (Chapter 3.1.4). Specifically, it remains unclear why ETP-46464 displayed no phenotypic effect in combination with GEM in

AsPC-1 cells despite the inhibitor's strong affinity and selectivity for ATR. Limited cellular uptake of this drug may possibly hamper target engagement *in cellulo*, while the drug can interact with the freely accessible protein *in lysate*. Another surprising observation was that Gartisertib exhibited only weak affinity and selectivity for ATR yet synergized heavily with GEM in the phenotypic assay. Potentially, this may be explained by distinct local concentrations and conformations of target proteins inside cells or by a difference in target engagement *in cellulo* vs. *in lysate*.

In conclusion, the chemoproteomic target profiling allowed the re-assessment of the previously reported target landscape and selectivity of seven ATRis, of which four are currently under clinical investigation. While most compounds exhibited high affinity and selectivity for ATR, others demonstrated unexpected off-target interactions, partly with cancer-related kinases. These previously unanticipated off-targets raise concerns regarding potential toxicity *in vivo*, as exemplified by the liver toxicity observed with Gartisertib in clinical trials. Notably, despite off-target effects, ATR inhibition remained the common mechanism shared by all inhibitors, indicating that ATR-mediated DNA damage response may play a pivotal role in drug synergy with GEM. However, discrepancies between target selectivity (in lysate) and phenotypic effects (in cells) warrant further investigation into the cellular engagement of ATR kinase by these compounds.

3.3 Blockage of GEM-induced replication stress response by ATRi explains synergy

Part of this work was included in the publication: Höfer, S.; Frasch, L.; Putzker, K.; Lewis, J.; Schürmann, H.; Leone, V.; Sakhteman, A.; The, M.; Bayer, F. P.; Müller, J.; Hamood, F.; Siveke, J. T.; Reichert, M.; Kuster, B. Gemcitabine and ATR inhibitors synergize to kill PDAC cells by blocking DNA damage response. Mol Syst Biol (2025)[153]. The article was published under a Creative Commons CC BY 4.0 license (https://creativecommons.org/licenses/by/4.0/). Some material published in the article, including several figure panels, have been adapted in this thesis.

3.3.1 High dose of GEM induces cellular DNA damage response within four hours

GEM induces DNA damage response and cell cycle control in AsPC-1 cells. To uncover the mechanism of synergy between GEM and ATR inhibition at the cellular signaling level, phosphoproteomic drug-perturbation experiments were conducted in AsPC-1 cells. Conceptually, the idea was to 1) induce DNA replication stress by GEM and 2) investigate the effect of ATR inhibition on the cellular signaling response to GEM.

First, the treatment duration for GEM-induced DNA damage was optimized in an initial time-series experiment. Therefore, AsPC-1 cells were treated with 1 µM GEM for intervals ranging from 15 minutes to 24 hours (8 time points), and changes in protein phosphorylation were analyzed compared to a vehicle control. In the experiment, 14,884 phosphorylated peptides (p-peptides) across 4,212 proteins were quantified, of which 1,141 p-peptides were regulated by the treatment with GEM (absolute $\log_2$ fold change > 1 in at least two consecutive time points; **Figure 23a**). One-third of the GEM-regulated p-peptides were up-regulated (389 out of 1,141, or 34%), and the remaining two-thirds were down-regulated (750, or 66%; defined as a positive or negative sum of $\log_2$ fold changes across all time points, respectively).

Sequence motif analysis of the regulated phosphoproteome was performed to identify upstream kinases. The analysis revealed an overrepresentation of pSQ (and, to a lesser extent, pTQ) among the up-regulated phosphorylation events (**Figure 23b**). This motif is highly specific for the PIKK kinase family, including ATR, ATM, and DNA-PK (Chapter 1.2.1), and its phosphorylation can serve as a proxy for cellular DNA damage signaling via these kinases[72,73,207]. The pSQ/pTQ motif was present in 38% of all up-regulation events (146 of 389) and < 2% of the down-regulated peptides (12 of 750). Strikingly, these GEM-regulated pSQ/pTQ sites comprised one-third of all pSQ/pTQ peptides quantified in the whole dataset (158 of 489, or 32%), underscoring the strong induction in the cellular DNA damage response by the chemodrug. Consistently, pathway

enrichment analysis revealed the affected proteins to be significantly involved in DNA damage repair processes (**c**).

Further, sequence motif analysis of the down-regulated phosphoproteome (> 700 p-sites) revealed an overrepresentation of a proline-directed (pSP) motif (**Figure 23b**). The pSP motif is specific to the CMGC kinase family, which includes cyclin-dependent kinases (CDK), mitogen-activated protein kinases (MAPK), glycogen synthase kinases (GSK), and CDK-like kinases[207]. Within this family, substrate specificity could be narrowed to CDKs and CDK-like kinases based on the overrepresentation of basic residues N- and C-terminal to the pSP-site (here, lysines; **Figure 23b**), as previously suggested by Johnson et al. (2023)[207]. CDKs and their phosphorylation are involved in cell cycle checkpoint regulation and transcriptional control[207]. Accordingly, pathway analysis on the down-regulated phosphoproteome revealed significant enrichment of cell cycle-related pathways (**Figure 23c**). This data implies direct activation of DNA damage response kinases and subsequent cell cycle control in response to GEM treatment.

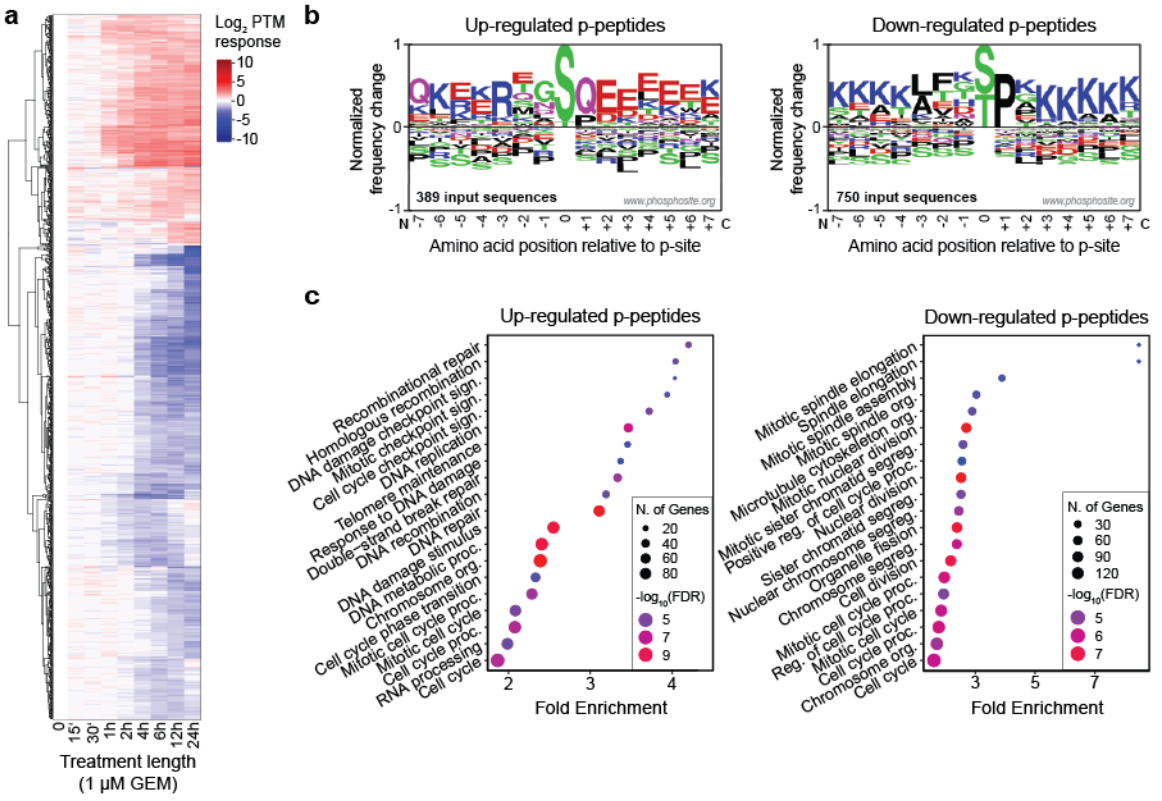

Figure 23. GEM induces phosphoproteome changes in AsPC-1 cells over time. a) Log_2 fold change in phosphorylation (PTM response) by 1 µM GEM compared to vehicle across different time points. The treatment length is in hours (h) or minutes (‘). Rows were sorted by hierarchical clustering. Regulation was defined as absolute log_2 fold change > 1 in at least two consecutive time points. **b)** Sequence logos generated from peptides either up-regulated (left) or down-regulated (right) by 1 µM GEM within 24 h. **c)** Top 20 enriched cellular processes, based on proteins that were up-regulated (left) or down-regulated (right) in phosphorylation by 1 µM GEM within 24 h.

GEM induces phosphorylation of DNA damage response kinases within 4 h. To pinpoint the onset of cellular DNA damage response, phosphorylation of key kinases involved in DNA damage signaling was studied. Earliest activation was found for ATM-pS1981 (1-2 h), followed by ATR-

pT1989, and PRKDC-pS3205 (2-4 h) and pS2612 (6-12 h; PRKDC is the gene name of DNA-PK; **Figure 24a**; **Appendix 8**). Some of these are known autophosphorylation sites that enhance kinase activity and, thus, cellular DNA damage response[60].

Another proxy of DNA damage signaling is the phosphorylation of downstream effector proteins. CHEK1-pS317, one of the best-known direct ATR substrates, was up-regulated after only 1 h of GEM treatment (log_2 fold change > 1; **Figure 24a,b**; **Appendix 8**). Early activation was also observed for CHEK1-pS286, although its levels dropped back to baseline between 6-12 h. CHEK1-pS286 is a known substrate of the cell cycle regulators CDK1 and CDK2 downstream of CHEK1[208], indicating a regulatory feedback mechanism after prolonged GEM exposure.

Apart from CHEK1, several sites of CHEK2, the putative effector protein of ATM[64], were phosphorylated as early as 2 h after exposure to GEM (pS120, pS260, p379, p387, T517; **Figure 24a,b**). Strikingly, their phosphorylation reached an exceptionally high level at 4-6 h, with a nearly 8-fold increase compared to vehicle control. Moreover, other commonly anticipated markers of DNA damage were only regulated within a few hours, including H2AX-pS139[209] and KAP1/TRIM28-pS473[210] (both log_2 fold change > 1 from 2 h onwards). Finally, the critical mediator of DNA repair via homologous recombination, BRCA1[211], exhibited elevated phosphorylation at multiple sites within 4 h (e.g., pS803, pS1524, pS1542; all log_2 fold change > 1.5; **Figure 24a,b; Appendix 8**). Based on the increased phosphorylation of the key DNA damage response kinases and their downstream effectors after 4 h of 1 µM GEM treatment, this time point was chosen for DNA damage induction in AsPC-1 cells in the following experiments.

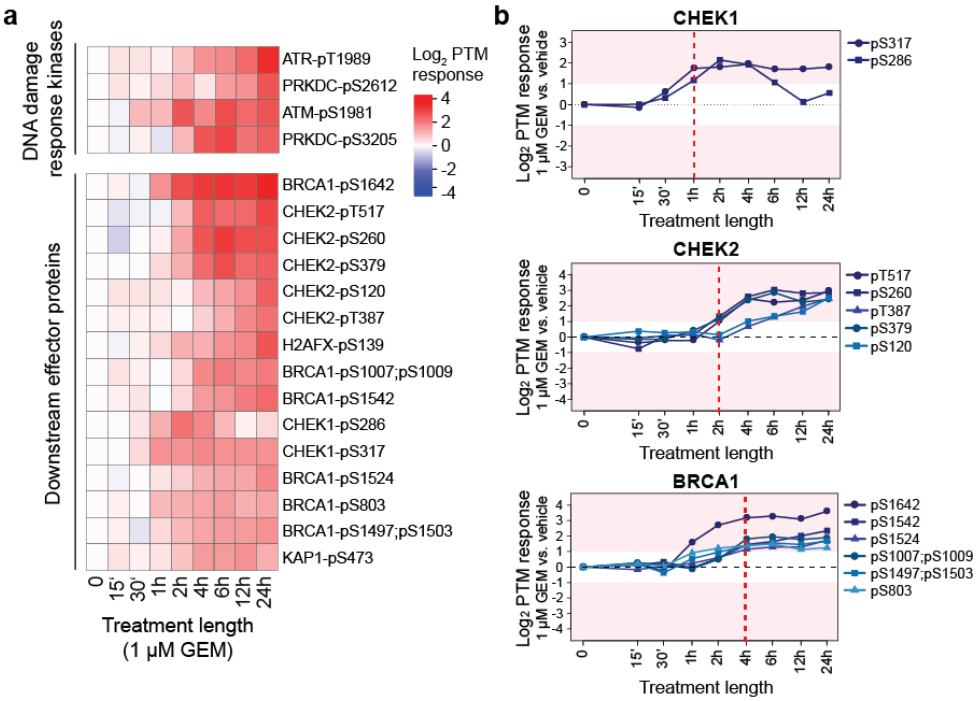

Figure 24. GEM induces cellular DNA damage response within 4 h. a) Heatmap showing the log_2 fold change in phosphorylation (PTM response) upon 1 µM GEM compared to vehicle in AsPC-1 cells over time. The gap separates the DNA damage response kinases ATR, ATM, and DNA-PK from downstream signal transducers. **b)** Log_2 PTM response

for different p-sites on CHEK1, CHEK2, and BRCA1. The red dashed line indicates the treatment length at which phosphorylation was increased by at least 2-fold. The treatment length in all plots is given in hours (h) or minutes (').

3.3.2 Four clinical inhibitors engage ATR kinase in cells at different potencies

Clinical inhibitors block the phosphorylation of ATR substrates. To shed light on the mechanistic interplay between GEM and ATRi, the cellular response to the combination treatment was investigated in AsPC-1 cells. This experiment used a previously published dose-dependent phosphoproteomics approach called decryptM[102] (Chapter 1.3.3). In brief, AsPC-1 cells were pre-incubated with 1 µM GEM for 3 h to induce DNA damage response, followed by co-treatment with either nine doses of ATRi (1 nM to 10,000 nM) or vehicle for 1 h (total treatment duration of 4 h; **Figure 25**). Tandem Mass Tag (TMT)[127] multiplexing was employed to simultaneously analyze cells treated with a combination of GEM and ATRi (TMT channels 1-9), GEM alone (TMT channel 10; control for combination treatment), and cells treated with a vehicle (TMT channel 11; control for GEM-only treatment, used in Chapter 3.3.3 below). Following phospho-proteomic analysis, the overlap in GEM- and ATRi-regulated phosphorylation sites was analyzed to infer drug synergy mechanisms.

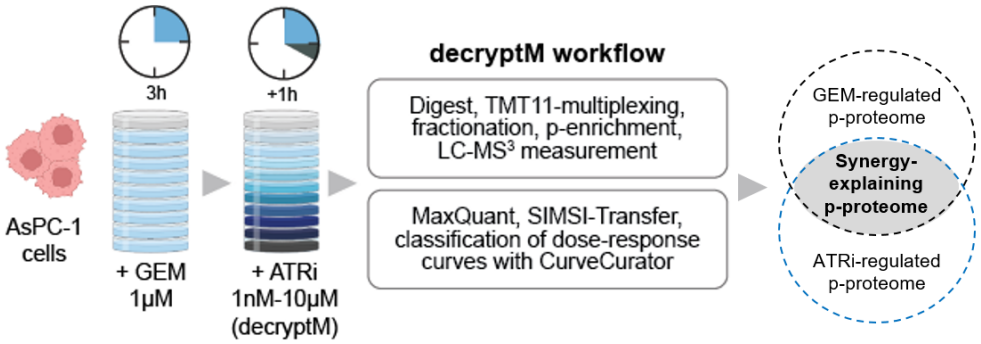

Figure 25. Schematic workflow of decryptM experiments with four clinical ATR inhibitors in DNA-damaged AsPC-1 cells. Cells were incubated with 1 µM GEM for 3 h, followed by nine doses of ATR inhibitor for 1 h (decryptM). TMT-labeled, fractionated, and phospho-enriched peptides were measured by LC-MS³. After data processing with MaxQuant[140] and SIMSI-Transfer[131], dose-response data was analyzed using CurveCurator[134]. The overlap in phosphoproteome regulation was investigated to study mechanisms of drug synergy.

Across all experiments, > 25,500 p-peptides on > 5,500 proteins were quantified. Of these, 20,784 p-peptides with site localization probability of at least 0.75 were used for subsequent analysis. This resulted in > 60,000 individual dose-response relationships across all measurements, which were fitted and classified into significantly up- and down-regulated phosphorylation events using CurveCurator[134]. The overall effect on the phosphoproteome varied among the four ATRi, with Ceralasertib and Elimusertib displaying the lowest (421 and 525, respectively) and Berzosertib and Gartisertib exhibiting the highest (840 and 1,015, respectively) number of regulated p-peptides (**Figure 26a**). Potentially, the higher degree of phospho-regulation of the latter two compounds may arise from cellular off-target engagement, as suggested by the aforementioned Kinobeads experiment (Chapter 3.2.3).

Despite these differences, the PIKK-specific pSQ/pTQ motif was over-represented among the down-regulated phosphoproteome for all four ATRis. Depending on the drug, 16-34% of all down-regulated phosphorylation events occurred on pSQ/pTQ peptides (42 to 57 peptides), while the fraction of quantified pSQ/pTQ peptides in the overall dataset was only 5% (981 of 20,784 peptides; **Figure 26a**). Noteworthy, the motif was present in only 1-4% of all up-regulation events (4 to 13 peptides, depending on the drug). This clearly demonstrates the repression of DNA damage response signaling by the four clinical ATR inhibitors in AsPC-1 cells.

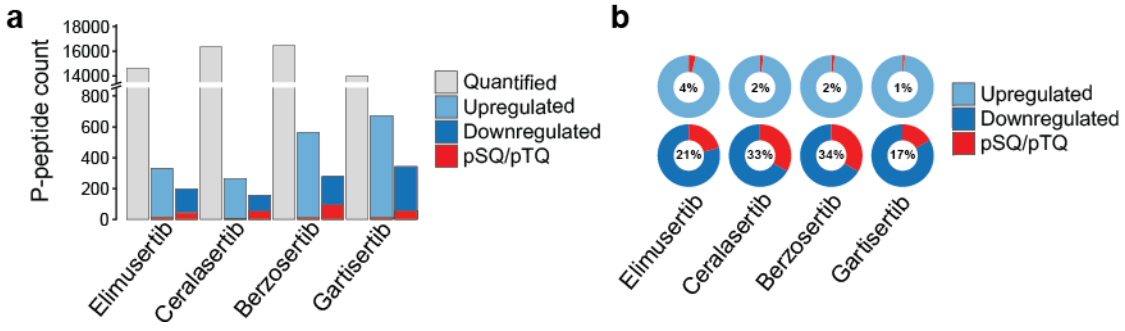

Figure 26. Overview of quantified and regulated phosphorylation events in decryptM experiments. a) Number of quantified (grey), up-regulated (light blue), or down-regulated (dark blue) phosphorylated peptides in the four decryptM experiments in GEM-pretreated AsPC-1 cells. Peptides containing the pSQ/pTQ motif are highlighted in red. **b)** Pie charts indicating the fraction of pSQ/pTQ-containing peptides among the up- or down-regulated phosphoproteomes.

Among the down-regulated pSQ/pTQ sites were known direct substrates of ATR kinase, indicating reduced ATR kinase activity. Most importantly, the direct ATR substrate CHEK1-pS317 was decreased in a dose-dependent fashion by all four drugs (**Figure 27**). CHEK1 is the best-known direct effector of ATR, and pS317 is frequently used as a direct proxy of ATR kinase activity[68-70] (Chapter 1.2.2). Moreover, phosphorylation was suppressed on other known ATR substrates, such as the ATR-activator TOPBP1[81] (pS1504) and the key mediator of homologous recombination BRCA1[211] (pS1239). Cellular target engagement was further evidenced by reduced phosphorylation of FANCD2-pS319, a known direct substrate of ATR in the repair of DNA interstrand crosslinks[75]. As mentioned, pSQ/pTQ sites may also be regulated by other PIKKs, such as ATM or DNA-PK[72] (Chapter 1.2.1). Nevertheless, the lack of interaction with ATM or DNA-PK by any of the drugs in the Kinobeads assay before (Chapter 3.2.1) suggests that the observed regulation of DNA damage response was exclusively due to ATR inhibition. In line with this, none of the autophosphorylation sites of ATM or DNA-PK nor any p-site of the direct ATM substrate CHEK2 (Chapter 0) were affected by the ATRis. Collectively, these findings confirm that all four inhibitors directly engage ATR kinase in cells and effectively block ATR-mediated DNA damage signaling.

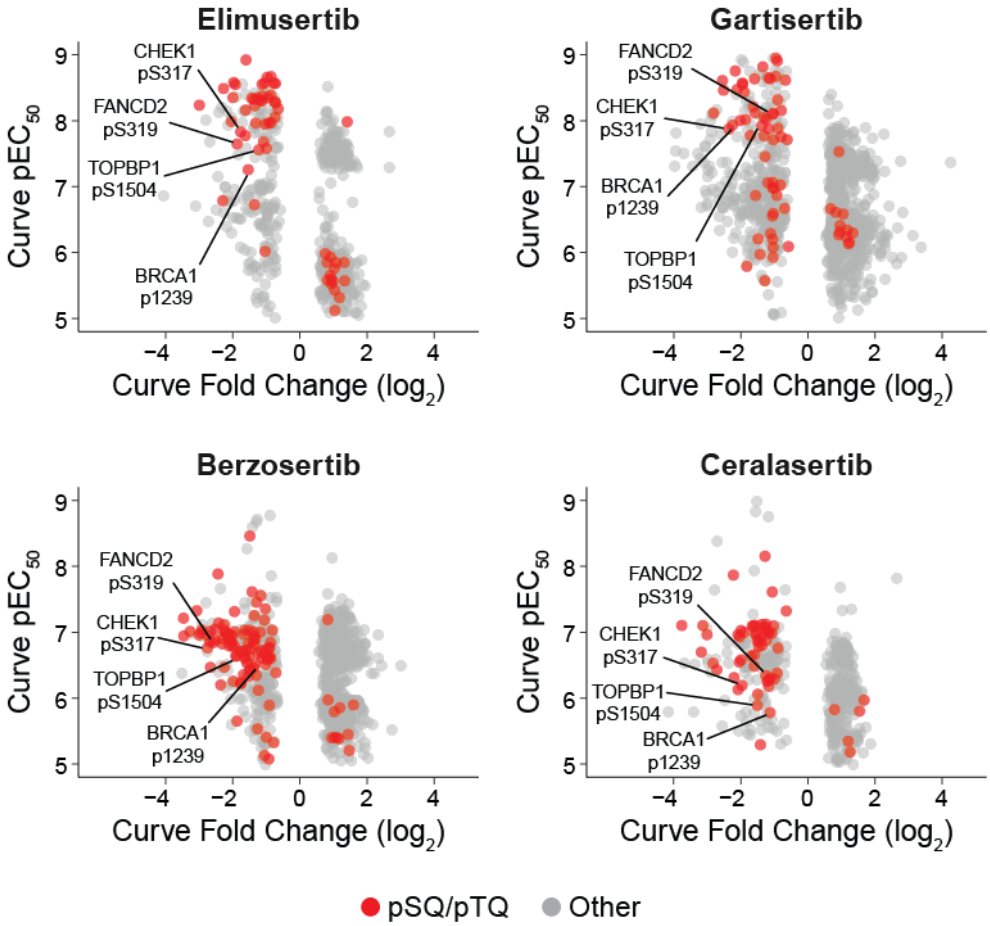

Figure 27. Potencies (-log$_{10}$ EC$_{50}$, or pEC$_{50}$) and curve fold changes (log$_2$) of regulated p-peptides from decryptM experiments with Elimusertib, Gartisertib (top), Berzosertib, and Ceralasertib (bottom) in GEM-pretreated AsPC-1 cells. Each dot represents one dose-response curve of a regulated p-peptide. Red dots indicate pSQ/pTQ peptides. Selected known substrates of ATR kinase are annotated by text.

Elimusertib and Gartisertib engage ATR kinase in cells most potently. In addition to the drugs' maximum effect on cellular signaling at high doses, decryptM provides information on their potency (measured in half-maximum effect concentration, or EC$_{50}$)[102]. Here, decryptM revealed varying potencies across drugs and p-sites, ranging from nanomolar to micromolar EC$_{50}$ (**Figure 27**). Although all four ATRis regulated pSQ/pTQ sites and thus direct DNA damage response at high potency (all median EC$_{50}$ < 200 nM), they also displayed differences. For instance, inhibition of CHEK1-pS317 by Elimusertib and Gartisertib occurred at > 10-fold higher potency (EC$_{50}$ of 13 nM and 15 nM, respectively) compared to Berzosertib and Ceralasertib (EC$_{50}$ of 173 nM and 642 nM, respectively). Similarly, phosphorylation on other pSQ/pTQ sites, such as the previously mentioned TOPBP1-pS1504, BRCA1-pS1239, and FANCD2-pS319, was repressed most potently by Elimusertib and Gartisertib (**Figure 28a**). Analysis of EC$_{50}$ distributions across all regulated pSQ/pTQ sites separated the ATRi based on their drug potency. On average, the efficacy at which Elimusertib and Gartisertib blocked these pSQ/pTQ sites (median EC$_{50}$ of 10 nM and 21 nM, respectively) was 10- to 20-fold higher than that of Berzosertib and Ceralasertib (median EC$_{50}$ of 154 nM and 188 nM, respectively; **Figure 28b**). Interestingly, the higher potency on the level of

phosphorylation mirrored the drugs' superior phenotypic efficacy in AsPC-1 cells observed before (viability EC_{50} < 130 nM of Elimusertib and Gartisertib vs. > 700 nM of Berzosertib and Ceralasertib; Chapter 3.1.4). This implies that the potent cellular engagement of ATR kinase is likely the primary mode of action via which these drugs induce cell death despite potential off-target interactions (Chapter 3.2.3).

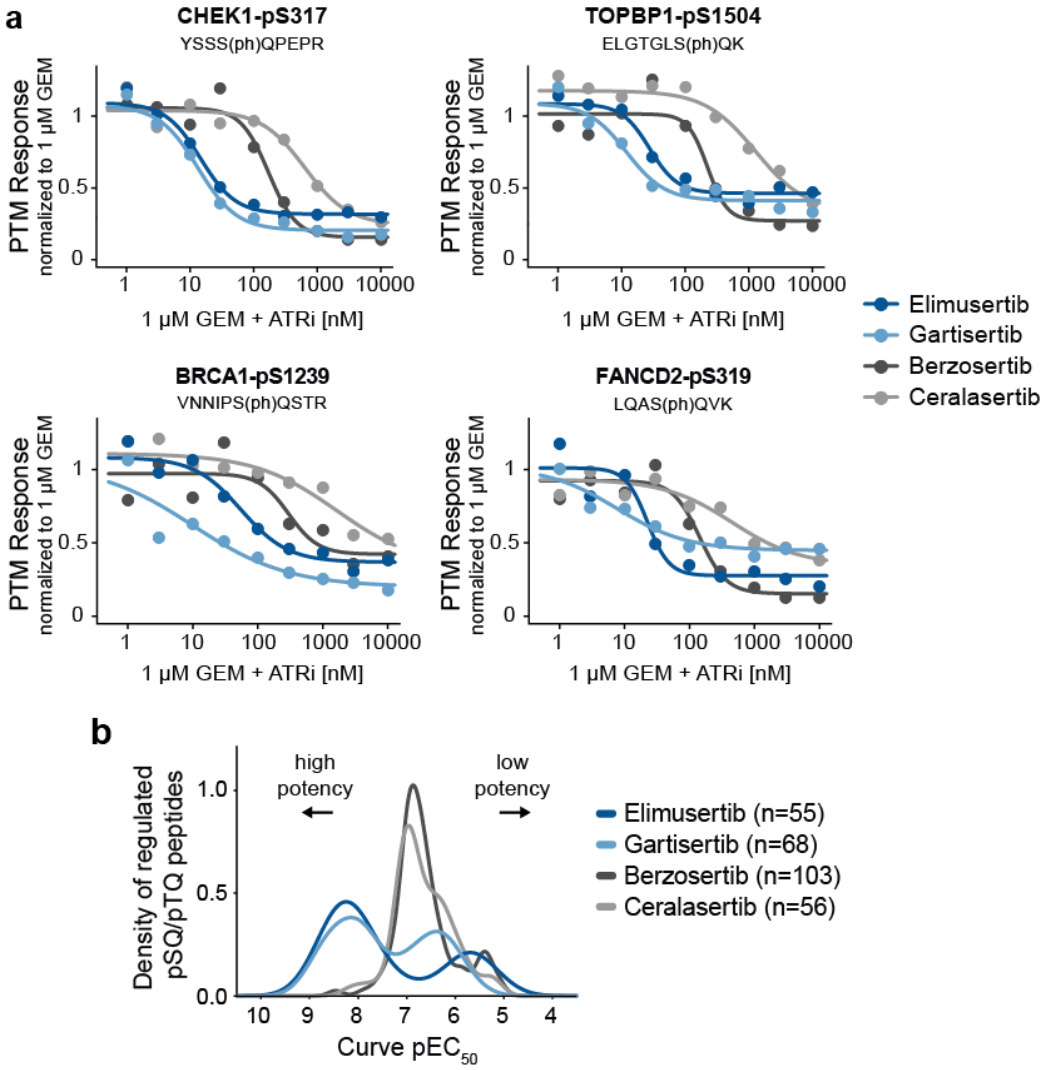

Figure 28. Clinical ATR inhibitors interfere with ATR kinase signaling at different potencies. a) Dose-dependent inhibition of the known ATR substrates CHEK1-pS317, TOPBP1-pS1504, BRCA1-pS1239, and FANCD2-pS319 by four ATR inhibitors in DNA-damaged AsPC-1 cells. The PTM response was normalized to 1 µM GEM. **b)** Density of potencies (pEC_{50}) of all pSQ/pTQ peptides regulated by each of the four ATR inhibitors in DNA-damaged AsPC-1 cells. The numbers of regulated pSQ/pTQ peptides are given in the legend.

Overlap in 248 ATRi-regulated phosphopeptides declared as *bona fide* ATR signaling events. To pinpoint the drugs' mechanism that corresponds specifically to the inhibition of ATR kinase, only sites regulated by at least three of the four ATRi were considered for all further analysis and declared *bona fide* ATR-dependent phosphorylation events. This resulted in 298 ATRi-regulated peptides attributed to ATR inhibition, including 42 pSQ/pTQ sites (**Figure 29**; pSQ/pTQ sites see **Appendix 9**). Among the commonly regulated sites lacking the pSQ/pTQ motif were over 35

known direct substrates of cyclin-dependent kinases CDK1 and CDK2 (based on kinase-substrate relationship annotations from PhosphoSitePlus[147], as of February 2024). These encompassed regulated p-sites on the cell cycle regulator CHEK1 (pS268), the spindle assembly proteins TPX2 (pT72) and PRC1 (pT481), and the proliferation marker MKI67/Ki67 (pT761; **Appendix 10**). CDK1 and CDK2 are critical cell cycle regulators downstream of the ATR-CHEK1 signaling axis, which generally remain inactivated in response to DNA damage to prevent cell cycle progression (Chapter 1.2.1). Hence, the observed increase in phosphorylation of CDK1 and CDK2 substrates indicates a failure to activate cell cycle checkpoints as a consequence of ATR pathway inhibition.

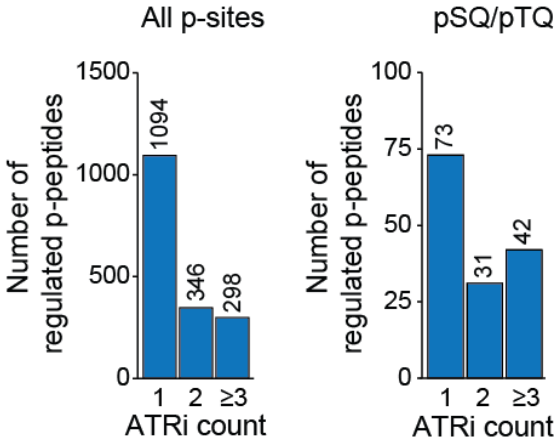

Figure 29. Numbers of all p-peptides (left) or pSQ/pTQ motif-containing peptides (right) regulated by one, two, or at least three ATR inhibitors in decryptM experiments.

3.3.3 Synergy with ATRi explained by partial blockage of GEM-induced DNA damage

GEM monotherapy activates DNA damage response and cell cycle control. To finally assess the molecular mechanism of synergy, the overlap in phospho-regulation between GEM and ATR inhibition was investigated. First, the cellular response to 1 µM GEM after 4 h (independent of ATRi) was compared to a vehicle control. From all quantified sites, GEM induced phosphorylation on 414 sites (216 up, 198 down; Student's t-test adjusted *p*-value < 0.01, absolute $\log_2$ fold change > 1, quantified in at least three of the four replicates). Strikingly, nearly two-thirds of all GEM-induced up-regulation events occurred on pSQ/pTQ peptides (135 of 216, or 62%; **Figure 30a**). Elevated phosphorylation occurred on the ATR substrate CHEK1 (e.g., pS286, pS317) and the ATM substrate CHEK2 (e.g., pS260, pS379: all $\log_2$ fold change > 1.5 and adj. *p*-value < $1e^{-4}$; **Figure 30b**). Moreover, GEM significantly induced phosphorylation of the known DNA damage response markers H2AX-pS319 and KAP1/TRIM28-pS473 ($\log_2$ fold change > 1 and adj. *p*-value < $1e^{-4}$). Also, the phosphorylation of several cell cycle-related proteins was elevated in response to GEM. Remarkably, the proliferation marker MKI67 was inhibited in phosphorylation at 23 p-sites, including the known CDK1 substrate MKI67-pT761[212] ($\log_2$ fold change = -1.5, adj. *p*-value < $1e^{-4}$). Also, reduced phosphorylation was observed on the MKI67-interacting protein NIFK (pT223,

T279) and MYBL2, a transcription factor of genes involved in cell cycle progression[213] (pT494; all log_2 fold changes < -1, adj. *p*-value < $1e^{-3}$). Further, the analysis revealed decreased phosphorylation on 11 p-sites on different histone H1 proteins, which control chromatin condensation and DNA accessibility throughout the cell cycle[214] (e.g., pT18 and pT147 on HIST1H1D; log_2 fold changes < -1.8, adj. *p*-value < $1e^{-4}$). Overall, this illustrates the activation of DNA damage response and cell cycle control in response to GEM, corroborating the findings of the time-course experiment with the chemodrug in AsPC-1 cells above (Chapter 0).

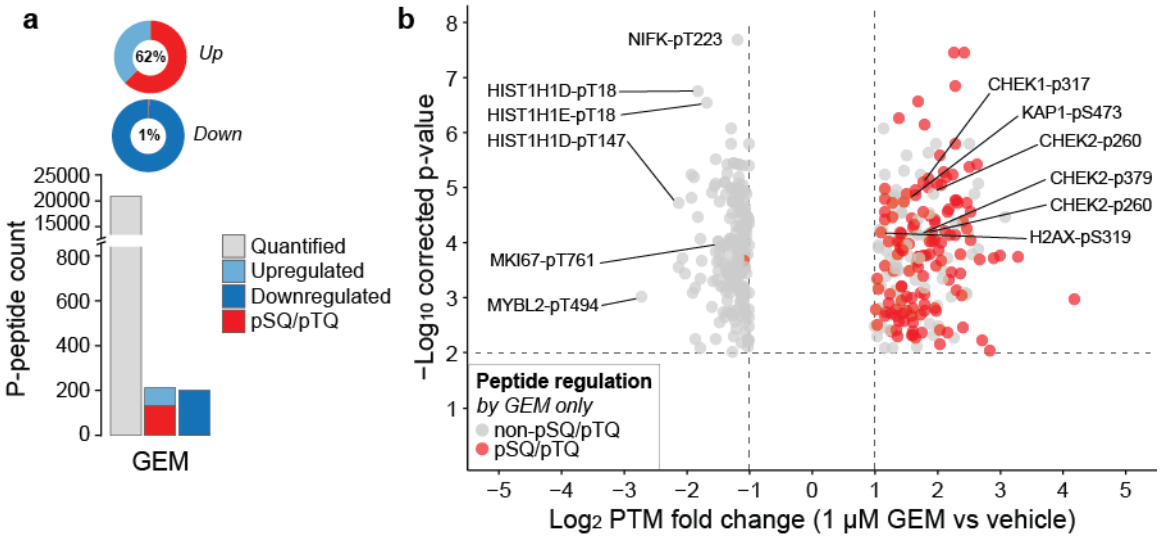

Figure 30. GEM induces DNA damage response in AsPC-1 cells after 4 h. a) Number of all quantified (grey), up-regulated (light blue), and down-regulated (dark blue) phosphorylated peptides upon treatment of AsPC-1 cells with 1 µM GEM for 4 h (n = 4). Peptides containing the pSQ/pTQ motif are highlighted in red. The pie charts indicate the fraction of pSQ/pTQ-containing peptides within the up- or down-regulated phospho-proteome. **b)** Volcano plot showing significantly regulated p-sites upon 1 µM GEM for 4 h in AsPC-1 cells (Student's t-test, n = 4; log_2 fold change > 1, adj. *p*-value < 0.01). *P*-values were corrected for multiple hypothesis testing using the Benjamini–Hochberg procedure. Peptides containing the pSQ/pTQ motif are shown in red. Selected sites are annotated by text.

The combination of GEM and ATRi regulates 164 p-peptides, including 36 pSQ/pTQ sites. Next, the overlap in GEM- and ATRi-regulated sites was investigated. From all GEM-affected p-peptides, 164 peptides (40%) were countered upon the combination with ATRi, potentially explaining drug synergy (**Figure 31a,b**). Thereby, ATR inhibition blocked GEM-induced phosphorylation on 62 p-peptides, including 36 pSQ/pTQ sites, and restored GEM-inhibited phosphorylation on 102 p-peptides (**Appendix 11**; **Appendix 12**). Interestingly, the ATRi-blocked 36 pSQ/pTQ sites comprised only one-third of all GEM-activated pSQ/pTQ phosphorylation events (36 of 135, or 28%). This illustrates that only a small part of the DNA damage response induced by GEM is responsible for drug synergy.

In line with this partial blockage in DNA damage response, ATR inhibition restored half of the GEM-blocked non-pSQ/pTQ sites involving cell cycle-regulated proteins (102 of 198, or 51%). For instance, 17 non-pSQ/pTQ sites were known CDK1 and/or CDK2 substrates (**Appendix 11**). Moreover, the combination treatment restored phosphorylation on 13 of the 23 GEM-blocked p-

sites on MKI67, as well as 8 of the 11 GEM-inhibited p-sites on different H1 histone proteins. Also, all four ATRis fully restored phosphorylation of the transcription factor MYBL2-pT494, the site most strongly inhibited by GEM monotherapy (see above and **Appendix 12**). This data demonstrates the perturbed cell cycle regulation in response to the combination treatment via specific sites on effector proteins downstream of ATR kinase.

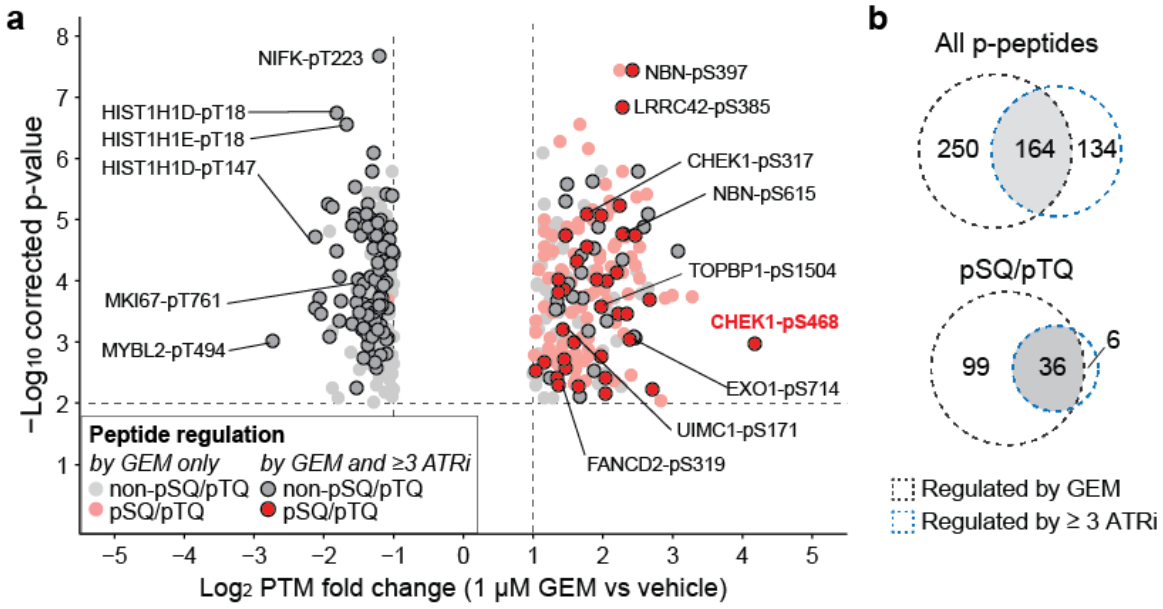

Figure 31. ATR inhibition counters 164 GEM-regulated p-sites, including 36 pSQ/pTQ sites. a) Significantly regulated p-peptides upon 1 µM GEM after 4 h in AsPC-1 cells compared to vehicle (Student's t-test, n = 4). *P*-values were corrected for multiple testing using the Benjamini–Hochberg procedure. P-peptides were either regulated by GEM but not ATRi (lighter color) or by GEM and at least three ATR inhibitors (darker color and encircled). Peptides with the pSQ/pTQ motif are shown in red. Selected sites are annotated by text. **b)** Venn diagram displaying the overlap in p-peptides regulated by GEM and at least three ATR inhibitors combined with GEM. Upper: all p-peptides, lower: pSQ/pTQ motif-containing peptides only.

The combination treatment affected different p-sites on the ATR effector protein CHEK1, including the previously mentioned pS317 (ATR substrate, pSQ/pTQ) and pS286 (CDK1/2 substrate, non-pSQ/pTQ). Both sites were significantly up-regulated by GEM by nearly 4-fold (log_2 fold change of 1.8 and 1.9; adj. *p*-values < $1e^{-5}$) and reduced back to baseline levels by all four ATRi (mean log_2 curve fold change < -2; **Figure 32a**). Nevertheless, the most strongly affected p-site in the dataset was CHEK1-pS468 (pSQ/pTQ), which was significantly increased > 18-fold in response to GEM (log_2 fold change of 4.2, adj. *p*-value ≈ $1e^{-3}$; **Figure 32a**) and erased by three of the four ATRi (mean log_2 curve fold change of -3.2; not quantified for Gartisertib; **Figure 32b**). The strong regulation by both GEM and ATRi suggests CHEK1-p468 as a potential pharmacodynamics biomarker for this combination.

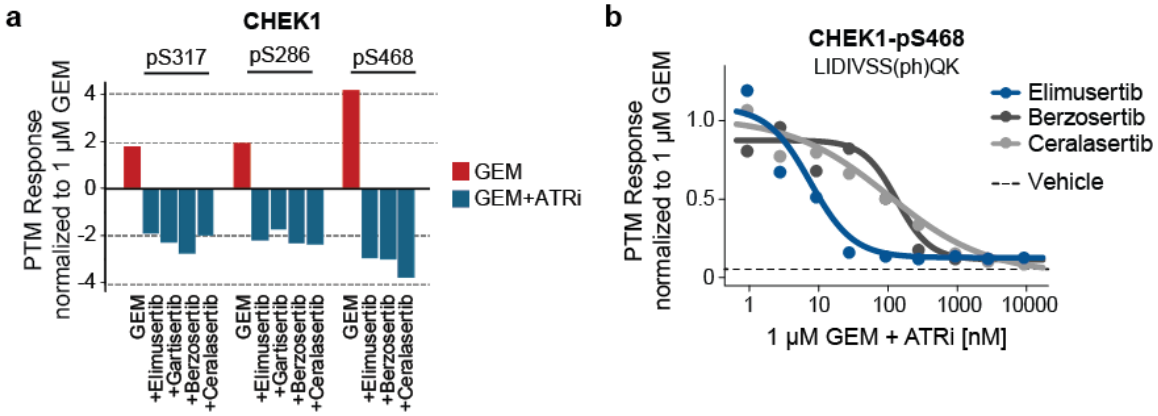

Figure 32. CHEK1 phosphorylation was induced by GEM and neutralized by subsequent ATR inhibition. a) Log_2 fold change in phosphorylation of CHEK1 pS317, pS286, and pS468 in AsPC-1 cells treated with GEM (red; n = 4) or GEM combined with ATR inhibitors (blue). **b)** Dose-dependent inhibition of CHEK1-pS468 by three ATR inhibitors in GEM-treated cells (not quantified for Gartisertib). The PTM response was normalized to 1 µM GEM. The dashed line marks the baseline phosphorylation in AsPC-1 cells treated with vehicle (normalized to 1 µM GEM).

The fact that large parts of the GEM-regulated phosphoproteome remained unaffected by ATR inhibition (60%; both pSQ/pTQ and non-pSQ/pTQ) indicates that GEM induces additional DNA damage response pathways, independent of ATR kinase. Although these non-overlapping phosphorylation events warrant further investigation, the following work was dedicated to characterizing only the counter-regulated, drug synergy-explaining p-sites.

3.3.4 Combined GEM and ATRi affect RNA processing and transcriptional control

Canonical ATR signaling covers one-quarter of the 36 synergy-explaining pSQ/pTQ sites. To further investigate the role of the regulated sites in cellular signaling, pathway enrichment, and visualization were performed using PTMNavigator[152]. The analysis was based on p-sites regulated by either GEM alone or both GEM and ATRi (in any direction; also non-pSQ/pTQ peptides). As expected, the two most enriched pathways were DNA damage response signaling via ATR (WikiPathways entry WP4016; enrichment score = 14.51) and cell cycle (KEGG pathway entry hsa04110; enrichment score = 11.50). The DNA damage signaling network covered 9 of the 36 ATRi-blocked pSQ/pTQ sites, including the aforementioned ATR substrates CHEK1 (pS317, pS468), TOPBP1 (pS1504), and FANCD2 (pS319; all pSQ/pTQ; **Figure 33**).

Interestingly, several proteins within this pathway were affected by GEM both in an ATR-dependent and ATR-independent fashion, depending on the phosphorylation site. For instance, on the DNA-crosslink repair protein FANCD2, the pSQ/pTQ site pS717 was induced by the chemodrug yet remained unaffected by ATR inhibition. Another example was BRCA1, a key mediator of homologous recombination, a DNA repair mechanism known to be orchestrated by ATM and ATR (Chapter 1.2.1). On BRCA1, seven p-sites were significantly elevated upon GEM, of which only two were blocked by subsequent ATR inhibition (pSQ/pTQ pS1239 and non-pSQ/pTQ pS1642; **Figure 33**). Similarly, other proteins involved in homologous recombination

were only partially affected in phosphorylation by the combination, namely BRCA1 interactor UIMC1 (or RAP80[215]; pS171 and pS597 ATR-dependent, pS250 ATR-independent) and NBN (or NBS1[216]; pS397 and pS615 ATR-dependent; pS58 and pS343 ATR-independent). Although heavily regulated by GEM, these sites do not explain drug synergy with ATRis and are likely phosphorylated by one of the other DNA damage response kinases.

Given that ATR and ATM share the same substrate preference (pSQ/pTQ) and both proteins were annotated within this signaling pathway, it was hypothesized that the ATR-independent cellular response to GEM likely occurred through activated ATM. This was supported by the fact that several proteins within the ATM-signaling axis were exclusively regulated by GEM but not ATRi (**Figure 33**). These included two sites on CHEK2, the well-described downstream effector of ATM (pS260 and pS379), and the commonly accepted marker of DNA double-strand breaks, H2AX[209] (pS139). Additional pSQ/pTQ sites affected by GEM but not ATRi were found on the chromatin-associated factors MDC1 (pS955, pS1086) and TP53BP1 (pS831), both of which are known to be recruited to the site of DNA damage, and more specifically, double-strand breaks, by H2AX[217]. Also, KAP1/TRIM28-pS473 was exclusively regulated by GEM but remained unaltered by ATR inhibition. These proteins are known to be involved in the ATM-mediated cell cycle regulation and repair of DNA double-strand breaks[218,219], clearly linking them to ATM kinase. This allows the assumption that the remaining ATR-independent phosphorylation events upon GEM found within this pathway were indeed likely orchestrated by ATM kinase.

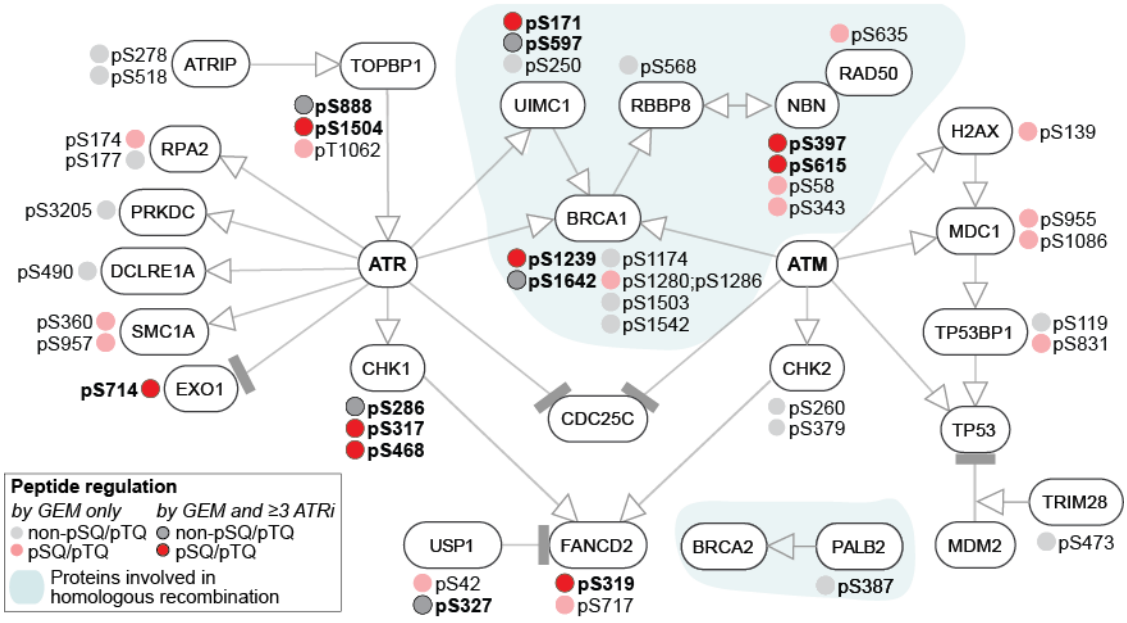

Figure 33. ATR signaling pathway (WP4016) and involved p-sites regulated by either GEM only (lighter color) or both GEM and ATR inhibition (darker color and encircled). Regulated pSQ/pTQ peptides are shown in red, and the quantified but non-regulated p-sites are shown in grey. The pathway was exported from pathway enrichment analysis using PTMNavigator[152]. Only selected pathway proteins are shown and p-site annotations were added manually.

STRING analysis links RNA processing and transcriptional regulation to canonical ATR signaling. The annotated ATR signaling network above included 9 of the 36 synergy-explaining pSQ/pTQ sites (on 7 different proteins), leaving the remaining sites without functional annotation (**Figure 34a**). However, given their similar regulation (induced by GEM and mitigated by ATRi) and the presence of the specific substrate motif, a connection to ATR kinase is likely. The data herein proposes these pSQ/pTQ sites to be potential novel ATR kinase substrates. Moreover, this data implies a crucial mechanistic role of these proteins in the ATR-mediated cellular response to GEM treatment.

To explore potential links to the DNA damage response pathway, STRING protein network analysis was performed on all proteins carrying the 36 pSQ/pTQ sites (32 proteins). Thereby, 12 proteins could be connected to the 7 proteins annotated in canonical ATR signaling based on evidence from curated databases, experimental data, or text mining (**Figure 34b**). These included proteins involved in protein homeostasis, such as the E3 ubiquitin ligases RAD18 (pS368) and UHRF1 (pS393) and the 26S proteasome component PSMD4 (pS266). Further, proteins involved in mRNA processing and transcriptional regulation were (indirectly) associated with the annotated ATR-signaling pathway proteins. These involved the spliceosome component SNRPA (pS115)[220], the splicing factor PNISR (pS706)[221], and the phosphatase PPM1G (pS201), which is involved in various cellular processes, including mRNA splicing[222]. Notably, these proteins were only indirectly linked to the ATR signaling members in the network *via* the chaperone HSP70 and the RNA helicase DHX9. Further evidence of the role of splicing in this context comes from non-pSQ/pTQ sites regulated by the combination treatment, e.g., PNN (pS66) or HNRNPM (pS481 and pS513; **Appendix 11**). Finally, the network analysis revealed an association to the three RNA elongation factors TCEB3 (pS251), TCEA1 (pS97;pS100)[223], and HTATSF1 (pS481)[224]. Noteworthy, the remaining 15 synergy-explaining pSQ/pTQ sites that could not be functionally linked to ATR signaling comprised multiple sites on transcriptional regulators, including HMGA1 (pS9, pS36, pS44), HDGF (pS103), and BRD8 (pS621; **Appendix 13**). Considering that overall, nearly one-third of all combination-affected pSQ/pTQ sites occurred on proteins involved in RNA processing or transcriptional regulation, this data implies a crucial mechanistic role of these cellular processes in drug synergy between GEM and ATRis.

Previously unknown ATR substrates emerge as potential biomarkers. Finally, a few of the combination-affected pSQ/pTQ sites lacked a clear association with ATR despite likely being direct substrates of this kinase. Intriguingly, these involved some of the most heavily GEM-induced sites in the dataset, including the cytosine methyltransferase NSUN5-pS432 (7-fold increase upon GEM, adj. p-value < $1e^{-2}$ and the leucine-rich protein LRRC42-pS385 (4.8-fold increase upon GEM, adj. p-value < $1e^{-6}$; **Figure 34a**; **Appendix 11**). Both sites were blocked in phosphorylation by at least three ATRis in a dose-dependent fashion, but the most outstanding counter-regulation was seen for

LRRC42-pS385, which was fully neutralized to baseline levels by all four ATRis, with EC_{50} values as low as < 10 nM (**Figure 34c**). The ATRi-blocked phosphorylation suggests a crucial functional role of LRRC42-pS385 and NSUN5-pS432 in (potentially non-canonical) ATR signaling after GEM treatment. Moreover, given their strong response, these sites may serve as pharmacological markers for the GEM-ATRi combination, in addition to the aforementioned CHEK1-pS468.

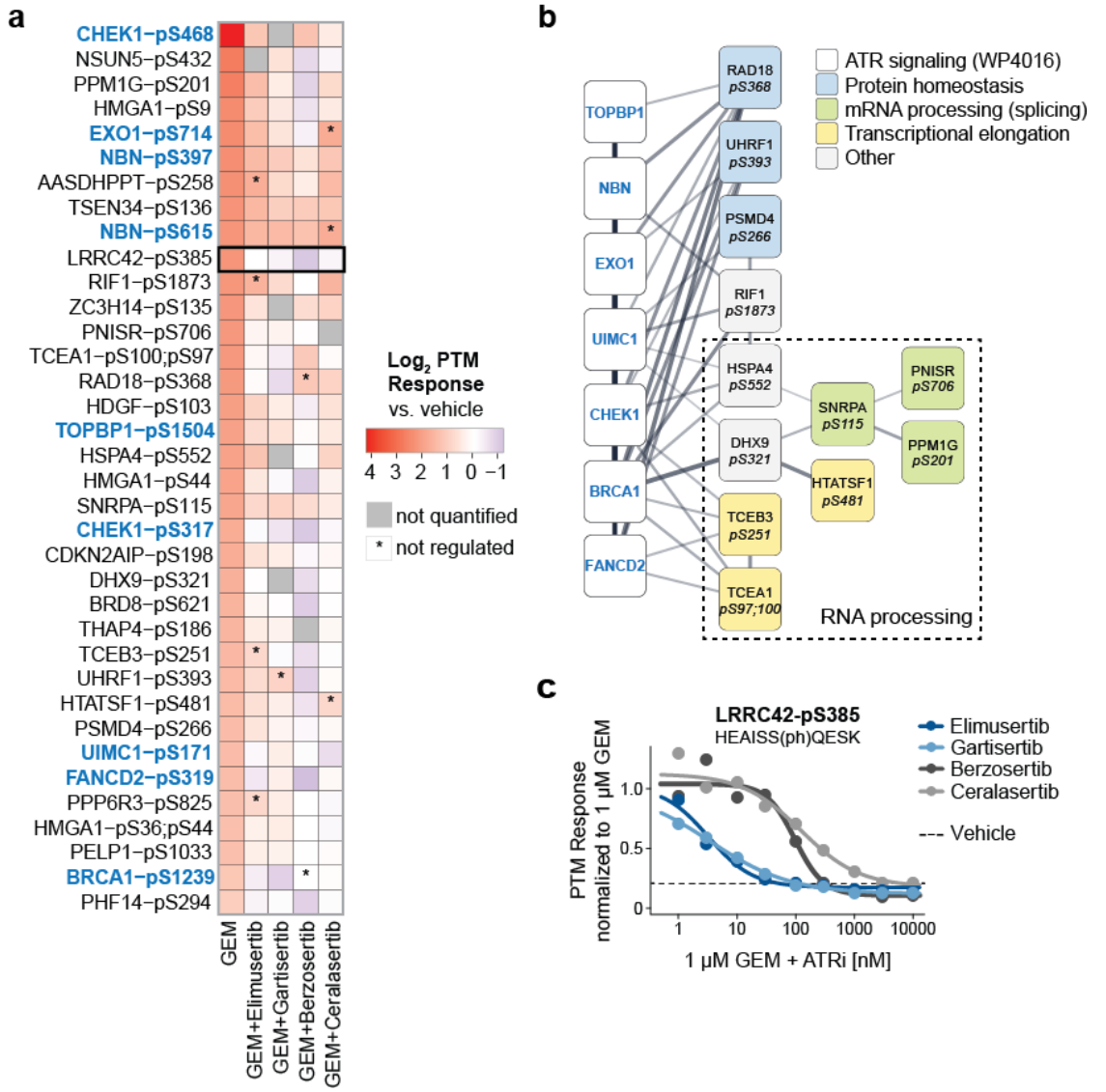

Figure 34. Analysis of the 36 synergy-explaining pSQ/pTQ sites. a) Heatmap showing the $\log_2$ PTM response of the 36 counter-regulated pSQ/pTQ peptides. Grey indicates missing values (not quantified), and asterisks indicate quantified but non-regulated peptides. The blue text highlights ATR signaling pathway proteins (WP4016). **b)** Resulting network from STRING analysis on all 32 proteins carrying the 36 pSQ/pTQ sites. Interaction information was based on experimental evidence, curated databases, or text mining. The blue text highlights ATR signaling pathway proteins (WP4016). Line thickness indicates the level of confidence. Functional annotations were retrieved from UniprotKB[139] and may not be complete. P-site information was added manually. **c)** Dose-dependent inhibition of LRRC42-pS385 by four ATR inhibitors in DNA-damaged AsPC-1 cells. The PTM response was normalized to 1 µM GEM. The red dashed line indicates the baseline phosphorylation in untreated cells relative to 1 µM GEM (n = 4).

3.3.5 GEM and Elimusertib conversely regulate expression of dNTP synthesis enzymes

GEM and Elimusertib regulate protein expression mainly after 12-24 h. Beyond sensing and tolerating DNA damage, ATR regulates cellular dNTP pools to preserve genome integrity (Chapter 1.2.2). Moreover, GEM is known to interfere with intracellular dNTP conversion enzymes, a drug action that has been linked to chemoresistance before (Chapter 1.1.2). However, the decryptM study above did not reveal mechanisms of drug synergy related to this function, as no enzymes involved in dNTP synthesis were directly affected in phosphorylation (based on the analysis of 101 proteins annotated in the nucleoside metabolism pathway HSA15869 in Reactome[225]). Investigating drug-induced changes in protein expression rather than phosphorylation might uncover such non-canonical activities of ATR kinase and their role in drug synergy with GEM. Therefore, two separate time-series experiments were conducted in AsPC-1 cells with either 1 µM GEM or 1 µM Elimusertib, and protein abundances were measured throughout 24 h (same time points as in Chapter 0). In total, 7,281 proteins were quantified, with an overlap of 6,386 proteins in both experiments. In response to GEM, 64 proteins displayed altered expression (17 up, 47 down; **Figure 35a**; **Appendix 14**). In contrast, treatment with the ATR inhibitor Elimusertib affected the expression of only 32 proteins (28 down, 4 up). The effect of protein expression by Elimusertib occurred at earlier time points yet was less extreme than that of the treatment with GEM (**Figure 35a**; **Appendix 14**).

GEM and Elimusertib conversely regulate the expression of RRM2, WDR76, and TK1. One protein counter-regulated by GEM and ATRi was the ribonucleotide reductase subunit RRM2. Protein levels of RRM2 increased in response to GEM (log_2 fold change = 1.6 at 24 h) and decreased in response to Elimusertib (log_2 fold change = -1.2 at 12 h; **Figure 35b**). Interestingly, the expression of RRM1, the other subunit of ribonucleotide reductase[29], remained unaffected by both treatments within 24 h (**Figure 35c**). The simultaneous but converse regulation of RRM2 levels highlights that ATR-driven dNTP pool regulation by RRM2, but not RRM1, is a critical mechanism of drug synergy. Additionally, WDR76, a protein possibly involved in various protein interactions at sites of DNA damage[226], was increased up to 2-fold in expression by GEM (log_2 fold change ≈ 1 at 24 h) and decreased up to 4-fold by Elimusertib (log_2 fold change = -2 at 24 h; **Figure 35b**).

Finally, to gain more insight into the regulation of dNTP metabolism proteins, other proteins involved in dNTP synthesis were examined based on the Reactome-annotated pathway HSA15869 (see above). Of the 101 annotated proteins, only four were regulated by GEM, ATRi, or both, including RRM2 (here, defined as abs. log_2 fold change > 1 at any time point; **Figure 35d**). These included thymidine kinase 1 (TK1) and carbamoyl-phosphate synthetase 2 (CAD), which were up-regulated more than 2-fold after 24 h of GEM exposure. However, only TK1 was mildly down-

regulated by ATR inhibition (log_2 fold change = -0.8 at 24 h), suggesting a potential role of TK1 in drug synergy. The third affected dNTP pool regulator, thymidylate synthase (TYMS), was steadily reduced by ATR inhibition from 12 h onward (down to log_2 fold change = -1.5 at 24 h). However, since no significant regulation was observed in response to GEM (log_2 fold change < -0.5), the contribution of TYMS to drug synergy remains unclear from this data. Nevertheless, the overall results suggest that perturbed dNTP homeostasis by GEM and ATR inhibition likely plays a mechanistic role in drug synergy.

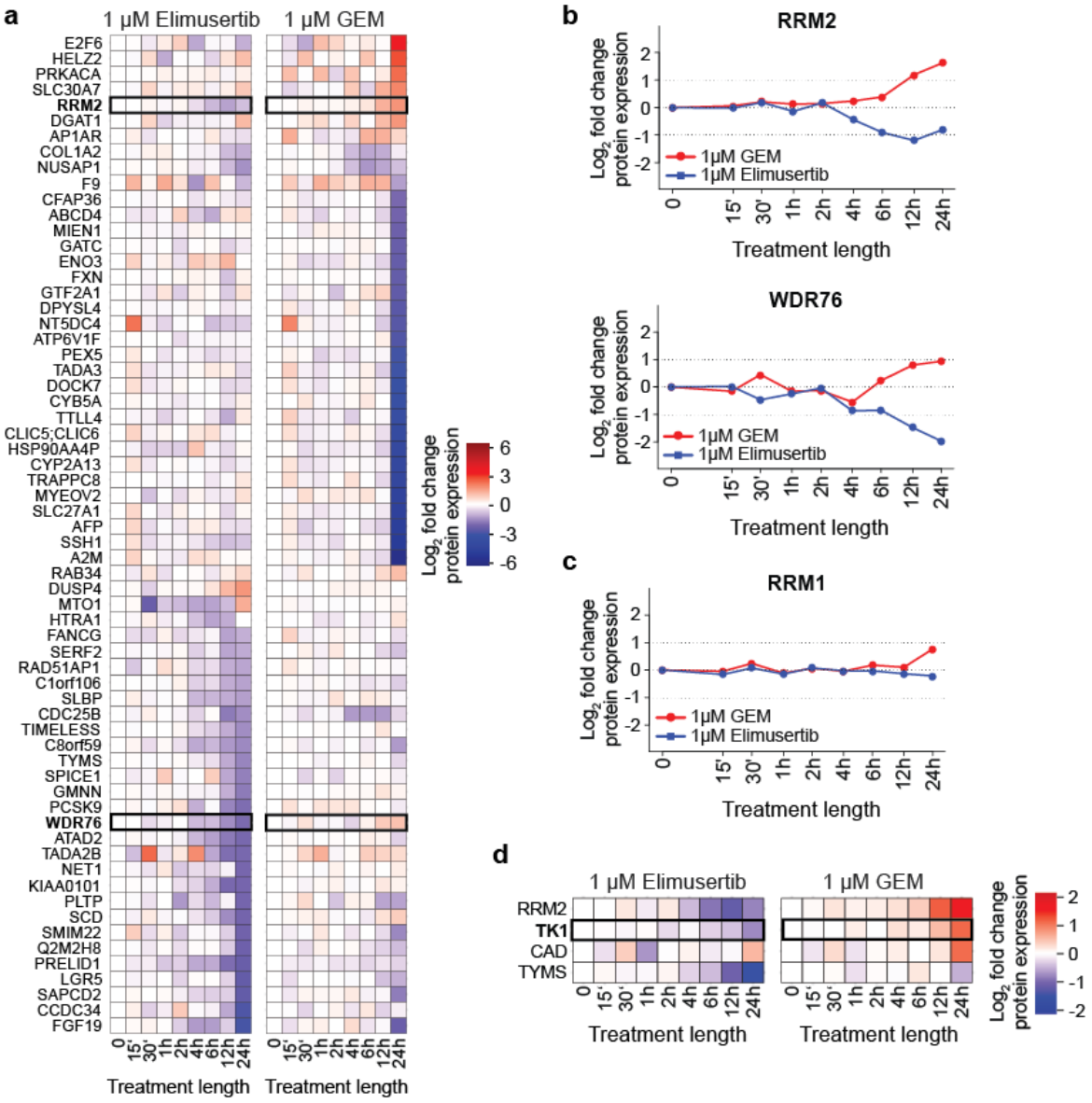

Figure 35. Time-series experiment reveals protein expression changes of enzymes involved in nucleotide synthesis. **a.** Log_2 fold changes in regulated protein expression in AsPC-1 cells treated with 1 µM GEM or 1 µM Elimusertib over time relative to untreated cells. Rectangles highlight the counter-regulated protein levels of RRM2 and WDR76. Regulation was defined as absolute log_2 fold change > 1 in at least two consecutive time points or > 2 at 24 h. **b-c.** Log_2 fold change in protein expression over time upon treatment with 1 µM GEM (red) or 1 µM Elimusertib (blue) of RRM2 (panel b, upper), WDR76 (panel b, lower), and RRM1 (panel c). **d.** Log_2 fold change in protein expression of four proteins involved in nucleotide metabolism. The rectangle highlights the counter-regulated protein levels of TK1. In all plots, the treatment length is given in hours (h) or minutes (').

3.3.6 Discussion

Synergy between GEM and ATRis is explained by the abrogation of ATR-mediated DNA damage response signaling. One primary goal of this study was to reveal potential mechanisms of drug synergy between GEM and ATR inhibition in PDAC cells. Therefore, the phosphoproteome changes upon GEM and its combination with ATR inhibition were investigated in the PDAC cell line AsPC-1. The analysis identified 164 p-peptides, including 36 pSQ/pTQ sites, to be blocked in phosphorylation by the combination treatment, explaining drug synergy. One-quarter of these 36 putative ATR substrates were on several known direct downstream effectors involved in cell cycle control and DNA repair, such as CHEK1, TOPBP1, FANCD2, and BRCA1 (Chapter 3.3.3), clearly linking canonical ATR signaling to the mechanism of drug synergy. These findings corroborate prior small-scale studies that reported the block of CHEK1-phosphorylation upon combined GEM and ATR inhibition[69,181] and align well with the anticipated mode of action of GEM to induce replication stress in cells (Chapter 1.1.2).

In addition, another important synergy mechanism revealed in this study was the ATR-mediated regulation of mRNA processing and translation in response to GEM. Several of the combination-affected phosphorylation events were on splicing factors (e.g., on SNRPA, PNISR, and PPM1G) and transcriptional elongation proteins (e.g., on TCEB3, TCEA1, and HTATSF1), indicating a crucial role of ATR kinase in RNA metabolism (Chapter 3.3.4). It has been widely recognized that the regulation of RNA metabolism is crucial in cellular DNA damage response[227-229]. For instance, splicing of mRNAs controls the expression of components for DNA damage repair, apoptosis, and cell cycle by creating splicing variants that harbor potentially distinct and sometimes opposite activities[228]. This implies that the regulation of RNA processing by ATR likely serves its canonical function in coping with GEM-induced replication stress, more specifically by cell cycle control and induction of DNA damage repair pathways.

Moreover, previous studies evidenced that already at the early steps of the DNA damage response, splicing-related proteins are regulated by phosphorylation, affecting their localization and activity directly at sites of DNA damage[230]. For example, in UV-treated cells, it was shown that ATM triggers the re-localization of the spliceosome to sites of newly formed R-loops, promoting the removal of these transcription-blocking lesions[230,231]. Although such evidence for ATR and GEM is lacking, the ATR-dependent regulation of the spliceosome subunit SNRPA[220] at pS115 (pSQ/pTQ) in response to the insertion of GEM into DNA could result from a similar mechanism. Another affected splicing factor was the phosphatase PPM1G, which is involved in pre-mRNA splicing[232] (pS201; pSQ/pTQ). PPM1G was previously shown to be phosphorylated in response to irradiation and subsequently recruited to the site of DNA damage[233]. However, the exact targets of this phosphatase and how they affect the cellular response to DNA damage, let alone GEM, remain

unclear at this stage[233]. In fact, the functional role of most of the newly discovered ATR substrates RNA processing substrates has not been elucidated yet in the context of ATR or GEM, warranting further investigation into their exact role in drug synergy. Taken together, this data provides strong evidence that the blockage of GEM-induced (non-)canonical ATR signaling in cell cycle control, DNA repair, and RNA processing, explains drug synergy with ATR inhibitors.

This study complements prior phosphoproteomic data on ATRis and the DNA damage response. MS-based phosphoproteomics has been employed before to investigate the molecular mechanism of ATR inhibitors in other cancer entities, including the clinical drugs Elimusertib (neuroblastoma)[234] and Ceralasertib (gastric cancer)[235], and the pre-clinical compounds VE-821 (leukemia)[236,237] and AZ20 (lymphoma)[238]. Most relevant to the current work is a very recent study in which Jadav et al. (2024) used phosphoproteomics to reveal the molecular mechanism of ATRis Berzosertib and Gartisertib in US-O2 osteosarcoma cells treated with the DNA-damaging agent hydroxyurea, an inhibitor of ribonucleotide reductase[239]. Despite specific differences, such as the selected chemodrug for DNA damage induction (GEM vs. hydroxyurea), the biological context (PDAC vs. sarcoma), and the experimental treatment design (4 vs. 2 ATRi, treatment dosing, and scheduling), half of the 36 regulated pSQ/pTQ sites presented herein were also regulated in their study[239] (**Appendix 13**). This partial overlap confirms the robustness of the ATRi-regulated phosphoproteome data presented herein. Moreover, the fact that GEM and hydroxyurea share similar modes of action supports the idea that the abrogation of the ATR-mediated replication stress response mainly drives drug synergy. This implies that ATRi may also synergize with other DNA-damaging chemotherapy, especially with antimetabolites.

A total of 18 synergy-explaining pSQ/pTQ sites were not found regulated in the work of Jadav et al.[239] (**Appendix 13**). These additional sites could arise from a greater phosphoproteomic depth or the aforementioned experimental differences. However, these phosphorylation events may also be unique to the mode of action of GEM, compared to hydroxyurea, and thus pinpoint potential differences in drug synergy between ATRis and other chemodrugs. Among these 18 pSQ/pTQ sites were 13 newly identified ATR substrates that have neither been reported by Jadav et al. nor by another large, pivotal phosphoproteomic study on the cellular DNA damage response, comprising > 700 putative ATM or ATR substrates (pSQ/pTQ sites; **Appendix 13**)[73,239]. This illustrates the depth of acquired data and the contribution of this phosphoproteomic resource to a better understanding of ATR kinase signaling.

Identification of novel phosphorylation biomarkers for the GEM-ATRi combination. In this work, several phosphorylation sites emerged as potential biomarkers. Notably, the pSQ/pTQ site CHEK1-pS468 exhibited an over 18-fold increase upon GEM treatment and complete reversion by ATR inhibition. This significant regulation was the highest among all quantified phosphorylation sites, underscoring CHEK1-pS468 as a promising mechanistic marker for the GEM-ATR inhibitor

combination. Despite the established role of CHEK1 in DNA damage signaling, the p-site pS468 is not well characterized, with only one prior study investigating its phosphorylation over 20 years ago[70]. Intriguingly, that study reported no change in CHEK1-pS468 levels in response to UV or hydroxyurea in HEK 293 cells[70]. These findings prompt further investigation into the functional role of CHEK1-pS468 in ATR signaling in response to GEM-induced replication stress. Given the established role of CHEK1, a function of CHEK1-pS468 in canonical ATR signaling and cell cycle control is likely.

Another potential pharmacodynamic marker was NSUN5-pS432 (pSQ/pTQ), which was increased seven-fold by GEM and neutralized by three ATR inhibitors. NSUN5 is an rRNA methyltransferase that affects the structural composition of ribosomes and promotes translational fidelity[240]. The pSQ/pTQ site pS432 was previously found to be regulated in response to ionizing radiation, though it remained unclear whether its phosphorylation was mediated by ATR or ATM[73]. The data herein suggest this site as a specific substrate of ATR kinase. In yeast, NSUN5 was shown to regulate the synthesis of oxidative stress-responsive proteins involved in cell cycle control and DNA damage repair[240], suggesting a similar role for NSUN5-pS432 in the GEM-mediated replication stress response.

LRRC42-pS385 (pSQ/pTQ) also emerged as a marker candidate, showing a nearly 5-fold increase upon GEM and complete blockage by all four clinical ATRi. LRRC42 belongs to the leucine-rich repeat protein family, which is involved in protein-protein interactions and found in various cellular processes, including signal transduction, transcriptional regulation, and immune response[241]. Although the exact function of LRRC42 remains largely uncharacterized, some cancer-related studies suggest a role in lung carcinogenesis[242] and report its overexpression in breast tumors[243]. Phosphorylation of LRRC42-pS385 has not been reported previously, rendering it a novel candidate for further investigation in the context of DNA damage and ATR signaling.

One of the aims of the ongoing clinical investigation of GEM with ATRi Elimusertib in PDAC is to establish pharmacodynamic biomarkers that confirm ATR target engagement *in vivo* (NCT04616534). While pH2AX and pKAP1/TRIM28 have been used in these trials as a marker of DNA damage response[244,245], they lack specificity to ATR, as they are more frequently reported as substrates of ATM[209,219]. The proposed biomarkers in this study are more closely associated with ATR-dependent signaling mechanisms and may offer greater specificity for the combination of GEM and ATRi. Nevertheless, the suggested phosphorylation markers require extensive validation in additional cell lines or clinically more advanced systems, such as patient-derived organoids or xenograft models.

Moreover, the functional role of these p-sites remains to be elucidated. This could be achieved by site-directed mutagenesis experiments to uncover their functional role in ATR-mediated replication

stress response and DNA repair efficiency. For LRCC42, protein-protein interaction assays, including yeast two-hybrid, co-immunoprecipitation, or proximity ligation experiments, could identify binding partners that may hint at a role in ATR-related cellular processes. Also, cellular knockdown or knockout models of these proteins could be tested for altered phenotypic and molecular readouts upon DNA damage induction and/or ATR inhibition.

This study allows to distinguish ATR-dependent from ATR-independent DNA damage response signaling. Large parts of the phosphoproteomic analysis in this work relied on the pSQ/pTQ substrate motif, which is specific to both ATR and ATM. This approach is common in the large-scale study of cellular DNA damage response[73,230,231,246], yet it hampers the differentiation between ATR- and ATM-mediated signaling. For instance, the work mentioned above by Matsuoka et al. (2007) generated an extensive resource of over 700 regulated pSQ/pTQ sites in cells treated with UV, representing one of the most frequently referenced ATM/ATR substrate datasets to date[73]. However, their data does not differentiate between ATR or ATM substrates, and the two kinases were mainly used synonymously in their study[73]. Similarly, another MS-based phosphoproteomics study identified over 80 p-peptides levels to change upon induction of DSBs via irradiation and assigned these *ad hoc* to ATM kinase[230] solely based on the presence of the pSQ/pTQ motif. However, it was previously shown that not all DSB-induced phosphorylation changes occur through ATM[231], and that ATR may be indirectly activated from single-stranded DNA at DSBs as well[247].

Herein, the phosphoproteomic profiling of four different ATR inhibitors, together with the fact that no off-target binding to ATM was observed (Chapter 3.2.1), clearly indicates that the observed drug synergy with GEM was rooted in abrogated DNA damage signaling via ATR and not ATM. This also aligns with the fact that ATM inhibition (via AZD-0156) did not display synergy with GEM in the initial phenotypic drug combination screen (median ΣAUC_{Δ} across all cell lines < 2%; Chapter 3.1.3). Although there is still the possibility that some of these pSQ/pTQ sites arise from signaling crosstalk between ATM and ATR[181,247], these data that combined target profiles with phosphoproteomic experiments show that these sites can indeed be distinguished. As a potential follow-up, experiments with ATM inhibitor(s) may verify ATR- and ATM-specific substrates in response to GEM-induced replication stress. This could complement the ATR inhibitor-specific data and provide a better understanding of the highly complex DNA damage signaling network.

In this work, a substantial number of peptides that explained drug synergy lacked the pSQ/pTQ motif (> 120). However, functional enrichment could link most of them to either cell cycle regulation (mostly down-regulated by GEM and rescued by ATRis) or DNA damage response-related processes (mainly up-regulated by GEM and blocked by ATRis). These were likely also the indirect downstream consequences of ATR and not ATM. However, the exact role of many of these sites in ATR-mediated replication stress response has yet to be explored by the community.

DecryptM revealed ATRi Elimusertib to have the most potent and selective on-target activity *in cellulo*. Prior phosphoproteomic studies on ATRi often applied single, arbitrarily high doses (up to 10 µM) and prolonged incubation times (10-24 h)[235-238]. Here, the use of decryptM provided information on the potency with which ATR inhibitors induce direct DNA damage response. Thereby, the evidence-based selection of 4 h pre-incubation with GEM guaranteed that activating phosphorylation sites on crucial and known ATR substrates are exactly then or shortly before that downregulated. This helped to limit the observed changes in the phosphoproteome to direct ATR inhibition.

An interesting discovery was that the four clinical ATRi Elimusertib, Gartisertib, Berzosertib, and Ceralasertib engaged their putative target in cells at different potencies, which corresponded to their phenotypic efficacy. A similar observation was shown in prior decryptM experiments on lysine deacetylase inhibitors, where direct substrate activity correlated with phenotypic outcome[135]. This demonstrates that cellular target engagement, as reflected by inhibition of these pSQ/pTQ sites indeed corresponds to the therapeutic efficacy, highlighting the validity of the proposed pharmacodynamics biomarkers herein. Also, the analysis demonstrated that decryptM could elucidate the complex interplay of overall effects and off-target modulation, revealing connections between the drugs' direct target engagement and indirect downstream signaling by their potency of regulation. Moreover, the comparative analysis of drug potencies revealed precise mechanistic differences between drugs, even from within the same target class. Here, the fact that ATRi Elimusertib revealed the highest on-target potency while displaying the least amount of potential off-target engagement among *in cellulo* suggests that Elimusertib should be prioritized in future clinical investigations over the other clinical ATRi. Overall, this highlights the potential of phosphoproteome potency to gain clinically relevant mechanistic details on therapeutics, as previously outlined by Zecha et al. (2023)[102].

Expression regulation of RRM2, TK1, and WDR76 levels indicates some known and novel non-canonical actions of ATR. In addition to phosphoproteomics, changes in protein expression were investigated over 24 h to reveal non-canonical mechanisms of ATR that could explain drug synergy with GEM. Most strikingly, expression levels of the regulatory subunit of ribonucleotide reductase RRM2 were elevated upon GEM and decreased by ATR inhibition from 12 h onwards. This observation aligns with the established role of ATR kinase in dNTP pool regulation. ATR kinase induces the accumulation of RRM2 in the nucleus during the S-phase to cope with replication stress[248], and the inhibition of ATR-CHEK1 signaling was shown to induce CDK2-mediated proteasomal degradation of RRM2[249]. This explains the active regulation of RRM2 levels by ATRi observed herein, even in the absence of GEM. Given GEM's known mechanism of blocking ribonucleotide reductase activity (Chapter 1.1.2), the elevated expression of RRM2 in response to GEM may arise as a compensatory mechanism to counteract the loss of this enzyme's activity. A

similar observation was reported in a prior study, where elevated RRM2 levels were seen in response to hydroxyurea and reduced levels upon CHEK1 depletion[250]. Simultaneous co-treatment with GEM and ATR inhibitors may prevent compensatory up-regulation of RRM2 by ATR, ultimately accelerating dNTP pool deficiencies and promoting cell death – explaining synergy.

Interestingly, protein levels of RRM1, the other subunit of ribonucleotide reductase, remained completely unaffected by both drugs, although prior studies have linked RRM1 to GEM. For instance, increased RRM1 levels were observed in PDAC patients 24 hours after GEM exposure[251] and were associated with chemoresistance[36,252]. Additionally, phosphorylation of RRM1 was shown to affect ATR activity[253]. These controversial findings *in vivo* indicate that RRM1 likely still plays a role in drug synergy, although this could not be confirmed by the data herein in a single PDAC cell line. Nevertheless, it would be interesting to learn why the combination of GEM and ATRi affected ribonucleotide reductase specifically by RRM2, and not RRM1, in AsPC-1 cells, and whether some tissue-specificity exists that may be of clinical relevance.

Another affected dNTP metabolism protein was the dTTP synthesis enzyme thymidylate kinase 1 (TK1). Although to a lesser extent than RRM2, TK1 was also elevated in response to GEM and decreased by ATRi Elimusertib. Although current literature does not suggest any link between ATR kinase and TK1 regulation, GEM is known to inhibit another enzyme involved in dTTP synthesis, thymidylate synthase (TYMS; Chapter 1.1.2). Hence, the increase in TK1 levels may be a compensatory mechanism (mediated by ATR) in response to GEM-inhibited TYMS activity. However, in this work, TYMS was only affected in expression by the ATRi but remained largely unaffected by GEM (Chapter 1.1.2), rendering it unclear whether GEM indeed affected TYMS activity. An alternative interpretation may be that TK1 expression levels were regulated by GEM directly, presenting a potential novel mode of action of the chemodrug. These hypotheses require further evaluation to understand the true mechanism by which GEM reduces TK1 levels. Moreover, no prior evidence of ATR-mediated regulation of neither TK1 nor TYMS has been reported. Hence, this work revealed a potential novel non-canonical activity of ATR in regulating these enzymes' expression levels, warranting further validation.

Finally, expression levels of WDR76 were also conversely regulated by GEM (up) and ATRi Elimusertib (down). WDR76 is a hub protein involved in over 100 protein interactions related to base excision repair, mismatch repair, and homologous recombination[226]. In response to GEM-induced replication stress, ATR kinase may increase WDR76 levels to enhance these DNA repair processes, providing a potential explanation for why ATR inhibition sensitizes cells to GEM treatment. However, this hypothesis necessitates further verification, as no established context currently links ATR kinase or GEM to WDR76 regulation.

Taken together, global proteome profiling linked non-canonical functions of ATR kinase, most importantly the regulation of dNTP pools, to the mechanism of drug synergy. The ATR-dependent regulation of these enzymes could be further validated on mRNA levels or by measuring enzyme activity in the presence of these drugs by metabolomics. Such novel insights into the non-canonical functions of ATR kinase could ultimately help the search for potential sensitivity-predicting markers or alternative therapies against these pathways.

4 General Discussion and Outlook

4.1 A phenotypic resource to explore the potential of targeted therapies in PDAC

Phenotypic screening reveals the unexplored potential of targeted therapies in PDAC. PDAC is a devastating disease in urgent need of novel therapeutics, as resistance to systemic chemotherapy, such as the DNA-damaging agent GEM, remains a persistent issue. In the effort to overcome chemoresistance, the community has recognized combining classical chemotherapy with targeted inhibitors as a promising strategy. Since the clinical approval of EGFR inhibitor Erlotinib with GEM some 15 years ago, a high interest in GEM-based combinations with molecularly targeted drugs emerged, with more than 50 additional inhibitors having been investigated in PDAC (Chapter 1.1.3). However, the fact that GEM combined with Erlotinib remains the only approved regimen implies significant hurdles in developing such clinically successful combinations.

The phenotypic characterization of drug efficacy in pre-clinical disease models is essential for advancing treatments to clinical settings. Despite extensive combination screenings of targeted inhibitors in other cancers, the systematic assessment of their efficacy, let alone their drug synergy with chemodrugs, in PDAC remains underrepresented[185,189-191,254]. This work addresses this critical gap by providing a comprehensive phenotypic profiling of 13 PDAC cell lines against 146 targeted inhibitors, alone and in combination with GEM. The drug screen stands out for its strong clinical relevance, as it covers most of the over 80 clinical inhibitors approved to date[51], along with many late-phase compounds (mostly phase III). By focusing on approved or clinically advanced drugs, this screen builds upon extensive *in vivo* investigations already made on these compounds. Since developing novel bioactive substances from scratch is extremely time-consuming, costly, and rarely leads to clinical success[255,256], this phenotypic resource of clinically relevant compounds provides an efficient alternative to identify new treatment options for PDAC.

Several clinically advanced or approved drugs emerged from this work as promising repurposing candidates based on their broad efficacy in monotherapy (22 drugs) and/or combined with GEM (18 drugs) in PDAC cells (Chapter 3.1.5). For example, this work suggested two potential candidates for drug repurposing (PLK1 inhibitor Volasertib and SRC inhibitor Tirbanibulin) and supported the ongoing clinical evaluation of Sapanisertib in PDAC. Moreover, although this work focused on the combination of GEM and ATR inhibitors, other (classes of) inhibitors synergized with GEM, albeit only in specific cellular contexts. For instance, three mTOR inhibitors synergized with GEM in a subset of 3 PDAC cell lines, and the inhibition of WEE1 chemo-sensitized near half of the cell line panel. These drugs and combinations represent only a few that emerged from this

screen as potential repurposing candidates and have not yet been investigated in PDAC (**Appendix 4** and **Appendix 5**). This illustrates the scope of this large phenotypic resource for further exploration and highlights the clinical potential of molecularly targeted therapy in PDAC, both alone and in combination with chemotherapy. Another insight was that phenotypic efficacy in PDAC is not limited to a specific class of targeted inhibitors. However, most drugs seemingly require specific molecular contexts to be efficacious, warranting the evaluation of responding PDAC subtypes for clinical follow-up.

The systemic lack of synergy between GEM and RTKi implies an urgent need for patient stratification. This phenotypic resource also illustrated challenges in developing effective GEM-based combination treatments in PDAC. One important finding was that drug synergy is a rare phenomenon, which has also been anticipated in prior large-scale combination studies [189-191]. Specifically, the drug screen herein was the first to reveal the systemic lack of drug synergy with GEM and RTK inhibitors (RTKis) *in vitro*, including Erlotinib. This aligns with post-approval clinical trials and meta-analyses reporting only a modest clinical benefit of GEM and Erlotinib or even the complete lack thereof[257-259]. Intriguingly, following negative clinical results of EGFR-directed therapy in KRAS-mutant colorectal cancer, Erlotinib has been 'effectively abandoned by the community' as stated by Luo (2021)[44].

All of the above raises concerns about the clinical use of GEM and Erlotinib in PDAC. Nevertheless, there remains a high clinical interest in other RTKis as anti-cancer therapeutics. For instance, RTKis have been most frequently tested in combination with GEM compared to other inhibitors (11 RTKis in total, including Erlotinib), and two novel trials on GEM and RTKis have been initiated in PDAC just within the past three years (Anlotinib and Surufatinib; **Appendix 1**). Based on this work, it is likely that such combinations may only be clinically successful in rare PDAC contexts, prompting the need for biomarkers to enable patient stratification. In non-small cell lung cancer, Erlotinib is explicitly approved for patients bearing activating mutations EGFR[260]. However, no such biomarker could be identified for PDAC yet, neither for Erlotinib alone nor combined GEM and Erlotinib[261-263], illustrating disease-specific challenges in this endeavor.

Future large-scale proteomic studies can maximize clinical impact of the phenotypic data. Beyond providing evidence for (and against) specific therapeutic strategies, this tissue-specific viability data also builds the basis for future proteomic research into drug sensitivity and resistance mechanisms in PDAC. For example, drug response biomarkers may be identified by correlating the phenotypic drug sensitivity data to the baseline (phospho-)proteome levels of the tested PDAC models, as demonstrated in a recent study comprising 17 sarcoma cell lines and a similarly extensive inhibitor library[133]. Such experiments could detect predictive biomarkers for the therapeutic response (or resistance) to, e.g., GEM combined with mTOR or WEE1 inhibition, or identify molecular backgrounds that benefit the most from the broadly active combination of GEM and

ATRi Elimusertib. Ultimately, such protein or phosphorylation biomarkers may inform clinical trial design or build the basis of personalized treatment recommendations in molecular tumor boards.

For more mechanistic follow-ups, additional drug-perturbation experiments with MS-based global proteomic readouts could be conducted. The recently developed decryptE approach, evaluating drug-induced changes in protein levels under conditions similar to the viability screen (e.g., dose-dependent, long drug exposure), may explain phenotypes and cellular processes by the activity of proteins[264]. When applied systematically to the whole cell line panel, one may unveil tissue-specific mechanistic details and dependencies underlying phenotypic sensitivity. To increase the confidence and the clinical relevance of the findings, drug response biomarkers and mechanistic rationales could be further evaluated in more advanced pre-clinical disease models, potentially even across entities.

To facilitate data accessibility to the community, all drug sensitivity results are available through an interactive online platform on ProteomicsDB[154] (www.proteomicsdb.org/analytics/cellSensitivity, dataset 'Pancreatic_cancer'). This open-access resource should encourage researchers and clinicians to leverage the data for future investigations, hopefully supporting the ongoing efforts to find better therapeutic options for this challenging disease.

4.2 Challenges in studying a drug's mode of action by phosphoproteomics

The ultimate goal of any drug development campaign is its clinical success. However, given that the probability of early clinical compounds to be eventually launched is below 10%[265], there is a strong need for improved drug development strategies and clinical trial designs. Pre-clinical evidence of a drug's phenotypic efficacy often drives clinical entry decisions, sometimes without prior knowledge of the mode of action (MoA). However, knowledge of a drug's MoA can provide valuable insights that ultimately aid in promoting clinical success and preventing failure. Specifically, MS-based phosphoproteomics significantly supports drug discovery and development by identifying new targets, constructing pathways, and predicting drug efficacy and toxicity (Chapter 1.3.3). Nevertheless, its full potential in routine drug development and clinical decision-making is yet to be realized.

Sparse functional annotation hampers the biological interpretation of phosphoproteomic data. One current challenge is the sparse functional annotation of phosphorylation sites, which hampers the biological interpretation of phosphoproteomic data. Fast and sensitive LC-MS/MS technologies, together with highly optimized proteomic sample preparation workflows, enable the

quantification of over 20,000 p-sites from a single drug-perturbation experiment within only a few hours. This rapid generation of large datasets necessitates high-throughput data interpretation, typically based on enrichment analysis. However, current enrichment tools predominantly annotate phosphoproteomic data at the protein level, thus neglecting valuable site-specific information. Also, the underlying databases often rely on well-established pathway databases (e.g., KEGG, Reactome, or WikiPathways), which creates a bias towards frequently studied proteins and hinders the characterization of novel kinase substrates. For example, in this work, only one-quarter of the 36 synergy-explaining pSQ/pTQ sites regulated by GEM and ATRi could be associated with the canonical ATR signaling pathway through enrichment analysis. The remaining p-sites implicated in DNA damage response signaling required extensive and low-throughput literature research to be linked to ATR, as they were not yet included in well-established pathway annotations (Chapter 3.3.4).

This challenge is expected to diminish over time as more functional insights on phosphorylation sites are acquired and curated. Nevertheless, this prospect is delayed by the complex nature of protein phosphorylation, which challenges their experimental characterization. One complicating factor is that phosphorylation can lead to diverse outcomes, such as altered protein activity, localization, stability, or interactions with other biomolecules[118]. Investigating these outcomes can be costly, labor-intensive, and require special expertise, often limiting studies to a few prioritized phosphorylation sites. Furthermore, the lack of site-specific commercial antibodies for highly understudied phosphorylation sites can limit the options for functional studies. For instance, CHEK1-pS468 was proposed as a promising mechanistic marker of synergy between GEM and ATRi (Chapter 3.3.3). Despite CHEK1 being the best-known direct substrate of ATR kinase, phosphorylation at p468 has received little recognition in the scientific community[70,266], and no commercial antibody currently exists for this site.

The biological interpretation of phosphorylation is further complicated by the fact that individual p-sites on the same protein may elicit different functional roles. For example, while BRCA1 was regulated in response to GEM at seven p-sites, only three were counter-regulated by ATR inhibition, suggesting that BRCA1 takes part in both ATR-dependent and ATR-independent DNA damage response signaling (Chapter 3.3.3). In this context, discovering novel kinase substrates from phosphoproteomic studies often prompts their verification in orthogonal assays. However, this is particularly difficult when multiple kinases display a substantial overlap in substrates. For instance, ATR and ATM both share a strong preference for phosphorylating the pSQ/pTQ motif and share some substrates, although these kinases orchestrate different DNA damage response pathways[72,73]. Typical *in vitro* kinase-substrate assays, which utilize recombinant kinases and synthetic peptides, often show substantial overlap in substrate specificity between ATR and ATM, making it nearly impossible to assign individual substrates[72,207]. In contrast, cellular drug

perturbation with GEM and ATRi in this work effectively pinpointed individual pSQ/pTQ sites as novel ATR-specific substrates. This exemplifies that certain kinase-substrate relationships require more elaborate verification methods than typical *in vitro* activity assays, further complicating their experimental characterization.

Complementary techniques are required to fully understand a drug's MoA. Phosphorylation analysis alone may not capture all drug mechanisms. This becomes particularly relevant when kinases not only trigger signal transduction through protein phosphorylation but also regulate metabolic processes. An example in this work was the non-canonical role of ATR kinase in nucleotide (dNTP) metabolism, which was also affected by the treatment with GEM and ATRi (Chapter 3.3.5). MS-based phosphoproteomics infers kinase activity from phosphorylation levels of (downstream) protein substrates. However, metabolic kinases, such as dNTP pathway enzymes, phosphorylate small molecules or metabolites rather than other proteins[267], and thus, their activity is not captured in typical phosphoproteomic workflows. In this work, protein expression changes upon prolonged drug exposure with GEM and ATRi revealed drug effects on metabolic kinases involved in dNTP synthesis. However, the direct consequence on enzyme activity remains unclear from this protein-level readout. As an alternative (or complementary) approach, metabolomics could provide more direct evidence of drug-induced changes in metabolic kinase activity and, thus, the drugs' MoA.

Moreover, other PTMs beyond phosphorylation, such as ubiquitination, acetylation, and methylation, can provide critical insights into the mode of action of drugs, particularly those targeting DNA damage responses[268,269]. Ubiquitination, for example, plays a pivotal role in regulating protein degradation and signal transduction during DNA repair processes[270]. By examining changes in ubiquitination patterns, researchers can identify stabilized or degraded proteins in response to drug treatment, providing insights into how a drug affects protein turnover and DNA repair pathways. Acetylation, which affects protein function and interaction by modifying lysine residues, can also reveal how drugs influence chromatin structure and gene expression[268]. Methylation of histones and other proteins is another key PTM that regulates DNA repair by modulating protein interactions and chromatin dynamics. In this work, combined GEM and ATRi affected the phosphorylation of several ubiquitin ligases (e.g., BRCA1, RAD18), proteasome subunits (e.g., PSMD4), and chromatin-associated transcriptional regulators (e.g., HMGA1, BRD8). Hence, analysis of these additional PTMs could provide insights into the indirect consequences of perturbed kinase signaling. Prior studies have extended the use of dose-resolved phosphoproteomics (decryptM) to other PTMs, including acetylation and ubiquitination, demonstrating the feasibility of these experiments and the value in potency information on drug MoA[102,135]. In future approaches, integrating dose-resolved data from different PTMs can provide a more comprehensive understanding of how drugs or their combination affect cellular processes.

The translation of pre-clinical phosphoproteomic data to clinical relevance is yet to be determined. Finally, one of the most significant issues remains the yet unclear physiological implications and clinical interpretation of pre-clinical (phospho-)proteomic data. Proteomic drug-perturbation experiments are typically still limited to cell line models, rendering the translation to *in vivo* systems, let alone patients, challenging. One critical aspect is the molecular background of the chosen pre-clinical model, which introduces a bias that may impact the clinical relevance of the obtained data. The ultimate goal of elucidating a drug's action in the context of cancer is to benefit patients eventually. However, tumors, and PDAC especially, are highly heterogeneous in their molecular features and thus their response to therapy[271]. Hence, proteomic studies typically require further follow-up experiments across diverse molecular contexts to draw general conclusions on the clinical implications of the identified drug MoA. Notably, the phosphoproteomic experiments in this study were confined to only a single PDAC cell line, AsPC-1. Although AsPC-1 cells carry alterations in KRAS and p53[272], the two most frequently altered genes in PDAC[44,54], it yet remains unclear whether the drug-induced phosphorylation changes were specific to other mutational contexts of PDAC. Understanding the implications of the models' molecular background is particularly relevant for the evaluation of pharmacodynamics biomarkers that emerge from such phosphoproteomic studies. To reveal their true clinical impact, it is essential to learn whether these markers robustly predict a response or synergy across a wide range of PDACs or only a specific molecular subset of tumors instead. Hence, pre-clinically suggested biomarkers require extensive and systematic testing in multiple disease models with genetically different backgrounds and, if possible, the integration of existing clinical data. Utilizing more advanced disease models, such as spheroids or organoids, could offer closer approximations to the clinical scenario in this context.

An outlook on how the systematic knowledge of drug mechanisms could inform future drug development. As exemplified herein on GEM and ATRi, MS-based phosphoproteomics is a powerful technique to investigate the MoA of drugs and how their clinical use can be rationalized. Extending such mechanistic studies systematically to other drugs, together with existing clinical data on the compounds, could ultimately gain a large knowledge base of drug MoAs to guide future drug development campaigns and improve clinical success. In this context, great learning could arise from retrospectively analyzing the MoA of compounds that previously failed clinical trials due to insufficient efficacy or lack of safety. Although rescuing previously failed drugs is not new to the pharmaceutical industry[273-275], the systematic integration of phosphoproteomic data could contribute in different ways. First, the proteomic study of clinically advanced drugs that have failed due to only partial, insufficient efficacy *in vivo* can identify molecular features that predict therapeutic sensitivity or resistance, guiding personalized medicine approaches. This approach may identify patient subgroups that still benefit from these regimens and reveal molecular characteristics, such as biomarkers, that could inform alternative trial design and patient selection.

The underlying clinical data may even be acquired from other cancer entities, as clinical data in PDAC is typically sparse due to small patient cohorts, given the low incidence and high mortality of the disease[276]. Second, the retrospective mechanistic understanding of drug toxicity could explain how future lead candidates can avoid these issues. Such mechanistic insights could help understand the structure-activity relationships of bioactive compounds and their scaffolds and guide drug prioritization and optimization towards safer compounds. Considering that toxicity is the leading cause of clinical attrition[265], such a mechanism-guided endeavor could ultimately enhance clinical success in future campaigns. Ultimately, such visionary, large-scale mechanistic analysis of clinically advanced (both approved and failed) compounds could support current repurposing campaigns and drastically change the clinical success rate in cancer in the long run.

In conclusion, several factors are holding back the streamlined use of MS-based phosphoproteomics in clinical drug development, including challenges in functional annotation, the need for complementary experimental strategies, and unclear clinical translation. Some of these issues can only be addressed over time as research progresses and functional insights on protein phosphorylation and its clinical implications accumulate. This gradual advancement will enhance our ability to interpret large-scale phosphoproteomic data, ultimately leading to more effective integration in clinical decision-making. Continued investigations and collaborative efforts in this field are essential to overcome current limitations and fully realize the potential of phosphoproteomics for clinical drug development.

4.3 Future clinical directions in targeting cellular DNA damage response in PDAC

Potential safety concerns of DNA-damage targeting therapy in PDAC. This work presents strong evidence of pre-clinical drug efficacy and provides a mechanistic rationale for the clinical use of GEM combined with ATRi in PDAC. Nevertheless, the true therapeutic benefit and clinical impact of GEM and ATR inhibitor combinations in PDAC patients are yet to be determined. Currently, the three ATR inhibitors Ceralasertib, Berzosertib, and Elimusertib are being investigated in PDAC, of which only Elimusertib is assessed in combination with GEM (phase I; Chapter 1.2.3). Although the results of these trials are pending, another recent safety and dose-escalation trial combining Elimusertib with Irinotecan or Topotecan reported high levels of myelosuppression in solid tumors, including PDAC (phase I, NCT04514497)[277,278]. Although the pharmacodynamics and response rates were not yet reported, the trial sponsor halted patient expansion and clinical follow-up[277,278]. Presumably, similar side effects may occur from combining Elimusertib and GEM, considering that bone marrow suppression is also a reported side effect of GEM monotherapy[279].

Despite these concerns, encouraging clinical evidence on the combination of GEM and ATRi comes from other cancer entities. For instance, a completed phase II trial in platinum-resistant ovarian cancer demonstrated that the combination of GEM and Berzosertib improved progression-free survival without significant toxicity issues (NCT02595892)[280]. Moreover, the same drug combination was well tolerated and showed preliminary efficacy in lung and breast cancer patients (phase I, NCT02157792)[90]. Nevertheless, the clinical data is sparse, and similar trials on other ATR inhibitors in combination with GEM, specifically in the context of PDAC, still seek completion. In any case, careful evaluation of dosing and treatment schedules is required to ensure the safety and efficacy of DNA damage-targeting combination therapies in clinical settings.

Exploring ATRi combinations beyond GEM-based therapies. This study focused solely on the combination of ATRi and GEM. GEM has been in clinical use for PDAC for nearly 20 years and is the basis of numerous clinical trials testing its combination with molecularly targeted agents (Chapter 1.1.3). Given that ATRi strongly synergized with GEM by blocking cellular DNA damage response, it is plausible that ATRi could also synergize with other DNA-damaging agents. In PDAC, individual components of FOLFIRINOX, such as 5-FU, present promising candidates for combination with ATRi. Similar to GEM, 5-FU is an antimetabolite that interferes with DNA replication by inhibiting thymidylate synthase and incorporating its metabolites into RNA and DNA[281,282]. Given the similarity in drug action, the combination of 5-FU and ATRi is expected to be broadly active in PDAC as well. However, at present, there is no clinical evidence on this regimen. Only a single trial has been initiated in gastric and colon cancer, testing the combination of Elimusertib with fluorouracil, irinotecan, and leucovorin (FOLFIRI), but the results are still pending (NCT04535401). Other relevant candidates include platinum-based chemotherapy agents such as Oxaliplatin, which induces DNA crosslinks that obstruct replication and transcription[283], and topoisomerase inhibitors such as Irinotecan, which prevent DNA replication by stabilizing the topoisomerase-DNA complex[284]. While the combination of ATR inhibitors and topoisomerase inhibitors presents a high safety risk (see above), platinum-based combination therapies with ATRi are gaining interest in clinical settings[198,285]. However, pre-clinical and clinical evidence in PDAC is sparse, and further investigations are needed to explore the potential synergy between ATRi and these agents.

In this work, drug synergy between GEM and ATRi was mechanistically explained by the partial blockage of GEM-induced DNA damage response in cells upon combination. As the aforementioned alternative chemotherapies comprise different MoAs, understanding how these impact drug synergism with ATRi would be of particular interest. Presumably, based on the learnings from this work, the degree of drug synergy will depend on their different induced DNA lesions and the extent by which they activate (non-)canonical ATR kinase functions (e.g., cell cycle control, DNA repair, RNA processing, or dNTP metabolism). Knowledge about these different

synergy mechanisms by phosphoproteomics could provide the basis for the rational prioritization of suitable regimens.

Summary and outlook on DNA-damage response targeted combination therapies in PDAC. In conclusion, the phenotypic and mechanistic insights gained from this study on GEM and ATRi, along with ongoing clinical investigations on GEM and Elimusertib, provide a promising outlook for DNA damage-targeting combination therapies in PDAC. However, the journey towards effective DNA damage-related therapies in PDAC has been initiated only recently, and their true clinical impact remains to be seen. One major challenge will be the tolerability of combining DNA-damaging chemotherapy with targeted inhibition.

The various available DNA-damaging chemotherapies and the increasing number of novel ATR inhibitors entering clinical trials demonstrate the potential for alternative combination regimens beyond GEM and Elimusertib. For future campaigns on DNA damage-directed therapies, the early implementation of MS-based proteomics will be crucial to promote clinical success. Specifically, mechanistic knowledge from these studies will help to 1) select potent and selective ATR inhibitors as more enter the clinics, 2) prioritize DNA-damaging chemotherapies for such combinations, and 3) stratify patients based on specific biomarkers to mitigate safety risks and enhance therapeutic outcomes in future trials.

This study exemplified how MS-based proteomics can be applied to unravel the molecular mechanism underlying drug action and synergy, potentially forming the basis for future implementation in clinical drug development pipelines. To focus future investigations on the most clinically relevant drugs and combinations, strong collaboration between clinicians and molecular researchers will be essential to maximize the clinical benefit for PDAC patients.

Abbreviations

5-FU	5-fluorouracil
AGC	Automatic gain control
ATM	Ataxia telangiectasia mutated
ATR	Ataxia telangiectasia and Rad3 related
ATRi	Inhibitor of ataxia telangiectasia and Rad3 related
AUC	Area-under-curve
CATDS	Concentration and target-dependent selectivity
CID	Collision-induced dissociation
dCTP	Deoxycytidine triphosphate
dFdC	Difluorodeoxycytidine
dFdCDP	Difluorodeoxycytidine diphosphate
dFdCMP	Difluorodeoxycytidine monophosphate
dFdCTP	Difluorodeoxycytidine triphosphate
dFdUMP	Deoxyuridine monophosphate
DMSO	Dimethyl sulfoxide
DNA	Deoxyribonucleic acid
DNA-PK	DNA-dependent protein kinase
dNTP	Deoxyribonucleotides
DSB	DNA double strand break
dTMP	Deoxythymidine monophosphate
dTTP	Deoxythymidine triphosphate
dUMP	Deoxyuridine monophosphate
EC50	Half-maximum effect concentration
EGFR	Epidermal growth factor receptor
FA	Formic acid
FDA	U.S. Food and Drug Administration
GEM	Gemcitabine
HCD	Higher energy collision dissociation
HPLC	High-performance liquid chromatography
HR	Homologous recombination
hTERT	Human telomerase reverse transcriptase
IMAC	Immobilized metal affinity chromatography
Kdapp	Apparent dissociation constant
LC-MS/MS	Liquid chromatography-tandem mass spectrometry
mFOLFIRINOX	Modified FOLFIRINOX
MoA	Mode of action
MS	Mass spectrometry
nab	Nanoparticle albumin-bound
NHEJ	Non-homologous end-joining
NSCLC	Non-small cell lung cancer

PDAC	Pancreatic adenocarcinoma
PDPD	Pulldown of pulldown
PI3K	Phosphatidylinositol 3-kinase
PIKK	Phosphatidylinositol 3-kinase-related kinase
pSQ/pTQ	Phosphorylated serine or threonine followed by glutamine
PTM	Posttranslational modification
RTK	Receptor tyrosine kinase
RTKi	Inhibitor of receptor tyrosine kinase
SD	Standard deviation
ssDNA	Single-stranded DNA
TMT	Tandem mass tag

Appendix

Appendix 1. Past and ongoing clinical trials in PDAC patients with GEM and small molecule targeted therapies (all time; according to *clinicaltrials.gov* as of June 2024). Only active, recruiting, and completed trials were considered. nabP.: nanoparticle albumin-bound Paclitaxel.

NCT Number	Status	Chemodrug	Inhibitor	Inhibitor Target	Phase	Start	Completion
NCT06360354	Recruiting	GEM+nabP.	AMG-193	PRMT5	I	2024	2027
NCT06447662	Recruiting	GEM+nabP.	PF-07934040	KRAS	I	2024	2028
NCT06445062	Recruiting	GEM+nabP.	RMC-6236	RAS	I/II	2024	2027
NCT06199466	Recruiting	GEM+nabP.	YL-13027	TGFBR	I	2024	2027
NCT05669482	Recruiting	GEM+nabP.	Avutometinib	MEK	I/II	2023	2025
NCT06015659	Recruiting	GEM	Azenosertib	WEE1	II	2023	2027
NCT06059001	Recruiting	GEM+nabP.	OMO-103	MYC	I	2023	2026
NCT05493995	Completed	GEM+nabP.	Anlotinib	RTK	II	2022	2024
NCT05580445	Recruiting	GEM	Conteltinib	FAK	I/II	2022	2024
NCT05827796	Recruiting	GEM+nabP.	Ifebemtinib	FAK	I/II	2022	2026
NCT04616534	Active	GEM	Elimusertib	ATR	I	2021	2024
NCT04827953	Active	GEM+nabP.	NLM-001	Hedgehog	I/II	2021	2024
NCT05218889	Recruiting	GEM+nabP.	Surufatinib	RTK	I/II	2021	2025
NCT04247126	Completed	GEM+nabP.	SY-5609	CDK	I	2020	2023
NCT03678883	Active	GEM+nabP.	Elraglusib	GSK3	II	2019	2025
NCT03997968	Active	GEM	Emzadirib	RAD51	I/II	2019	2024
NCT06278493	Completed	GEM	AL2846	MET	I/II	2018	2023
NCT02981342	Completed	GEM	Samotolisib	CDK	II	2017	2018
NCT02632448	Recruiting	GEM	LY2880070	CHEK1	I/II	2016	2025
NCT02436668	Completed	GEM+nabP.	Ibrutinib	BTK	III	2015	2019
NCT02574663	Completed	GEM+nabP.	Umbralisib	PI3K	I	2015	2018
NCT02194829	Completed	GEM+nabP.	Adavosertib	WEE1	I/II	2014	2022
NCT02155088	Completed	GEM+nabP.	Alpelisib	PI3K	I	2014	2020
NCT02231723	Completed	GEM+nabP.	Napabucasin	STAT3	I	2014	2020
NCT01924260	Completed	GEM	Alisertib	AURORA	I	2013	2017
NCT01858883	Completed	GEM+nabP.	Itacitinib	JAK1	I/II	2013	2016
NCT01663272	Completed	GEM	Cabozantinib	RTK	I	2012	2017
NCT01660971	Active	GEM	Dasatinib	BCR-ABL	I	2012	2025
NCT01487785	Completed	GEM	Sonidegib	Hedgehog	I	2012	2014
NCT01585805	Active	GEM	Veliparib	PARP	II	2012	2024
NCT01373164	Completed	GEM	Galunisertib	TGFBR	I/II	2011	2016
NCT01251640	Completed	GEM	Refametinib	MEK	I/II	2011	2013
NCT01360853	Completed	GEM	Rigosertib	PLK1	III	2011	2015
NCT01130142	Completed	GEM	Saridegib	Hedgehog	I/II	2010	2012
NCT01231581	Completed	GEM	Trametinib	MEK	II	2010	2013
NCT01088815	Completed	GEM+nabP.	Vismodegib	Hedgehog	II	2010	2018
NCT01016483	Completed	GEM	Pimasertib	MEK	I/II	2009	2015
NCT00839332	Completed	GEM	Rabusertib	CHEK1	I/II	2009	2013
NCT00898287	Completed	GEM	Riviciclib	CDK	I/II	2009	NA
NCT00862524	Completed	GEM	Varlitinib	RTK	I/II	2009	2011
NCT00709826	Completed	GEM	Apricoxib	COX	II	2008	2011
NCT00789633	Completed	GEM	Masitinib	KIT	III	2008	2012
NCT01097512	Completed	GEM	Cenisertib	AURORA	I	2007	2011
NCT00560963	Completed	GEM	Everolimus	mTOR	I/II	2007	2011
NCT00515866	Completed	GEM	Olaparib	PARP	I	2007	2012
NCT00462553	Completed	GEM	Sunitinib	RTK	I	2007	NA
NCT00551096	Completed	GEM	Vandetanib	RTK	I	2007	2013
NCT00379639	Completed	GEM	Romidepsin	HDAC	I	2006	2008
NCT00265876	Completed	GEM	Saracatinib	BCR-ABL	I/II	2006	2012
NCT00219557	Completed	GEM	Axitinib	RTK	II	2005	2008

NCT00161213	Completed	GEM	Imatinib	BCR-ABL	II	2005	2010
NCT00327327	Completed	GEM	Imexon	RRM1/2	I	2004	2009
NCT00095966	Completed	GEM	Sorafenib	RTK	II	2004	NA
NCT00185588	Completed	GEM	Vatalanib	RTK	I/II	2004	2009
NCT00176813	Completed	GEM	Celexocib	COX	II	2003	2006
NCT00064051	Completed	GEM	Triapine	RRM1/2	II	2003	2008
NCT00234416	Completed	GEM	Gefitinib	RTK	I/II	2002	2005
NCT00026338	Completed	GEM	Erlotinib	RTK	III	2001	2009

Appendix 2. Cell lines used for phenotypic drug screening with information on supplier and order number (if applicable), and if KRAS or TP53 are mutated (indicated by `+`). Cell culture medium with supplements and cell seeding densities per well of a 384-well are provided. For high-throughput drug screening, all cell culture medium was supplemented with 1% 100 U/ml penicillin and 100 µg/ml streptomycin. *Cell lines were kindly provided by Prof Kisten Lauber (Molecular Oncology Department of Radiation, LMU).

Cell line	**Supplier**	**Supplier order #**	**KRAS mut.**	**TP53 mut.**	**Culture Medium**	**Culture medium supplements**	**Cell density (384-well)**
AsPC-1	ATCC	CRL-1682	+	+	DMEM	10% FBS, 1% non-essential amino acids	1000
Panc-1	ATCC	CRL-1469	+	+	DMEM	10% FBS	2000
PSN-1	ATCC	CRL-3211	+	+	RPMI	10% FBS	1000
BxPC-3	ATCC	CRL-1687		+	RPMI	10% FBS	1000
MiaPaCa-2	ATCC	CRL-1420	+	+	DMEM	10% FBS	1000
Capan-1	CLS	300143	+	+	RPMI	10% FBS, 1% HEPES	2000
FAMPAC	CLS	300309	+	+	RPMI	10% FBS, 1% HEPES	1000
HuP-T4	creative-bioarray	CSC-C0333	+	+	DMEM/Hams-F12 (1:1)	10% FBS, 15 mM HEPES	1000
Dan-G	DSMZ	ACC-249	+	+	RPMI	10% FBS	1000
PaTu-8988-T	DSMZ	ACC-162	+	+	DMEM	10% FBS	1000
Colo-357*	-	-	+	+	DMEM	10% FBS	2000
HPDE*	-	-			RPMI/keratinocyte serum-free medium (1:1)	10% FBS, 5 ng/ml human epi-dermal growth factor, 50 µg/ml bovine pituitary extract	1000
Suit2-07*	-	-	+	+	RPMI	10% FBS	1000

Appendix 3. Inhibitors used for phenotypic drug screening, with information on supplier, catalog number, and if the drug is a kinase inhibitor (indicated by `+`). Designated targets are given based on *drugbank.com*. At maximum, only four designated targets are shown. Clinical status indicates the highest reached clinical phase according to *clinicaltrials.gov* (as of 06/2023).

Drug	Supplier	Supplier order #	Kinase Inhibitor	Designated targets	Clinical status
Abemaciclib	Selleckchem	S7158	+	CDK4,CDK6	approved
Abrocitinib	MedChemExpress	HY-107429	+	JAK	approved
Acalabrutinib	Selleckchem	S8116	+	BTK	approved
Afatinib	Selleckchem	S1011	+	EGFR	approved
Alectinib	MedChemExpress	HY-13011	+	ALK	approved
Alpelisib	Selleckchem	S2814	+	PIK3CA	approved
Asciminib	MedChemExpress	HY-104010	+	ABL	approved
Avapritinib	Selleckchem	S8553	+	PDGFRa, KIT	approved
Axitinib	Selleckchem	S1005	+	FLT1,KDR,FLT4	approved
Baricitinib	MedChemExpress	HY-15315	+	JAK1,JAK2	approved
Binimetinib	Selleckchem	S7007	+	MAP2K1,MAP2K2	approved
Bosutinib	Selleckchem	S1014	+	SRC,ABL1	approved
Brigatinib	Selleckchem	S7000	+	ALK, ROS1	approved
Cabozantinib	Selleckchem	S1119	+	KDR	approved
Capmatinib	Selleckchem	S2788	+	MET	approved
Ceritinib	MedChemExpress	HY-15656	+	ALK	approved
Cobimetinib	Selleckchem	S8041	+	MAP2K1	approved
Copanlisib	MedChemExpress	HY-15346	+	PIK3CA,PIK3CB,PIK3CD+more	approved
Crizotinib	Selleckchem	S1068	+	MET,ALK	approved
Dabrafenib	Selleckchem	S2807	+	BRAF	approved
Dacomitinib	Selleckchem	S2727	+	EGFR	approved
Dasatinib	Selleckchem	S1021	+	ABL1,SRC	approved
Deucravacitinib	MedChemExpress	HY-117287	+	TYK2	approved
Duvelisib	Selleckchem	S7028	+	PIK3CD, PIK3CG	approved
Encorafenib	Selleckchem	S7108	+	BRAF	approved
Entrectinib	MedChemExpress	HY-12678	+	NTRK1,NTRK2,NTRK3,ROS1+more	approved
Erdafitinib	Selleckchem	S8401	+	FGFR	approved
Erlotinib	Selleckchem	S1023	+	EGFR	approved
Everolimus	Selleckchem	S1120	+	mTOR	approved
Fedratinib	Selleckchem	S2736	+	JAK2	approved
Fostamatinib	Selleckchem	S2625	+	SYK	approved
Gefitinib	Selleckchem	S1025	+	EGFR	approved
Glasdegib	Selleckchem	S7160		SMO	approved
Ibrutinib	Selleckchem	S2680	+	BTK	approved
Idelalisib	Selleckchem	S2226	+	PIK3CD	approved
Imatinib	Selleckchem	S1026	+	ABL1,KIT,PDGFRA,PDGFRB	approved
Lapatinib	Selleckchem	S1028	+	EGFR,ERBB2	approved
Larotrectinib	Selleckchem	S7960	+	TRK	approved
Leniolisib	MedChemExpress	HY-17635	+	PIK3CD	approved
Lenvatinib	Selleckchem	S1164	+	KDR,FLT4	approved
Lorlatinib	MedChemExpress	HY-12215	+	ALK, ROS1	approved
Midostaurin	MedChemExpress	HY-10230	+	PRKCA,PRKCB,PRKCG,SYK+more	approved
Neratinib	Selleckchem	S2150	+	ERBB2,EGFR	approved
Netarsudil	Selleckchem	S8226	+	ROCK	approved
Nilotinib	Selleckchem	S1033	+	ABL1	approved
Nintedanib	Selleckchem	S1010	+	FLT1,KDR,FLT4,FGFR1+more	approved
Niraparib	Selleckchem	S2741		PARP	approved
Olaparib	Selleckchem	S1060		PARP	approved
Osimertinib	Selleckchem	S7297	+	EGFR	approved
Pacritinib	MedChemExpress	HY-16379	+	JAK2,FLT3	approved
Palbociclib	Selleckchem	S1116	+	CDK4,CDK6	approved
Pazopanib	Selleckchem	S1035	+	FLT1,KDR,FLT4	approved
Pemigatinib	MedChemExpress	HY-109099	+	FGFR1,FGFR2,FGFR3	approved
Pexidartinib	Selleckchem	S7818	+	CSF1R	approved
Ponatinib	Selleckchem	S1490	+	ABL1	approved
Pralsetinib	Selleckchem	S8716	+	RET	approved
Rapamycin	Selleckchem	S1039	+	mTOR	approved

Regorafenib	Selleckchem	S1178	+	KDR,RET,RAF1	approved
Ribociclib	Selleckchem	S7440	+	CDK4,CDK6	approved
Ripretinib	Selleckchem	S8757	+	KIT, PDGFRa	approved
Ruxolitinib	Selleckchem	S1378	+	JAK1,JAK2	approved
Selinexor	Selleckchem	S7252		XPO1	approved
Selpercatinib	Selleckchem	S8781	+	RET	approved
Selumetinib	Selleckchem	S1008	+	MAP2K1	approved
Sorafenib	Selleckchem	S1040	+	RAF1,BRAF	approved
Sunitinib	Selleckchem	S1042	+	KDR,PDGFRB	approved
Talazoparib	Selleckchem	S7048		PARP	approved
Temsirolimus	Selleckchem	S1044	+	mTOR	approved
Tepotinib	Selleckchem	S7067	+	MET	approved
Tirbanibulin	Selleckchem	S2700	+	SRC	approved
Tivozanib	Selleckchem	S1207	+	FLT1,KDR,FLT4	approved
Tofacitinib	Selleckchem	S5001	+	JAK3	approved
Trametinib	MedChemExpress	HY-10999	+	MAP2K1,MAP2K2	approved
Tucatinib	Selleckchem	S8362	+	ERBB2	approved
Umbralisib	Selleckchem	S8194	+	PIK3CD	approved
Upadacitinib	MedChemExpress	HY-19569	+	JAK1	approved
Vandetanib	Selleckchem	S1046	+	KDR	approved
Vemurafenib	Selleckchem	S1267	+	BRAF	approved
Volasertib	Selleckchem	S2235	+	PLK1	approved
Zanubrutinib	MedChemExpress	HY-101474A	+	BTK	approved
Anlotinib	Selleckchem	S8726	+	VEGFR2	approved (China)
Apatinib	Selleckchem	S2221	+	KDR	approved (China)
Fasudil	Selleckchem	S1573	+	ROCK	approved (China)
Fruquintinib	MedChemExpress	HY-19912	+	VEGFR	approved (China)
Icotinib	MedChemExpress	HY-15164	+	EGFR	approved (China)
Filgotinib	MedChemExpress	HY-18300	+	JAK1	approved (EMA)
Olmutinib	MedChemExpress	HY-19730	+	EGFR	approved (Korea)
AZD-0156	Selleckchem	S8375	+	ATM	Phase I
Belizatinib	Selleckchem	S8511	+	ALK, TRK	Phase I/II
Elimusertib	Selleckchem	S8666	+	ATR	Phase I/II
Lifirafenib	Selleckchem	S7926	+	RAF	Phase I/II
Roblitinib	MedChemExpress	HY-101568	+	FGFR4	Phase I/II
Adavosertib	Selleckchem	S1525	+	WEE1	Phase II
Defactinib	Selleckchem	S7654	+	FAK	Phase II
Edicotinib	MedChemExpress	HY-109086	+	CSF1R	Phase II
GSK-2256098	Selleckchem	S8523	+	FAK	Phase II
GSK-3145095	MedChemExpress	HY-111946	+	RIPK1	Phase II
Nemiralisib	Selleckchem	S7937	+	PIK3CD	Phase II
Sapanisertib	Selleckchem	S2811	+	mTOR	Phase II
Vactosertib	Selleckchem	S7530	+	TFGBR	Phase II
AZD-4547	Selleckchem	S2801	+	FGFR1,FGFR2,FGFR3	Phase II/III
Barasertib	MedChemExpress	HY-10127	+	AURKB	Phase II/III
Galunisertib	Selleckchem	S2230	+	TGFBR1	Phase II/III
Rogaratinib	MedChemExpress	HY-100019	+	FGFR	Phase II/III
Saracatinib	Selleckchem	S1006	+	SRC	Phase II/III
Tideglusib	Selleckchem	S2823	+	GSK3B	Phase II/III
Varlitinib	Selleckchem	S2755	+	EGFR,ERBB2	Phase II/III
Zorifertinib	Selleckchem	S7971	+	EGFR	Phase II/III
Alisertib	Selleckchem	S1133	+	AURKA	Phase III
Brivanib	Selleckchem	S1084	+	KDR	Phase III
Brivanib alaninate	Selleckchem	S1138	+	KDR	Phase III
Buparlisib	Selleckchem	S2247	+	PIK3CA,PIK3CB,PIK3CD,PIK3CG	Phase III
Cediranib	Selleckchem	S1017	+	KDR	Phase III
Crenolanib	Selleckchem	S2730	+	PDGFRA,PDGFRB	Phase III
Dinaciclib	Selleckchem	S2768	+	CDK2,CDK5,CDK1,CDK9	Phase III
Dovitinib	Selleckchem	S1018	+	FLT3,KIT	Phase III
Ensartinib	Selleckchem	S2934	+	ALK	Phase III
Enzastaurin	Selleckchem	S1055	+	PRKCB	Phase III
Evobrutinib	MedChemExpress	HY-101215	+	BTK	Phase III
Ipatasertib	Selleckchem	S2808	+	AKT	Phase III
Itacitinib	MedChemExpress	HY-16997	+	JAK1	Phase III

Lestaurtinib	MedChemExpress	HY-50867	+	JAK2,FLT3,NTRK1	Phase III
Linifanib	Selleckchem	S1003	+	KDR,CSF1R,FLT1,FLT3	Phase III
Linsitinib	Selleckchem	S1091	+	IGF1R	Phase III
Losmapimod	Selleckchem	S7215	+	MAPK14,MAPK11	Phase III
Lucitanib	MedChemExpress	HY-15391	+	FLT1,KDR,FLT4,FGFR1+more	Phase III
Masitinib	Selleckchem	S1064	+	KIT,PDGFRA,PDGFRB	Phase III
Momelotinib	Selleckchem	S2219	+	JAK1,JAK2	Phase III
Motesanib	Selleckchem	S1032	+	FLT1,KDR,FLT4	Phase III
Napabucasin	Selleckchem	S7977		STAT3	Phase III
Orantinib	Selleckchem	S1470	+	PDGFRA,PDGFRB	Phase III
Peficitinib	Selleckchem	S7650	+	JAK	Phase III
Perifosine	Selleckchem	S1037	+	AKT1	Phase III
Quizartinib	MedChemExpress	HY-13001	+	FLT3	Phase III
Radotinib	Selleckchem	S8134	+	BCR-ABL1	Phase III
Ridaforolimus	MedChemExpress	HY-50908	+	mTOR	Phase III
Rigosertib	Selleckchem	S1362	+	PLK1	Phase III
Rociletinib	MedChemExpress	HY-15729	+	EGFR	Phase III
Ruboxistaurin	Selleckchem	S7663	+	PRKCB	Phase III
Selonsertib	Selleckchem	S8292	+	MAP3K5	Phase III
Semaxanib	Selleckchem	S2845	+	VEGFR	Phase III
Sulfatinib	MedChemExpress	HY-12297	+	VEGFR, FGFR, CSF1R	Phase III
Taselisib	Selleckchem	S7103	+	PIK3CA,PIK3CB,PIK3CD,PIK3CG	Phase III
Tivantinib	Selleckchem	S2753	+	MET	Phase III
Vatalanib	Selleckchem	S1101	+	KDR	Phase III
Volitinib	Selleckchem	S7674	+	MET	Phase III

Appendix 4. Designated target proteins, count of affected cell lines, and median AUC (in %) of the 22 drugs that displayed an AUC of < 80% in the single-drug screen. Information on clinical trials in PDAC is shown (only when tested in monotherapy).

Drug	**Target(s)**	**Cell line count**	**median AUC [%]**	**Clinical trials in PDAC (in monotherapy)**	**Trial results**	**Source**
Dinaciclib	CDK	13	40	-	-	-
Volasertib	PLK1	12	54	Phase II, MATCH screening trial NCT02465060 (active, start 2015)	-	-
Tirbanibulin	SRC	12	60	-	-	-
Elimusertib	ATR	12	76	-	-	-
Sapanisertib	mTOR	11	54	Phase I, NCT04005690 (recruiting, start 2019)	-	-
Copanlisib	MEK1/2	11	67	Phase II, MATCH screening trial NCT02465060 (active, start 2015)	-	-
Selinexor	XPO1	11	68	Phase II, MATCH screening trial NCT02465060 (active, start 2015)	-	-
Adavosertib	WEE1	11	72	-	-	-
Brigatinib	Multiple	11	73	-	-	-
Neratinib	RTK	11	74	Phase II, MATCH screening trial NCT02465060, active since 2015); Phase II, NCT00474812 (completed 2014)	NCT00474812: No clinical activity	Chee et al. (2013)[286]
Rigosertib	PLK1	11	76	Phase II, MATCH screening trial NCT02465060 (active, start 2015)	-	-
Trametinib	MEK1/2	10	67	-	-	-
Lestaurtinib	Multiple	10	70	Phase I/II, NCT03919292 (recruiting, start 2019)	-	-
Dasatinib	Multiple	10	71	-	-	-
Fedratinib	JAK	10	77	Phase II, MATCH screening trial NCT02465060 (active, start 2015)	-	-
Ponatinib	ABL1	9	78	-	-	-
Cobimetinib	MEK1/2	8	66	-	-	-
Taselisib	PI3K	8	76	-	-	-
Napabucasin	STAT3	8	76	-	-	-
Buparlisib	PI3K	8	79	-	-	-
Temsirolimus	mTOR	8	80	-	-	-
Netarsudil	ROCK	1	79	-	-	-

Appendix 5. Designated target proteins, count of affected cell lines and median ΣAUC_{Δ} (in %) of the 18 drugs that synergized with GEM in PDAC cells. Information on clinical trials with these drugs in combination with GEM in PDAC is shown.

Drug	**Target(s)**	**Cell line count**	**median ΣAUC_{Δ} [%]**	**Clinical trials in PDAC (combined with GEM)**	**Trial results**	**Source**
Elimusertib	ATR	11	23	Phase I, NCT04616534 (active, start 2021)	-	-
Lestaurtinib	Multi	7	20	-	-	-
Brigatinib	Other	5	15	-	-	-
Adavosertib	WEE1	5	19	Phase I/II, NCT02037230 (completed 2018) Phase I/II, NCT02194829 (completed 2022)	NCT02037230: Preliminary efficacy	Cuneo et al. (2019)[287]
Ridaforolimus	mTOR	4	26	-	-	-
Everolimus	mTOR	3	25	Phase I/II, NCT00560963 (completed 2011)	Unknown results	-
Rapamycin	mTOR	3	21	-	-	-
Temsirolimus	mTOR	2	14	Phase I, NCT00593008 (terminated 2009)	-	-
Talazoparib	PARP1	2	19	-	-	-
Ibrutinib	BTK	1	13	Phase I/II, NCT02562898 (completed 2020) Phase III, NCT02436668 (completed 2019)	NCT02436668: No clinical efficacy	Tempero et al. (2021)[288]
Binimetinib	MEK1/2	1	14	-	-	-
Cobimetinib	MEK1/2	1	20	-	-	-
Trametinib	MEK1/2	1	12	Phase II, NCT01231581 (completed 2013)	No clinical efficacy	Infante et al. (2014)[289]
Selumetinib	MEK1/2	1	21	-	-	-
Dasatinib	Multi	1	17	Phase II, NCT01395017 (completed 2015)	No clinical efficacy	Evans et al. (2012)[290]
Copanlisib	PI3K	1	19	-	-	-
Ruboxistaurin	PKC	1	25	-	-	-
Netarsudil	ROCK	1	25	-	-	-

Appendix 6. External datasets on Kinobeads pulldown experiments of inhibitors Adavosertib, Lestaurtinib (Klaeger et al. 2017) and Brigatinib (Reinecke 2020). For each target protein, the EC_{50} (in nM) and K_D^{app} (in nM) are given, and information on the used Kinobeads is provided. The target kinases WEE1 (of Adavosertib) and CHEK1 (of Brigatinib and Lestaurtinib) are highlighted in blue text.

Drug	Kinobeads	Source	Target	EC_{50} [nM]	K_D^{app} [nM]
Adavosertib	Kinobeads γ	Klaeger et al. (2017)	**WEE1**	19	12
Adavosertib	Kinobeads γ	Klaeger et al. (2017)	ADK	13	13
Adavosertib	Kinobeads γ	Klaeger et al. (2017)	MAP3K4	77	52
Brigatinib	Kinobeads ε	Reinecke (2020)	TNK1	2	1
Brigatinib	Kinobeads ε	Reinecke (2020)	FER	4	2
Brigatinib	Kinobeads ε	Reinecke (2020)	TNK2	6	3
Brigatinib	Kinobeads ε	Reinecke (2020)	PTK2B	12	5
Brigatinib	Kinobeads ε	Reinecke (2020)	PTK2	13	5
Brigatinib	Kinobeads ε	Reinecke (2020)	GAK	10	6
Brigatinib	Kinobeads ε	Reinecke (2020)	CLK1	13	9
Brigatinib	Kinobeads ε	Reinecke (2020)	PHKA2	20	20
Brigatinib	Kinobeads ε	Reinecke (2020)	SIK2	47	24
Brigatinib	Kinobeads ε	Reinecke (2020)	PRKD1	46	31
Brigatinib	Kinobeads ε	Reinecke (2020)	ULK1	57	38
Brigatinib	Kinobeads ε	Reinecke (2020)	RPS6KA6	94	39
Brigatinib	Kinobeads ε	Reinecke (2020)	CAMKK2	61	40
Brigatinib	Kinobeads ε	Reinecke (2020)	PTK6	86	41
Brigatinib	Kinobeads ε	Reinecke (2020)	CLK4	49	42
Brigatinib	Kinobeads ε	Reinecke (2020)	CAMK2B	323	48
Brigatinib	Kinobeads ε	Reinecke (2020)	PLK4	95	49
Brigatinib	Kinobeads ε	Reinecke (2020)	FRK	156	53
Brigatinib	Kinobeads ε	Reinecke (2020)	**CHEK1**	71	58
Brigatinib	Kinobeads ε	Reinecke (2020)	MAPKAPK5	63	58
Brigatinib	Kinobeads ε	Reinecke (2020)	FES	170	63
Brigatinib	Kinobeads ε	Reinecke (2020)	NUAK2	89	68
Brigatinib	Kinobeads ε	Reinecke (2020)	FLT3	142	76
Brigatinib	Kinobeads ε	Reinecke (2020)	CAMK2D	424	86
Brigatinib	Kinobeads ε	Reinecke (2020)	CAMK2G	429	93
Lestaurtinib	Kinobeads γ	Klaeger et al. (2017)	PDPK1;PDPK2P	11	11
Lestaurtinib	Kinobeads γ	Klaeger et al. (2017)	RASSF3	14	14
Lestaurtinib	Kinobeads γ	Klaeger et al. (2017)	RASSF2	24	22
Lestaurtinib	Kinobeads γ	Klaeger et al. (2017)	AURKA	70	25
Lestaurtinib	Kinobeads γ	Klaeger et al. (2017)	LATS1	32	25
Lestaurtinib	Kinobeads γ	Klaeger et al. (2017)	MAPK10	33	28
Lestaurtinib	Kinobeads γ	Klaeger et al. (2017)	PAK4	48	29
Lestaurtinib	Kinobeads γ	Klaeger et al. (2017)	STK3	39	30
Lestaurtinib	Kinobeads γ	Klaeger et al. (2017)	MOB1A;MOB1B	34	31
Lestaurtinib	Kinobeads γ	Klaeger et al. (2017)	CDK3	37	37
Lestaurtinib	Kinobeads γ	Klaeger et al. (2017)	MINK1	41	41
Lestaurtinib	Kinobeads γ	Klaeger et al. (2017)	ERN1	51	42
Lestaurtinib	Kinobeads γ	Klaeger et al. (2017)	STK4	59	45
Lestaurtinib	Kinobeads γ	Klaeger et al. (2017)	PRKD2	69	46
Lestaurtinib	Kinobeads γ	Klaeger et al. (2017)	PRKD3	71	53
Lestaurtinib	Kinobeads γ	Klaeger et al. (2017)	SIK2	106	55
Lestaurtinib	Kinobeads γ	Klaeger et al. (2017)	MAP4K2	107	63
Lestaurtinib	Kinobeads γ	Klaeger et al. (2017)	TNK2	143	64
Lestaurtinib	Kinobeads γ	Klaeger et al. (2017)	AAK1	97	66
Lestaurtinib	Kinobeads γ	Klaeger et al. (2017)	RASSF5	73	72
Lestaurtinib	Kinobeads γ	Klaeger et al. (2017)	**CHEK1**	87	72
Lestaurtinib	Kinobeads γ	Klaeger et al. (2017)	MARK4	88	73
Lestaurtinib	Kinobeads γ	Klaeger et al. (2017)	AP2A1	84	77
Lestaurtinib	Kinobeads γ	Klaeger et al. (2017)	Q6ZSR9	105	80
Lestaurtinib	Kinobeads γ	Klaeger et al. (2017)	MAP2K6	87	87
Lestaurtinib	Kinobeads γ	Klaeger et al. (2017)	IRAK4	114	88
Lestaurtinib	Kinobeads γ	Klaeger et al. (2017)	PLK4	177	90
Lestaurtinib	Kinobeads γ	Klaeger et al. (2017)	MYLK3	109	95
Lestaurtinib	Kinobeads γ	Klaeger et al. (2017)	STK10	107	98

Appendix 7. Verification of drug synergy between Elimusertib and six other ATRi in AsPC-1 cells.

ATR inhibitor	Treatment	EC_{50} [nM]	EC_{50} s.d. [nM]	EC_{50} fold change relative to GEM
Elimusertib	ATRi	54	9	NA
Elimusertib	GEM	57	7	1.0
Elimusertib	GEM+3nM ATRi	9	< 1	0.2
Elimusertib	GEM+10nM ATRi	5	< 1	0.1
Elimusertib	GEM+30nM ATRi	17	2	0.3
Gartisertib	ATRi	127	8	NA
Gartisertib	GEM	51	5	1.0
Gartisertib	GEM+3nM ATRi	10	< 1	0.2
Gartisertib	GEM+10nM ATRi	6	< 1	0.1
Gartisertib	GEM+30nM ATRi	20	2	0.4
Berzosertib	ATRi	725	75	NA
Berzosertib	GEM	47	5	1.0
Berzosertib	GEM+30nM ATRi	22	2	0.5
Berzosertib	GEM+100nM ATRi	14	2	0.3
Berzosertib	GEM+300nM ATRi	32	3	0.7
Ceralasertib	ATRi	1,798	233	NA
Ceralasertib	GEM	55	9	1.0
Ceralasertib	GEM+100nM ATRi	9	2	0.2
Ceralasertib	GEM+300nM ATRi	36	6	0.6
Ceralasertib	GEM+1000nM ATRi	26	3	0.5
AZ-20	ATRi	649	61	NA
AZ-20	GEM	36	4	1.0
AZ-20	GEM+30nM ATRi	23	2	0.6
AZ-20	GEM+100nM ATRi	10	1	0.3
AZ-20	GEM+300nM ATRi	33	4	0.9
VE-821	ATRi	> 10,000	> 10,000	NA
VE-821	GEM	41	5	1.0
VE-821	GEM+300nM ATRi	16	2	0.4
VE-821	GEM+3000nM ATRi	7	1	0.2
VE-821	GEM+1000nM ATRi	26	4	0.6
ETP-46464	ATRi	> 10,000	> 10,000	NA
ETP-46464	GEM	51	7	1.0
ETP-46464	GEM+30nM ATRi	48	11	0.9
ETP-46464	GEM+100nM ATRi	52	18	1.0
ETP-46464	GEM+300nM ATRi	61	9	1.2

Appendix 8. Time-dependent log_2 fold changes in phosphorylation of proteins involved in DNA damage response signaling upon 1 µM GEM in AsPC-1 cells. The table provides information on the presence of the pSQ/pTQ motif.

Gene	P-site	pSQ/pTQ	15 min	30 min	1 h	2 h	4 h	8 h	12 h	24 h
ATM	S1981	TRUE	-0.2	0.7	0.8	1.9	1.3	2.0	1.7	2.0
ATR	T1989	FALSE	0.2	0.3	0.1	0.6	1.2	1.4	1.7	2.5
BRCA1	S1007;S1009	FALSE	0.3	0.2	-0.1	0.5	1.8	1.9	1.8	1.9
BRCA1	S1497;S1503	FALSE	0.2	-0.4	0.6	1.0	1.3	1.5	1.4	1.7
BRCA1	S1524	TRUE	-0.2	0.1	0.2	0.6	1.1	1.3	1.3	1.7
BRCA1	S1542	FALSE	0.1	0.3	0.0	0.6	1.4	1.6	2.0	2.3
BRCA1	S1642	FALSE	0.2	-0.2	1.6	2.7	3.2	3.3	3.1	3.6
BRCA1	S803	TRUE	0.2	0.1	0.9	1.2	1.4	1.5	1.1	1.2
CHEK1	S286	FALSE	0.0	0.3	1.2	2.1	1.9	1.0	0.1	0.5
CHEK1	S317	TRUE	-0.1	0.5	1.7	1.7	1.8	1.6	1.6	1.7
CHEK2	S120	FALSE	0.4	0.3	0.3	0.2	1.0	1.3	1.6	2.5
CHEK2	S260	FALSE	-0.8	0.1	0.2	1.3	2.6	3.0	2.8	2.9
CHEK2	S379	FALSE	-0.2	-0.1	0.4	1.2	2.4	2.8	2.3	2.4
CHEK2	T387	FALSE	0.1	0.1	0.1	-0.1	0.6	1.2	1.8	2.2
CHEK2	T517	FALSE	-0.4	-0.2	-0.2	1.0	2.4	2.2	2.4	2.9
H2AFX	S139	TRUE	-0.2	0.1	0.4	1.2	1.2	1.7	1.8	2.6
PRKDC	S2612	TRUE	0.3	0.1	0.3	0.7	0.2	1.1	1.2	2.0
PRKDC	S2624	FALSE	0.3	-0.4	0.4	0.8	-0.8	-0.1	1.1	1.5
PRKDC	S3205	FALSE	-0.2	0.1	-0.3	0.8	2.0	2.3	1.5	1.9
KAP1	S473	FALSE	0.4	0.1	0.4	0.7	1.4	1.5	1.6	1.1

Appendix 9. Information on the 42 pSQ/pTQ sites regulated by at least three of the four clinical ATR inhibitors. The table includes the 36 pSQ/pTQ sites also affected by GEM (indicated by 'up' in column 'GEM Regulation'). Information on kinase-substrate relationships was derived from PhosphoSitePlus[147] as of February 2024.

Gene	P-site	Site sequence window	SQ/TQ	ATRi count	ATRi regulation	GEM regulation	Annotated kinase(s)
AASDHPPT	S258	SRHQDVPsQDDSKPT	TRUE	3	down	up	-
BRCA1	S1239	GKVNNIPsQSTRHST	TRUE	3	down	up	-
BRD8	S621	ESGTIFGsQIKDAPG	TRUE	4	down	up	-
CDKN2AIP	S198	ARSSGISsQNSSTSD	TRUE	4	down	up	-
CHEK1	S317	ENVKYSSsQPEPRTG	TRUE	4	down	up	ATR
CHEK1	S468	KLIDIVSsQKIWLPA	TRUE	3	down	up	-
DHX9	S321	KLAQFEPsQRQNQVG	TRUE	3	down	up	-
EXO1	S714	CNIKLLDsQSDQTSK	TRUE	3	down	up	-
FANCD2	S319	LPSRLQAsQVKLKSK	TRUE	4	down	up	-
HDGF	S103	KASGYQSsQKKSCVE	TRUE	4	down	up	-
HMGA1	S9	SESSSKSsQPLASKQ	TRUE	4	down	up	-
HMGA1	S44	PGTALVGsQKEPSEV	TRUE	4	down	up	PRKCD;PRKCA; PRKCB;PRKCG
HMGA1	S36;S44	PGTALVGsQKEPSEV	TRUE	4	down	up	PRKCD;PRKCA; PRKCB;PRKCG
HSPA4	S552	ESEEMETsQAGSKDK	TRUE	3	down	up	-
HTATSF1	S481	RGFEGSCsQKESEEG	TRUE	3	down	up	-
LRRC42	S385	LKHEAISsQESKKSK	TRUE	4	down	up	-
NBN	S397	EQKFRMLsQDAPTVK	TRUE	4	down	up	ATM
NBN	S615	VPESSKIsQENEIGK	TRUE	3	down	up	ATR;ATM
NSUN5	S432	VEVPSSAsQAKASAP	TRUE	3	down	up	-
PELP1	S1033	LAPEALPsQGEVERE	TRUE	4	down	up	PRKDC;ATR;ATM
PHF14	S294	TNDSLTLsQSKSNED	TRUE	4	down	up	ATR
PNISR	S706	EKDFKFSsQDDRLKR	TRUE	3	down	up	-
PPM1G	S201	DSTRETPsQENGPTA	TRUE	4	down	up	-
PPP6R3	S825	EEGKLSTsQDAACKD	TRUE	3	down	up	-
PSMD4	S266	ALLKMTIsQQEFGRT	TRUE	4	down	up	-
RAD18	S368	YKKIAGMsQKTVTIT	TRUE	3	down	up	-
RIF1	S1873	LGDSKNVsQESLETK	TRUE	3	down	up	-
SNRPA	S115	REKRKPKsQETPATK	TRUE	4	down	up	-
TCEA1	S100;S97	PAITSQNsPEAREES	TRUE	4	down	up	-
TCEB3	S251	FQDRLGAsQERHLGE	TRUE	3	down	up	-
THAP4	S186	LATMVAGsQGKAEAS	TRUE	3	down	up	-
TOPBP1	S1504	KELGTGLsQKRKAPT	TRUE	4	down	up	-
TSEN34	S136	QASGASSsQEAGSSQ	TRUE	4	down	up	-
UHRF1	S393	MASATSSsQRDWGKG	TRUE	3	down	up	-
UIMC1	S171	LFKGSHIsQGNEAEE	TRUE	4	down	up	-
ZC3H14	S135	DSRVSTSsQESKTTN	TRUE	3	down	up	-
PCNP	S77	KFGFAIGsQTTKKAS	TRUE	3	down	-	-
WDHD1	S907	SGAVTFSsQGRVNPF	TRUE	3	down	-	-
ACIN1	S710	SVQARRLsQPESAEK	TRUE	4	up	-	-
MISP	S541	PALRLQKsQSSDLLE	TRUE	3	up	-	-
PML	S480	TAQKRKCsQTQCPRK	TRUE	4	up	-	-
RECQL4	S27	RQRGRRPsQDDVEAA	TRUE	3	up	-	-

Appendix 10. Information on known CDK1 and/or CDK2 substrates regulated by at least three of four clinical ATR inhibitors. Information on kinase-substrate relationships was derived from PhosphoSitePlus[147] as of February 2024.

Gene	P-site	Site sequence window	SQ/TQ	ATRi count	ATRi regulation	Annotated kinase(s)
CD3EAP	S285	PLEDTVLsPTKKRKR	FALSE	4	up	CDK1
HJURP	S412	RTLKWLIsPVKIVSR	FALSE	4	up	CDK1
KIF20B	T1644	VKHPGCTtPVTVKIP	FALSE	4	up	CDK1
MKI67	T761	GIAEMFKtPVKEQPQ	FALSE	4	up	CDK1
RNMT	T77	SSSCGKDtPSKKRKL	FALSE	4	up	CDK1
NCL	T121	PGKALVAtPGKKGAA	FALSE	3	up	CDK1;CDC7;CDK2
HIST1H1E	S2;T18	APAPAEKtPVKKKAR	FALSE	4	up	CDK1;CDK2
HIST1H1E	T18	APAPAEKtPVKKKAR	FALSE	4	up	CDK1;CDK2
TPX2	T72	NLQQAIVtPLKPVDN	FALSE	3	up	CDK1;CDK2
ZC3H11A	T321	PETNIDKtPKKAQVS	FALSE	4	up	CDK1;CDK2
HMGA1	T42	KEPSEVPtPKRPRGR	FALSE	4	up	CDK1;HIPK2
PRC1	T481	RRGLAPNtPGKARKL	FALSE	4	up	CDK16;CDK1
EIF4G1	T647	VLDKANKtPLRPLDP	FALSE	3	up	CDK2
HIST1H1E	T146	KKATGAAtPKKSAKK	FALSE	4	up	CDK2
LIG1	T233	KTLSSFFtPRKPAVK	FALSE	4	up	CDK2
RAD18	S99	LLQFALEsPAKSPAS	FALSE	4	up	CDK2
THRAP3	T874	EEWDPEYtPKSKKYY	FALSE	3	up	CDK2
LIN9	T96	KFTATMStPDKKASQ	FALSE	4	up	CDK3
TPX2	S486	LPITVPKsPAFALKN	FALSE	3	up	CDK5
CHEK1	S286	TSGGVSEsPSGFSKH	FALSE	4	down	CDK1;CDK2
EIF4EBP1	S65;T70	RNSPVTKtPPRDLPT	FALSE	3	down	CDK1;GSK3B;MAPK1; MTOR;MAP3K8
GMPS	T318	PISDEDRtPRKRISK	FALSE	3	up	CDK1
LMNA	S22;T19	SGAQASStPLSPTRI	FALSE	4	up	CDK1
TCOF1	T983	AQAQAAStPRKARAS	FALSE	4	up	CDK1
TCOF1	S156	ANLLSGKsPRKSAEP	FALSE	4	up	CDK1
TERF1	T371	VSKSQPVtPEKHRAR	FALSE	3	up	CDK1
BARD1	T299	KSRNEVVtPEKVCKN	FALSE	3	up	CDK1;CDK2
NPM1	T234;T237	SFKKQEKtPKTPKGP	FALSE	3	up	CDK1;CDK2
HMGA1	T78	KTRKTTTtPGRKPRG	FALSE	4	up	CDK1;HIPK2
ORC1	S273	VAFSEITsPSKRSQP	FALSE	3	up	CDK2
ORC2	T226	SAPVGKEtPSKRMKR	FALSE	3	up	CDK2
SF3B1	T211	ADQTPGAtPKKLSSW	FALSE	3	up	CDK2
ZNF609	T722	FTVNPALtPAKDKKK	FALSE	3	up	CDK2
NUP50	S221	KVAAETQsPSLFGST	FALSE	4	up	MAPK3;CDK1;MAPK1
STMN1	S16;S25	QAFELILsPRSKESV	FALSE	3	up	MAPK3;CDK1;MAPK14; CDK2;MAPK1;CDK5; MAPK9;MAPK13;MAPK8; PRKCB;MAPK10

Appendix 11. Information on the 164 p-sites regulated by GEM and at least three of the four clinical ATR inhibitors. The table includes 36 pSQ/pTQ sites that were significantly induced by GEM and mitigated by ATR inhibition.

Gene	P-site	Site sequence window	SQ/TQ	GEM log2 FC	GEM adj. *p*-value	GEM Regulation	ATRi Regulation	ATRi Count
AASDHPPT	S258	SRHQDVPsQDDSKPT	TRUE	2.4	3.6E-04	up	down	3
BRCA1	S1239	GKVNNIPsQSTRHST	TRUE	1.2	2.2E-03	up	down	3
BRD8	S621	ESGTIFGsQIKDAPG	TRUE	1.6	4.8E-05	up	down	4
CDKN2AIP	S198	ARSSGISsQNSSTSD	TRUE	1.8	2.8E-05	up	down	4
CHEK1	S317	ENVKYSSsQPEPRTG	TRUE	1.8	8.2E-06	up	down	4
CHEK1	S468	KLIDIVSsQKIWLPA	TRUE	4.2	1.1E-03	up	down	3
DHX9	S321	KLAQFEPsQRQNQVG	TRUE	1.7	5.4E-03	up	down	3
EXO1	S714	CNIKLLDsQSDQTSK	TRUE	2.4	9.4E-04	up	down	3
FANCD2	S319	LPSRLQAsQVKLKSK	TRUE	1.4	5.0E-03	up	down	4
HDGF	S103	KASGYQSsQKKSCVE	TRUE	2.0	1.0E-04	up	down	4
HMGA1	S36;S44	PGTALVGsQKEPSEV	TRUE	1.4	1.6E-04	up	down	4
HMGA1	S44	PGTALVGsQKEPSEV	TRUE	2.0	8.8E-06	up	down	4
HMGA1	S9	SESSSKSsQPLASKQ	TRUE	2.5	1.9E-05	up	down	4
HSPA4	S552	ESEEMETsQAGSKDK	TRUE	2.0	1.7E-03	up	down	3
HTATSF1	S481	RGFEGSCsQKESEEG	TRUE	1.5	1.8E-05	up	down	3
LRRC42	S385	LKHEAISsQESKKSK	TRUE	2.3	1.4E-07	up	down	4
NBN	S397	EQKFRMLsQDAPTVK	TRUE	2.4	3.6E-08	up	down	4
NBN	S615	VPESSKIsQENEIGK	TRUE	2.3	1.7E-05	up	down	3
NSUN5	S432	VEVPSSAsQAKASAP	TRUE	2.7	5.9E-03	up	down	3
PELP1	S1033	LAPEALPsQGEVERE	TRUE	1.4	9.5E-05	up	down	4
PHF14	S294	TNDSLTLsQSKSNED	TRUE	1.0	3.1E-03	up	down	4
PNISR	S706	EKDFKFSsQDDRLKR	TRUE	2.2	7.5E-05	up	down	3
PPM1G	S201	DSTRETPsQENGPTA	TRUE	2.7	2.0E-04	up	down	4
PPP6R3	S825	EEGKLSTsQDAACKD	TRUE	1.3	3.9E-03	up	down	3
PSMD4	S266	ALLKMTIsQQEFGRT	TRUE	1.4	1.4E-04	up	down	4
RAD18	S368	YKKIAGMsQKTVTIT	TRUE	2.0	3.8E-03	up	down	3
RIF1	S1873	LGDSKNVsQESLETK	TRUE	2.2	5.9E-06	up	down	3
SNRPA	S115	REKRKPKsQETPATK	TRUE	1.9	9.6E-05	up	down	4
TCEA1	S100;S97	PAITSQNsPEAREES	TRUE	2.0	7.0E-03	up	down	4
TCEB3	S251	FQDRLGAsQERHLGE	TRUE	1.5	2.6E-03	up	down	3
THAP4	S186	LATMVAGsQGKAEAS	TRUE	1.6	1.0E-03	up	down	3
TOPBP1	S1504	KELGTGLsQKRKAPT	TRUE	2.0	2.7E-04	up	down	4
TSEN34	S136	QASGASSsQEAGSSQ	TRUE	2.3	1.7E-05	up	down	4
UHRF1	S393	MASATSSsQRDWGKG	TRUE	1.4	2.0E-03	up	down	3
UIMC1	S171	LFKGSHIsQGNEAEE	TRUE	1.4	6.3E-04	up	down	4
ZC3H14	S135	DSRVSTSsQESKTTN	TRUE	2.2	3.5E-04	up	down	3
BRCA1	S1642	EKPELTAsTERVNKR	FALSE	2.5	8.9E-04	up	down	4
BTAF1	S224	KLFAKQRsRDAVETN	FALSE	1.5	5.0E-06	up	down	3
C7orf50	S23	NKKLKKAsAEGPLLG	FALSE	1.9	2.9E-05	up	down	3
CHEK1	S286	TSGGVSEsPSGFSKH	FALSE	1.9	1.3E-05	up	down	4
CWC25	S337	PGYTRKLsAEELERK	FALSE	2.4	8.2E-04	up	down	4
HNRNPM	S481	QTMERIGsGVERMGA	FALSE	1.6	1.8E-04	up	down	4
HNRNPM	S513	QTIERMGsGVERMGP	FALSE	1.8	2.4E-06	up	down	4
MKI67	T1764	RSLRKADtEEEFLAF	FALSE	1.5	1.1E-04	up	down	4
MYBBP1A	S1310	SLVIRSPsLLQSGAK	FALSE	1.5	1.8E-05	up	down	4
NEB	S2439;S2443	KRASEIIsEKKYRQP	FALSE	2.5	1.6E-06	up	down	3
NELFE	T91	SGFKRSRtLEGKLKD	FALSE	2.1	4.5E-04	up	down	4
NIPBL	S256	HMVHRLSsDDGDSST	FALSE	1.7	1.9E-04	up	down	4
NIPBL	T592	IVGSLKStPENHPET	FALSE	1.3	2.2E-04	up	down	4
PARN	S557	NHYYRNNsFTAPSTV	FALSE	1.8	6.7E-04	up	down	4
PNN	S66	LLLRRGFsDSGGGPP	FALSE	1.5	2.6E-06	up	down	3
RALY	S106	KGLKRAAsAIYRLFD	FALSE	2.6	8.4E-06	up	down	4
RALY	S176	RSTAVTTsSAKIKLK	FALSE	3.1	3.4E-05	up	down	4
SGOL2	T845	KDNFFSLtPKDKETI	FALSE	1.2	4.0E-03	up	down	3
TCEA1	S135	SSFPRAPsTSDSVRL	FALSE	2.6	1.3E-05	up	down	3
THRAP3	S377	EKIKEKGsFSDTGLG	FALSE	1.4	2.9E-04	up	down	3
THRAP3	S560	DFPTGKSsFSITREA	FALSE	1.7	7.9E-03	up	down	4
TOPBP1	S888	NAVALSAsPQLKEAQ	FALSE	1.7	7.5E-05	up	down	4
TRIP12	S1078	SGLARAAsKDTISNN	FALSE	1.3	3.0E-04	up	down	4

UIMC1	S597	QGDGPEGsGRACSTV	FALSE	2.3	4.5E-05	up	down	4
UVSSA	S657	GKKRRYPsLTNLKAQ	FALSE	1.7	3.9E-05	up	down	4
WDR55	S354	ALSSKTWsTDDFFAG	FALSE	1.9	3.0E-03	up	down	4
AHCTF1	S1283	TTSFFLNsPEKEHQE	FALSE	-1.0	3.4E-05	down	up	3
AHCTF1	T1257	SKLEVFTtPKKCAVP	FALSE	-1.3	1.6E-06	down	up	4
ANLN	S449	FDKGNIWsAEKGGNS	FALSE	-1.1	1.6E-03	down	up	3
ANLN	S471	KQETHCQsTPLKKHQ	FALSE	-1.3	1.9E-03	down	up	3
ARHGAP11A	S422	SGKAGCFsPKISHKE	FALSE	-1.1	1.2E-04	down	up	4
ARHGAP11A	T323	SESPVILtPNAKRTL	FALSE	-1.0	3.8E-05	down	up	3
BOD1L1	S2905	GIVTVEQsPSSSKLK	FALSE	-1.3	3.5E-04	down	up	4
C5orf34	S616	EVNENRVsIALKKTS	FALSE	-1.2	3.4E-04	down	up	3
CD3EAP	S285	PLEDTVLsPTKKRKR	FALSE	-1.0	1.3E-05	down	up	4
CHAMP1	S286;S297	RKPSPSEsPEPWKPF	FALSE	-1.1	7.0E-04	down	up	3
CHTF18	S225	LLGVSLAsLKKQVDG	FALSE	-1.9	8.2E-04	down	up	3
CIZ1	T585	STPAATStPSKQALQ	FALSE	-1.3	2.9E-05	down	up	4
DNTTIP2	S117	RQILIACsPVSSVRK	FALSE	-1.1	1.1E-04	down	up	3
DTL	S676	KRKAENPsPRSPSSQ	FALSE	-1.1	2.9E-05	down	up	4
E2F8	S71	KMLISAVsPEIRNRD	FALSE	-1.9	5.8E-06	down	up	4
EIF4G1	T647	VLDKANKtPLRPLDP	FALSE	-1.0	5.5E-05	down	up	3
GSG2	T112	ARPSLTVtPRRLGLR	FALSE	-1.5	8.4E-06	down	up	4
GSG2	T97	DRPSLTVtPKRWKLR	FALSE	-1.3	5.9E-04	down	up	3
GTF2I	T558	VTQPRTNtPVKEDWN	FALSE	-1.4	1.9E-03	down	up	3
HIST1H1C	T146	KKAAGGAtPKKSAKK	FALSE	-2.1	1.9E-04	down	up	4
HIST1H1D	S2;T18	IPAPAEKtPVKKKAK	FALSE	-1.2	5.4E-04	down	up	3
HIST1H1D	T147	KKVAGAAtPKKSIKK	FALSE	-2.1	1.9E-05	down	up	4
HIST1H1D	T18	IPAPAEKtPVKKKAK	FALSE	-1.8	1.8E-07	down	up	4
HIST1H1E	S2;T18	APAPAEKtPVKKKAR	FALSE	-1.2	1.9E-05	down	up	4
HIST1H1E	T146	KKATGAAtPKKSAKK	FALSE	-2.1	2.8E-04	down	up	4
HIST1H1E	T18	APAPAEKtPVKKKAR	FALSE	-1.7	2.9E-07	down	up	4
HJURP	S412	RTLKWLIsPVKIVSR	FALSE	-1.4	8.1E-06	down	up	4
HMGA1	T42	KEPSEVPtPKRPRGR	FALSE	-1.3	1.6E-05	down	up	4
HP1BP3	S465	QKKTPAKsPGKAASV	FALSE	-1.5	1.8E-05	down	up	3
INCENP	S275	DSPAFPDsPWRERVL	FALSE	-1.5	6.3E-04	down	up	4
INCENP	T292	ILPDNFStPTGSRTD	FALSE	-1.3	6.2E-04	down	up	3
INO80E	T90	GTPKLSDtPAPKRKR	FALSE	-1.2	2.0E-04	down	up	4
INTS3	S995	RRKAALSsPRSRKNA	FALSE	-1.1	3.2E-05	down	up	3
KIF20B	S1756	KKIIETMsSSKLSNV	FALSE	-1.8	4.6E-04	down	up	3
KIF20B	T1644	VKHPGCTtPVTVKIP	FALSE	-1.2	1.1E-05	down	up	4
KMT2A	T2525	RTVKVTLtPLKMENE	FALSE	-1.2	1.7E-03	down	up	4
LIG1	T233	KTLSSFFtPRKPAVK	FALSE	-1.5	1.5E-04	down	up	4
LIN54	S310;S314	TPNKIAIsPLKSPNK	FALSE	-1.4	1.3E-05	down	up	4
LIN9	T96	KFTATMStPDKKASQ	FALSE	-1.3	8.4E-07	down	up	4
MASTL	S453	NFELVDSsPCKKIIQ	FALSE	-1.0	4.0E-06	down	up	4
MCM4	S120	RQRPDLGsAQKGLQV	FALSE	-1.6	9.7E-06	down	up	4
MEPCE	S254	EGHVVLAsPLKTGRK	FALSE	-1.1	5.6E-05	down	up	3
MKI67	S1636	SKRRLKTsLGKVGVK	FALSE	-1.2	2.8E-04	down	up	3
MKI67	S1937;S2420	LLGNLPGsKRQPQTP	FALSE	-1.2	1.2E-04	down	up	3
MKI67	S648	MICSKRRsGASEANL	FALSE	-1.2	1.8E-05	down	up	3
MKI67	T1193;T1557;T2285	DIKAFMGtPVQKLDL	FALSE	-1.1	8.6E-04	down	up	3
MKI67	T1315	DIIIFVGtPVQKLDL	FALSE	-1.2	9.6E-05	down	up	3
MKI67	T1327;T1569	LDLTENLtGSKRRLQ	FALSE	-1.2	2.0E-04	down	up	3
MKI67	T1355	GFKELFQtPGHTEEA	FALSE	-1.2	2.7E-04	down	up	4
MKI67	T1747	SQPDLVDtPTSSKPQ	FALSE	-1.3	2.1E-03	down	up	3
MKI67	T1801	DINTFLGtPVQKLDQ	FALSE	-1.4	2.4E-04	down	up	3
MKI67	T2325	GFKELFQtPGTDKPT	FALSE	-1.3	2.6E-04	down	up	3
MKI67	T328	RDVESVQtPSKAVGA	FALSE	-1.4	8.2E-06	down	up	4
MKI67	T761	GIAEMFKtPVKEQPQ	FALSE	-1.5	9.6E-05	down	up	4
MTA1	S562	SVSSVLSsLTPAKVA	FALSE	-1.5	5.7E-03	down	up	3
MTA1	S576	APVINNGsPTILGKR	FALSE	-1.3	1.8E-05	down	up	3
MTA1	T564	SSVLSSLtPAKVAPV	FALSE	-1.4	3.7E-04	down	up	4
MTA2	T505	RLPKAAKtPLKIHPL	FALSE	-1.8	8.6E-05	down	up	4
MYBL2	T494	TPLHRDKtPLHQKHA	FALSE	-2.7	9.6E-04	down	up	3
NCL	T121	PGKALVAtPGKKGAA	FALSE	-1.4	6.2E-04	down	up	3

NCL	T84	PAKKAAVtPGKKAAA	FALSE	-1.3	4.7E-04	down	up	3
NCL	T99	TPAKKTVtPAKAVTT	FALSE	-1.5	3.3E-04	down	up	3
NIFK	T223	KVSGTLDtPEKTVDS	FALSE	-1.2	2.1E-08	down	up	3
NIFK	T279	EEIQETQtPTHSRKK	FALSE	-1.1	3.9E-06	down	up	3
NOLC1	T597	EAAKEAEtPQAKKIK	FALSE	-1.4	3.3E-04	down	up	4
NUP153	T699	AKQTGIEtPNKSGKT	FALSE	-1.2	1.8E-04	down	up	4
ORC1	S287	PDKLQTLsPALKAPE	FALSE	-1.1	4.9E-05	down	up	3
PDS5A	T1208	PVRIISVtPVKNIDP	FALSE	-1.5	3.0E-06	down	up	4
PDS5B	T1121	PEMKSFFtPGKPKTT	FALSE	-1.4	7.9E-04	down	up	3
POLA2	T127;T130	SQKRAIStPETPLTK	FALSE	-1.3	8.3E-04	down	up	3
POM121	T474	QNSNSQStPGSSGQR	FALSE	-1.8	2.1E-04	down	up	3
PRC1	T481	RRGLAPNtPGKARKL	FALSE	-1.3	3.3E-04	down	up	4
PSIP1	T141	TKAVDITtPKAARRG	FALSE	-1.2	5.1E-05	down	up	3
RAD18	S99	LLQFALEsPAKSPAS	FALSE	-1.4	5.7E-06	down	up	4
RB1	T841	SIGESFGtSEKFQKI	FALSE	-1.6	1.2E-05	down	up	4
RBM27	T888	KTSSAVStPSKVKTK	FALSE	-1.4	1.1E-03	down	up	4
RFC1	S312	DKIGEVSsPKASSKL	FALSE	-1.5	9.6E-05	down	up	3
RIF1	S2161	SLVSANDsPSGMQTR	FALSE	-1.2	6.7E-05	down	up	3
RIF1	S2196	SQEDEISsPVNKVRR	FALSE	-1.9	6.4E-06	down	up	4
RNMT	T77	SSSCGKDtPSKKRKL	FALSE	-1.2	2.6E-04	down	up	4
RRP15	S226	GSTNETAsSRKKPKA	FALSE	-1.2	9.4E-05	down	up	3
RSL1D1	S427;T423	ESETPGKsPEKKPKI	FALSE	-1.1	9.1E-04	down	up	3
RSL1D1	T401	AKSPNPStPRGKKRK	FALSE	-1.6	5.1E-04	down	up	4
RSL1D1	T415	KALPASEtPKAAESE	FALSE	-1.4	1.1E-04	down	up	4
SLTM	T74	ELTVSTDtPNKKPTK	FALSE	-1.2	4.5E-04	down	up	3
SMARCC1	T398	LKKDSENtPVKGGTV	FALSE	-1.1	2.2E-05	down	up	3
SRRM2	T2599	EGRPPEPtPAKRKRR	FALSE	-1.5	2.3E-04	down	up	3
STAU1	T372	ALKSEEKtPIKKPGD	FALSE	-1.1	2.9E-05	down	up	3
TCEB3	T397	KGSNNLKtPEGKVKT	FALSE	-1.4	2.9E-04	down	up	3
TCF7L2	NA	DKQPGETNDANtPK	FALSE	-1.2	6.3E-04	down	up	3
TCOF1	T249	PGKVGDVtPQVKGGA	FALSE	-1.3	1.8E-03	down	up	4
THRAP3	T874	EEWDPEYtPKSKKYY	FALSE	-1.2	1.0E-05	down	up	3
TLK2	T52	LSDKEVEtPEKKQND	FALSE	-2.0	3.6E-04	down	up	3
TPR	T1677	KPTPVVStPSKVTAA	FALSE	-1.2	2.7E-05	down	up	4
TPX2	S486	LPITVPKsPAFALKN	FALSE	-1.1	2.8E-04	down	up	3
TPX2	T369	KICRDPQtPVLQTKH	FALSE	-1.3	8.7E-05	down	up	4
TPX2	T72	NLQQAIVtPLKPVDN	FALSE	-1.2	2.6E-04	down	up	3
USP1	S327	KYISENEsPRPSQKK	FALSE	-1.2	2.6E-03	down	up	3
VPRBP	S255	KTSSRVNsTTKPEDG	FALSE	-1.8	3.4E-05	down	up	4
WIZ	S996	TPLALAGsPTPKNPE	FALSE	-1.1	2.8E-05	down	up	4
ZC3H11A	T321	PETNIDKtPKKAQVS	FALSE	-1.3	9.5E-05	down	up	4
ZNF318	S1896	APELLLHsPARSAMC	FALSE	-1.3	1.0E-05	down	up	3

Appendix 12. Log_2 fold change in phosphorylation (PTM) of p-sites regulated by GEM and at least three of the four clinical ATR inhibitors. Only the 30 most strongly affected sites that were inhibited by GEM and induced by ATR inhibition are shown. Blue text highlights proteins annotated within the ATR signaling pathway (WP4016).

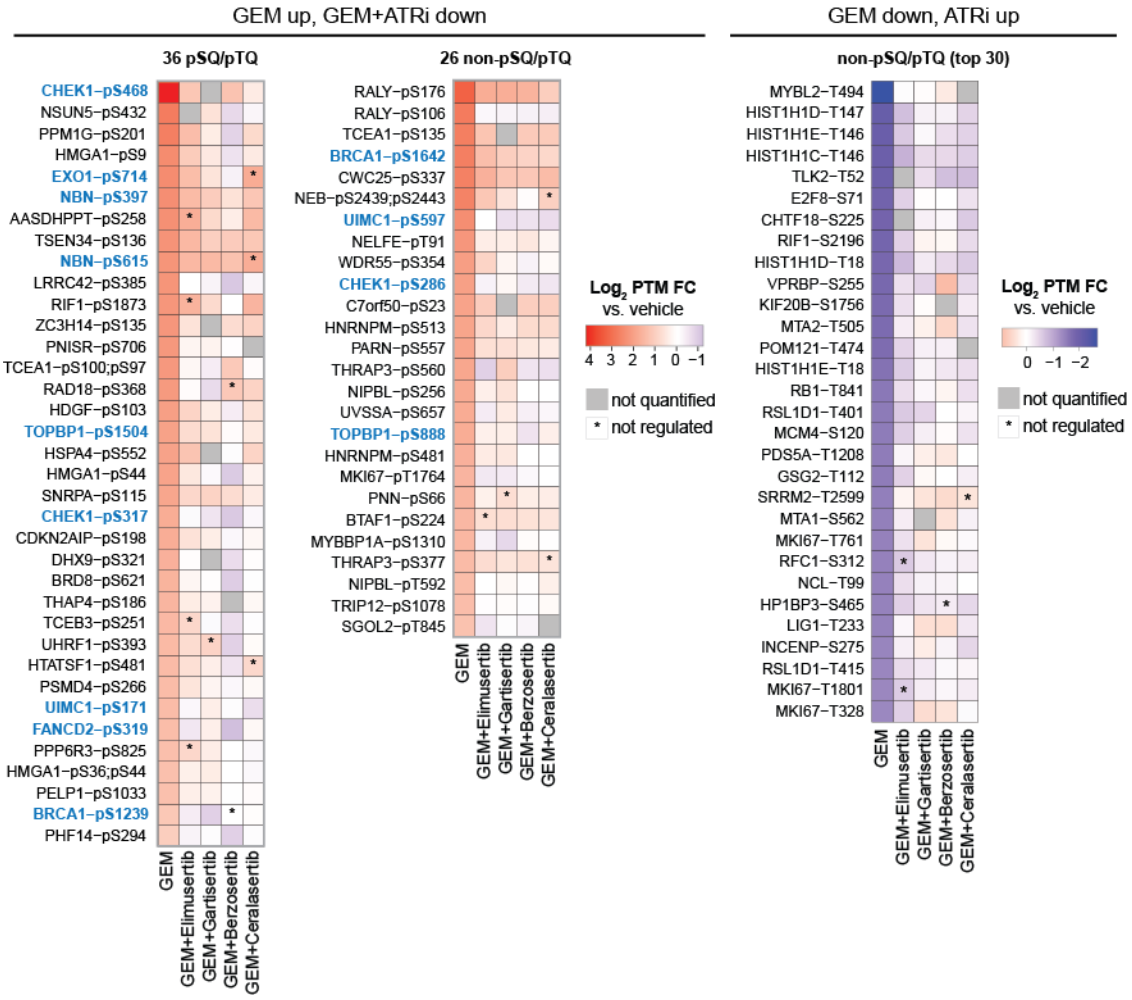

Appendix 13. Functional annotation of the 32 proteins carrying the 36 pSQ/pTQ sites explaining drug synergy based on information from UniProtKB (https://uniprot.org/). Table provides information whether the proteins were involved in the ATR signaling pathway (Wikipathways entry WP4016) and the STRING network described in Chapter 3.3.4, and whether p-sites were found in the work of Matsuoka et al. (2007)[73] or Jadav et al. (2024)[239].

Gene	P-site	WP4016	STRING	Functional annotation	Matsuoka et al. (2007)	Jadav et al. (2024)
CHEK1	S468	y	y	Cell cycle regulation	-	-
CHEK1	S317	y	y	Cell cycle regulation	y	y
EXO1	S714	y	y	DNA repair	y	y
FANCD2	S319	y	y	DNA repair	-	y
NBN	S615	y	y	DNA repair	-	y
NBN	S397	y	y	DNA repair	y	y
TOPBP1	S1504	y	y	DNA repair	-	y
UIMC1	S171	y	y	DNA repair	-	-
BRCA1	S1239	y	y	DNA repair, Cell cycle regulation	y	y
RIF1	S1873	-	y	DNA repair	-	-
PSMD4	S266	-	y	Protein homeostasis	-	y
UHRF1	S393	-	y	Protein homeostasis	-	-
RAD18	S368	-	y	Protein homeostasis, DNA repair	-	y
SNRPA	S115	-	y	RNA processing	-	-
HTATSF1	S481	-	y	RNA processing (elongation)	y	y
TCEA1	S100;S97	-	y	RNA processing (elongation)	-	-
TCEB3	S251	-	y	RNA processing (elongation)	-	y
DHX9	S321	-	y	RNA processing (helicase)	y	y
PNISR	S706	-	y	RNA processing (splicing)	y	y
PPM1G	S201	-	y	RNA processing (splicing)	-	y
HSPA4	S552	-	y	Various	y	-
CDKN2AIP	S198	-	-	Cell cycle regulation	-	-
AASDHPPT	S258	-	-	NA	y	y
LRRC42	S385	-	-	NA	-	-
NSUN5	S432	-	-	NA	y	-
PPP6R3	S825	-	-	NA	-	-
ZC3H14	S135	-	-	NA	-	y
THAP4	S186	-	-	RNA processing (splicing)	-	-
TSEN34	S136	-	-	RNA processing (splicing)	-	-
HDGF	S103	-	-	Transcriptional regulation	-	-
HMGA1	S44	-	-	Transcriptional regulation	y	-
HMGA1	S9	-	-	Transcriptional regulation	-	y
HMGA1	S36;S44	-	-	Transcriptional regulation	y	-
PELP1	S1033	-	-	Transcriptional regulation	y	-
PHF14	S294	-	-	Transcriptional regulation	-	y
BRD8	S621	-	-	Transcriptional regulator	-	-

Appendix 14. Proteins affected in expression by treatment with either 1 µM Elimusertib or 1 µM GEM. The table provides the log_2 fold changes for each tested incubation time. Regulation was defined by abs. log_2 fold changes > 1 for two consecutive time points or abs. log_2 fold changes > 2 at 24 h (annotated with '(24h)'). The proteins RRM2 and WDR76 are highlighted in blue text.

Gene	15 min	30 min	1 h	2 h	4 h	8 h	12 h	24 h	Drug (1 µM)	Regulated
FGF19	0.1	0.2	0.0	-0.6	-1.3	-1.3	-0.6	-2.9	Elimusertib	down
CCDC34	0.3	-0.6	-0.2	0.8	-0.1	-0.2	-1.1	-2.8	Elimusertib	down
PRELID1	-0.3	-0.3	-0.7	-0.6	-1.1	-1.1	-1.9	-2.3	Elimusertib	down
SCD	-0.2	0.3	-0.1	-0.1	-0.4	-0.7	-1.5	-2.1	Elimusertib	down
KIAA0101	0.0	-0.1	0.0	-0.4	-0.6	-1.1	-2.0	-2.1	Elimusertib	down
ATAD2	0.1	-0.2	0.0	-0.2	-0.9	-1.2	-1.7	-2.0	Elimusertib	down
WDR76	0.0	-0.5	-0.2	0.0	-0.9	-0.8	-1.5	-2.0	**Elimusertib**	**down**
PCSK9	0.2	-0.1	0.3	0.5	-1.0	-0.1	-1.6	-1.9	Elimusertib	down
GMNN	0.1	-0.1	0.1	-0.1	-0.2	-0.2	-1.0	-1.7	Elimusertib	down
SPICE1	-0.3	-0.2	0.8	-0.1	0.0	0.8	-1.1	-1.7	Elimusertib	down
TYMS	0.1	-0.1	-0.1	0.1	-0.3	-0.4	-1.1	-1.6	Elimusertib	down
C8orf59	0.2	-0.4	0.1	-0.4	-1.1	-0.9	-1.3	-1.5	Elimusertib	down
TIMELESS	-0.1	0.0	0.0	0.2	-0.4	-0.6	-1.1	-1.5	Elimusertib	down
CDC25B	-0.2	0.3	-0.1	-0.2	-0.5	0.1	-1.7	-1.5	Elimusertib	down
SLBP	0.3	-0.2	-0.1	0.1	-0.9	-0.9	-1.1	-1.2	Elimusertib	down
C1orf106	0.0	-0.1	-0.1	0.2	-0.6	-0.5	-1.1	-1.2	Elimusertib	down
RAD51AP1	-0.7	-0.1	0.5	0.2	-0.5	-0.4	-1.1	-1.2	Elimusertib	down
SERF2	-0.1	-0.1	-0.1	0.1	-0.6	-0.2	-1.2	-1.1	Elimusertib	down
FANCG	-0.5	-0.5	0.2	-0.5	-0.3	-0.2	-1.2	-1.0	Elimusertib	down
MZT1	0.0	-0.2	-1.4	-1.0	-0.3	0.2	-0.1	-0.4	Elimusertib	down
HTRA1	-0.1	0.3	-0.3	-0.1	-0.8	-1.2	-1.1	0.0	Elimusertib	down
MTO1	0.1	-2.3	-0.7	-0.9	-1.2	-1.2	-0.9	1.3	Elimusertib	down
KCTD20	-0.2	0.2	0.3	0.2	0.4	0.4	-1.0	-1.3	GEM	down
F9	0.8	-0.3	1.2	0.8	0.4	1.2	1.2	-1.3	GEM	down
PLTP	0.2	0.6	0.0	-0.8	0.2	0.2	-1.2	-1.2	GEM	down
NUSAP1	0.1	0.0	0.0	-0.2	-0.8	-1.4	-1.2	-0.8	GEM	down
CDC25B	-0.2	-0.5	-0.1	-0.2	-1.3	-1.3	-1.3	-0.5	GEM	down
COL1A2	-0.1	0.0	0.2	-0.2	-0.9	-1.1	-1.1	-0.3	GEM	down
DCAF12	0.2	0.5	-0.2	-1.1	-1.5	-1.1	-0.2	-0.2	GEM	down
KLHL12	-0.2	1.0	1.3	-1.5	-0.1	-1.0	-0.6	1.0	GEM	down
SAPCD2	0.1	0.0	0.1	-0.2	-0.5	-0.6	-0.6	-2.4	Elimusertib	down (24h)
LGR5	-0.2	-0.1	0.0	-0.5	0.1	0.0	-0.5	-2.4	Elimusertib	down (24h)
Q2M2H8	-0.1	-0.3	0.1	-0.4	0.1	0.1	-0.7	-2.2	Elimusertib	down (24h)
SMIM22	0.8	-0.4	0.3	-0.7	-0.1	-0.1	-0.6	-2.2	Elimusertib	down (24h)
PLTP	-0.1	-0.4	0.0	-1.3	-0.5	-0.9	-0.2	-2.1	Elimusertib	down (24h)
NET1	-0.2	-0.4	0.4	-0.7	-0.5	-0.5	-0.2	-2.0	Elimusertib	down (24h)
ETNPPL	0.0	-0.1	-0.1	-0.3	0.3	0.3	-0.3	-8.9	GEM	down (24h)
IQGAP2	-0.2	-1.2	-0.8	-0.7	-0.6	-0.5	-0.7	-5.9	GEM	down (24h)
TTC16	0.3	-0.3	-0.2	-0.2	0.1	-0.1	-0.2	-5.8	GEM	down (24h)
A2M	0.2	-0.1	-0.2	-0.1	0.3	-0.3	-0.5	-5.7	GEM	down (24h)
FHAD1	0.7	0.4	-0.4	-0.4	0.3	0.1	-0.2	-5.4	GEM	down (24h)
PRDM12	0.5	-0.6	-0.1	-0.4	0.0	0.0	-0.2	-5.1	GEM	down (24h)
SSH1	0.3	-0.3	-0.2	-0.5	0.1	0.1	-0.3	-4.8	GEM	down (24h)
AFP	0.3	-0.7	-0.2	-0.3	0.0	-0.4	-0.6	-4.7	GEM	down (24h)
SLC27A1	0.3	-0.2	-0.3	-0.2	-0.1	-0.1	-0.3	-4.6	GEM	down (24h)
MYEOV2	-0.1	0.5	0.2	0.4	0.3	0.4	-0.1	-4.5	GEM	down (24h)
GRID2	-0.1	-0.3	-0.6	-0.1	-0.1	0.1	-0.5	-4.2	GEM	down (24h)
TRAPPC8	0.5	-0.2	-0.3	0.0	0.5	0.0	-0.5	-4.2	GEM	down (24h)
CYP2A13	0.4	-0.4	-0.3	-0.2	0.1	-0.1	-0.2	-4.1	GEM	down (24h)
HSP90AA4P	0.1	-0.5	-0.2	-0.3	-0.2	-0.2	-0.6	-4.0	GEM	down (24h)
CLIC5;CLIC6	0.5	-0.3	-0.2	-0.1	0.3	0.2	-0.4	-3.9	GEM	down (24h)
TLR6	0.2	-0.2	-0.4	-0.2	-0.2	-0.1	-0.3	-3.5	GEM	down (24h)
TTLL4	0.7	-0.3	-0.2	-0.2	-0.6	0.0	-0.1	-3.5	GEM	down (24h)
ADAM12	0.4	-0.4	-0.3	-0.4	0.3	0.0	-0.7	-3.5	GEM	down (24h)
CCDC18	0.4	-0.3	-0.4	0.0	0.5	0.0	-0.5	-3.5	GEM	down (24h)
ARID1A	1.1	0.3	0.2	0.2	0.4	0.2	-0.7	-3.4	GEM	down (24h)
CYB5A	0.0	0.4	-0.1	-0.2	0.1	0.4	0.0	-3.4	GEM	down (24h)
DOCK7	0.5	-0.2	-0.4	-0.1	0.1	0.2	-0.3	-3.2	GEM	down (24h)
TADA3	0.7	-0.2	-0.4	-0.1	-0.2	0.3	-0.6	-2.9	GEM	down (24h)

PEX5	0.3	0.1	-0.6	-0.3	-0.4	-0.1	-0.2	-2.9	GEM	down (24h)
TFAP2D	0.4	-0.2	-0.2	-0.3	0.1	-0.1	-0.8	-2.8	GEM	down (24h)
ARHGEF39	0.4	-0.9	-0.4	-0.1	-0.1	-0.2	-0.7	-2.7	GEM	down (24h)
ATP6V1F	-0.1	-0.1	-0.1	-0.2	0.1	0.0	0.3	-2.7	GEM	down (24h)
NT5DC4	1.8	0.2	-0.2	-0.2	0.1	0.0	-0.7	-2.6	GEM	down (24h)
DPYSL4	0.4	-0.3	-0.1	-0.1	0.3	0.0	-0.5	-2.6	GEM	down (24h)
GTF2A1	-0.4	0.2	0.0	-0.8	0.1	0.4	0.7	-2.5	GEM	down (24h)
FXN	0.1	0.0	0.0	0.1	0.1	0.0	-0.2	-2.4	GEM	down (24h)
ENO3	0.2	-0.5	-0.3	-0.4	0.2	-0.2	-0.5	-2.4	GEM	down (24h)
GATC	0.1	0.1	0.1	-0.1	0.2	0.2	-0.1	-2.3	GEM	down (24h)
FGF19	-0.4	0.2	0.3	0.0	0.5	-0.4	-0.1	-2.3	GEM	down (24h)
MIEN1	0.0	-0.3	0.3	0.2	0.2	0.0	-0.3	-2.2	GEM	down (24h)
YDJC	-0.2	-0.2	-0.1	0.1	0.3	0.2	-0.7	-2.2	GEM	down (24h)
ABCD4	0.4	-0.3	-0.6	0.0	-0.3	-0.1	-0.5	-2.1	GEM	down (24h)
MYL3;MYL1	0.1	-0.3	-0.3	0.0	0.1	-0.2	-0.3	-2.0	GEM	down (24h)
CFAP36	0.2	-0.3	-0.2	-0.2	0.0	0.0	-0.3	-2.0	GEM	down (24h)
TADA2B	-0.8	2.2	-0.3	0.4	1.8	-1.1	-1.9	-2.0	Elimusertib	up
RAB38	-0.8	0.5	-0.7	1.3	1.1	0.6	0.6	0.7	Elimusertib	up
GJB3	0.1	0.0	0.4	0.6	0.3	0.0	1.4	1.1	Elimusertib	up
DUSP4	0.1	-0.6	0.1	0.1	0.1	0.4	1.1	1.6	Elimusertib	up
PUM2	0.6	0.2	1.5	1.2	0.5	-0.9	-0.6	-0.1	GEM	up
AP1AR	1.3	0.1	-0.5	-0.2	-0.4	1.2	1.2	0.6	GEM	up
ACSF2	-0.4	0.7	1.2	1.2	-0.5	0.4	-0.2	0.7	GEM	up
SYNJ1	0.8	-0.5	0.0	-0.5	-0.2	-0.2	1.1	1.1	GEM	up
CUL7	1.0	1.9	-0.7	-0.2	-1.0	0.8	0.2	1.5	GEM	up
DGAT1	-0.1	0.4	0.6	-0.1	0.7	-0.1	1.0	1.6	GEM	up
RRM2	0.1	0.2	0.1	0.1	0.2	0.4	1.2	1.6	**GEM**	**up**
GBA2	0.0	-0.4	0.4	0.1	0.0	-1.1	1.3	1.8	GEM	up
SLC30A7	-0.5	-0.2	-0.1	-0.1	0.8	-0.6	1.2	1.8	GEM	up
KDELR1	1.2	0.1	-0.1	0.4	-0.2	-0.5	0.5	2.0	GEM	up (24h)
BSCL2	-0.5	0.4	-0.6	0.3	0.0	-0.5	0.4	2.1	GEM	up (24h)
TMEM202	-0.3	0.7	-0.2	0.9	0.0	1.3	-0.2	2.1	GEM	up (24h)
PRKACA	1.0	-0.1	1.0	-0.5	0.9	0.0	0.3	2.2	GEM	up (24h)
CLN6	0.0	1.1	-0.8	0.0	-1.2	0.5	0.1	2.4	GEM	up (24h)
RASSF10	-0.2	0.5	0.1	0.8	-0.3	1.7	-0.5	2.6	GEM	up (24h)
HELZ2	-0.3	1.0	0.0	0.2	0.0	0.9	-0.1	2.6	GEM	up (24h)
E2F6	-0.5	-1.1	1.0	0.6	0.2	0.3	0.1	3.1	GEM	up (24h)

Acknowledgements

Firstly, I would like to thank my doctoral advisor, Bernhard, for giving me the opportunity to pursue my PhD on such an exciting and important topic. Our collaboration was the ideal balance of your support and my freedom to shape the project in my own way. Thank you also for granting me the necessary space at work when I needed it during challenging personal times, it helped me a lot.

I am also grateful to all the members of TTTT who spent the past few years with me at the Chair, making it such a wonderful experience. The numerous fun moments and experiences we shared will always be fond memories. In particular, I want to highlight the Flamingos – Polina, Nicole, Lapo, Julian, and Firas. Our unforgettable celebrations and trips, along with the amusing office days, have fostered friendships that mean a great deal to me. My time with you at the Chair has been incredibly helpful in getting back on my feet after difficult times, and for that, I will always be very grateful.

Two Flamingos who have been with me from the beginning of my Ph.D. journey are Polina and Nicole. PP, you quickly transitioned from being my supervisor to becoming my friend, and I am still so grateful to have you. NK, we share something truly special. Being hired for the same project back then meant we went through a lot together – both the good and the challenging times. Needless to say, this entire journey would have been only half as entertaining and enjoyable without you.

Special thanks also go to the whole team for the many helpful discussions and inputs that advanced my project significantly, with particular thanks to Flo and Steffi W. Additionally, I want to thank Teresa Rogler and Larissa Frasch, whom I had the pleasure of mentoring during their internships and master's theses. A further big thank you to Polina and Larissa for taking the time to provide valuable feedback on my written dissertation.

Finally, my heartfelt thanks to my family. Dear Mom and Dad, thank you for always supporting me and allowing me the freedom to pursue my goals. You have been through so much, and I am truly proud of you. Thanks also to C., my loving partner and husband. I want to thank you for your patience and understanding over the past years and for always believing in me. Without you, I would not have had the confidence to take many important steps in my life, and I would not be where I am today.

I dedicate this dissertation to my beloved sister, Melli. She was always the one who celebrated the successes of others as joyfully as if they were her own.

List of Publications

Main publications:

2024 **Gemcitabine and ATRi synergize to kill PDAC cells by blocking DNA damage response**
Stefanie Höfer, Larissa Frasch, Kerstin Putzker, Joe Lewis, Hendrik Schürmann, Valentina Leone, Amirhossein Sakhteman, Matthew The, Florian P. Bayer, Julian Müller, Firas Hamood, Jens T. Siveke, Maximilian Reichert, Bernhard Kuster (2025), *Molecular Systems Biology*
https://doi.org/10.1038/s44320-025-00085-6

Additional publications during PhD:

2024 **A Novel AMPK Inhibitor Sensitizes Pancreatic Cancer Cells to Ferroptosis Induction**
Carolin Schneider, Jorina Hilbert, Franziska Genevaux, Stefanie Höfer, Lukas Krauß, Felix Schicktanz, Constanza Tapia Contreras, Shaishavi Jansari, Aristeidis Papargyriou, Thorsten Richter, Abdallah M. Alfayomy, Chiara Falcomatà, Christian Schneeweis, Felix Orben, Ruppert Öllinger, Florian Wegwitz, Angela Boshnakovska, Peter Rehling, Denise Müller, Philipp Ströbel, Volker Ellenrieder, Lena Conradi, Elisabeth Hessmann, Michael Ghadimi, Marian Grade, Matthias Wirth, Katja Steiger, Roland Rad, Bernhard Kuster, Wolfgang Sippl, Maximilian Reichert, Dieter Saur, Günter Schneider (2024), *Advanced Sciences, 2307695*

2022 **Merits of Diazirine Photo-Immobilization for Target Profiling of Natural Products and Cofactors**
Polina Prokofeva, Stefanie Höfer, Maximilian Hornisch, Miriam Abele, Bernhard Kuster, Guillaume Médard (2022), *ACS Chemical Biology 17 (11), 3100-3109*

2021 **Robust microflow LC-MS/MS for proteome analysis: 38 000 runs and counting**
Yangyang Bian, Florian P Bayer, Yun-Chien Chang, Chen Meng, Stefanie Höfer, Nan Deng, Runsheng Zheng, Oleksandr Boychenko, Bernhard Kuster (2021), *Analytical Chemistry 93 (8), 3686-3690*

Additional publication before PhD:

2018 **Near-native, site-specific and purification-free protein labeling for quantitative protein interaction analysis by MicroScale Thermophoresis**
Tanja Bartoschik, Stefanie Galinec, Christian Kleusch, Katarzyna Walkiewicz, Dennis Breitsprecher, Sebastian Weigert, Yves A. Muller, Changjiang You, Jacob Piehler, Thomas Vercruysse, Dirk Daelemans, Nuska Tschammer (2018), *Scientific reports 8 (1), 1-10*

References

1 Schawkat, K., Manning, M. A., Glickman, J. N. & Mortele, K. J. Pancreatic Ductal Adenocarcinoma and Its Variants: Pearls and Perils. *Radiographics* **40**, 1219-1239 (2020). https://doi.org:10.1148/rg.2020190184

2 Siegel, R. L., Miller, K. D., Wagle, N. S. & Jemal, A. Cancer statistics, 2023. *CA Cancer J Clin* **73**, 17-48 (2023). https://doi.org:10.3322/caac.21763

3 National Cancer Institute. *Surveillance, Epidemiology, and End Results program*, <https://seer.cancer.gov/statistics-network/explorer/> (2024).

4 Jiang, Y. & Sohal, D. P. S. Pancreatic Adenocarcinoma Management. *JCO Oncol Pract* **19**, 19-32 (2023). https://doi.org:10.1200/OP.22.00328

5 Kolbeinsson, H. M., Chandana, S., Wright, G. P. & Chung, M. Pancreatic Cancer: A Review of Current Treatment and Novel Therapies. *J Invest Surg* **36**, 2129884 (2023). https://doi.org:10.1080/08941939.2022.2129884

6 Wood, L. D., Canto, M. I., Jaffee, E. M. & Simeone, D. M. Pancreatic Cancer: Pathogenesis, Screening, Diagnosis, and Treatment. *Gastroenterology* **163**, 386-402 e381 (2022). https://doi.org:10.1053/j.gastro.2022.03.056

7 Burris, H. A., 3rd *et al.* Improvements in survival and clinical benefit with gemcitabine as first-line therapy for patients with advanced pancreas cancer: a randomized trial. *J Clin Oncol* **15**, 2403-2413 (1997). https://doi.org:10.1200/JCO.1997.15.6.2403

8 Plunkett, W. *et al.* Gemcitabine: metabolism, mechanisms of action, and self-potentiation. *Semin Oncol* **22**, 3-10 (1995).

9 Gradishar, W. J. Albumin-bound paclitaxel: a next-generation taxane. *Expert Opin Pharmacother* **7**, 1041-1053 (2006). https://doi.org:10.1517/14656566.7.8.1041

10 Von Hoff, D. D. *et al.* Increased survival in pancreatic cancer with nab-paclitaxel plus gemcitabine. *N Engl J Med* **369**, 1691-1703 (2013). https://doi.org:10.1056/NEJMoa1304369

11 Conroy, T. *et al.* FOLFIRINOX versus gemcitabine for metastatic pancreatic cancer. *N Engl J Med* **364**, 1817-1825 (2011). https://doi.org:10.1056/NEJMoa1011923

12 Raphael, M. J. *et al.* The Association of Drug-Funding Reimbursement With Survival Outcomes and Use of New Systemic Therapies Among Patients With Advanced Pancreatic Cancer. *JAMA Netw Open* **4**, e2133388 (2021). https://doi.org:10.1001/jamanetworkopen.2021.33388

13 Tong, H., Fan, Z., Liu, B. & Lu, T. The benefits of modified FOLFIRINOX for advanced pancreatic cancer and its induced adverse events: a systematic review and meta-analysis. *Sci Rep* **8**, 8666 (2018). https://doi.org:10.1038/s41598-018-26811-9

14 O'Reilly, E. M. *et al.* Randomized, Multicenter, Phase II Trial of Gemcitabine and Cisplatin With or Without Veliparib in Patients With Pancreas Adenocarcinoma and a Germline BRCA/PALB2 Mutation. *J Clin Oncol* **38**, 1378-1388 (2020). https://doi.org:10.1200/JCO.19.02931

15 Wang-Gillam, A. *et al.* Nanoliposomal irinotecan with fluorouracil and folinic acid in metastatic pancreatic cancer after previous gemcitabine-based therapy (NAPOLI-1): a global, randomised, open-label, phase 3 trial. *The Lancet* **387**, 545-557 (2016).

16 Neoptolemos, J. P. *et al.* Comparison of adjuvant gemcitabine and capecitabine with gemcitabine monotherapy in patients with resected pancreatic cancer (ESPAC-4): a multicentre, open-label, randomised, phase 3 trial. *The Lancet* **389**, 1011-1024 (2017).

17 Moore, M. J. *et al.* Erlotinib plus gemcitabine compared with gemcitabine alone in patients with advanced pancreatic cancer: a phase III trial of the National Cancer Institute of Canada Clinical Trials Group. *J Clin Oncol* **25**, 1960-1966 (2007). https://doi.org:10.1200/JCO.2006.07.9525

18 Golan, T. *et al.* Maintenance Olaparib for Germline BRCA-Mutated Metastatic Pancreatic Cancer. *N Engl J Med* **381**, 317-327 (2019). https://doi.org:10.1056/NEJMoa1903387

19 Le, D. T. *et al.* Mismatch repair deficiency predicts response of solid tumors to PD-1 blockade. *Science* **357**, 409-413 (2017). https://doi.org:10.1126/science.aan6733

20 Doebele, R. C. *et al.* Entrectinib in patients with advanced or metastatic NTRK fusion-positive solid tumours: integrated analysis of three phase 1-2 trials. *Lancet Oncol* **21**, 271-282 (2020). https://doi.org:10.1016/S1470-2045(19)30691-6

21 Hong, D. S. *et al.* Larotrectinib in patients with TRK fusion-positive solid tumours: a pooled analysis of three phase 1/2 clinical trials. *Lancet Oncol* **21**, 531-540 (2020). https://doi.org:10.1016/S1470-2045(19)30856-3

22 de Sousa Cavalcante, L. & Monteiro, G. Gemcitabine: metabolism and molecular mechanisms of action, sensitivity and chemoresistance in pancreatic cancer. *Eur J Pharmacol* **741**, 8-16 (2014). https://doi.org:10.1016/j.ejphar.2014.07.041

23 Mackey, J. R. *et al.* Functional Nucleoside Transporters Are Required for Gemcitabine Influx and Manifestation of Toxicity in Cancer Cell Lines1. *Cancer Research* **58**, 4349-4357 (1998).

24 Plunkett, W., Huang, P. & Gandhi, V. Preclinical characteristics of gemcitabine. *Anti-Cancer Drugs* **6**, 7-13 (1995).

25 Cappella, P. *et al.* Cell cycle effects of gemcitabine. *Int J Cancer* **93**, 401-408 (2001). https://doi.org:10.1002/ijc.1351

26 Yang, S. *et al.* New Mechanism of Gemcitabine and Its Phosphates: DNA Polymerization Disruption via 3'-5' Exonuclease Inhibition. *Biochemistry* **59**, 4344-4352 (2020). https://doi.org:10.1021/acs.biochem.0c00543

27 Huang, P., Chubb, S., Hertel, L. W., Grindey, G. B. & Plunkett, W. Action of 2′,2′-Difluorodeoxycytidine on DNA Synthesis1. *Cancer Research* **51**, 6110-6117 (1991).

28 Heinemann, V. *et al.* Inhibition of ribonucleotide reduction in CCRF-CEM cells by 2',2'-difluorodeoxycytidine. *Molecular Pharmacology* **38**, 567-572 (1990).

29 Aye, Y., Li, M., Long, M. J. & Weiss, R. S. Ribonucleotide reductase and cancer: biological mechanisms and targeted therapies. *Oncogene* **34**, 2011-2021 (2015). https://doi.org:10.1038/onc.2014.155

30 Honeywell, R. J., Ruiz van Haperen, V. W., Veerman, G., Smid, K. & Peters, G. J. Inhibition of thymidylate synthase by 2',2'-difluoro-2'-deoxycytidine (Gemcitabine) and its metabolite 2',2'-difluoro-2'-deoxyuridine. *Int J Biochem Cell Biol* **60**, 73-81 (2015). https://doi.org:10.1016/j.biocel.2014.12.010

31 Koltai, T. *et al.* Resistance to Gemcitabine in Pancreatic Ductal Adenocarcinoma: A Physiopathologic and Pharmacologic Review. *Cancers (Basel)* **14** (2022). https://doi.org:10.3390/cancers14102486

32 Amrutkar, M. & Gladhaug, I. P. Pancreatic Cancer Chemoresistance to Gemcitabine. *Cancers (Basel)* **9** (2017). https://doi.org:10.3390/cancers9110157

33 Sierzega, M., Pach, R., Kulig, P., Legutko, J. & Kulig, J. Prognostic Implications of Expression Profiling for Gemcitabine-Related Genes (hENT1, dCK, RRM1, RRM2) in Patients With Resectable Pancreatic Adenocarcinoma Receiving Adjuvant Chemotherapy. *Pancreas* **46**, 684-689 (2017). https://doi.org:10.1097/MPA.0000000000000807

34 Greenhalf, W. *et al.* Pancreatic cancer hENT1 expression and survival from gemcitabine in patients from the ESPAC-3 trial. *J Natl Cancer Inst* **106**, djt347 (2014). https://doi.org:10.1093/jnci/djt347

35 Bergman, A. M., Pinedo, H. M. & Peters, G. J. Determinants of resistance to 2',2'-difluorodeoxycytidine (gemcitabine). *Drug Resist Updat* **5**, 19-33 (2002). https://doi.org:10.1016/s1368-7646(02)00002-x

36 Nakano, Y. *et al.* Gemcitabine chemoresistance and molecular markers associated with gemcitabine transport and metabolism in human pancreatic cancer cells. *Br J Cancer* **96**, 457-463 (2007). https://doi.org:10.1038/sj.bjc.6603559

37 Nakahira, S. *et al.* Involvement of ribonucleotide reductase M1 subunit overexpression in gemcitabine resistance of human pancreatic cancer. *Int J Cancer* **120**, 1355-1363 (2007). https://doi.org:10.1002/ijc.22390

38 Bergman, A. M. *et al.* In vivo induction of resistance to gemcitabine results in increased expression of ribonucleotide reductase subunit M1 as the major determinant. *Cancer Res* **65**, 9510-9516 (2005). https://doi.org:10.1158/0008-5472.CAN-05-0989

39 Giroux, V., Iovanna, J. & Dagorn, J. C. Probing the human kinome for kinases involved in pancreatic cancer cell survival and gemcitabine resistance. *FASEB J* **20**, 1982-1991 (2006). https://doi.org:10.1096/fj.06-6239com

40 Ng, S. S. W., Tsao, M.-S., Chow, S. & Hedley, D. W. Inhibition of Phosphatidylinositide 3-Kinase Enhances Gemcitabine-induced Apoptosis in Human Pancreatic Cancer Cells1. *Cancer Research* **60**, 5451-5455 (2000).

41 Neesse, A. *et al.* Stromal biology and therapy in pancreatic cancer. *Gut* **60**, 861-868 (2011). https://doi.org:10.1136/gut.2010.226092

42 Mahadevan, D. & Von Hoff, D. D. Tumor-stroma interactions in pancreatic ductal adenocarcinoma. *Mol Cancer Ther* **6**, 1186-1197 (2007). https://doi.org:10.1158/1535-7163.MCT-06-0686

43 Jones, S. *et al.* Core signaling pathways in human pancreatic cancers revealed by global genomic analyses. *Science* **321**, 1801-1806 (2008). https://doi.org:10.1126/science.1164368

44 Luo, J. KRAS mutation in pancreatic cancer. *Semin Oncol* **48**, 10-18 (2021). https://doi.org:10.1053/j.seminoncol.2021.02.003

45 Singhal, A., Li, B. T. & O'Reilly, E. M. Targeting KRAS in cancer. *Nat Med* **30**, 969-983 (2024). https://doi.org:10.1038/s41591-024-02903-0

46 Strickler, J. H. *et al.* Sotorasib in KRAS p.G12C-Mutated Advanced Pancreatic Cancer. *N Engl J Med* **388**, 33-43 (2023). https://doi.org:10.1056/NEJMoa2208470

47 Bekaii-Saab, T. S. *et al.* Adagrasib in Advanced Solid Tumors Harboring a KRAS(G12C) Mutation. *J Clin Oncol* **41**, 4097-4106 (2023). https://doi.org:10.1200/JCO.23.00434

48 National Comprehensive Cancer Network. *NCCN Guidelines for Patients: Pancreatic Cancer*, <https://www.nccn.org/patients/guidelines/content/PDF/pancreatic-patient.pdf> (2023).

49 Wang, X. *et al.* Identification of MRTX1133, a Noncovalent, Potent, and Selective KRAS(G12D) Inhibitor. *J Med Chem* **65**, 3123-3133 (2022). https://doi.org:10.1021/acs.jmedchem.1c01688

50 Zeissig, M. N., Ashwood, L. M., Kondrashova, O. & Sutherland, K. D. Next batter up! Targeting cancers with KRAS-G12D mutations. *Trends Cancer* **9**, 955-967 (2023). https://doi.org:10.1016/j.trecan.2023.07.010

51 Ayala-Aguilera, C. C. *et al.* Small Molecule Kinase Inhibitor Drugs (1995-2021): Medical Indication, Pharmacology, and Synthesis. *J Med Chem* **65**, 1047-1131 (2022). https://doi.org:10.1021/acs.jmedchem.1c00963

52 Kun, E., Tsang, Y. T. M., Ng, C. W., Gershenson, D. M. & Wong, K. K. MEK inhibitor resistance mechanisms and recent developments in combination trials. *Cancer Treatment Reviews* **92**, 102137 (2021). https://doi.org:https://doi.org/10.1016/j.ctrv.2020.102137

53 Nikiforov, Y. E. & Nikiforova, M. N. Molecular genetics and diagnosis of thyroid cancer. *Nat Rev Endocrinol* **7**, 569-580 (2011). https://doi.org:10.1038/nrendo.2011.142

54 Crowley, F., Park, W. & O'Reilly, E. M. Targeting DNA damage repair pathways in pancreas cancer. *Cancer Metastasis Rev* **40**, 891-908 (2021). https://doi.org:10.1007/s10555-021-09983-1

55 Kuo, K. K. *et al.* Therapeutic Strategies Targeting Tumor Suppressor Genes in Pancreatic Cancer. *Cancers (Basel)* **13** (2021). https://doi.org:10.3390/cancers13153920

56 Zhao, D. & DePinho, R. A. Synthetic essentiality: Targeting tumor suppressor deficiencies in cancer. *Bioessays* **39** (2017). https://doi.org:10.1002/bies.201700076

57 Hu, H. F. *et al.* Mutations in key driver genes of pancreatic cancer: molecularly targeted therapies and other clinical implications. *Acta Pharmacol Sin* **42**, 1725-1741 (2021). https://doi.org:10.1038/s41401-020-00584-2

58 Lindahl, T. Instability and decay of the primary structure of DNA. *Nature* **362**, 709-715 (1993). https://doi.org:10.1038/362709a0

59 Jackson, S. P. & Bartek, J. The DNA-damage response in human biology and disease. *Nature* **461**, 1071-1078 (2009). https://doi.org:10.1038/nature08467

60 Blackford, A. N. & Jackson, S. P. ATM, ATR, and DNA-PK: The Trinity at the Heart of the DNA Damage Response. *Mol Cell* **66**, 801-817 (2017). https://doi.org:10.1016/j.molcel.2017.05.015

61 Roos, W. P., Thomas, A. D. & Kaina, B. DNA damage and the balance between survival and death in cancer biology. *Nat Rev Cancer* **16**, 20-33 (2016). https://doi.org:10.1038/nrc.2015.2

62 Hanahan, D. & Weinberg, R. A. Hallmarks of cancer: the next generation. *Cell* **144**, 646-674 (2011). https://doi.org:10.1016/j.cell.2011.02.013

63 Yates, L. R. & Campbell, P. J. Evolution of the cancer genome. *Nat Rev Genet* **13**, 795-806 (2012). https://doi.org:10.1038/nrg3317

64 Kantidze, O. L., Velichko, A. K., Luzhin, A. V., Petrova, N. V. & Razin, S. V. Synthetically Lethal Interactions of ATM, ATR, and DNA-PKcs. *Trends Cancer* **4**, 755-768 (2018). https://doi.org:10.1016/j.trecan.2018.09.007

65 Lovejoy, C. A. & Cortez, D. Common mechanisms of PIKK regulation. *DNA Repair (Amst)* **8**, 1004-1008 (2009). https://doi.org:10.1016/j.dnarep.2009.04.006

66 Chapman, J. R., Taylor, M. R. & Boulton, S. J. Playing the end game: DNA double-strand break repair pathway choice. *Mol Cell* **47**, 497-510 (2012). https://doi.org:10.1016/j.molcel.2012.07.029

67 Chaplin, A. K. & Blundell, T. L. Structural biology of multicomponent assemblies in DNA double-strand-break repair through non-homologous end joining. *Curr Opin Struct Biol* **61**, 9-16 (2020). https://doi.org:10.1016/j.sbi.2019.09.008

68 Guo, Z., Kumagai, A., Wang, S. X. & Dunphy, W. G. Requirement for Atr in phosphorylation of Chk1 and cell cycle regulation in response to DNA replication blocks and UV-damaged DNA in Xenopus egg extracts. *Genes Dev* **14**, 2745-2756 (2000). https://doi.org:10.1101/gad.842500

69 Liu, Q. *et al.* Chk1 is an essential kinase that is regulated by Atr and required for the G(2)/M DNA damage checkpoint. *Genes Dev* **14**, 1448-1459 (2000).

70 Zhao, H. & Piwnica-Worms, H. ATR-mediated checkpoint pathways regulate phosphorylation and activation of human Chk1. *Mol Cell Biol* **21**, 4129-4139 (2001). https://doi.org:10.1128/MCB.21.13.4129-4139.2001

71 Zou, L. & Elledge, S. J. Sensing DNA damage through ATRIP recognition of RPA-ssDNA complexes. *Science* **300**, 1542-1548 (2003). https://doi.org:10.1126/science.1083430

72 Kim, S. T., Lim, D. S., Canman, C. E. & Kastan, M. B. Substrate specificities and identification of putative substrates of ATM kinase family members. *J Biol Chem* **274**, 37538-37543 (1999). https://doi.org:10.1074/jbc.274.53.37538

73 Matsuoka, S. *et al.* ATM and ATR substrate analysis reveals extensive protein networks responsive to DNA damage. *Science* **316**, 1160-1166 (2007). https://doi.org:10.1126/science.1140321

74 Gatei, M. *et al.* Ataxia telangiectasia mutated (ATM) kinase and ATM and Rad3 related kinase mediate phosphorylation of Brca1 at distinct and overlapping sites. In vivo assessment using phospho-specific antibodies. *J Biol Chem* **276**, 17276-17280 (2001). https://doi.org:10.1074/jbc.M011681200

75 Kupculak, M. *et al.* Phosphorylation by ATR triggers FANCD2 chromatin loading and activates the Fanconi anemia pathway. *Cell Rep* **42**, 112721 (2023). https://doi.org:10.1016/j.celrep.2023.112721

76 Taniguchi, T. *et al.* Convergence of the fanconi anemia and ataxia telangiectasia signaling pathways. *Cell* **109**, 459-472 (2002). https://doi.org:10.1016/s0092-8674(02)00747-x

77 Cimprich, K. A. & Cortez, D. ATR: an essential regulator of genome integrity. *Nature Reviews Molecular Cell Biology* **9**, 616-627 (2008). https://doi.org:10.1038/nrm2450

78 da Costa, A., Chowdhury, D., Shapiro, G. I., D'Andrea, A. D. & Konstantinopoulos, P. A. Targeting replication stress in cancer therapy. *Nat Rev Drug Discov* **22**, 38-58 (2023). https://doi.org:10.1038/s41573-022-00558-5

79 Branzei, D. & Foiani, M. Maintaining genome stability at the replication fork. *Nat Rev Mol Cell Biol* **11**, 208-219 (2010). https://doi.org:10.1038/nrm2852

80 Byun, T. S., Pacek, M., Yee, M. C., Walter, J. C. & Cimprich, K. A. Functional uncoupling of MCM helicase and DNA polymerase activities activates the ATR-dependent checkpoint. *Genes Dev* **19**, 1040-1052 (2005). https://doi.org:10.1101/gad.1301205

81 Kumagai, A., Lee, J., Yoo, H. Y. & Dunphy, W. G. TopBP1 activates the ATR-ATRIP complex. *Cell* **124**, 943-955 (2006). https://doi.org:10.1016/j.cell.2005.12.041

82 Delacroix, S., Wagner, J. M., Kobayashi, M., Yamamoto, K. & Karnitz, L. M. The Rad9-Hus1-Rad1 (9-1-1) clamp activates checkpoint signaling via TopBP1. *Genes Dev* **21**, 1472-1477 (2007). https://doi.org:10.1101/gad.1547007

83 Austin, W. R. *et al.* Nucleoside salvage pathway kinases regulate hematopoiesis by linking nucleotide metabolism with replication stress. *J Exp Med* **209**, 2215-2228 (2012). https://doi.org:10.1084/jem.20121061

84 Le, T. M. *et al.* ATR inhibition facilitates targeting of leukemia dependence on convergent nucleotide biosynthetic pathways. *Nat Commun* **8**, 241 (2017). https://doi.org:10.1038/s41467-017-00221-3

85 Zeman, M. K. & Cimprich, K. A. Causes and consequences of replication stress. *Nature Cell Biology* **16**, 2-9 (2014). https://doi.org:10.1038/ncb2897

86 Bester, C., Assaf *et al.* Nucleotide Deficiency Promotes Genomic Instability in Early Stages of Cancer Development. *Cell* **145**, 435-446 (2011). https://doi.org:10.1016/j.cell.2011.03.044

87 Foote, K. M. *et al.* Discovery and Characterization of AZD6738, a Potent Inhibitor of Ataxia Telangiectasia Mutated and Rad3 Related (ATR) Kinase with Application as an Anticancer Agent. *J Med Chem* **61**, 9889-9907 (2018). https://doi.org:10.1021/acs.jmedchem.8b01187

88 Middleton, G. *et al.* MA06.06 A Phase II Trial of Ceralasertib and Durvalumab in Advanced Non-Small Cell Lung Cancer (NSCLC) with and without RAS Mutations: Results of NLMT Arm J. *Journal of Thoracic Oncology* **18**, S119-S120 (2023). https://doi.org:10.1016/j.jtho.2023.09.154

89 Yap, T. A. *et al.* Phase I Trial of First-in-Class ATR Inhibitor M6620 (VX-970) as Monotherapy or in Combination With Carboplatin in Patients With Advanced Solid Tumors. *J Clin Oncol* **38**, 3195-3204 (2020). https://doi.org:10.1200/JCO.19.02404

90 Middleton, M. R. *et al.* Phase 1 study of the ATR inhibitor berzosertib (formerly M6620, VX-970) combined with gemcitabine +/- cisplatin in patients with advanced solid tumours. *Br J Cancer* **125**, 510-519 (2021). https://doi.org:10.1038/s41416-021-01405-x

91 Luecking, U. T. *et al.* Abstract 983: Identification of potent, highly selective and orally available ATR inhibitor BAY 1895344 with favorable PK properties and promising efficacy in monotherapy and combination in preclinical tumor models. *Cancer Research* **77**, 983-983 (2017). https://doi.org:10.1158/1538-7445.Am2017-983

92 Yap, T. A. *et al.* First-in-Human Study of the Ataxia Telangiectasia and Rad3-related (ATR) Inhibitor Tuvusertib (M1774) as Monotherapy in Patients with Solid Tumors. *Clin Cancer Res* (2024). https://doi.org:10.1158/1078-0432.CCR-23-2409

93 Roulston, A. *et al.* RP-3500: A Novel, Potent, and Selective ATR Inhibitor that is Effective in Preclinical Models as a Monotherapy and in Combination with PARP Inhibitors. *Mol Cancer Ther* **21**, 245-256 (2022). https://doi.org:10.1158/1535-7163.MCT-21-0615

94 Moore, K. *et al.* 680P First results from the phase I trial of the ATR inhibitor, ART0380, in advanced solid tumors. *Annals of Oncology* **34**, S475-S476 (2023). https://doi.org:10.1016/j.annonc.2023.09.1866

95 Yuwen, H. *et al.* Abstract 2604: The novel ATR inhibitor ATG-018 is efficacious in preclinical cancer models. *Cancer Research* **82**, 2604-2604 (2022). https://doi.org:10.1158/1538-7445.Am2022-2604

96 Singh, S., Malik, B. K. & Sharma, D. K. Molecular drug targets and structure based drug design: A holistic approach. *Bioinformation* **1**, 314-320 (2006). https://doi.org:10.6026/97320630001314

97 Aebersold, R. & Mann, M. Mass spectrometry-based proteomics. *Nature* **422**, 198-207 (2003). https://doi.org:10.1038/nature01511

98 Meissner, F., Geddes-McAlister, J., Mann, M. & Bantscheff, M. The emerging role of mass spectrometry-based proteomics in drug discovery. *Nat Rev Drug Discov* **21**, 637-654 (2022). https://doi.org:10.1038/s41573-022-00409-3

99 Schirle, M., Bantscheff, M. & Kuster, B. Mass spectrometry-based proteomics in preclinical drug discovery. *Chem Biol* **19**, 72-84 (2012). https://doi.org:10.1016/j.chembiol.2012.01.002

100 KhalKhal, E., Rezaei-Tavirani, M. & Rostamii-Nejad, M. Pharmaceutical Advances and Proteomics Researches. *Iran J Pharm Res* **18**, 51-67 (2019). https://doi.org:10.22037/ijpr.2020.112440.13758

101 Anighoro, A., Bajorath, J. & Rastelli, G. Polypharmacology: Challenges and Opportunities in Drug Discovery. *Journal of Medicinal Chemistry* **57**, 7874-7887 (2014). https://doi.org:10.1021/jm5006463

102 Zecha, J. *et al.* Decrypting drug actions and protein modifications by dose- and time-resolved proteomics. *Science*, eade3925 (2023). https://doi.org:10.1126/science.ade3925

103 Morris, M. K., Chi, A., Melas, I. N. & Alexopoulos, L. G. Phosphoproteomics in drug discovery. *Drug Discovery Today* **19**, 425-432 (2014). https://doi.org:https://doi.org/10.1016/j.drudis.2013.10.010

104 Klaeger, S. *et al.* The target landscape of clinical kinase drugs. *Science* **358** (2017). https://doi.org:10.1126/science.aan4368

105 De Lellis, L. *et al.* Drug Repurposing, an Attractive Strategy in Pancreatic Cancer Treatment: Preclinical and Clinical Updates. *Cancers (Basel)* **13** (2021). https://doi.org:10.3390/cancers13163946

106 Gao, Y., Ma, M., Li, W. & Lei, X. Chemoproteomics, A Broad Avenue to Target Deconvolution. *Adv Sci (Weinh)* **11**, e2305608 (2024). https://doi.org:10.1002/advs.202305608

107 Kubota, K., Funabashi, M. & Ogura, Y. Target deconvolution from phenotype-based drug discovery by using chemical proteomics approaches. *Biochim Biophys Acta Proteins Proteom* **1867**, 22-27 (2019). https://doi.org:10.1016/j.bbapap.2018.08.002

108 Heinzlmeir, S. *When chemical proteomics meets medicinal chemistry: Guided drug discovery towards EPHA2 inhibitors*, Technische Universität München, (2017).

109 Rix, U. & Superti-Furga, G. Target profiling of small molecules by chemical proteomics. *Nat Chem Biol* **5**, 616-624 (2009). https://doi.org:10.1038/nchembio.216

110 Bantscheff, M. *et al.* Quantitative chemical proteomics reveals mechanisms of action of clinical ABL kinase inhibitors. *Nat Biotechnol* **25**, 1035-1044 (2007). https://doi.org:10.1038/nbt1328

111 Lemeer, S., Zorgiebel, C., Ruprecht, B., Kohl, K. & Kuster, B. Comparing immobilized kinase inhibitors and covalent ATP probes for proteomic profiling of kinase expression and drug selectivity. *J Proteome Res* **12**, 1723-1731 (2013). https://doi.org:10.1021/pr301073j

112 Currie, G. M. Pharmacology, Part 1: Introduction to Pharmacology and Pharmacodynamics. *J Nucl Med Technol* **46**, 81-86 (2018). https://doi.org:10.2967/jnmt.117.199588

113 Tonge, P. J. Drug-Target Kinetics in Drug Discovery. *ACS Chem Neurosci* **9**, 29-39 (2018). https://doi.org:10.1021/acschemneuro.7b00185

114 Reinecke, M. *et al.* Chemical proteomics reveals the target landscape of 1,000 kinase inhibitors. *Nat Chem Biol* (2023). https://doi.org:10.1038/s41589-023-01459-3

115 Medard, G. *et al.* Optimized chemical proteomics assay for kinase inhibitor profiling. *J Proteome Res* **14**, 1574-1586 (2015). https://doi.org:10.1021/pr5012608

116 Reinecke, M. *et al.* Chemoproteomic Selectivity Profiling of PIKK and PI3K Kinase Inhibitors. *ACS Chem Biol* **14**, 655-664 (2019). https://doi.org:10.1021/acschembio.8b01020

117 Reinecke, M. *et al.* in *Target Discovery and Validation* 97-130 (2019).

118 Johnson, L. N. & Barford, D. The Effects of Phosphorylation on the Structure and Function of Proteins. *Annual Review of Biophysics* **22**, 199-232 (1993). https://doi.org:https://doi.org/10.1146/annurev.bb.22.060193.001215

119 Hunter, T. Protein kinases and phosphatases: the yin and yang of protein phosphorylation and signaling. *Cell* **80**, 225-236 (1995).

120 Gerritsen, J. S. & White, F. M. Phosphoproteomics: a valuable tool for uncovering molecular signaling in cancer cells. *Expert Rev Proteomics* **18**, 661-674 (2021). https://doi.org:10.1080/14789450.2021.1976152

121 Schmelzle, K. & White, F. M. Phosphoproteomic approaches to elucidate cellular signaling networks. *Curr Opin Biotechnol* **17**, 406-414 (2006). https://doi.org:10.1016/j.copbio.2006.06.004

122 Sharma, K. *et al.* Ultradeep human phosphoproteome reveals a distinct regulatory nature of Tyr and Ser/Thr-based signaling. *Cell Rep* **8**, 1583-1594 (2014). https://doi.org:10.1016/j.celrep.2014.07.036

123 Hunter, T. & Sefton, B. M. Transforming gene product of Rous sarcoma virus phosphorylates tyrosine. *Proceedings of the National Academy of Sciences* **77**, 1311-1315 (1980).

124 Singh, V. *et al.* Phosphorylation: Implications in Cancer. *Protein J* **36**, 1-6 (2017). https://doi.org:10.1007/s10930-017-9696-z

125 Andersson, L. & Porath, J. Isolation of phosphoproteins by immobilized metal (Fe3+) affinity chromatography. *Anal Biochem* **154**, 250-254 (1986). https://doi.org:10.1016/0003-2697(86)90523-3

126 Qiu, W., Evans, C. A., Landels, A., Pham, T. K. & Wright, P. C. Phosphopeptide enrichment for phosphoproteomic analysis - A tutorial and review of novel materials. *Analytica Chimica Acta* **1129**, 158-180 (2020). https://doi.org:https://doi.org/10.1016/j.aca.2020.04.053

127 Thompson, A. *et al.* Tandem mass tags: a novel quantification strategy for comparative analysis of complex protein mixtures by MS/MS. *Anal Chem* **75**, 1895-1904 (2003). https://doi.org:10.1021/ac0262560

128 Rauniyar, N. & Yates, J. R., III. Isobaric Labeling-Based Relative Quantification in Shotgun Proteomics. *Journal of Proteome Research* **13**, 5293-5309 (2014). https://doi.org:10.1021/pr500880b

129 Li, J. *et al.* TMTpro-18plex: The Expanded and Complete Set of TMTpro Reagents for Sample Multiplexing. *J Proteome Res* **20**, 2964-2972 (2021). https://doi.org:10.1021/acs.jproteome.1c00168

130 O'Connell, J. D., Paulo, J. A., O'Brien, J. J. & Gygi, S. P. Proteome-Wide Evaluation of Two Common Protein Quantification Methods. *Journal of Proteome Research* **17**, 1934-1942 (2018). https://doi.org:10.1021/acs.jproteome.8b00016

131 Hamood, F., Bayer, F. P., Wilhelm, M., Kuster, B. & The, M. SIMSI-Transfer: Software-Assisted Reduction of Missing Values in Phosphoproteomic and Proteomic Isobaric Labeling Data Using Tandem Mass Spectrum Clustering. *Mol Cell Proteomics* **21**, 100238 (2022). https://doi.org:10.1016/j.mcpro.2022.100238

132 Olsen, J. V. *et al.* Global, In Vivo, and Site-Specific Phosphorylation Dynamics in Signaling Networks. *Cell* **127**, 635-648 (2006). https://doi.org:10.1016/j.cell.2006.09.026

133 Lee, C. Y. *et al.* Illuminating phenotypic drug responses of sarcoma cells to kinase inhibitors by phosphoproteomics. *Mol Syst Biol* **20**, 28-55 (2024). https://doi.org:10.1038/s44320-023-00004-7

134 Bayer, F. P., Gander, M., Kuster, B. & The, M. CurveCurator: a recalibrated F-statistic to assess, classify, and explore significance of dose-response curves. *Nat Commun* **14**, 7902 (2023). https://doi.org:10.1038/s41467-023-43696-z

135 Chang, Y.-C. *et al.* Decrypting lysine deacetylase inhibitor action and protein modifications by dose-resolved proteomics. *Cell Reports* **43**, 114272 (2024). https://doi.org:https://doi.org/10.1016/j.celrep.2024.114272

136 Zhang, J. H., Chung, T. D. & Oldenburg, K. R. A Simple Statistical Parameter for Use in Evaluation and Validation of High Throughput Screening Assays. *J Biomol Screen* **4**, 67-73 (1999). https://doi.org:10.1177/108705719900400206

137 Bliss, C. I. THE TOXICITY OF POISONS APPLIED JOINTLY1. *Annals of Applied Biology* **26**, 585-615 (1939).

138 Ritz, C., Baty, F., Streibig, J. C. & Gerhard, D. Dose-Response Analysis Using R. *PLoS One* **10**, e0146021 (2015). https://doi.org:10.1371/journal.pone.0146021

139 UniProt, C. UniProt: a worldwide hub of protein knowledge. *Nucleic Acids Res* **47**, D506-D515 (2019). https://doi.org:10.1093/nar/gky1049

140 Cox, J. & Mann, M. MaxQuant enables high peptide identification rates, individualized p.p.b.-range mass accuracies and proteome-wide protein quantification. *Nat Biotechnol* **26**, 1367-1372 (2008). https://doi.org:10.1038/nbt.1511

141 Cox, J. *et al.* Andromeda: a peptide search engine integrated into the MaxQuant environment. *J Proteome Res* **10**, 1794-1805 (2011). https://doi.org:10.1021/pr101065j

142 Seber, G. A. & Lee, A. J. *Linear regression analysis*. (John Wiley & Sons, 2012).

143 Zecha, J. *et al.* Data, Reagents, Assays and Merits of Proteomics for SARS-CoV-2 Research and Testing. *Mol Cell Proteomics* **19**, 1503-1522 (2020). https://doi.org:10.1074/mcp.RA120.002164

144 Hughes, C. S. *et al.* Single-pot, solid-phase-enhanced sample preparation for proteomics experiments. *Nat Protoc* **14**, 68-85 (2019). https://doi.org:10.1038/s41596-018-0082-x

145 Tyanova, S. *et al.* The Perseus computational platform for comprehensive analysis of (prote)omics data. *Nat Methods* **13**, 731-740 (2016). https://doi.org:10.1038/nmeth.3901

146 Benjamini, Y. & Hochberg, Y. Controlling the False Discovery Rate: A Practical and Powerful Approach to Multiple Testing. *Journal of the Royal Statistical Society: Series B (Methodological)* **57**, 289-300 (1995). https://doi.org:https://doi.org/10.1111/j.2517-6161.1995.tb02031.x

147 Hornbeck, P. V. *et al.* PhosphoSitePlus, 2014: mutations, PTMs and recalibrations. *Nucleic Acids Res* **43**, D512-520 (2015). https://doi.org:10.1093/nar/gku1267

148 Hornbeck, P. V. *et al.* PhosphoSitePlus: a comprehensive resource for investigating the structure and function of experimentally determined post-translational modifications in man and mouse. *Nucleic Acids Res* **40**, D261-270 (2012). https://doi.org:10.1093/nar/gkr1122

149 Ge, S. X., Jung, D. & Yao, R. ShinyGO: a graphical gene-set enrichment tool for animals and plants. *Bioinformatics* **36**, 2628-2629 (2020). https://doi.org:10.1093/bioinformatics/btz931

150 Szklarczyk, D. *et al.* STRING v10: protein-protein interaction networks, integrated over the tree of life. *Nucleic Acids Res* **43**, D447-452 (2015). https://doi.org:10.1093/nar/gku1003

151 Shannon, P. *et al.* Cytoscape: a software environment for integrated models of biomolecular interaction networks. *Genome Res* **13**, 2498-2504 (2003). https://doi.org:10.1101/gr.1239303

152 Müller, J. *et al.* PTMNavigator: interactive visualization of differentially regulated post-translational modifications in cellular signaling pathways. *Nat Commun* **16**, 510 (2025). https://doi.org:10.1038/s41467-024-55533-y

153 Höfer, S. *et al.* Gemcitabine and ATR inhibitors synergize to kill PDAC cells by blocking DNA damage response. *Mol Syst Biol* (2025). https://doi.org:10.1038/s44320-025-00085-6

154 Lautenbacher, L. *et al.* ProteomicsDB: toward a FAIR open-source resource for life-science research. *Nucleic Acids Res* **50**, D1541-D1552 (2022). https://doi.org:10.1093/nar/gkab1026

155 Tallarida, R. J. Drug synergism: its detection and applications. *J Pharmacol Exp Ther* **298**, 865-872 (2001).

156 Reinecke, M. *Identifying small molecule probes for kinases by chemical proteomics*, Technische Universität München, (2020).

157 O'Connell, M. J., Raleigh, J. M., Verkade, H. M. & Nurse, P. Chk1 is a wee1 kinase in the G2 DNA damage checkpoint inhibiting cdc2 by Y15 phosphorylation. *EMBO J* **16**, 545-554 (1997). https://doi.org:10.1093/emboj/16.3.545

158 Zhu, J. *et al.* Gemcitabine induces apoptosis and autophagy via the AMPK/mTOR signaling pathway in pancreatic cancer cells. *Biotechnol Appl Biochem* **65**, 665-671 (2018). https://doi.org:10.1002/bab.1657

159 Yong-Xian, G., Xiao-Huan, L., Fan, Z. & Guo-Fang, T. Gemcitabine inhibits proliferation and induces apoptosis in human pancreatic cancer PANC-1 cells. *J Cancer Res Ther* **12**, 1-4 (2016). https://doi.org:10.4103/0973-1482.191615

160 Schniewind, B. *et al.* Resistance of pancreatic cancer to gemcitabine treatment is dependent on mitochondria-mediated apoptosis. *Int J Cancer* **109**, 182-188 (2004). https://doi.org:10.1002/ijc.11679

161 Dohner, H. *et al.* Adjunctive Volasertib in Patients With Acute Myeloid Leukemia not Eligible for Standard Induction Therapy: A Randomized, Phase 3 Trial. *Hemasphere* **5**, e617 (2021). https://doi.org:10.1097/HS9.0000000000000617

162 Stadler, W. M. *et al.* An open-label, single-arm, phase 2 trial of the Polo-like kinase inhibitor volasertib (BI 6727) in patients with locally advanced or metastatic urothelial cancer. *Cancer* **120**, 976-982 (2014). https://doi.org:10.1002/cncr.28519

163 Ellis, P. M. *et al.* A Randomized, Open-Label Phase II Trial of Volasertib as Monotherapy and in Combination With Standard-Dose Pemetrexed Compared With Pemetrexed Monotherapy in Second-Line Treatment for Non-Small-Cell Lung Cancer. *Clin Lung Cancer* **16**, 457-465 (2015). https://doi.org:10.1016/j.cllc.2015.05.010

164 Pujade-Lauraine, E. *et al.* Volasertib Versus Chemotherapy in Platinum-Resistant or -Refractory Ovarian Cancer: A Randomized Phase II Groupe des Investigateurs Nationaux pour l'Etude des Cancers de l'Ovaire Study. *J Clin Oncol* **34**, 706-713 (2016). https://doi.org:10.1200/JCO.2015.62.1474

165 U.S. Food & Drug Administration. *Volasertib Orphan Designation*, <https://www.accessdata.fda.gov/scripts/opdlisting/oopd/detailedIndex.cfm?cfgridkey=771420> (2020).

166 Li, J. *et al.* Plk1 inhibition enhances the efficacy of gemcitabine in human pancreatic cancer. *Cell Cycle* **15**, 711-719 (2016). https://doi.org:10.1080/15384101.2016.1148838

167 Gilmartin, A. G. *et al.* Distinct concentration-dependent effects of the polo-like kinase 1-specific inhibitor GSK461364A, including differential effect on apoptosis. *Cancer Res* **69**, 6969-6977 (2009). https://doi.org:10.1158/0008-5472.CAN-09-0945

168 Steegmaier, M. *et al.* BI 2536, a potent and selective inhibitor of polo-like kinase 1, inhibits tumor growth in vivo. *Curr Biol* **17**, 316-322 (2007). https://doi.org:10.1016/j.cub.2006.12.037

169 Markham, A. & Duggan, S. Tirbanibulin: First Approval. *Drugs* **81**, 509-513 (2021). https://doi.org:10.1007/s40265-021-01479-0

170 Naing, A. *et al.* A phase I trial of KX2-391, a novel non-ATP competitive substrate-pocket- directed SRC inhibitor, in patients with advanced malignancies. *Invest New Drugs* **31**, 967-973 (2013). https://doi.org:10.1007/s10637-013-9929-8

171 Voss, M. H. *et al.* Phase 1 study of mTORC1/2 inhibitor sapanisertib (TAK-228) in advanced solid tumours, with an expansion phase in renal, endometrial or bladder cancer. *Br J Cancer* **123**, 1590-1598 (2020). https://doi.org:10.1038/s41416-020-01041-x

172 Pelosci, A. *Sapanisertib Receives Fast Track Designation by the FDA for Advanced NSCLC*, <https://www.cancernetwork.com/view/sapanisertib-receives-fast-track-designation-by-the-fda-for-advanced-nsclc> (2022).

173 US National Library of Medicine. *ClinicalTrials.gov (NCT02465060)*, <https://clinicaltrials.gov/study/NCT02465060?cond=pancreatic%20cancer&intr=sapanisertib&viewType=Table&rank=3> (2024).

174 Rajdev, L. *et al.* A phase II study of sapanisertib (TAK-228) a mTORC1/2 inhibitor in rapalog-resistant advanced pancreatic neuroendocrine tumors (PNET): ECOG-ACRIN EA2161. *Invest New Drugs* **40**, 1306-1314 (2022). https://doi.org:10.1007/s10637-022-01311-w

175 Khan, T. *et al.* Synergistic activity of agents targeting growth factor receptors, CDKs and downstream signaling molecules in a panel of pancreatic cancer cell lines and the identification of antagonistic combinations: Implications for future clinical trials in pancreatic cancer. *Oncol Rep* **44**, 2581-2594 (2020). https://doi.org:10.3892/or.2020.7822

176 Feldmann, G. *et al.* Cyclin-dependent kinase inhibitor Dinaciclib (SCH727965) inhibits pancreatic cancer growth and progression in murine xenograft models. *Cancer Biol Ther* **12**, 598-609 (2011). https://doi.org:10.4161/cbt.12.7.16475

177 Yang, J. *et al.* Dinaciclib prolongs survival in the LSL-Kras(G12D/+) ; LSL-Trp53(R172H/+) ; Pdx-1-Cre (KPC) transgenic murine models of pancreatic ductal adenocarcinoma. *Am J Transl Res* **12**, 1031-1043 (2020).

178 Murphy, A. G. *et al.* A Phase I Study of Dinaciclib in Combination With MK-2206 in Patients With Advanced Pancreatic Cancer. *Clinical and Translational Science* **13**, 1178-1188 (2020). https://doi.org:https://doi.org/10.1111/cts.12802

179 Yamaguchi, H. *et al.* Effects of Clostridium perfringens enterotoxin via claudin-4 on normal human pancreatic duct epithelial cells and cancer cells. *Cellular & Molecular Biology Letters* **16**, 385-397 (2011). https://doi.org:10.2478/s11658-011-0014-z

180 Ju, H.-Q. *et al.* Mutant Kras- and p16-regulated NOX4 activation overcomes metabolic checkpoints in development of pancreatic ductal adenocarcinoma. *Nature Communications* **8**, 14437 (2017). https://doi.org:10.1038/ncomms14437

181 Wallez, Y. *et al.* The ATR Inhibitor AZD6738 Synergizes with Gemcitabine In Vitro and In Vivo to Induce Pancreatic Ductal Adenocarcinoma Regression. *Mol Cancer Ther* **17**, 1670-1682 (2018). https://doi.org:10.1158/1535-7163.MCT-18-0010

182 Fokas, E. *et al.* Targeting ATR in vivo using the novel inhibitor VE-822 results in selective sensitization of pancreatic tumors to radiation. *Cell Death Dis* **3**, e441 (2012). https://doi.org:10.1038/cddis.2012.181

183 Liu, S. *et al.* Inhibition of ATR potentiates the cytotoxic effect of gemcitabine on pancreatic cancer cells through enhancement of DNA damage and abrogation of ribonucleotide reductase induction by gemcitabine. *Oncol Rep* **37**, 3377-3386 (2017). https://doi.org:10.3892/or.2017.5580

184 Prevo, R. *et al.* The novel ATR inhibitor VE-821 increases sensitivity of pancreatic cancer cells to radiation and chemotherapy. *Cancer Biology & Therapy* **13**, 1072-1081 (2012). https://doi.org:10.4161/cbt.21093

185 Zhang, H. *et al.* Mapping combinatorial drug effects to DNA damage response kinase inhibitors. *Nat Commun* **14**, 8310 (2023). https://doi.org:10.1038/s41467-023-44108-y

186 Shon, H. W. *et al.* Abstract 6217: Inhibiting ataxia-telangiectasia mutated and RAD3-related (ATR) by BAY 1895344 overcomes chemoresistance to oxaliplatin and promotes synergistic anti-tumor effect in pancreatic cancer. *Cancer Research* **83**, 6217-6217 (2023). https://doi.org:10.1158/1538-7445.Am2023-6217

187 Lucking, U. *et al.* Damage Incorporated: Discovery of the Potent, Highly Selective, Orally Available ATR Inhibitor BAY 1895344 with Favorable Pharmacokinetic Properties and Promising Efficacy in Monotherapy and in Combination Treatments in Preclinical Tumor Models. *J Med Chem* **63**, 7293-7325 (2020). https://doi.org:10.1021/acs.jmedchem.0c00369

188 Wengner, A. M. *et al.* The Novel ATR Inhibitor BAY 1895344 Is Efficacious as Monotherapy and Combined with DNA Damage-Inducing or Repair-Compromising Therapies in Preclinical Cancer Models. *Mol Cancer Ther* **19**, 26-38 (2020). https://doi.org:10.1158/1535-7163.MCT-19-0019

189 Jaaks, P. *et al.* Effective drug combinations in breast, colon and pancreatic cancer cells. *Nature* **603**, 166-173 (2022). https://doi.org:10.1038/s41586-022-04437-2

190 Nair, N. U. *et al.* A landscape of response to drug combinations in non-small cell lung cancer. *Nat Commun* **14**, 3830 (2023). https://doi.org:10.1038/s41467-023-39528-9

191 O'Neil, J. *et al.* An Unbiased Oncology Compound Screen to Identify Novel Combination Strategies. *Mol Cancer Ther* **15**, 1155-1162 (2016). https://doi.org:10.1158/1535-7163.MCT-15-0843

192 Heinzlmeir, S. *et al.* Chemoproteomics-Aided Medicinal Chemistry for the Discovery of EPHA2 Inhibitors. *ChemMedChem* **12**, 999-1011 (2017). https://doi.org:10.1002/cmdc.201700217

193 Charrier, J. D. *et al.* Discovery of potent and selective inhibitors of ataxia telangiectasia mutated and Rad3 related (ATR) protein kinase as potential anticancer agents. *J Med Chem* **54**, 2320-2330 (2011). https://doi.org:10.1021/jm101488z

194 Das, A., Bhattacharya, B. & Roy, S. Decrypting a path based approach for identifying the interplay between PI3K and GSK3 signaling cascade from the perspective of cancer. *Genes Dis* **9**, 868-888 (2022). https://doi.org:10.1016/j.gendis.2021.12.025

195 Duda, P. *et al.* Targeting GSK3 and Associated Signaling Pathways Involved in Cancer. *Cells* **9** (2020). https://doi.org:10.3390/cells9051110

196 Toledo, L. I. *et al.* A cell-based screen identifies ATR inhibitors with synthetic lethal properties for cancer-associated mutations. *Nat Struct Mol Biol* **18**, 721-727 (2011). https://doi.org:10.1038/nsmb.2076

197 Reaper, P. M. *et al.* Selective killing of ATM- or p53-deficient cancer cells through inhibition of ATR. *Nat Chem Biol* **7**, 428-430 (2011). https://doi.org:10.1038/nchembio.573

198 Shapiro, G. I. *et al.* Phase 1 study of the ATR inhibitor berzosertib in combination with cisplatin in patients with advanced solid tumours. *Br J Cancer* **125**, 520-527 (2021). https://doi.org:10.1038/s41416-021-01406-w

199 Yew, M. J. *et al.* ACAD10 is not required for metformin's metabolic actions or for maintenance of whole-body metabolism in C57BL/6J mice. *Diabetes Obes Metab* **26**, 1731-1745 (2024). https://doi.org:10.1111/dom.15484

200 Janda, E., Boutin, J. A., De Lorenzo, C. & Arbitrio, M. Polymorphisms and Pharmacogenomics of NQO2: The Past and the Future. *Genes* **15**, 87 (2024).

201 Zenke, F. T. *et al.* Abstract 369: Antitumor activity of M4344, a potent and selective ATR inhibitor, in monotherapy and combination therapy. *Cancer Research* **79**, 369-369 (2019). https://doi.org:10.1158/1538-7445.Am2019-369

202 Syed, V. TGF-beta Signaling in Cancer. *J Cell Biochem* **117**, 1279-1287 (2016). https://doi.org:10.1002/jcb.25496

203 Strum, S. W., Gyenis, L. & Litchfield, D. W. CSNK2 in cancer: pathophysiology and translational applications. *Br J Cancer* **126**, 994-1003 (2022). https://doi.org:10.1038/s41416-021-01616-2

204 Unbekandt, M. *et al.* A novel small-molecule MRCK inhibitor blocks cancer cell invasion. *Cell Commun Signal* **12**, 54 (2014). https://doi.org:10.1186/s12964-014-0054-x

205 Peters, J.-U. Polypharmacology – Foe or Friend? *Journal of Medicinal Chemistry* **56**, 8955-8971 (2013). https://doi.org:10.1021/jm400856t

206 Burris, H. A. *et al.* A phase I study of ATR inhibitor gartisertib (M4344) as a single agent and in combination with carboplatin in patients with advanced solid tumours. *Br J Cancer* **130**, 1131-1140 (2024). https://doi.org:10.1038/s41416-023-02436-2

207 Johnson, J. L. *et al.* An atlas of substrate specificities for the human serine/threonine kinome. *Nature* **613**, 759-766 (2023). https://doi.org:10.1038/s41586-022-05575-3

208 Xu, N. *et al.* Cdk-mediated phosphorylation of Chk1 is required for efficient activation and full checkpoint proficiency in response to DNA damage. *Oncogene* **31**, 1086-1094 (2012). https://doi.org:10.1038/onc.2011.310

209 Rogakou, E. P., Pilch, D. R., Orr, A. H., Ivanova, V. S. & Bonner, W. M. DNA double-stranded breaks induce histone H2AX phosphorylation on serine 139. *J Biol Chem* **273**, 5858-5868 (1998). https://doi.org:10.1074/jbc.273.10.5858

210 Hu, C. *et al.* Roles of Kruppel-associated Box (KRAB)-associated Co-repressor KAP1 Ser-473 Phosphorylation in DNA Damage Response. *J Biol Chem* **287**, 18937-18952 (2012). https://doi.org:10.1074/jbc.M111.313262

211 Moynahan, M. E., Chiu, J. W., Koller, B. H. & Jasin, M. Brca1 controls homology-directed DNA repair. *Molecular cell* **4**, 511-518 %@ 1097-2765 (1999).

212 Blethrow, J. D., Glavy, J. S., Morgan, D. O. & Shokat, K. M. Covalent capture of kinase-specific phosphopeptides reveals Cdk1-cyclin B substrates. *Proc Natl Acad Sci U S A* **105**, 1442-1447 (2008). https://doi.org:10.1073/pnas.0708966105

213 Bessa, M., Joaquin, M., Tavner, F., Saville, M. K. & Watson, R. J. Regulation of the cell cycle by B-Myb. *Blood Cells Mol Dis* **27**, 416-421 (2001). https://doi.org:10.1006/bcmd.2001.0399

214 Izzo, A. & Schneider, R. The role of linker histone H1 modifications in the regulation of gene expression and chromatin dynamics. *Biochim Biophys Acta* **1859**, 486-495 (2016). https://doi.org:10.1016/j.bbagrm.2015.09.003

215 Yan, J. *et al.* The ubiquitin-interacting motif containing protein RAP80 interacts with BRCA1 and functions in DNA damage repair response. *Cancer Res* **67**, 6647-6656 (2007). https://doi.org:10.1158/0008-5472.CAN-07-0924

216 Tauchi, H. *et al.* Nbs1 is essential for DNA repair by homologous recombination in higher vertebrate cells. *Nature* **420**, 93-98 (2002). https://doi.org:10.1038/nature01125

217 Xie, A. *et al.* Distinct roles of chromatin-associated proteins MDC1 and 53BP1 in mammalian double-strand break repair. *Mol Cell* **28**, 1045-1057 (2007). https://doi.org:10.1016/j.molcel.2007.12.005

218 Kim, J. E., Minter-Dykhouse, K. & Chen, J. Signaling networks controlled by the MRN complex and MDC1 during early DNA damage responses. *Mol Carcinog* **45**, 403-408 (2006). https://doi.org:10.1002/mc.20221

219 Stucki, M. & Jackson, S. P. gammaH2AX and MDC1: anchoring the DNA-damage-response machinery to broken chromosomes. *DNA Repair (Amst)* **5**, 534-543 (2006). https://doi.org:10.1016/j.dnarep.2006.01.012

220 Kambach, C., Walke, S. & Nagai, K. Structure and assembly of the spliceosomal small nuclear ribonucleoprotein particles. *Curr Opin Struct Biol* **9**, 222-230 (1999). https://doi.org:10.1016/s0959-440x(99)80032-3

221 Zhou, Z. & Fu, X.-D. Regulation of splicing by SR proteins and SR protein-specific kinases. *Chromosoma* **122**, 191-207 (2013). https://doi.org:10.1007/s00412-013-0407-z

222 Gudipaty, S. A. & D'Orso, I. Functional interplay between PPM1G and the transcription elongation machinery. *RNA Dis* **3** (2016).

223 Aso, T., Lane, W. S., Conaway, J. W. & Conaway, R. C. Elongin (SIII): A Multisubunit Regulator of Elongation by RNA Polymerase II. *Science* **269**, 1439-1443 (1995). https://doi.org:doi:10.1126/science.7660129

224 Corsini, N. S. *et al.* Coordinated Control of mRNA and rRNA Processing Controls Embryonic Stem Cell Pluripotency and Differentiation. *Cell Stem Cell* **22**, 543-558.e512 (2018). https://doi.org:https://doi.org/10.1016/j.stem.2018.03.002

225 Milacic, M. *et al.* The Reactome Pathway Knowledgebase 2024. *Nucleic Acids Res* **52**, D672-D678 (2024). https://doi.org:10.1093/nar/gkad1025

226 Gilmore, J. M. *et al.* WDR76 Co-Localizes with Heterochromatin Related Proteins and Rapidly Responds to DNA Damage. *PLoS One* **11**, e0155492 (2016). https://doi.org:10.1371/journal.pone.0155492

227 Shkreta, L. & Chabot, B. The RNA Splicing Response to DNA Damage. *Biomolecules* **5**, 2935-2977 (2015).

228 Naro, C., Bielli, P., Pagliarini, V. & Sette, C. The interplay between DNA damage response and RNA processing: the unexpected role of splicing factors as gatekeepers of genome stability. *Frontiers in Genetics* **6** (2015). https://doi.org:10.3389/fgene.2015.00142

229 Lenzken, S. C., Loffreda, A. & Barabino, S. M. L. RNA Splicing: A New Player in the DNA Damage Response. *International Journal of Cell Biology* **2013**, 153634 (2013). https://doi.org:https://doi.org/10.1155/2013/153634

230 Bennetzen, M. V. *et al.* Site-specific phosphorylation dynamics of the nuclear proteome during the DNA damage response. *Mol Cell Proteomics* **9**, 1314-1323 (2010). https://doi.org:10.1074/mcp.M900616-MCP200

231 Bensimon, A. *et al.* ATM-dependent and -independent dynamics of the nuclear phosphoproteome after DNA damage. *Sci Signal* **3**, rs3 (2010). https://doi.org:10.1126/scisignal.2001034

232 Murray, M. V., Kobayashi, R. & Krainer, A. R. The type 2C Ser/Thr phosphatase PP2Cγ is a pre-mRNA splicing factor. *Genes & development* **13**, 87-97 (1999).

233 Beli, P. *et al.* Proteomic Investigations Reveal a Role for RNA Processing Factor THRAP3 in the DNA Damage Response. *Molecular Cell* **46**, 212-225 (2012). https://doi.org:10.1016/j.molcel.2012.01.026

234 Szydzik, J. *et al.* ATR inhibition enables complete tumour regression in ALK-driven NB mouse models. *Nat Commun* **12**, 6813 (2021). https://doi.org:10.1038/s41467-021-27057-2

235 O'Leary, P. C. *et al.* Resistance to ATR Inhibitors Is Mediated by Loss of the Nonsense-Mediated Decay Factor UPF2. *Cancer Research* **82**, 3950-3961 (2022). https://doi.org:10.1158/0008-5472.Can-21-4335

236 Salovska, B. *et al.* Radiosensitization of human leukemic HL-60 cells by ATR kinase inhibitor (VE-821): phosphoproteomic analysis. *Int J Mol Sci* **15**, 12007-12026 (2014). https://doi.org:10.3390/ijms150712007

237 Salovska, B. *et al.* Radio-sensitizing effects of VE-821 and beyond: Distinct phosphoproteomic and metabolomic changes after ATR inhibition in irradiated MOLT-4 cells. *PLoS One* **13**, e0199349 (2018). https://doi.org:10.1371/journal.pone.0199349

238 Schlam-Babayov, S. *et al.* Phosphoproteomics reveals novel modes of function and inter-relationships among PIKKs in response to genotoxic stress. *EMBO J* **40**, e104400 (2021). https://doi.org:10.15252/embj.2020104400

239 Jadav, R. *et al.* Chemo-phosphoproteomic profiling with ATR inhibitors berzosertib and gartisertib uncovers new biomarkers and DNA damage response regulators. *Mol Cell Proteomics*, 100802 (2024). https://doi.org:10.1016/j.mcpro.2024.100802

240 Schosserer, M. *et al.* Methylation of ribosomal RNA by NSUN5 is a conserved mechanism modulating organismal lifespan. *Nat Commun* **6**, 6158 (2015). https://doi.org:10.1038/ncomms7158

241 Kobe, B. & Kajava, A. V. The leucine-rich repeat as a protein recognition motif. *Curr Opin Struct Biol* **11**, 725-732 (2001). https://doi.org:10.1016/s0959-440x(01)00266-4

242 Fujitomo, T., Daigo, Y., Matsuda, K., Ueda, K. & Nakamura, Y. Identification of a nuclear protein, LRRC42, involved in lung carcinogenesis. *Int J Oncol* **45**, 147-156 (2014). https://doi.org:10.3892/ijo.2014.2418

243 Moody, L., Chen, H. & Pan, Y. X. Considerations for feature selection using gene pairs and applications in large-scale dataset integration, novel oncogene discovery, and interpretable cancer screening. *BMC Med Genomics* **13**, 148 (2020). https://doi.org:10.1186/s12920-020-00778-x

244 Lecona, E. & Fernandez-Capetillo, O. Targeting ATR in cancer. *Nat Rev Cancer* **18**, 586-595 (2018). https://doi.org:10.1038/s41568-018-0034-3

245 Yap, T. A. *et al.* First-in-Human Trial of the Oral Ataxia Telangiectasia and RAD3-Related (ATR) Inhibitor BAY 1895344 in Patients with Advanced Solid Tumors. *Cancer Discov* **11**, 80-91 (2021). https://doi.org:10.1158/2159-8290.CD-20-0868

246 Mu, J. J. *et al.* A proteomic analysis of ataxia telangiectasia-mutated (ATM)/ATM-Rad3-related (ATR) substrates identifies the ubiquitin-proteasome system as a regulator for DNA damage checkpoints. *J Biol Chem* **282**, 17330-17334 (2007). https://doi.org:10.1074/jbc.C700079200

247 Fedak, E. A., Adler, F. R., Abegglen, L. M. & Schiffman, J. D. ATM and ATR activation through crosstalk between DNA damage response pathways. *Bulletin of mathematical biology* **83**, 38 (2021).

248 Buisson, R., Boisvert, J. L., Benes, C. H. & Zou, L. Distinct but Concerted Roles of ATR, DNA-PK, and Chk1 in Countering Replication Stress during S Phase. *Mol Cell* **59**, 1011-1024 (2015). https://doi.org:10.1016/j.molcel.2015.07.029

249 Koppenhafer, S. L., Goss, K. L., Terry, W. W. & Gordon, D. J. Inhibition of the ATR-CHK1 Pathway in Ewing Sarcoma Cells Causes DNA Damage and Apoptosis via the CDK2-Mediated Degradation of RRM2. *Mol Cancer Res* **18**, 91-104 (2020). https://doi.org:10.1158/1541-7786.MCR-19-0585

250 Bertoli, C., Herlihy, A. E., Pennycook, B. R., Kriston-Vizi, J. & de Bruin, R. A. M. Sustained E2F-Dependent Transcription Is a Key Mechanism to Prevent Replication-Stress-Induced DNA Damage. *Cell Rep* **15**, 1412-1422 (2016). https://doi.org:10.1016/j.celrep.2016.04.036

251 Kato, T. *et al.* Cytoplasmic RRM1 activation as an acute response to gemcitabine treatment is involved in drug resistance of pancreatic cancer cells. *PLoS One* **16**, e0252917 (2021). https://doi.org:10.1371/journal.pone.0252917

252 Han, Q. L., Zhou, Y. H., Lyu, Y., Yan, H. & Dai, G. H. Effect of ribonucleotide reductase M1 expression on overall survival in patients with pancreatic cancer receiving gemcitabine chemotherapy: A literature-based meta-analysis. *J Clin Pharm Ther* **43**, 163-169 (2018). https://doi.org:10.1111/jcpt.12655

253 Shu, Z. *et al.* Cell-cycle-dependent phosphorylation of RRM1 ensures efficient DNA replication and regulates cancer vulnerability to ATR inhibition. *Oncogene* **39**, 5721-5733 (2020). https://doi.org:10.1038/s41388-020-01403-y

254 Falcomata, C. *et al.* Selective multi-kinase inhibition sensitizes mesenchymal pancreatic cancer to immune checkpoint blockade by remodeling the tumor microenvironment. *Nat Cancer* **3**, 318-336 (2022). https://doi.org:10.1038/s43018-021-00326-1

255 Schlander, M., Hernandez-Villafuerte, K., Cheng, C.-Y., Mestre-Ferrandiz, J. & Baumann, M. How Much Does It Cost to Research and Develop a New Drug? A Systematic Review and Assessment. *PharmacoEconomics* **39**, 1243-1269 (2021). https://doi.org:10.1007/s40273-021-01065-y

256 Waring, M. J. *et al.* An analysis of the attrition of drug candidates from four major pharmaceutical companies. *Nature Reviews Drug Discovery* **14**, 475-486 (2015). https://doi.org:10.1038/nrd4609

257 Abrams, R. A. *et al.* Results of the NRG Oncology/RTOG 0848 Adjuvant Chemotherapy Question-Erlotinib+Gemcitabine for Resected Cancer of the Pancreatic Head: A Phase II Randomized Clinical Trial. *Am J Clin Oncol* **43**, 173-179 (2020). https://doi.org:10.1097/COC.0000000000000633

258 Sinn, M. *et al.* CONKO-005: Adjuvant Chemotherapy With Gemcitabine Plus Erlotinib Versus Gemcitabine Alone in Patients After R0 Resection of Pancreatic Cancer: A Multicenter Randomized Phase III Trial. *J Clin Oncol* **35**, 3330-3337 (2017). https://doi.org:10.1200/JCO.2017.72.6463

259 Yang, Z.-Y. *et al.* Gemcitabine Plus Erlotinib for Advanced Pancreatic Cancer: A Systematic Review with Meta-Analysis. *PLOS ONE* **8**, e57528 (2013). https://doi.org:10.1371/journal.pone.0057528

260 O'Leary, C. *et al.* Epidermal Growth Factor Receptor (EGFR)-Mutated Non-Small-Cell Lung Cancer (NSCLC). *Pharmaceuticals* **13** (2020).

261 da Cunha Santos, G. *et al.* Molecular predictors of outcome in a phase 3 study of gemcitabine and erlotinib therapy in patients with advanced pancreatic cancer. *Cancer* **116**, 5599-5607 (2010). https://doi.org:https://doi.org/10.1002/cncr.25393

262 Boeck, S. *et al.* EGFR pathway biomarkers in erlotinib-treated patients with advanced pancreatic cancer: translational results from the randomised, crossover phase 3 trial AIO-PK0104. *British Journal of Cancer* **108**, 469-476 (2013). https://doi.org:10.1038/bjc.2012.495

263 Propper, D. *et al.* Phase II, randomized, biomarker identification trial (MARK) for erlotinib in patients with advanced pancreatic carcinoma. *Annals of Oncology* **25**, 1384-1390 (2014). https://doi.org:https://doi.org/10.1093/annonc/mdu176

264 Eckert, S. *et al.* Decrypting the molecular basis of cellular drug phenotypes by dose-resolved expression proteomics. *Nat Biotechnol* (2024). https://doi.org:10.1038/s41587-024-02218-y

265 Dowden, H. & Munro, J. Trends in clinical success rates and therapeutic focus. *Nat Rev Drug Discov* **18**, 495-496 (2019). https://doi.org:10.1038/d41573-019-00074-z

266 Tapia-Alveal, C., Calonge, T. M. & O'Connell, M. J. Regulation of chk1. *Cell Div* **4**, 8 (2009). https://doi.org:10.1186/1747-1028-4-8

267 Mullen, N. J. & Singh, P. K. Nucleotide metabolism: a pan-cancer metabolic dependency. *Nature Reviews Cancer* **23**, 275-294 (2023). https://doi.org:10.1038/s41568-023-00557-7

268 Huen, M. S. Y. & Chen, J. The DNA damage response pathways: at the crossroad of protein modifications. *Cell Research* **18**, 8-16 (2008). https://doi.org:10.1038/cr.2007.109

269 Elia, Andrew E. H. *et al.* Quantitative Proteomic Atlas of Ubiquitination and Acetylation in the DNA Damage Response. *Molecular Cell* **59**, 867-881 (2015). https://doi.org:10.1016/j.molcel.2015.05.006

270 Al-Hakim, A. *et al.* The ubiquitous role of ubiquitin in the DNA damage response. *DNA Repair* **9**, 1229-1240 (2010). https://doi.org:https://doi.org/10.1016/j.dnarep.2010.09.011

271 Espinet, E., Klein, L., Puré, E. & Singh, S. K. Mechanisms of PDAC subtype heterogeneity and therapy response. *Trends in Cancer* **8**, 1060-1071 (2022). https://doi.org:10.1016/j.trecan.2022.08.005

272 Moore, P. S. *et al.* Genetic profile of 22 pancreatic carcinoma cell lines. *Virchows Archiv* **439**, 798-802 (2001). https://doi.org:10.1007/s004280100474

273 Pushpakom, S. *et al.* Drug repurposing: progress, challenges and recommendations. *Nature Reviews Drug Discovery* **18**, 41-58 (2019). https://doi.org:10.1038/nrd.2018.168

274 Naylor, D. M., Kauppi, D. & Schonfeld, J. Therapeutic drug repurposing, repositioning and rescue. *Drug Discovery* **57**, 1-16 (2015).

275 Begley, C. G. *et al.* Drug repurposing: Misconceptions, challenges, and opportunities for academic researchers. *Science Translational Medicine* **13**, eabd5524 (2021). https://doi.org:doi:10.1126/scitranslmed.abd5524

276 American Cancer Society. *Cancer Facts & Figures 2023*, <https://www.cancer.org/content/dam/cancer-org/research/cancer-facts-and-statistics/annual-cancer-facts-and-figures/2023/2023-cancer-facts-and-figures.pdf> (2023).

277 Stockton, S. *et al.* A phase I study of ATR inhibitor BAY1895344 (elimusertib) plus topotecan (ETCTN 10402): Results of dose escalation. *Journal of Clinical Oncology* **42**, 3076-3076 (2024). https://doi.org:10.1200/JCO.2024.42.16_suppl.3076

278 Heumann, T. R. *et al.* A phase I study of irinotecan combined with BAY1895344 (ATR inhibitor) in advanced solid tumors: Results of ETCTN 10402 dose escalation. *Journal of Clinical Oncology* **42**, 3077-3077 (2024). https://doi.org:10.1200/JCO.2024.42.16_suppl.3077

279 Zhang, Z., He, S., Wang, P. & Zhou, Y. The efficacy and safety of gemcitabine-based combination therapy vs. gemcitabine alone for the treatment of advanced pancreatic cancer: a systematic review and meta-analysis. *J Gastrointest Oncol* **13**, 1967-1980 (2022). https://doi.org:10.21037/jgo-22-624

280 Konstantinopoulos, P. A. *et al.* Randomized Phase II Study of Gemcitabine With or Without ATR Inhibitor Berzosertib in Platinum-Resistant Ovarian Cancer: Final Overall Survival and Biomarker Analyses. *JCO Precis Oncol* **8**, e2300635 (2024). https://doi.org:10.1200/PO.23.00635

281 Cohen, S. S., Flaks, J. G., Barner, H. D., Loeb, M. R. & Lichtenstein, J. THE MODE OF ACTION OF 5-FLUOROURACIL AND ITS DERIVATIVES[*]. *Proceedings of the National Academy of Sciences* **44**, 1004-1012 (1958). https://doi.org:doi:10.1073/pnas.44.10.1004

282 Chalabi-Dchar, M. *et al.* A novel view on an old drug, 5-fluorouracil: an unexpected RNA modifier with intriguing impact on cancer cell fate. *NAR Cancer* **3** (2021). https://doi.org:10.1093/narcan/zcab032

283 Raymond, E., Faivre, S., Woynarowski, J. M. & Chaney, S. G. Oxaliplatin: mechanism of action and antineoplastic activity. *Semin Oncol* **25**, 4-12 (1998).

284 Dodds, H. M., Haaz, M.-C., Riou, J.-F., Robert, J. & Rivory, L. P. Identification of a New Metabolite of CPT-11 (Irinotecan): Pharmacological Properties and Activation to SN-38. *Journal of Pharmacology and Experimental Therapeutics* **286**, 578 (1998).

285 Pal, S. K. *et al.* Effect of Cisplatin and Gemcitabine With or Without Berzosertib in Patients With Advanced Urothelial Carcinoma: A Phase 2 Randomized Clinical Trial. *JAMA Oncology* **7**, 1536-1543 (2021). https://doi.org:10.1001/jamaoncol.2021.3441

286 Chee, C. E. *et al.* Phase II study of dasatinib (BMS-354825) in patients with metastatic adenocarcinoma of the pancreas. *Oncologist* **18**, 1091-1092 (2013). https://doi.org:10.1634/theoncologist.2013-0255

287 Cuneo, K. C. *et al.* Dose Escalation Trial of the Wee1 Inhibitor Adavosertib (AZD1775) in Combination With Gemcitabine and Radiation for Patients With Locally Advanced Pancreatic Cancer. *J Clin Oncol* **37**, 2643-2650 (2019). https://doi.org:10.1200/JCO.19.00730

288 Tempero, M. *et al.* Ibrutinib in combination with nab-paclitaxel and gemcitabine for first-line treatment of patients with metastatic pancreatic adenocarcinoma: phase III RESOLVE study. *Ann Oncol* **32**, 600-608 (2021). https://doi.org:10.1016/j.annonc.2021.01.070

289 Infante, J. R. *et al.* A randomised, double-blind, placebo-controlled trial of trametinib, an oral MEK inhibitor, in combination with gemcitabine for patients with untreated metastatic adenocarcinoma of the pancreas. *Eur J Cancer* **50**, 2072-2081 (2014). https://doi.org:10.1016/j.ejca.2014.04.024

290 Evans, T. R. J. *et al.* Dasatinib combined with gemcitabine (Gem) in patients (pts) with locally advanced pancreatic adenocarcinoma (PaCa): Design of CA180-375, a placebo-controlled, randomized, double-blind phase II trial. *Journal of Clinical Oncology* **30**, TPS4134-TPS4134 (2012). https://doi.org:10.1200/jco.2012.30.15_suppl.tps4134